Novel Strategies for the Preparation and Functionalization of Noble Metallic and Titanium Dioxide Nanoparticles

Zur Erlangung des akademischen Grades eines

DOKTORS DER NATURWISSENSCHAFTEN

(Dr. rer. nat.)

Fakultät für Chemie und Biowissenschaften

Karlsruher Institut für Technologie (KIT) - Universitätsbereich

genehmigte

DISSERTATION

von

M.Eng. Cheng Chen

aus

<Baotou, China>

Dekan: Prof. Dr. Peter Roesky

Referent: Priv.-Doz. Dr. Ljiljana Fruk

Korreferent: Prof. Dr. Christof Niemeyer

Tag der mündlichen Prüfung: 24.10.2014

I hereby declare that the entire work embodied in this thesis is the based on the experimental results carried out by me independently at Center for Functional Nanostructures in Karlsruhe Institute of Technology, under the supervision and guidance of Dr. Ljiljana Fruk. The experimental results and conclusions presented in this thesis have not been submitted previously for the application for any other degrees. According to the regulations of Karlsruhe Institute of Technology concerning the protection of a proper scientific praxis, all quotations have been distinguished by quotation marks and the sources of information specifically acknowledged, and nothing beyond the listed sources and aids have been used.

<div align="right">

Cheng Chen

Karlsruhe, 24.10.2014

</div>

Table of Contents

Kurzzusammenfassung

Nanopartikel (NP) haben für große Aufmerksamkeit aufgrund ihrer neuartigen Eigenschaften und ihrer Charakteristiken gesorgt, die sich von den äquivalenten „bulk" Materialien unterscheiden. Während der letzten Jahrzehnte sind gewaltige Fortschritte im Forschungsbereich der Edelmetall- und Halbleiternanomaterialien sowie deren Hybriden mit Biomolekülen gemacht worden und es wird ein steigender Bedarf für die Entwicklung von neuen, milden und effizienten Methoden für ihre Herstellung und die Erforschung neuer Anwendungen geben. Um Nanomaterialien kompatibel und anwendbar für verschiedene chemische und biologische Umgebungen zu machen ist es auch wichtig grundsätzlich aktive NPs und multifunktionale oberflächenstabilisierte Linker mit Potential für weitere Modifikation zu entwickeln.

Im Rahmen dieser Arbeit wurden verschiedene Nanopartikel einschließlich Silber (Ag), Kupfer (Cu) und Titaniumdioxid (TiO$_2$) mit ihren interessanten Eigenschaften erforscht wie beispielsweise die lokalisierte Oberflächenplasmonenresonanz, fluoreszierende Eigenschaften, Leitfähigkeit und katalytische Aktivität, die in den unterschiedlichsten Bereichen wie der Photonik, Elektronik, Sensorik, Katalyse und biomedizinischen Diagnostik angewendet werden können.[1-5]

Aufgrund der Oxidationsanfälligkeit bei Lufteinwirkung stellt die reproduzierbare Synthese von stabilen und reinen Ag und Cu NPs unter wässrigen Bedingungen immer noch eine Herausforderung dar. Einer der entscheidenden Faktoren, um dies zu erreichen, ist die Wahl geeigneter bedeckender Stoffe zum Schutz und zur Stabilisierung der Nanopartikeloberfläche, da unbedeckte Ag und Cu NPs oxidiert werden können und zur Aggregation neigen, um ihre Oberflächenenergie zu reduzieren, was ihre chemischen, optischen und katalytischen Eigenschaften massiv beeinflussen könnte.

Wasserlösliche und monodisperse Ag NPs wurden erfolgreich mit Polyacrylsäure und Benzotriazole-Maleinimid synthetisiert und die plasmonischen und fluoreszierenden Eigenschaften der erhaltenen Ag NPs wurden untersucht. Des Weiteren wurden die Ag NPs zum Aufbau von DNA-AgNP Konjugaten mittels Ligandenaustausch oder milder Diels-Alder Reaktionen verwendet. Die erhaltenen DNA-AgNP Konjugate wurden dann zur weiteren Anbindung von Gold (Au) NPs verwendet, welche als Oberflächen-verstärkte Raman Spektroskopie Substrate, oder zur gerichteten Immobilisierung von DNA auf Enzyme verwendet werden könnten, und ihre Aktivität nach dem Immobilisierungsprozess beibehalten.

Kurzzusammenfassung

Im Gegensatz zu Au und Ag NPs wurden die potentiellen Anwendungen von Cu NPs aufgrund ihrer Anfälligkeit zur Oberflächenoxidation noch nicht vollständig erschlossen. Es ist lohnend die Anwendungen von Cu NPs zu erforschen, da Kupfer interessante Eigenschaften wie etwa Oberflächenplasmonenresonanz, katalytische Aktivität und antibakterielle Wirkung besitzt und es wesentlich billiger als Au und Ag ist. Deshalb ist es besser geeignet für die großindustrielle Produktion und Anwendungen. Im Rahmen dieser Arbeit wurde die Herstellung von stabilen Cu NPs in wässrigen Lösungen mit Ascorbinsäure und Dopamin basierten Linkern erforscht. Die hergestellten Cu NPs besitzen die Fähigkeit zur „reactive oxygen species" (ROS) Produktion und können als leistungsstarke Enzymmimetika genutzt werden, wie etwa die Aktivierung des Enzyms Peroxidase oder der Nachahmung von Superoxid Dismutase. Aufgrund der exzellenten Fähigkeit zur ROS Bildung könnten solche Cu NPs auch als Katalysator zur Degradierung von schädlichen fluoreszierenden Farbstoffen und Antibiotika verwendet werden.

Zuletzt wurden zwei klickbare Dopaminlinker für die Herstellung und Modifikation von Cu NPs und TiO_2 Nanomaterialien entwickelt, da die Katecholgruppe von Dopamin eine starke Affinität zu beiden hat, Cu und TiO_2. Da Cu NPs zu einer Gruppe von plasmonischen und ROS produzierenden Nanopartikel gehören und TiO_2 Nanomaterialien ebenfalls die Fähigkeit zur lichtinduzierte ROS-Bildung besitzen, ist es interessant zu untersuchen ob die Kombination von Cu NPs und TiO_2 Nanomaterialien einen Einfluss auf die katalytischen Eigenschaften von TiO_2 Nanomaterialien haben würden. Die Kombination von TiO_2 und Cu könnte neue, hochaktive und effiziente Nanomaterialien erzeugen, die zur Enzymmimetika und für Umweltanwendungen nützlich sind.

Abstract

Nanoparticles (NPs) have attracted lots of attention due to their novel properties and characteristics that differ from the equivalent bulk counterparts. During the past decades tremendous progress has been made in the research fields of noble metallic and semiconductor nanomaterials as well as their hybrids with biomolecules, and there will be an increasing need for the development of new, mild and efficient methods for their preparation, and the exploration of novel applications. In order to make the nanomaterials compatible and applicable in different chemical and biological environments, it is also important to develop inherently active NPs and multifunctional surface stabilizing linkers with potentials for further modifications.

Within this thesis, several types of nanoparticles, including silver (Ag), copper (Cu) and titanium dioxide (TiO_2), were explored due to their interesting properties, such as localized surface plasmon resonance, fluorescence properties, conductivity and catalytic activity, which can be applied in various fields, such as photonics, electronics, sensing, catalysis and biomedical diagnostics.[1-5]

Due to the ease of oxidation upon air exposure, the reproducible synthesis of stable and pure Ag and Cu NPs under aqueous conditions still poses challenge. One of the crucial factors to achieve this is the choice of proper capping agents for the protection and stabilization of nanoparticles' surface, as bare Ag and Cu NPs can be oxidized and tend to aggregate to reduce their surface energy, which could severely influence their chemical, optical and catalytic properties.

Water-soluble and monodispersed Ag NPs were successfully synthesized using polyacrylic acid and benzotriazole-maleimide, and the plasmonic and fluorescent properties of the obtained Ag NPs were investigated. In addition, the Ag NPs were used for the construction of DNA-AgNP conjugates through ligand exchange or mild Diels-Alder cycloaddition. The obtained DNA-AgNP conjugates were then employed for the further assembly with gold (Au) NPs which could be used as substrates for surface enhanced Raman Scattering, or utilized for DNA-directed immobilization of enzyme which retained its activity after the immobilization process.

Unlike Au and Ag NPs, the potential applications of Cu NPs have not yet been fully tapped due to the ease of surface oxidation. It is worthwhile to explore the applications of Cu NPs, because copper possess interesting properties such as surface plasmon resonance,

Abstract

catalytic activity and antibacterial properties, and it is much cheaper than Au and Ag, so it is more suitable for large scale industrial production and applications. Within this thesis, the preparation of stable Cu NPs in aqueous solutions using ascorbic acid and dopamine-based linkers was explored. The as-prepared Cu NPs possess reactive oxygen species (ROS) production ability, and could be employed as powerful enzyme mimetics, such as the activation of peroxidase enzyme or the mimicking of superoxide dismutase. Due to the excellent ROS generation ability, such Cu NPs could also be used as catalysts for the degradation of harmful fluorescent dyes and antibiotics.

Finally, two clickable dopamine linkers were designed for the preparation or modification of Cu NPs and TiO_2 nanomaterials, as the catechol groups of dopamine have strong affinity to both Cu and TiO_2. Since Cu NPs are a group of plasmonic and ROS producing nanoparticles and TiO_2 nanomaterials also possess photo-induced ROS generation ability, it is interesting to investigate if the combination of Cu NPs and TiO_2 nanomaterials would have any influence on the catalytic property of TiO_2 nanomaterials. The combination of TiO_2 and Cu might afford novel, highly active and efficient nanomaterials that are useful for enzyme mimetics and environmental applications.

Chapter 1

Introduction

1 Introduction

1.1 Syntheses of Nanoparticles

Nanoparticles (NPs) are materials with dimension between 1 and 100 nm, which possess novel properties and characteristics that differ from the equivalent bulk counterparts, for example, surface plasmon resonance in metallic particles,[6, 7] quantum confinement in semiconductor materials,[8, 9] superparamagnetism in magnetic materials,[10, 11] and high surface area in nanocatalysts.[12, 13] Normally their properties are tunable through the control of their size, morphologies, structures and compositions.[13, 14]

During the past decades tremendous progress has been made in the research fields of noble metallic and semiconductor nanomaterials. They are widely applied in photonics, electronics, sensing, catalysis and biomedical diagnostics,[15-19] because they possess range of fascinating properties, such as localized surface plasmon resonance (LSPR), fluorescence properties, conductivity, and catalytic activity,[1-5] all of which can be applied to various research field.

Within this thesis, several classes of NPs, including silver (Ag), copper (Cu) and titanium dioxide (TiO$_2$) were explored due to their interesting properties such as LSPR, fluorescence and reactive oxygen species production, and their potential applications in sensing, catalysis and enzyme mimetics.[20-22] Different synthetic strategies of these NPs have been developed up to date, and the size, morphology and properties of the NPs vary greatly depending on the methods. Herewith, a few synthetic methods for Ag, Cu and TiO$_2$ NPs as well as their properties and applications will be introduced.

1.1.1 Silver Nanoparticles

Among all the metallic nanoparticles, silver nanoparticles (Ag NPs) have found numerous uses in biosensor design, in particular, as effective substrates for surface enhanced Ramam scattering[23, 24] and as ideal building blocks for plasmonic sensors,[25, 26] because they offer many advantages over the other noble metals, such as higher extinction coefficients, extremely high field enhancements, high electrical and thermal conductivity, which permit more accurate and highly sensitive optical and electrical measurements.[27] However, their applications have been limited by the lower chemical stability in comparison with gold, for example, ease of surface oxidation and lower compatibility with physiological buffers conditions.[28] Therefore, there is a continuous search for efficient synthetic methods to obtain

stable Ag NPs, such as chemical reduction,[29, 30] polyol method,[31] seed mediated growth,[32] and photochemical method.[33]

1.1.1.1 Citrate Reduction

Citrate is one of the most used reducing agents for the synthesis of noble metallic (Au, Ag, and Cu) NPs in aqueous phase.[34-36] The reduction of $AgNO_3$ to Ag NPs by citrate in water was first reported by Lee and Meisel in 1982.[36] In this reaction, citrate served not only as a reducing agent, but also as a capping agent for the stabilization of Ag NPs. However, the obtained nanocrystals were polydispersed and had different morphologies, including nanorods, nanoprisms, nanospheres and nanoplates. Different strategies have been attempted to improve the citrate reduction method for the preparation of uniform Ag NPs. Kamali *et al*., prepared Ag NPs from 10 to 40 nm by adjusting the pH of the solution, and it was found that the pH value had a significant influence on the size and crystallinity of Ag NPs due to the influence of pH on the distribution of citrate.[37] Yang's group obtained relatively uniform spherical Ag NPs using a stepwise citrate reduction method at different pH conditions.[38] Laser irradiation was also employed to make citrate-coated Ag NPs with different morphologies into spherical NPs.[39] Recently, Li and coworkers have obtained monodispersed, quasi-spherical Ag nanocrystals by reducing $AgNO_3$ with both citrate and ascorbic acid in the presence of iodide ions (Figure 1.1).[29] The synergy effects of ascorbic acid, citrate and KI significantly narrowed the size distribution and controlled the shape of the Ag nanocrystals.
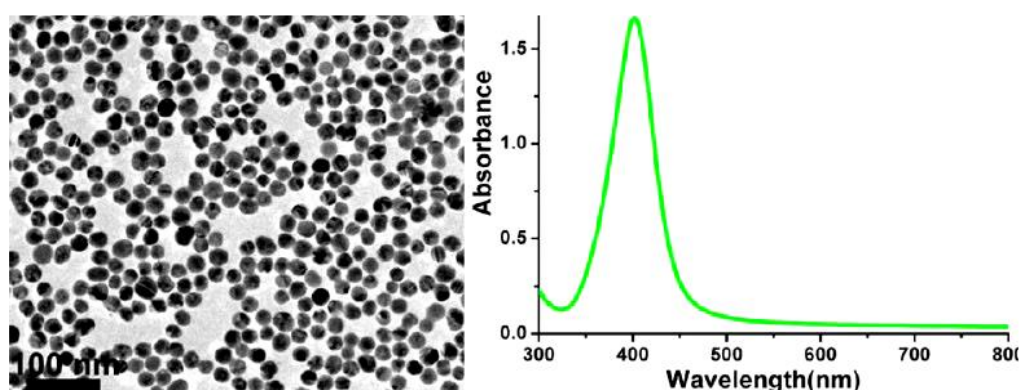
Figure 1. 1 TEM image (left) and UV-Vis spectrum (right) of Ag NPs synthesized by KI-assisted citrate/ascorbic acid reduction method. Figure reprinted with permission from Ref 29. Copyright © 2013 American Chemical Society

The citrate reduction method enables reproducible production of noble metal NPs with tunable sizes, and the obtained NPs could exhibit long-term stability due to the strong

affinities between the carboxylic groups of citrate and the metal surfaces. But this method also has several drawbacks, for example, the concentrations of NPs obtained by citrate reduction are often very low,[40] and the highly negatively charged citrate-coated NPs are vulnerable at high ionic conditions due to the change of the surface charge,[41] which has limited their applications in biological media.

1.1.1.2 Polyol Method

Polyol method, which was firstly developed by Fievet et al,[42] is a simple and robust route for the preparation of highly crystallized and monodispersed colloid NPs with different morphologies, such as, Au nanostructures with well-defined shapes[43] and single crystalline nanowires of Pt.[44] Although different capping agents might be needed to get shape-controlled NPs, a typical procedure involves the reduction of a precursor salt by polyol (i.e. polyethylene glycol) at an elevated temperature (normally at the boiling point of the polyol).[45] The size of the colloid NPs could be controlled through the temperature-dependent reducing ability of polyol.[46] By using ethylene glycol as a reducing agent, Kim and coworkers prepared spherical Ag NPs with various sizes by tuning the heating rate and the reaction temperature.[47] Jiang et al. reported the control over the size distribution of Ag NPs by adjusting the microwave frequency in a microwave-assisted polyol method.[48] Wiley et al. synthesized a number of Ag nanocrystals with different morphologies (nanowires, monodispersed nanocubes and nanospheres) in ethylene glycol by tuning the ratio between the capping agent polyvinylpyrrolidone and the precursor AgNO$_3$ (Scheme 1.1 and Figure 1.2).[31]
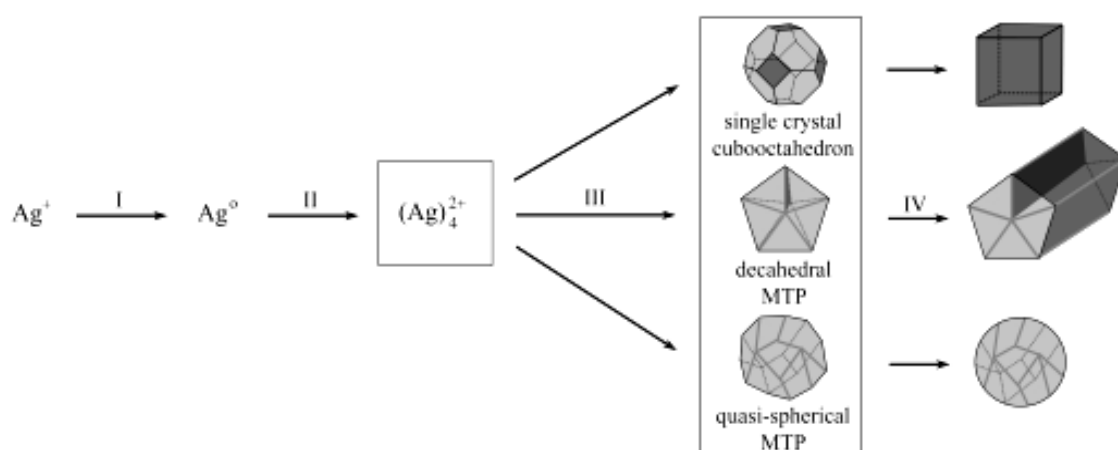
Scheme 1. 1 Schematic illustration of (I) the reduction of Ag$^+$ by ethylene glycol; (II) the formation of Ag clusters; (III) the nucleation of seeds; and (IV) the growth of seeds into Ag nanocubes, nanorods or nanowires, and nanospheres. Figure reprinted with permission from Ref 31. Copyright © 2005 WILEY-VCH Verlag GmbH & Co. KGaA, Weinheim
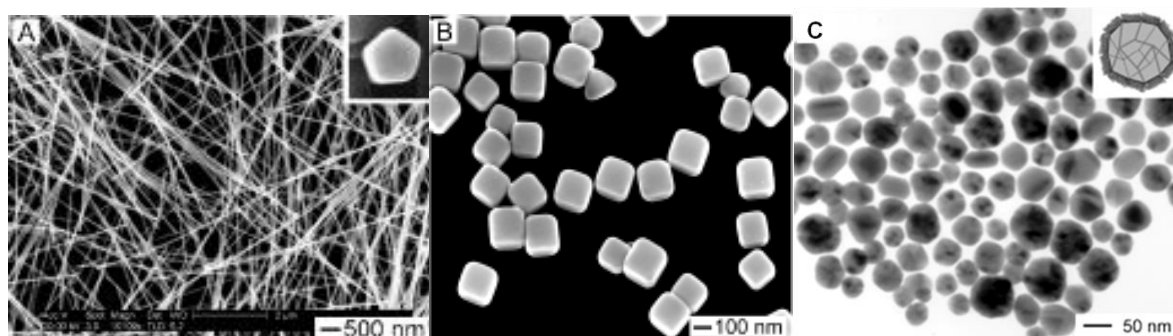
Figure 1. 2 TEM images of (a) Ag nanowires, (b) Ag nanocubes and (c) Ag nanospheres. Figure adapted with permission from Ref 31. Copyright © 2005 WILEY-VCH Verlag GmbH & Co. KGaA, Weinheim

The advantage of this method is that polyol could simultaneously act as solvent, reducing agent, and sometimes capping agent, thus no further reducing agent or capping agent is required.[49] The flexible control over the size, shape and crystallinity of nanocrystals could also be realized by the polyol approach through the adjusting of the reaction temperature.[49] However, suitable and appropriate amount of polyhydroxyl alcohol needs to be chosen for individual processes in order to realize the ideal control over the growth of NPs, and the high boiling point of polyol makes the removal of solvent and the purification of NPs difficult.[50, 51]

1.1.1.3 Thiols and Disulfides Stabilization

The use of thiols or disulfides as stabilizers is another possibility for the preparation of metallic NPs, because the organosulfur groups could strongly coordinate with many metals, such as Au, Ag, Pt and Fe.[52, 53] Spherical Ag NPs with an average diameter of 17 nm were synthesized using mercaptoacetic acid as a capping agent and then employed as SERS substrates for the detection of Rhodamine 6G.[54] Both cubic and hexagonal crystals phases of Ag NPs could be obtained using the combination of cysteine and glutathione as the surface stabilizers.[55] Chin and coworkers reported the preparation of fluorescent ultra-small Ag nanoclusters (< 2 nm) by reducing $AgNO_3$ with $NaBH_4$ in the presence dihydrolipoic acid (DHLA).[30] Through the control over the pH value of the solution, the interaction between the disulfide group and Ag nanoclusters could be changed, which could in turn affect the absorbance and fluorescence of the Ag nanoclusters (Figure 1.3).
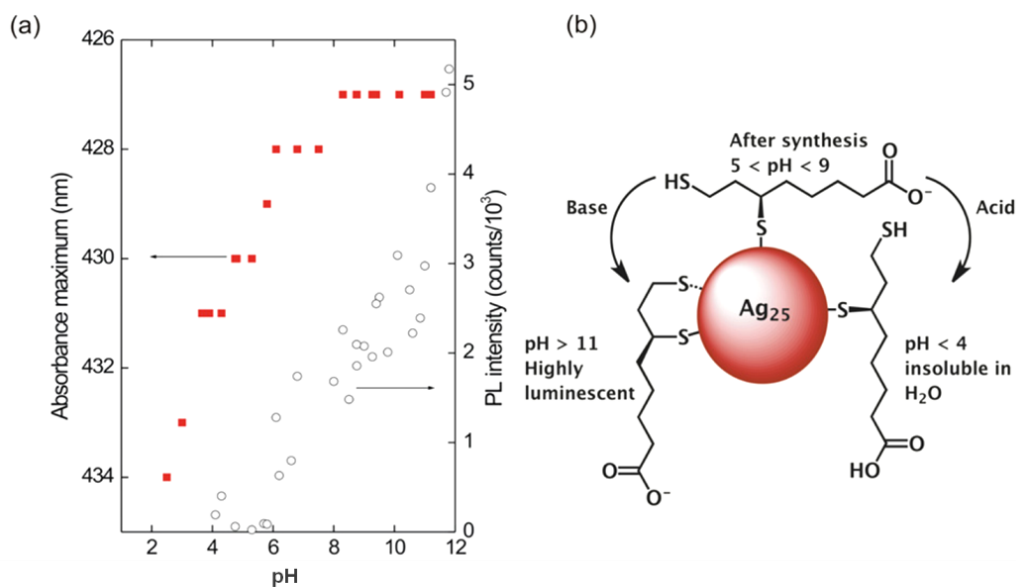
Figure 1. 3 (a) Photoluminescence intensity and absorbance peak position as function of the pH; (b) schematic representation of the coordination possibilities for DHLA towards the Ag nanoclusters under different pH conditions. Figure reprinted with permission from Ref 30. Copyright © 2013 IOP Publishing, LTD

Recently, Andrieux-Ledier *et al*. prepared alkylthiol-coated monodispersed spherical Ag NPs.[56] The stability tests showed that the obtained Ag NPs could be stable for month under nitrogen atmosphere. However, rapid corrosion of Ag NPs occurred when they were exposed to air under ambient conditions, and the corrosion process would become faster when the humidity in the air was increased (Figure 1.4).
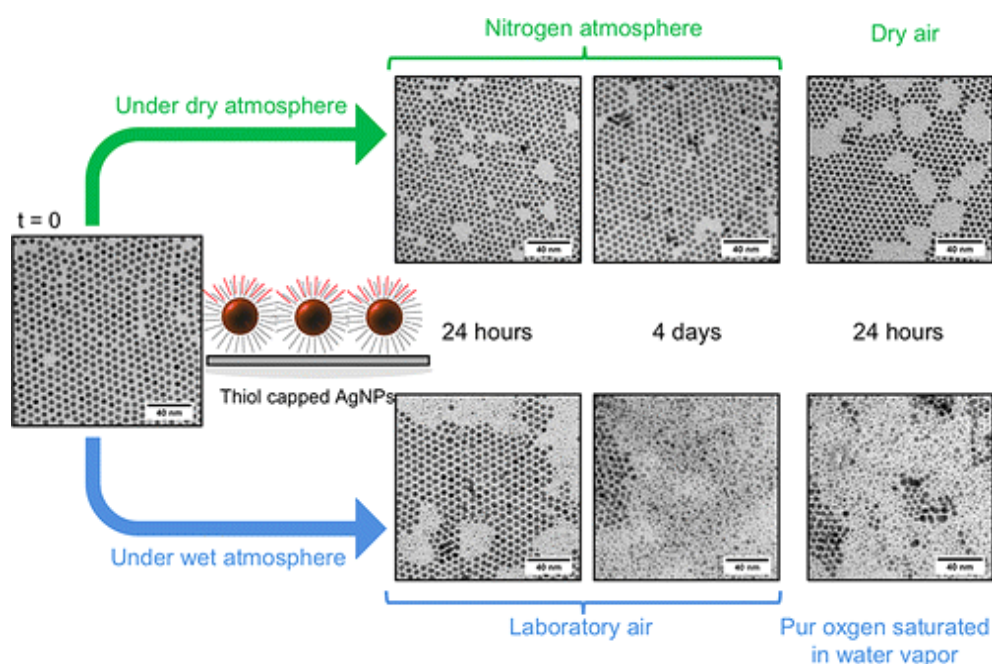
Figure 1. 4 The stability of thiol-coated Ag NPs under different environmental conditions. Figure reprinted with permission from Ref 56. Copyright © 2013 American Chemical Society

It has been reported that the affinity between thiol and Ag is weaker in comparison to that between thiol and Au.[57] Thus, the alkylthiol-Ag interaction was not strong enough to provide sufficient protection for the Ag NPs when they were exposed to humid air. Therefore, improvements and optimizations are still needed in order to obtain stable thiol-coated Ag NPs.

1.1.1.4 Seed-Mediated Growth

Seed-mediated approach is another alternative for the preparation of colloid nanocrystals, which involves two separated steps: nucleation and growth. Typically, the seeds were first prepared through the reduction of precursor salts and then added as nucleation centers to a solution containing additional precursors and reducing agents for the further growth of NPs.[58] Xia's group has demonstrated the preparation of Ag nanocubes with controllable size between 30 and 200 nm using spherical or cubic Ag seeds, and the size control was realized by changing the amount of $AgNO_3$ or Ag seeds in the step of growth.[59] The seed-mediated growth method is not only useful for size control, but also crucial for the manipulation of the aspect ratio of nanocrystals. Monodisperse Ag nanorods with a pentagonal cross section could be obtained by thermal regrowth of decahedral Ag seeds at 95 °C (Figure 1.5).[32] The aspect ratio of the nanorods could be adjusted from 1 to 12 through semi-continuous addition of Ag seeds, and the uniform Ag nanorods could easily self-assemble to 3D arrays.
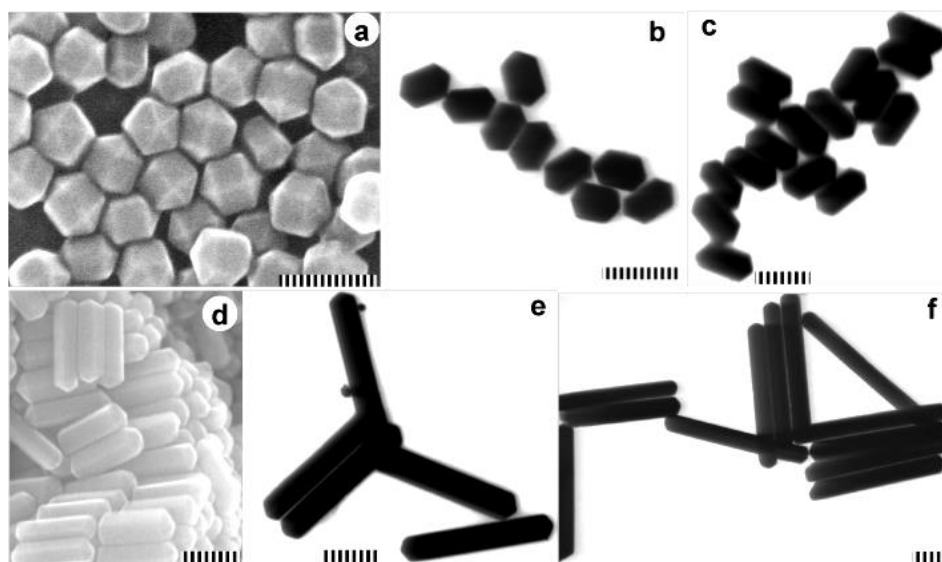
Figure 1. 5 SEM and TEM images of faceted Ag nanorods prepared by the regrowth of Ag seeds in aqueous solution. The rods' length are (a) 62 ±3 nm; (b) 75 ±3 nm; (c) 108 ±5 nm; (d) 142 ±7 nm; (e) 260 ±10 nm; (f) 430 ±15 nm. The rods' width is 49.5 ±2.5 nm. Figure adapted with permission from Ref 32. Copyright © 2009 American Chemical Society

In addition to the size and morphology control, seed-mediated approach could help to propose the possible growth mechanism of nanocrystals. For example, Zong *et al*. employed Au seeds for the growth of polyhedral Ag NPs, and differently sized NPs were obtained through the continuous addition of the reactants.[60] It was found that the choice of weak reducing agent and the proper addition rate of reagent in the growth step could prevent additional nucleation in the growth step, and facilitate the formation of narrow dispersed NPs.

Although the multi-step procedures of seed-mediated growth is time consuming and complicated, the nucleation and growth processes can provide useful information about the mechanism of nanocrystals formation.[61] Furthermore, seed-mediated approach enables stoichiometric control over the size and shape of nanocrystals and affords monodispersed nanocrystals with narrow size distribution, which are very important for size-dependent property studies.[62]

1.1.1.5 Photo-induced Approach

Green chemistry has been drawing more and more attention during the development process of nanotechnology as the improper release of harmful chemicals could cause contaminations to the environment and disturb the balance of the eco-system. As a novel and environmental friendly energy source, light has already been applied for the preparation of different nanomaterials. Small and stable Pt NPs were obtained by the visible light irradiation of a host-guest inclusion complex between β-cyclodextrin and platinum acetylacetonate.[63] Water-soluble Au NPs were synthesized using a photo initiator, Irgacure-2959 (1-[4-(2-hydroxyethoxy)phenyl]-2-hydroxy-2-methyl-1-propane-1-one), upon excitation at 350 nm.[64] Ag NPs with narrow size distribution were prepared using a higher power (14.4 W/cm^2) monochromatic laser line (514.5 nm).[65] El-Sheikh reported the synthesis of carboxymethyl starch-coated spherical Ag NPs under UV irradiation using a different photo initiator, 4-(trimethyl ammonium methyl) benzophenone chloride.[66] Mirkin's group employed the photo-induced approach to prepare Ag triangular nanoplates with different sizes.[33] The synthesis of Ag nanoprisms was performed under a dual-beam irradiation mode, and the size of the nanoprisms could be controlled by tuning the wavelength of the primary beam (Figure 1.6). It was found that the growth of Ag nanoprisms could be driven by surface plasmon excitation, and the edge length of the Ag nanoprisms increased with the increase of the primary excitation wavelength, which might be because that the plasmon excitation could facilitate the dissociation of ligand at the edge of nanoprisms and led to the fusion of nanoprisms in an edge-selective manner.
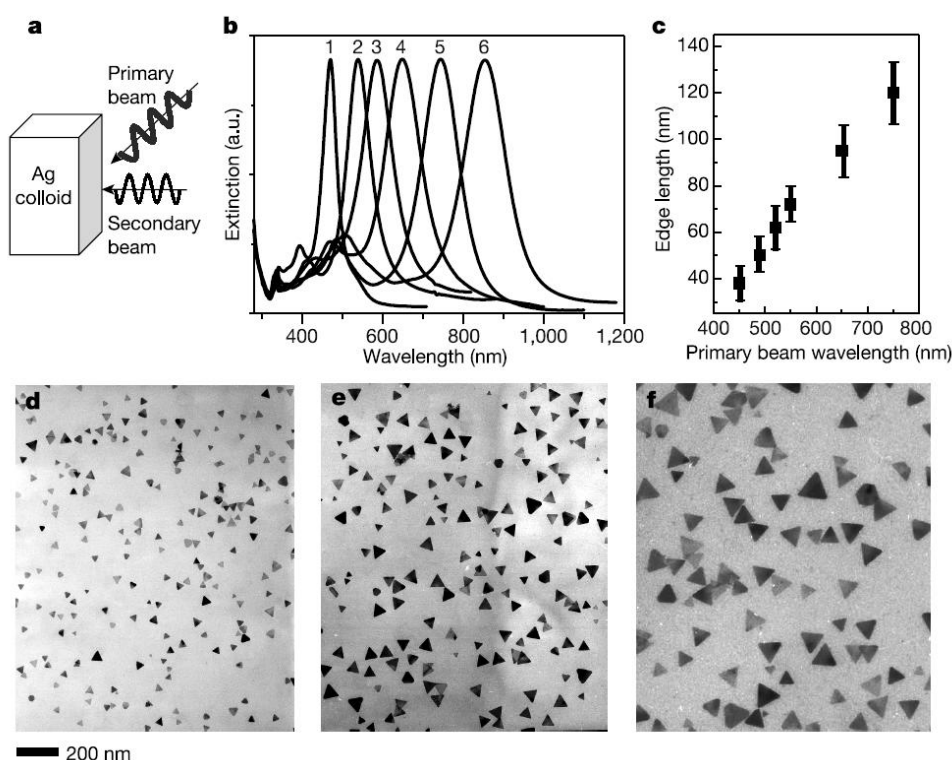
Figure 1. 6 (a) Schematic diagram of dual-beam excitation, (b) The optical spectra (normalized) for six different sized nanoprisms (1–6 edge length: 38 ± 7 nm, 50 ± 7 nm, 62 ± 9 nm, 72 ± 8 nm, 95 ± 11 nm and 120 ± 14 nm) prepared by varying the primary excitation wavelength (central wavelength at 450, 490, 520, 550, 650 and 750 nm, respectively; width, 40 nm) coupled with a secondary wavelength (340 nm; width, 10 nm), (c) The edge lengths as a function of the primary excitation wavelength, and (d–f) TEM images of Ag nanoprisms with average edge lengths of (d) 38 ± 7 nm, (e) 72 ± 8 nm and (f) 120 ± 14 nm. Figure reprinted with permission from Ref 33. Copyright © 2003 Nature Publishing Group

Light-induced synthesis is a simple and environment-friendly method that can be carried out at mild conditions, such as room temperature and normal pressure. Its tunable wavelength and intensity make it a unique tool in comparison to typical reducing agent. However, it is difficult to predict the chemical transition during the reaction and to understand the light induced redox processes.[67]

Many efforts have been devoted to the preparation of stable and monodispersed Ag nanocrystals with different morphologies and sizes, including nanoparticles, nanorods, nanoplates, and nanocubes. However, in order to make them more favourable and compatible for the applications in catalysis, antibacterial agents, analytical chemistry, sensing, biology and medicine,[68] further improvements of these synthetic strategies or the development of novel efficient methods are still required for the controllable and reproducible synthesis of hydrophilic Ag NPs with high stability under different chemical and biological conditions.

1.1.2 Copper Nanoparticles

Copper nanoparticles (Cu NPs) are beginning to attract more attention of the science community due to their potential applications as lubricants, catalysts, electronics elements and antibacterial materials.[69-71] As a member of noble metal group, Cu NPs possess similar antibacterial, electrical and optical properties (such as LSPR and SERS) as Au and Ag NPs.[72-74] However, only a few reports about the preparation of Cu NPs have been published during the last decades due to their instability against air oxidation, not to mention their further applications. Most of the reported synthetic procedures for Cu NPs were carried out in organic solvents or oxygen-free environments.[75, 76] Several reports described the preparation of Cu NPs in aqueous solutions using citrate,[21] polyvinylpyrrolidone[77] or cetyltrimethylammonium bromide[78] as capping agents, but the obtained NPs could be stable for only a couple of days or even shorter. Therefore, the preparation of stable Cu NPs in aqueous phase still poses a great challenge.

1.1.2.1 Thermal Decomposition

Thermal decomposition method, which was first employed by both Alivisatos' and Yan's research groups for nanomaterials production, involves the chemical decomposition of precursors through the breaking of chemical bonds in a high boiling point organic solvent.[79, 80] It is a perfect method for the preparation of various kinds of nanomaterials, such as upconversion NPs, metal oxides, magnetic materials, quantum dots, as well as noble metals.[80-83] This method was also successfully employed for the preparation of stable Cu NPs. Kim *et al*. prepared narrowly dispersed Cu NPs through the thermal decomposition of Cu-oleate complex at 295 °C in an autoclave.[84] Shi and coworkers described the synthesis of uniform spherical Cu NPs through the thermal decomposition of copper acetylacetonate in oleylamine at 230 °C (Figure 1.7a and b).[76] The obtained Cu NPs showed excellent reactive oxygen species (ROS) production ability, which could be used for the activation of peroxidase enzymes and the oxidation of nonfluorescent substrate 2,7-dichlorodihydroflurescein diacetate to fluorescent 2,7-dichloro-fluorescein. They have also demonstrated that the ROS production ability of Cu NPs could be significantly suppressed by the formation of cuprous oxide layer or the surface modification with long carbon chain ligands (Figure 1.7 c).
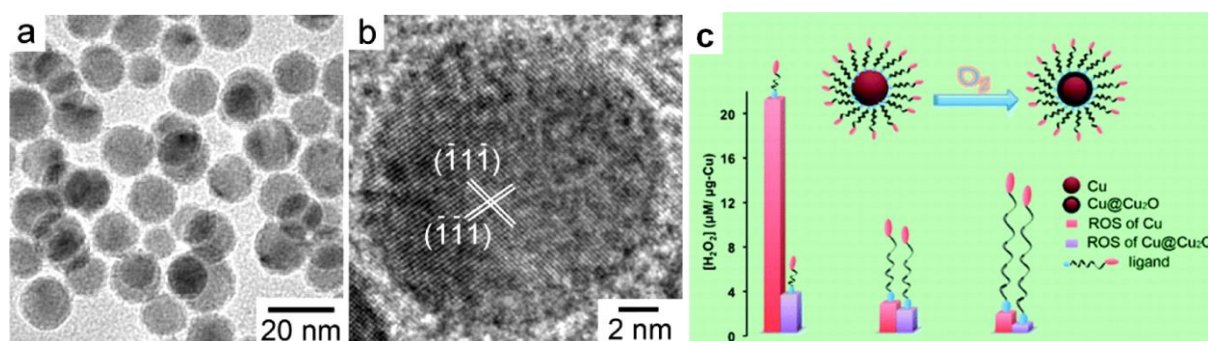
Figure 1. 7 (a) TEM and (b) HRTEM micrographs of oleylamine-coated Cu NPs; and (c) the influence of surface oxidation and surface modification with long carbon chain ligands on the ROS production ability of Cu NPs. Figure adapted with permission from Ref 76. Copyright © 2012 American Chemical Society

Although thermal decomposition method could afford monodispersed and stable Cu NPs, the hydrophobic property of OA on the surface on Cu NPs has significantly limited their further applications in aqueous phase or polar solvents. In addition, ligand exchange on the surface might cause the surface oxidation of Cu NPs and lead to the loss of their ROS production ability. Therefore, other methods still need to be explored for the synthesis of stable and water-soluble Cu NPs.

1.1.2.2 Polyol Method

As a simple solution route for the preparation of water-soluble metal colloids such as Au and Ag,[31, 43] polyol method could also be applied to the synthesis of Cu NPs. Well-defined Cu nanocubes have been prepared in ethylene glycol in the presence of polyvinylpyrrolidone (PVP), which could serve as both surface stabilizer and soft template for Cu NPs (Figure 1.8).[77] Instead of using polyol itself as a reducing agent for Cu precursor, Park *et al*. employed $NaH_2PO_2 \cdot H_2O$ for the reduction of Cu^{2+} in diethylene glycol, and the size distribution of Cu NPs could be controlled by adjusting the amount of $NaH_2PO_2 \cdot H_2O$.[85]
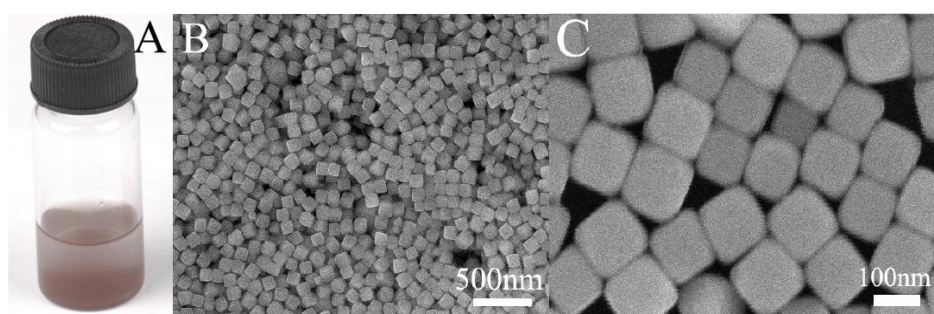
Figure 1. 8 (a) Ethanol solution of Cu nanocubes; (b) and (c) SEM images of Cu nanocubes. Figure reprinted with permission from Ref 77. Copyright © 2006 IOP Publishing, LTD

Feldmann's group also reported the use of diethylene glycol as both the solvent and the surface protecting agent for the synthesis of non-agglomerated citrate-coated Cu NPs with an average diameter of 20 nm, which showed a plasmonic absorption band at 614 nm in the UV-Vis spectrum (Figure 1.9).[86] The as-prepared Cu NPs turned out to be highly stable against air oxidation even after storage for a long time (14 months) or treatment at elevated temperature (120 °C). The obtained Cu NPs were used to make porous Cu thin-film electrode through the solvent evaporation of Cu suspension onto Al_2O_3 substrates, and the obtained electrode exhibited high conductivity.
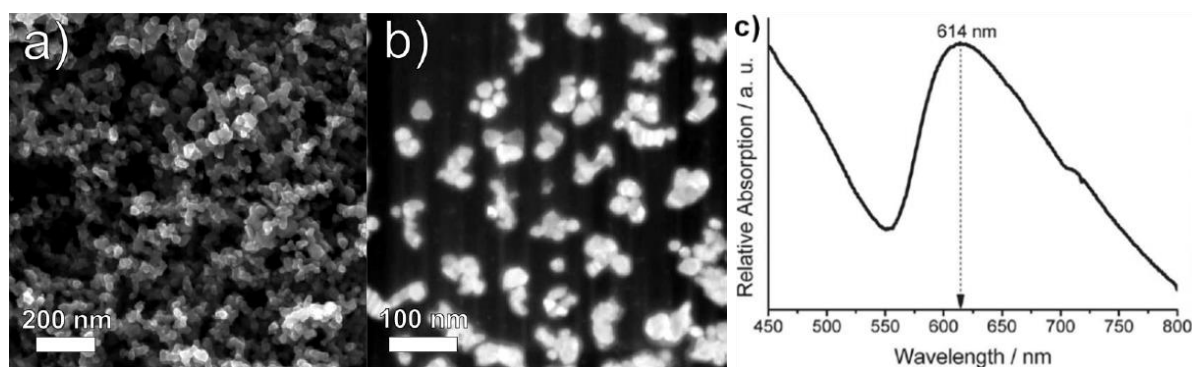
Figure 1. 9 (a) SEM image, (b) dark-field STEM image, and (c) UV-Vis spectrum of citrate-capped Cu NPs. Figure adapted with permission from Ref 86. Copyright © 2012 the Royal Society of Chemistry

The use of non-aqueous (polyol) solvent can minimize surface oxidation of Cu NPs and also protect them from agglomeration.[87] In the meanwhile, the hydrophilic property of polyol makes the obtained NPs easily dispersible in polar solvents.[49] Furthermore, the high yield of NPs through polyol approach facilitates its applications in large-scale NP production.

1.1.2.3 Electrochemical Approach

Electrochemical procedures, in which minimal numbers of chemical reagents are needed, are of great interest as they are environmental friendly and they result in products with high purity.[88] Electrochemical methods include electrodeposition, electrochemical etching and electrochemical reduction,[88] and they have already been used for the shape-controlled synthesis of different metals (Pb, Zn)[89, 90], metal oxides (Cu_2O),[91] and semiconductor nanomaterials.[92] The control over the size and morphology of nanomaterials using electrochemistry method could be achieved by varying either the current density or the applied potential.[93, 94] Gao and coworkers used porous anodic alumina as templates for the large-scale preparation of Cu nanowires, and the single crystal and polycrystal Cu nanowires

could be obtained by changing the applied potential.[95] By employing a conventional electrode system and an electrolyte made of 0.1 M copper sulfate and 1 M citric acid, well-defined, uniform and spherical Cu NPs could be successfully deposited on a glass substrate coated with fluorine doped tin oxide.[96] It was found that the deposition time and electrode potential played important roles in controlling the growth of Cu nanocrystals during the electrodeposition process (Figure 1.10). This template free method provides an economically favorable route for the preparation of well-defined spherical Cu NPs.
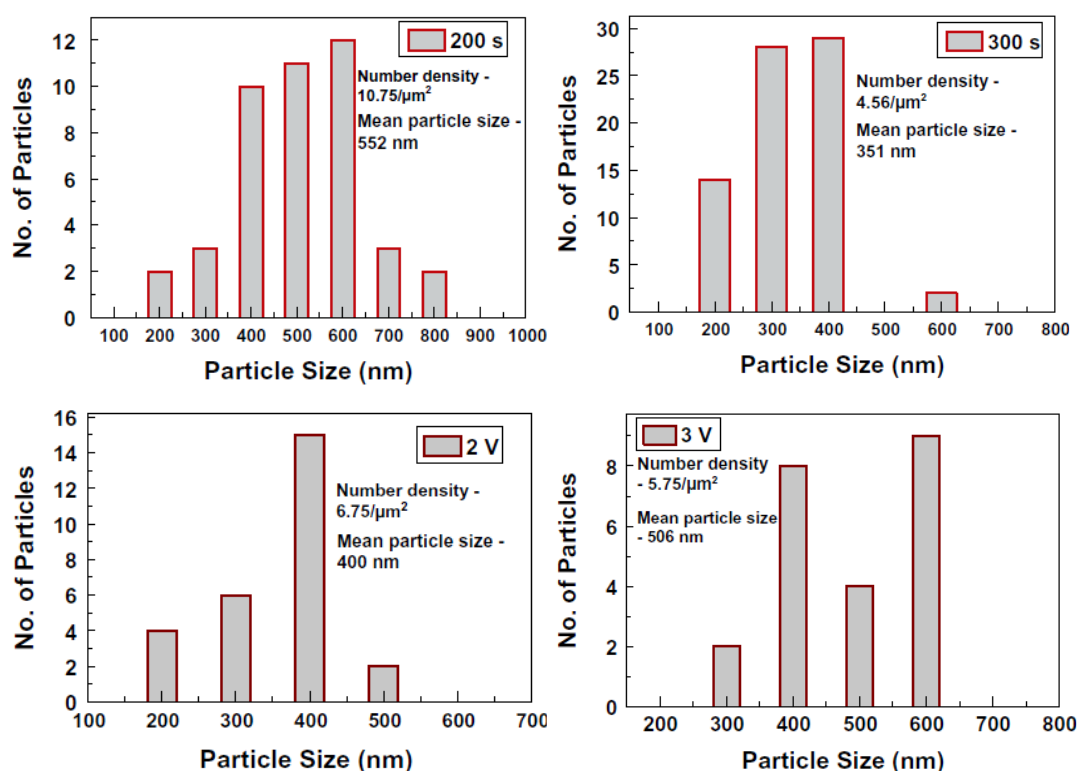
Figure 1. 10 Size distributions of Cu NPs at different deposition time and electrode potentials. Figure adapted with permission from Ref 96. Copyright © 2012 Elsevier

The main advantages of electrochemical method are the high purity of obtained NPs and the easy control over the size and shape of NPs by adjusting the electrode potential or the current density.[97] The advantages are particularly attractive for biochemical applications because the synthetic steps are clean, and few chemicals are used.[98] Thus there are less harmful substances in the solution of NPs, which might affect the structure and activity of biomolecules.

1.1.2.4 Surfactant Stabilization

Surfactants, consisting of a polar hydrophilic head and a lipophilic tail, tend to self assemble to minimize the contact with aqueous solutions, leading to the formation of microemulsions, which could be utilized as nanocontainers for the controlled synthesis of metal colloids.[99] The most commonly used surfactants are the single-chained, anionic sodium dodecylsulphate (SDS), cationic cetyltrimethylammonium bromide (CTAB), and double-chained, anionic sodium bis(2-ethylhexyl) sulphosuccinate (Na(AOT)).[99] Recently, Soomro *et al.* employed SDS as a surface stabilizer and $NaBH_4$ as a reducing agent to prepare stable spherical Cu NPs, which were then used as catalysts for the degradation of fluorescent dye Eosin B.[100] Monodispersed Cu NPs with an average diameter of 5.1 nm was also prepared by the reduction of $CuCl_2$ with hydrazine in the presence of CTAB.[78] Na(AOT) was also used for the preparation of Cu NPs with different shapes. Figure 1.11 shows the Cu nanorods and nanospheres prepared using interconnected cylinder templates in the $Cu(AOT)_2$-isooctane-water system.[101] As can be seen from Figure 1.11 b, the morphology of the NPs could not be precisely controlled. However, different salts were added to the template leading to significant change of the NPs' shape and enabling a control over the morphology of NPs (Figure 1.12).
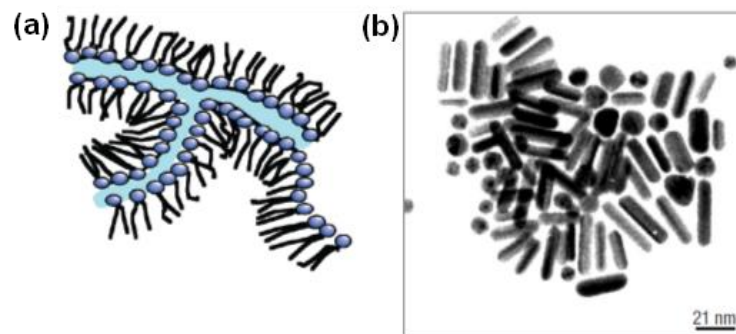
Figure 1. 11 (a) Scheme of interconnected cylinders template, and (b) formation of spherical and cylindrical Cu NPs. Figure adapted with permission from Ref 101. Copyright © 2003 Nature Publishing Group
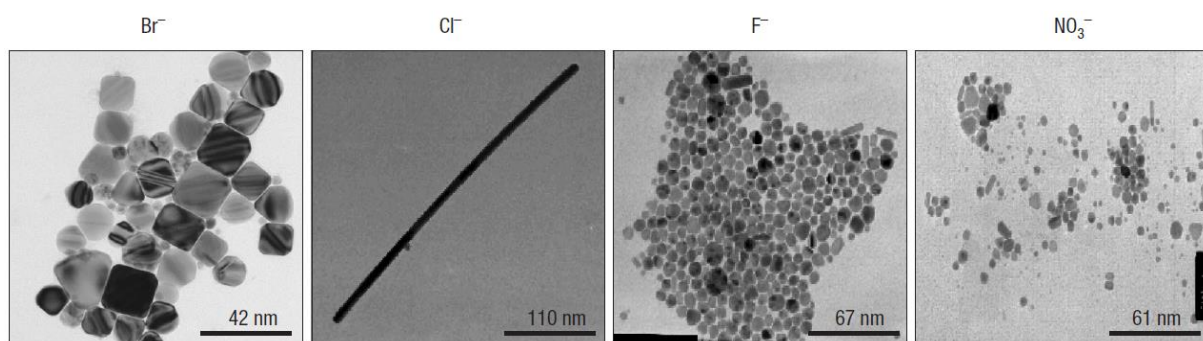
Figure 1. 12 Various shapes of Cu nanocrystals produced in interconnected cylinders in the presence of different salt ions. Figure reprinted with permission from Ref 101. Copyright © 2003 Nature Publishing Group

Although surfactants could serve as excellent templates to control the growth of NPs, stabilize NPs' surface and prevent NPs' agglomeration, they still have putative disadvantages, such as questionable biocompatibility, irreversible incorporation in NPs, and alternation of NPs' surface properties,[102] which might limit the applications of NPs in biological systems and catalysis.[103, 104]

1.1.2.5 Biotemplate-Assisted Growth

Since the late 1990s, biomolecules such as DNAs and proteins have also been utilized as templates to produce metal nanostructures. For instance, Wang *et al.* utilized DNA as scaffolds to prepare fluorescent Ag nanoclusters and used them to identify single nucleotide mutation.[105] Ying and coworkers reported protein (bovine serum albumin)-directed synthesis of fluorescent Au nanoclusters and their application for the detection of Hg^{2+} ions.[106, 107] Recently, Mokhir's group employed double stranded DNA (*ds*DNA) as templates to produce fluorescent Cu NPs, while no NPs were obtained in the control experiments where single stranded DNA (*ss*DNA) was used.[108] It was also found that the size and the fluorescence intensity of Cu NPs could be controlled by changing the length of DNA sequences (Figure 1.13), and longer DNA strands would lead to the formation of bigger NPs and subsequently higher fluorescence intensity.
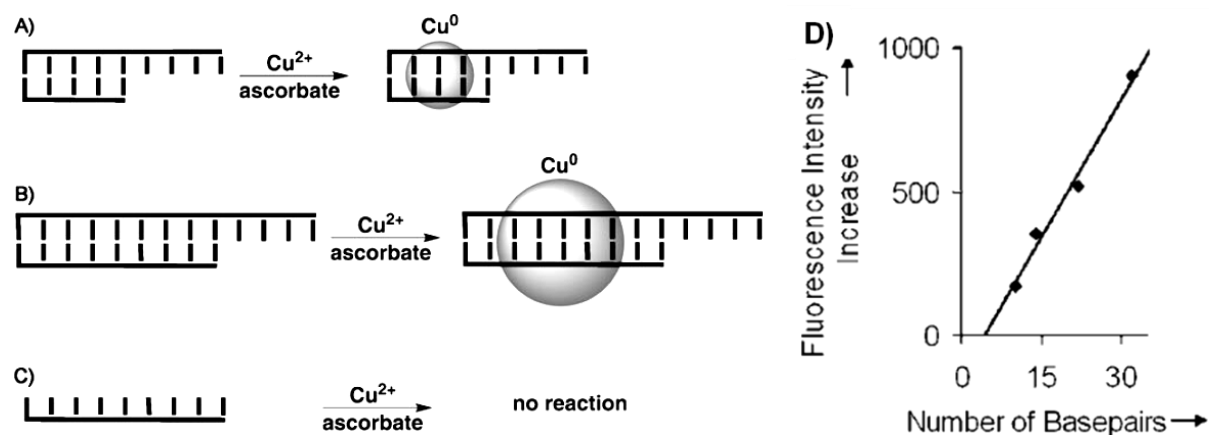
Figure 1. 13 (A and B) Formation of Cu NPs in solution of Cu^{2+} and ascorbate in the presence of a DNA duplex, and the size of the NPs is dependent on the number of base pairs in the *ds*DNA template, (C) *ss*DNA do not promote this reaction, and (D) fluorescence intensity increase of Cu NPs when *ds*DNA of different lengths were used. Figure adapted with permission from Ref 108. Copyright © 2010 WILEY-VCH Verlag GmbH & Co. KGaA, Weinheim

The Cu NPs formed by the *ds*DNA templated method have also been employed as fluorescent probes for the detection of adenosine triphosphate (ATP), which acts as a coenzyme in cells for intracellular energy transfer.[109] The presence of ATP could induce the structure switching of reporter DNA to form aptamer-ATP complex, leading to the disappearance of the double helix structure (Scheme 1.2), and in turn inhibit the formation of Cu NPs, which resulted in the decrease of fluorescence intensity. On the other hand, *ds*DNA would maintain its duplex structure in the absence of ATP, and highly fluorescent Cu NPs could be obtained. This demonstrates that *ds*DNA-Cu NPs can be used as a platform for the design of biosensors.
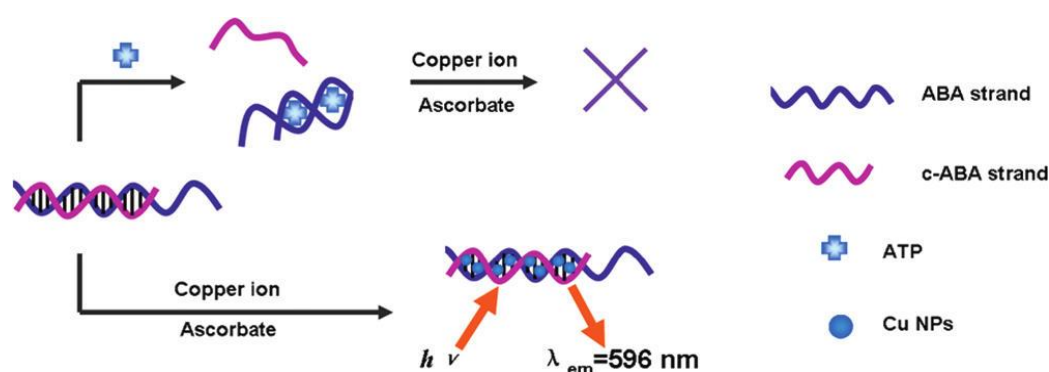
Scheme 1. 2 Schematic illustration of the influence of ATP on the formation of *ds*DNA-Cu NPs. Scheme adapted with permission from Ref 109. Copyright © 2011 American Chemical Society

The use of biotemplates can afford uniform NPs and avoid the production of harmful waste by the traditional chemical reduction method. However, biotemplated approach also has its drawbacks, for example, biomolecules are difficult to handle, expensive, and insufficient for large-scale production of NPs.[110]

Cu nanomaterials have aroused many research interests in the past few years, because they are useful for the design of electronic devices, catalysis and antimicrobial activity studies.[74, 111, 112] Due to the relatively low cost, copper is more useful for large-scale industrial productions when compared to the expensive gold, platinum and silver. However, the instability of Cu nanocrystals upon air-exposure has severely limited their applications. Although different strategies have been attempted to synthesize Cu nanocrystals, most of them requires the use of organic solvents, inert gas atmosphere or surfactants to protect the Cu NPs from being oxidized.[75, 76, 113] Therefore, it is still of great importance to develop new methods for the preparation of Cu nanomaterials with higher stability in aqueous solutions.

1.1.3 Titanium Dioxide Nanoparticles

Semiconductor nanomaterials have been drawing the attentions of both industry and research communities for several decades due to their promising applications in various fields, such as solar cells design,[114] catalysis,[115] electronic and electrochemical energy storage.[116] Among all the semiconductor nanomaterials, titanium dioxide (TiO_2), a large band gap semiconducting material with band gaps of 3.20 and 3.02 eV for anatase and rutile crystal phases, has been extensively explored for applications in solar cells, water splitting, paints, photocatalysis and the degradation of contaminants.[117] The mechanism for the photoactivity of TiO_2 nanocrystals is demonstrated in Scheme 1.3.[118] When TiO_2 is irradiated by UV light, whose energy is equal to or higher than the band gap of TiO_2, an electron (e^-) could be excited and transfer from the valence band to the conduction band leaving a positive hole (h^+) in the valence band, which results in the formation of electron-hole pairs on TiO_2 (Scheme 1.3). These electrons and holes could react with oxygen and water to produce superoxide and hydroxyl radicals, which have strong redox potential and are responsible for the excellent photoactivity of TiO_2. However, due to the large band gap and the easy recombination of electron-hole pairs, the application of TiO_2 has been limited. Many methods have been used for the preparation of size- and shape-controlled TiO_2 nanocrystals,[119] and different strategies, such as doping with metallic ions or NPs and dye sensitization,[117] have been developed to reduce the energy gap (Scheme 1.3), or to trap the electrons and inhibit their recombination with holes,[118] which would help to improve the photoactivity of TiO_2. Herewith, only a few most widely used synthetic methods for TiO_2 nanomaterials will be introduced.
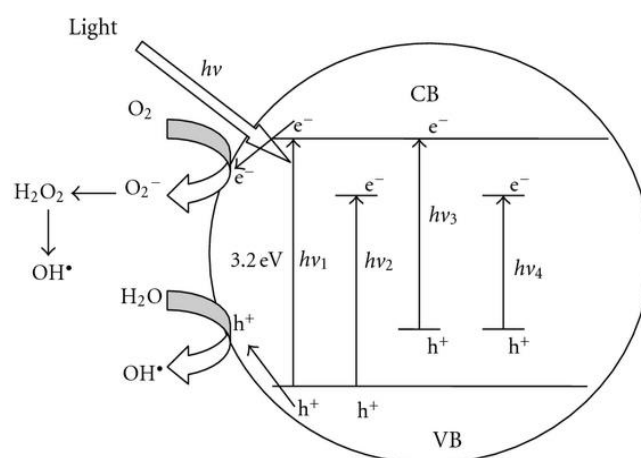
Scheme 1. 3 Schematic representation of the mechanism of photo activation of titanium dioxide particles (TiO_2: hv_1, metal-doped TiO_2: hv_2, N-doped TiO_2: hv_3, metal-N-codoped TiO_2: hv_4) and generation of reactive oxygen species. Scheme reprinted with permission from Ref 118. Copyright © 2012 Hindawi Publishing Corporation

1.1.3.1 Sol-Gel Method

Sol-gel method has been one of the most used wet-chemical methods for the preparation of TiO₂ nanomaterials with high crystallinity. It involves the formation of a sol by the hydrolysis and polymerization of titanium precursor, and the subsequent transformation from sol to gel caused by complete polymerization and loss of solvent.[120] The size, shape and crystal phase of the nanoparticles could be controlled by tuning the pH and the reaction temperature.[121]

Sugimoto and coworkers employed the sol-gel method for the preparation of TiO₂ nanomaterials with different shapes and sizes.[122] The morphologies TiO₂ nanocrystals could be tuned from spherical NPs to spindle-like structures by adjusting the pH of the solution (Figure 1.14), and the aspect ratio of spindle-like structures could be controlled using different primary, secondary and tertiary amines as complexing agent for Ti^{4+} ions. The obtained different nanocrystals were narrowly dispersed and highly crystallized.

a) pH 9.6　　　　　　　　b) pH 10.5　　　　　　　　c) pH 11.5

200 nm
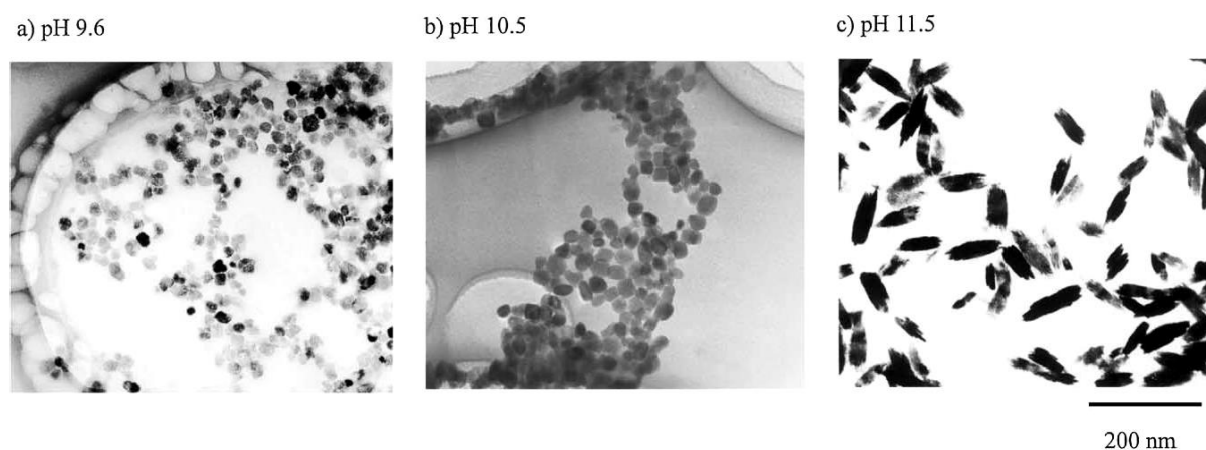
Figure 1. 14 Effect of pH on the shape control of TiO₂ nanocrystals. Figure reprinted with permission from Ref 122. Copyright © 2003 Elsevier

Lee *et al*. reported the synthesis of TiO₂ nanospheres, nanorods and nanowires through the similar sol-gel procedures as above,[123] which were then used for the dye (N719) sensitized solar cell studies, and the results indicated that the TiO₂ nanospheres obtained by sol-gel method showed higher photo-to-current conversion efficiency (5.3%) than the commercial TiO₂ NPs (P25) (4.0%). The photo-to-current conversion efficiencies for the nanorods and nanowires were 4.7% and 4.2%, respectively, and the lower efficiencies was caused by their reduced specific surface area when compared to TiO₂ nanospheres, which led to the decrease of dye adsorption on the surface and the subsequent decrease in light absorption. In addition,

Guo and coworkers prepared transparent nanoporous polyethylene golcol (PEG) modified-TiO_2 film using sol-gel method, and the incorporation of PEG improved the photocatalytic activity of TiO_2 film for the degradation of a harmful dye methyl orange.[124] Recently, enhanced photocatalytic activity for the degradation of indoor volatile organic compounds, including benzene, toluene, ethylbenzene and o-xylene, was demonstrated by Li's group using Ln^{3+}-doped TiO_2 photocatalysts.[125]

Modified sol-gel methods have also been developed, including calcination-assisted sol-gel method, ultra-sonic assisted sol-gel method, aerogel method, and two-step wet-chemical method, to facilitate the preparation of TiO_2 NPs with different crystal phases and shapes.[126]

1.1.3.2 Solvothermal/Hydrothermal Method

Solvothermal or hydrothermal method is normally carried out in different organic solvents or aqueous solutions using a Teflon-lined autoclave at elevated temperatures.[127] The size and morphology of nanomaterials could be controlled by adjusting the pressure in the autoclave, which could be easily realized by tuning the volume of solvents and the reaction temperature.

TiO_2 nanocrystals (undoped or doped) with different shapes, such as spherical NPs, nanorods, nanowires, nanocubes and core-shell nanostructures, or in different crystal phases, such as rutile and anatase, have been synthesized using solvothermal or hydrothermal method.[128-131]

Yang and coworkers prepared well-faceted single crystal TiO_2 nanosheets using a water-2-propanol solvothermal synthetic route.[132] Bian *et al*. employed carbon nanotubes as templates to synthesize TiO_2 mesoporous nanotubes through the solvothermal alcoholysis of titanium precursor in the mixture of ethanol, glycerol and diethyl ether.[133] Li's group have reported the solvothermal synthesis of highly crystallized and monodispersed TiO_2 NPs and nanorods through the hydrolysis of tetrabutyl titanate in the mixture of linoleic acid, NH_4HCO_3, triethylamine and cyclohexane.[134] It was observed that the morphologies of the TiO_2 nanocrystals could be easily controlled by tuning the amount of linoleic acid and NH_4HCO_3 (Figure 1.15). It was also found that the reaction temperature and time would also affect the formation of TiO_2. Higher temperature (> 120 °C) and longer reaction time would result in TiO_2 NPs or nanorods with higher crystallinity.
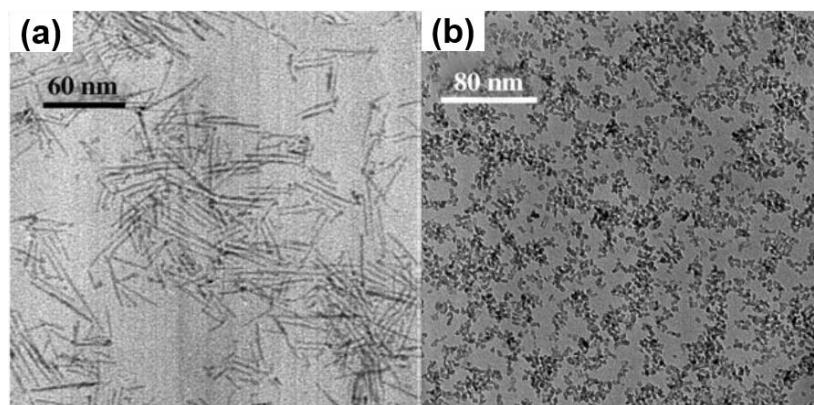
Figure 1. 15 TEM images of TiO_2 (a) nanorods and (b) nanoparticles. Figure adapted with permission from Ref 134. Copyright © 2006 WILEY-VCH Verlag GmbH & Co.KGaA, Weinheim

Instead of organic solvent, aqueous solution should be used for hydrothermal reactions. Zhang's group prepared Pt-loaded rutile TiO_2 spheres through a hydrothermal process, which showed excellent photocatalytic activity towards the degradation of methyl orange.[135] Mesoporous TiO_2 with high surface area and crystallinity obtained *via* hydrothermal method were used for the photocatalytic degradation of methylene blue.[136] Recently, Mali *et al*. prepared a series of TiO_2 nanostructures using hydrothermal method without the assistance of any surfactants.[137] Through the controlled hydrolysis of tetrabutyl titanate in H_2O at different temperatures, different morphologies of TiO_2 were obtained, such as the clusters of NPs (100 ℃), nanorods (120 ℃), and nanodendrites (160 ℃) (Figure 1.16).
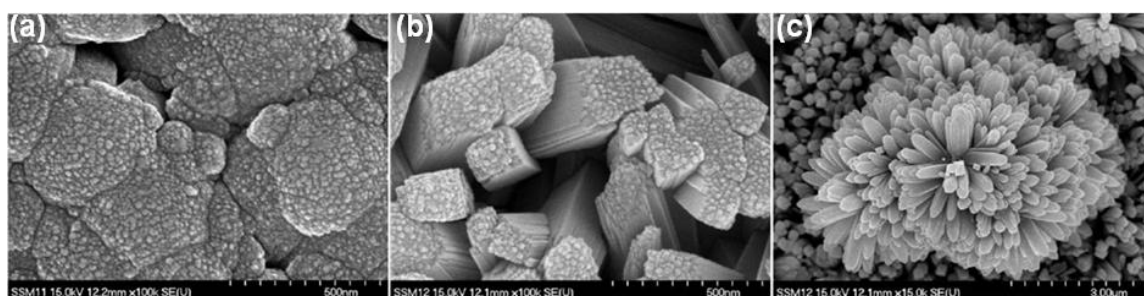
Figure 1. 16 SEM images of different TiO_2 nanostructure obtained by hydrothermal method at different temperatures: (a) 100 ℃, (b) 120 ℃, and (c) 160 ℃. Figure adapted with permission from Ref 137. Copyright © 2013 Nature Publishing Group

Hydrothermal and solvothermal methods are suitable for the growth of highly crystallized nanomaterials, and allow the control over their composition, size, and shapes. But it is impossible to monitor the growth process of nanocrystals during the reaction. In addition, the formation of harmful substance with high volatility and the pressure surge might be dangerous to human bodies; therefore, it is necessary to check the autoclaves before experiments.[138]

1.1.3.3 Polyol Method

Polyol synthesis, is not only useful for the synthesis of metallic colloids, but also a suitable method for the preparation metal oxides nanomaterials.[139] It has been reported that one-dimensional Ag/TiO_2 core-shell nanocables could be obtained through the reduction of $AgNO_3$ and the hydrolysis of titanium isopropoxide in ethylene glycol.[140] Geiseler employed the polyol method to prepare TiO_2 NPs in diethlyene glycol, and the obtained NPs were used for the design of peptide-TiO_2NP conjugates.[141] TiO_2 rutile (R) and anatase (A) nanocrystals with an average diameter of 20 to 40 nm could also be obtained *via* the hydrolysis of titanium isopropoxide in mixture of ethylene glycol, acetone and H_2O.[142] In order to get TiO_2 NPs with high purity and crystallinity, the materials were calcined at higher temperatures. Anatase could be obtained after calcinations at 400 $^{\circ}$C and rutile at 1000 $^{\circ}$C (Figure 1.17a and b). The photocatalytic activity tests of TiO_2 NPs towards the degradation of acetaldehyde showed that the degradation efficiencies of the as-synthesized TiO_2 rutile and anatase NPs were higher than the commercial TiO_2 NPs (P-25) (Figure 1.17c).
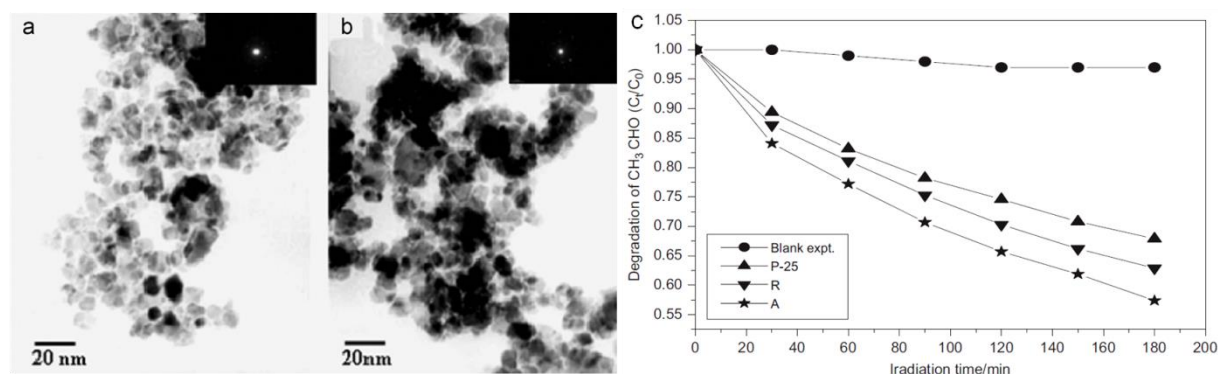
Figure 1. 17 (a) and (b) TEM images of TiO_2 calcined at 400 ℃ and 1000 ℃; (c) photocatalytic activities of commercial TiO_2 and as-prepared TiO_2 calcined at 400 and 1000 $^{\circ}$C, indicated as P-25, A and R, respectively. Figure adapted with permission from Ref 142. Copyright © 2009 Elsevier

Besides the three methods mentioned above, other synthetic strategies, such as micelle and inverse micelle methods, chemical/physical vapour deposition, microwave-assisted method, and electrodecomposition, have also been employed for the preparation of TiO_2 nanomaterials, such as nanoparticles, nanorods, nanowires, nanotubes, and mesoporous structures, which have been widely investigated as photocatalytic and photovoltaic materials.[119, 143] The numerous research works about TiO_2 nanomaterials prove that they have been and will still be useful for the treatments of environmental contaminants and the design of clean and renewable energy devices.

1.2 Properties of Nanoparticles

1.2.1 Localized Surface Plasmon Resonance (LSPR)

Localized surface plasmon resonance (LSPR) is an important property associated with nanoscaled noble metals. Surface plasmons are the oscillations of free electrons confined at the boundaries between metals and dielectrics.[144] When a surface plasmon is excited by an incident light, the electron magnetic field of the light exerts a force on the negatively charged electrons in the conduction band of the metal and drives them to oscillate collectively.[27] When the frequency of the incident light matches the frequency of the electrons oscillating against the restoring force of the positive nuclei, the oscillation will be in resonance with the incident light, leading to a strong oscillation of the surface electrons (Scheme 1.4),[145] which is known as surface plasmon resonance (SPR). SPR in nanoscaled structures, whose size is comparable with the wavelength of the incident light, is called LSPR.
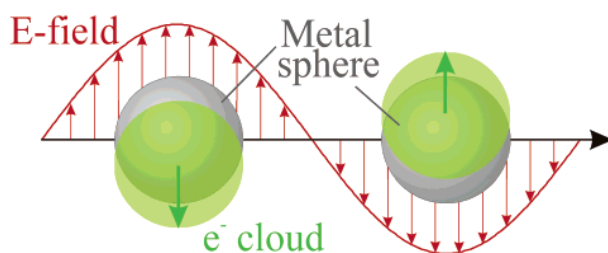
Scheme 1. 4 Schematic of plasmon oscillation for a sphere, showing that the conduction electron charge cloud can be displaced from the positive nuclei and collectively oscillates in resonance with the incident light. Figure reprinted with permission from Ref 145. Copyright © 2003 American Chemical Society

The LSPR of metallic NPs falls into the visible region of the UV-Vis absorption spectrum, and one effect of this is the intense colour displayed by the solution of metallic NPs. For example, the LSPR of monodispersed Au NPs (8 ~ 12 nm) caused an absorption of green light at ~ 527 nm, while red light is reflected, so the solution of Au NPs exhibited a ruby-red colour.[146] Ag (5-10 nm) and Cu (30-80 nm) NPs displayed yellow and wine-red colours due to their absorption of violet-blue light (350-450 nm) and green-orange light (525-620 nm), respectively.[147, 148]

Furthermore, the SPR of metallic NPs could be strongly influenced by the size, shape, and the surface chemistry of NPs. Wang's group showed that the plasmonic bands of Au nanocrystals could be tuned from 527 to 1096 nm upon their morphology change (including nanoparticles, nanocubes, nanobranches, nanorods and nanopyramids) and size control (i.e.

different aspect ratios of nanorods and nanopyramids).[149] Similar as Au NPs, the control over the shape of Ag NPs could also greatly affect their plasmonic properties. The LSPR bands of Ag triangular nanoplates blue shifted from 800 nm to 400 nm upon the corner truncation (Figure 1.18),[150] which is because that sharp structures could increase charge separation on NPs, reduce the restoring force for electron oscillation, and in turn reduce the resonance frequency.[151]Additionally, when the size of NPs is comparable with the electron free path, the charge separation on the NPs increases with the increase of NPs' size, which can also lead to the decrease of the resonance frequency.[152] For example, the LSPR bands of Ag nanocubes red-shifted from 430 to 550 nm when the size of the Ag nanocubes increased from 36 to 172 nm,[59] while the LSPR band of Au nanocubes shifted from 579 to 670 nm when their size increased from 20 to 100 nm.[152]
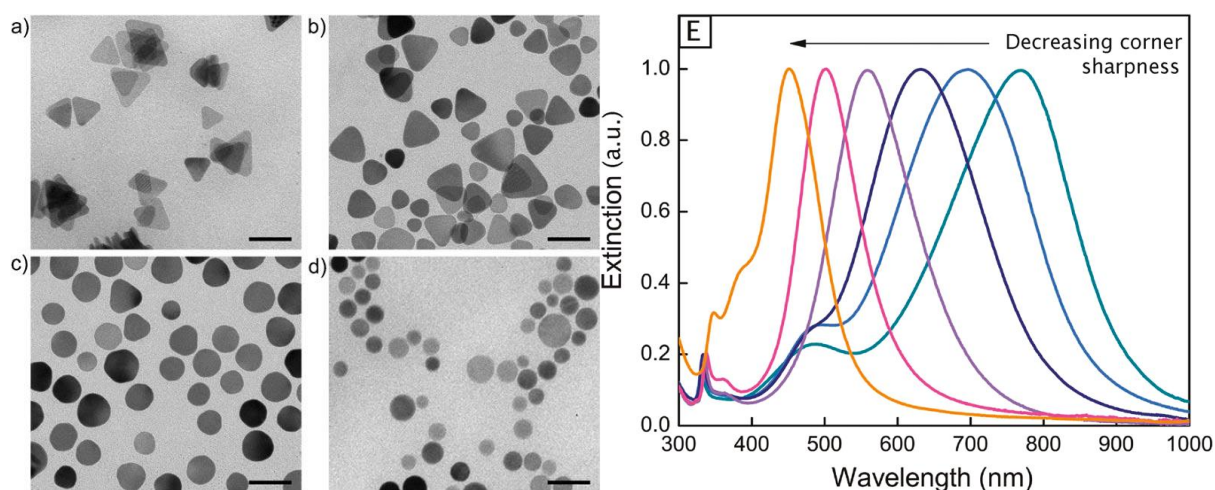
Figure 1. 18 (a-d) TEM images of the truncation process of Ag NPs. The sharp corners of the Ag nanoplates (a) were gradually truncated to circular disks (d) with reduced lateral dimensions (Scale bars is 50 nm.). (e) The decreasing corner sharpness is correlated with a blue-shift in the extinction spectra of Ag NPs in solution. Figure adapted with permission from Ref 150. Copyright © 2010 WILEY-VCH Verlag GmbH & Co. KGaA, Weinheim

Interestingly, the LSPR band of NPs smaller than 5 nm could become weak and broad and it could disappear completely when the NPs are smaller than 2 nm (Figure 1.19).[153, 154] Kreibig *et al*. proposed that electron-surface scattering could be enhanced in small NPs because the mean free path of the conduction electrons is limited by the small dimension of NPs.[155] The electrons could reach the surface of NPs very quickly, and then scatter on the surface, which will lead to the loss of the coherent plasmon oscillation. Therefore, the bandwidth of the plasmon peak increases with the decrease of NPs' size.
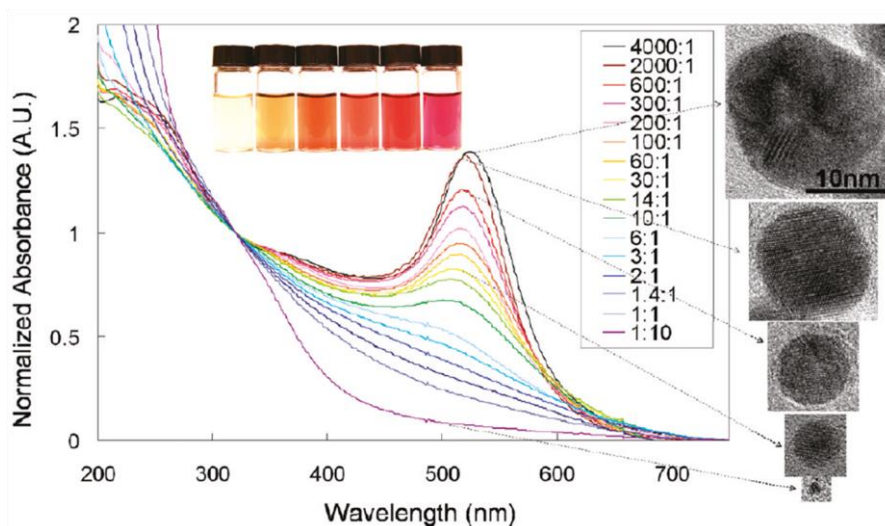
Figure 1. 19 Normalized UV-Vis absorption spectra for AuNPs with different sizes prepared with different Au/ligand molar ratios, along with a few representative TEM images. (Inset: images for a series of AuNP dispersions in deionized water; colour change from light to red reflecting the increase of AuNPs' size.) Figure adapted with permission from Ref 153. Copyright © 2010 American Chemical Society

Later, Persson proposed that the chemical environment surrounding the surface of NPs could also lead to the broadening and damping of the LSPR band due to the electron transfer between the NPs and the absorbates on their surface and the subsequent loss of the coherent electron oscillation.[156] Henglein and coworkers also experimentally proved that chemisorbed molecules on the surface of Ag NPs could lead to significant broadening and damping of the LSPR band.[157]

In addition to size, shape and surface chemistry, different crystallinity and chemical compositions of nanocrystals could also lead to the change of their plasmonic properties.[158, 159] Through the optimization of these conditions, LSPR applications at desired resonance wavelengths could be realized. Other applications such as detection and sensing of different molecules could also be achieved by monitoring the change in the LSPR of noble metallic NPs.

1.2.2 Photoluminescence Property

Photoluminescence refers to the light emission from certain kinds of materials upon the absorption of photons (excitation with a light source).[160] According to the delay time (the period between light absorption and emission) photoluminescence can be divided in to two classes: fluorescence with a shorter delay time ($10^{-12} \sim 10^{-7}$ s) and phosphorescence with a longer delay time up to milliseconds.[161] Photoluminescence property of metallic NPs was first reported by Wilcoxon *et al.* in 1998, and relatively intense blue emission at 440 nm could be

observed only from the small Au NPs (less than 5 nm), while Au NPs bigger than 15 nm were nonluminescent.[162] Later, Au NPs with an average diameter form 1.1 to 1.7 nm were shown to be photoluminescent in the near infrared region with a quantum yield of $(4.4 \pm 1.5) \times 10^{-5}$.[163] Under the excitations at 500 nm and 514 nm, Au_{28} nanoclusters showed fluorescence at 1.55 eV (800 nm) and 1.13 eV (1100 nm) with quantum yields of 1.5×10^{-3} and 2.0×10^{-3}, respectively.[164] Since the HOMO-LUMO gap for Au was 1.15 eV, so the emission at 1.55 eV could not be originated from the intraband transition alone, therefore, Link and coworkers proposed that the emission from Au_{28} nanoclusters was caused by both intraband (sp-sp) and interband (sp-d) transitions (Scheme 1.5).[164]
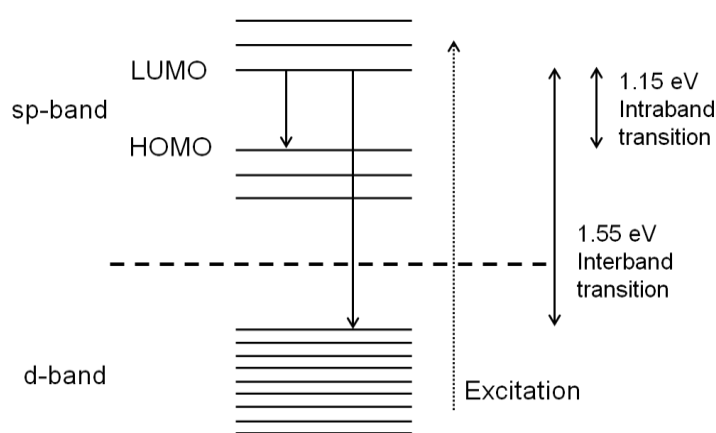
Scheme 1. 5 The combination of intraband (sp-sp) and interband (sp-d) electronic transition mechanisms for the fluorescence of Au nanoclusters. Scheme adapted with permission from Ref 164. Copyright © 2002 American Chemical Society

Similar to plasmonic property, the fluorescent property of NPs could also be affected by the size, shape, surface chemistry and chemical compositions of NPs.[165-170]

To investigate the size-dependent emission from Au nanocrystals, Zheng *et al*. prepared a series of Au nanoclusters (Au_5, Au_8, Au_{13}, Au_{23} and Au_{31}), which showed emissions from UV to near infrared region, and the emission blue-shifted with the decrease of the nanoclusters' size (Figure 1.20).[165] Water soluble mercaptosuccinic acid-coated Ag nanoclusters composed of 7 and 8 Ag atoms showed fluorescence blue-green and red emission at 440 and 650 nm.[171] The size effect on fluorescence is that in small NPs the interaction between d electrons and nuclei are stronger than that between s electrons and nuclei, thus the energy gap between s and d bands is increased, leading to the blue-shift of the emission.[172] The morphologies of NPs could also affect the fluorescence property of NPs. For example, the quantum yield of Au nanocubes was 200 times higher than cylindrical Au nanorods, due to the well overlapping of the SPR band and the photoluminescence band of Au nanocubes.[173]

40
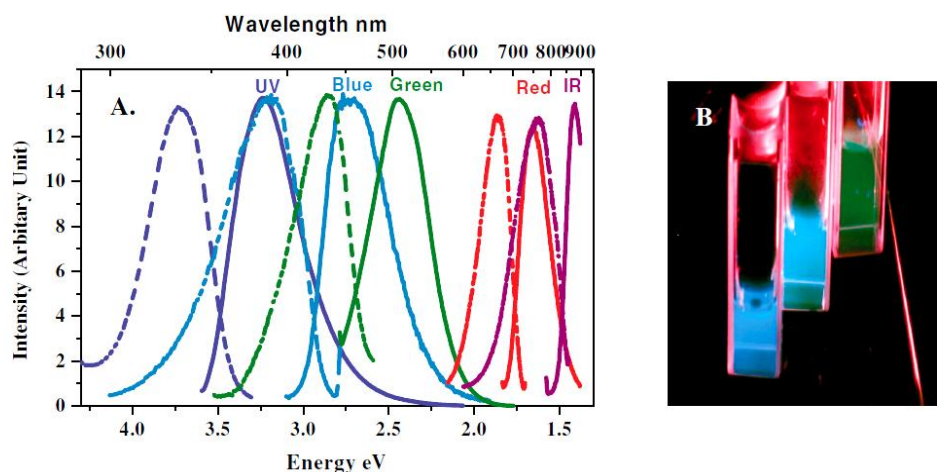
Figure 1. 20 (a) Excitation (dashed) and emission (solid) spectra of different gold nanoclusters. Excitation and emission maxima blue-shifted with the decrease of the nanocluster size. (b) Emission from the three shortest wavelength emitting gold nanocluster solutions (from left to right) under UV irradiation (366 nm). Figure reprinted with permission from Ref 165. Copyright © 2004 American Physical Society

In addition, chemical compositions of NPs or the chemical environments around NPs could also influence their fluorescence property. Ag/Au alloy nanodots prepared with different molar ratios of $AgNO_3$ to $HAuCl_4$ (0, 0.125, 0.8 and 2) showed different emissions (yellow, green, turquoise and blue) at 525, 500, 478 and 456 nm (Figure 1.21).[170] Ag NPs prepared by electro-expolosion of Ag wire showed specific fluorescence emissions at 300, 310, and 325 nm in different solvent systems such as water, methanol and hexane.[174] Au nanoclusters coated with three different polymers, poly(t-butyl methacrylate), poly(n-butyl methacrylate), and poly(methyl methacrylate) exhibited different quantum yields (3.8%, 14.3% and 20.1%, respectively), which might because that the increasing steric hindrance of the polymers could protect the Au nanoclusters against the solvent quenching effect.[167]
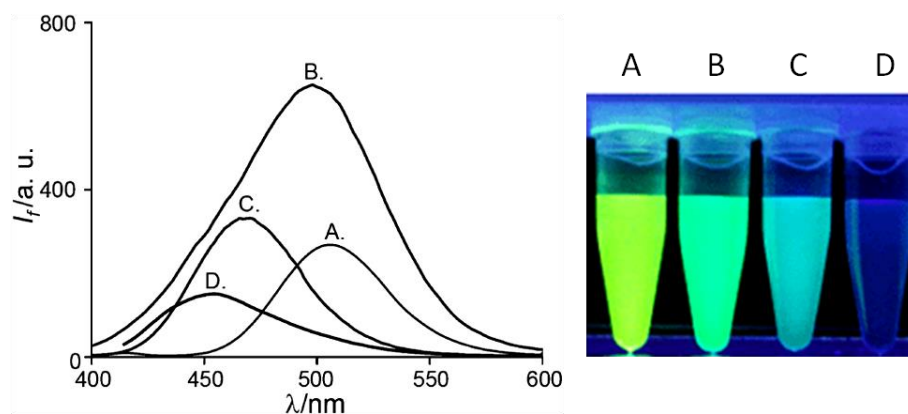
Figure 1. 21 (left) Photoluminescence spectra of Au/Ag nanodots prepared at different $AgNO_3$-to-$HAuCl_4$ molar ratios, (A) 0, (B) 0.125, (C) 0.800, and (D) 2.000; (right) Image of Au/Ag nanodots under UV light irradiation. Figure adapted with permission from Ref 170. Copyright © 2008 the Royal Society of Chemistry

Great efforts have been devoted to the preparation of highly fluorescent NPs, and their emission wavelengths and quantum yields could be tuned through the control over the size, shape, chemical compositions and surface chemistry. The tunable emission, brightness, high photochemical stability and high quantum yields of fluorescent NPs have made them useful for applications in the design of optical devices, sensing and imaging.[175-177]

1.2.3 Surface Enhanced Raman Scattering (SERS)

Raman Scattering is the inelastic scattering of photons by molecules, and Raman spectra could provide vibrational "fingerprint" information that are useful for the detection and identification of molecules.[178] However, the application of traditional Raman spectroscopy was limited due to the relatively weak Raman signal resulted from the low efficiency of inelastic scattering.[179] This problem was solved by surface enhanced Raman scattering (SERS), which refers to the enhancement of Raman scattering signals from molecules absorbed on the rough surfaces of metal substrates (Figure 1.22).[178, 180]
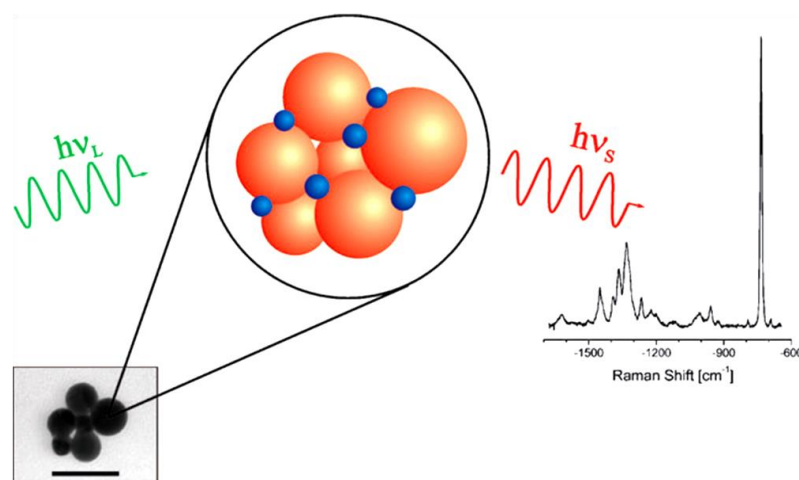
Figure 1. 22 Surface-enhanced Raman scattering. Molecules (blue) are adsorbed onto metallic NPs (orange) either in suspension or on a surface. As in ordinary Raman scattering, the SERS spectrum reveals molecular-vibration energies based on the frequency shift between incident (green) and scattered (red) laser light. The SERS spectrum shown as example was collected from 10^{-9} M adenine in a solution of Ag nanoaggregates. Figure adapted with permission from Ref 180. Copyright © 2007 AIP Publishing LLC

Two different mechanisms for SERS have been proposed.[181] One is electromagnetic theory, which says electromagnetic field can be enhanced when the localized surface plasmon of metallic NPs is excited by an incident light, and the enhancement reaches maximum when the frequency of the incident light is in resonance with the plasmon frequency. The electromagnetic field enhancement then magnifies the intensity of the incident light for

exciting the Raman scattering of molecules, which finally leads to the enhancement of Raman scattering signals. Scattering occurs only when the plasmon oscillations are perpendicular to the surface of substrates, therefore, rough surfaces or arrangements of NPs are needed for SERS measurements. The other mechanism for SERS is charge-transfer theory, which involves the charge transfer between chemisorbed molecules and the metal surface due to the formation of metal-analyte complex. When the excitation frequency is in resonance with the energy for metal-analyte charge transfer, the enhancement of Raman scattering signal occurs. It is generally considered that electromagnetic enhancement contributes more to SERS than charge transfer enhancements.

Noble metallic nanomaterials, such as Au, Ag and Cu, are suitable substrates for SERS as they are excellent plasmonic materials.[182] However, the most used SERS-active substrates are Au and Ag because they are more air stable than Cu,[182] and Ag nanocrystals have been found to be more SERS active than Au in many studies due to their narrower and more intense plasmons than Au.[183, 184] For example, Mahmoud *et al*. showed that Ag nanorods were more efficient for Ramam enhancement than Au nanorods with comparable aspect ratios and diameters, and the SERS enhancement factor for Ag nanorods was $0.1 \sim 2 \times 10^{14}$, while that for Au nanorods was $0.3 \sim 2.2 \times 10^{12}$.[185] Ag NPs also exhibited better ability for the SERS detection of fluorescent dye Cy5.5 than Au NPs, and the detection limit of Cy5.5 using Ag NPs was 5.2×10^{-12} M in contrast to 7.3×10^{-11} M when Au NPs were used.[186] In comparison to simplex Au NPs, Au cores coated with Ag shells showed better enhancement ability of the Raman signals from Rhodamine 6G and crystal violet (Figure 1.23), and the enhancement factor of Au@Ag core-shell NPs was 10~100 times more than that of the Au NPs.[187]
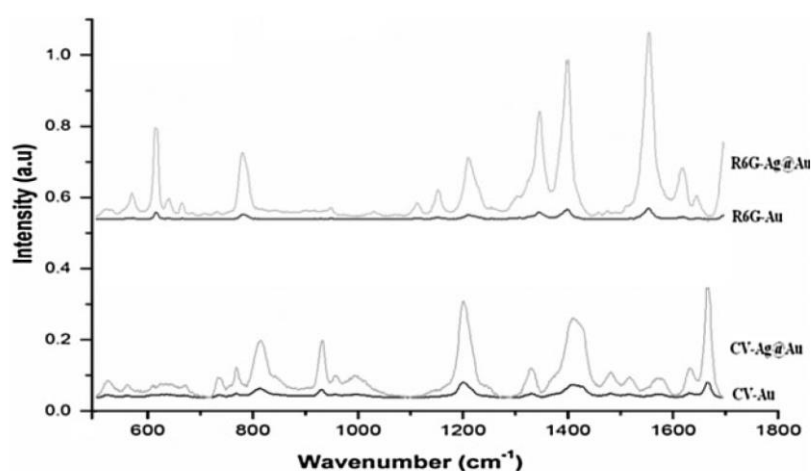
Figure 1. 23 SERS spectra of crystal violet (CV) and Rhodamine 6G (R6G) using Au NPs and Au@Ag core-shell NPs as SERS substrates. Figure reprinted with permission from Ref 187. Copyright © 2010 WILEY-VCH Verlag GmbH & Co. KGaA, Weinheim

Many research works have demonstrated that the size and shape of metallic NPs could influence their SERS activity due to the difference in their localized surface plasmon.[188-190] Jang *et al*. employed Au NPs with different sizes (from 6 to 97 nm) for the SERS studies of 4-biphenylmethanethiolate, which showed that the SERS enhancement was very weak when smaller Au NPs (< 11 nm) were used.[188] Nie's group investigated the SERS activity of Ag NPs with different sizes showing that there was a linear correlation between the size of Ag NPs and the optical excitation wavelength (Figure 1.24).[189] In order to get better SERS signals, a proper excitation wavelength need to be chosen to excite the localized surface plasmon of different-sized NPs. NPs with different morphologies, such as rod, prisms, and cubes, were also employed as excellent SERS active substrates, and it has been both theoretically and experimentally proved that the sharp edges or angles of NPs could result in the enhancement of the electromagnetic field of plasmonic nanocrystals and lead to the enhancement of Raman scattering.[191] Flower-like Ag nanoplates displayed excellent SERS property in comparison to anisotropic Ag NPs and nanodiscs.[192] Xia's group demonstrated that sharp or truncated Ag nanocubes exhibited higher SERS enhancement efficiencies than spherical Ag NPs.[193, 194]
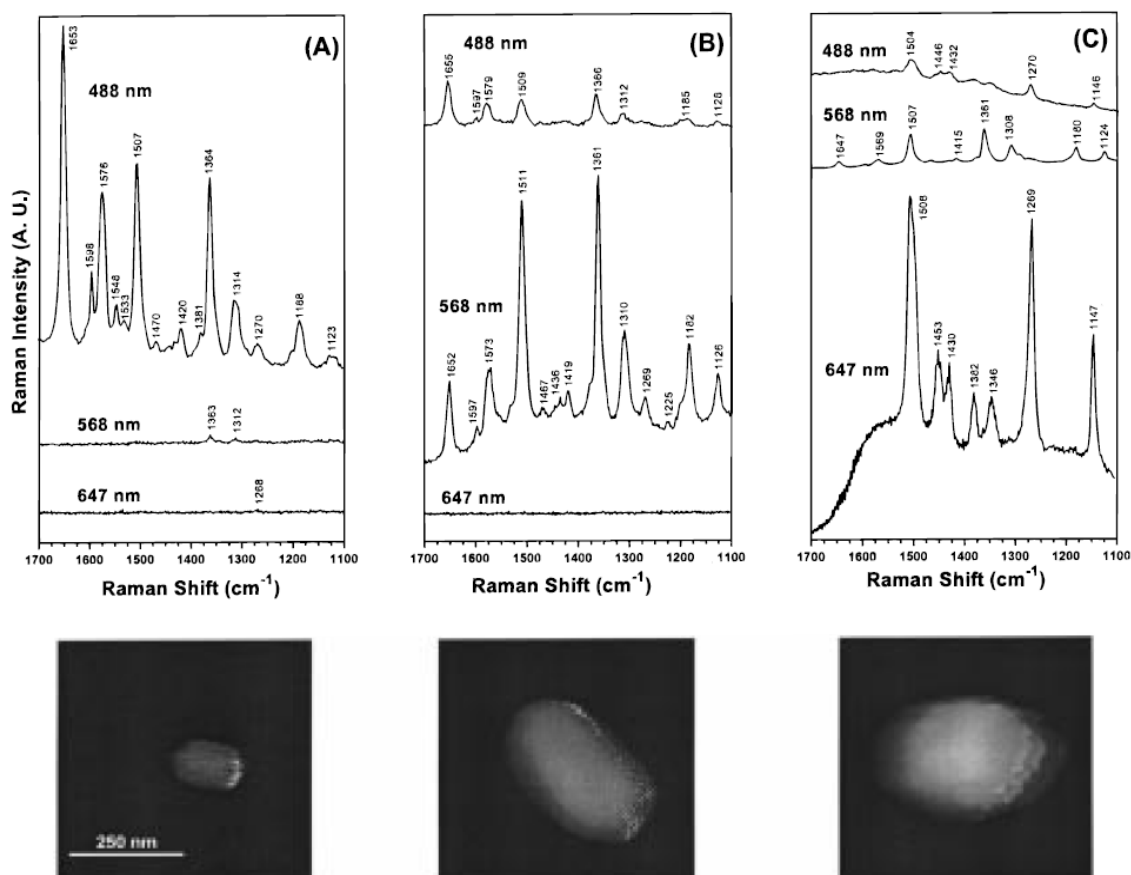
Figure 1. 24 Correlated SERS spectra and AFM images obtained from spatially isolated single Ag NPs. The NPs were selected by wide-field screening for maximum enhancement at (A) 488 nm, (B) 567 nm, and (C) 647 nm, respectively. Figure reprinted with permission from Ref 189. Copyright © 1998 American Chemical Society

44

In addition to nanocrystals with sharp features, aggregations of metallic NPs are often needed for SERS studies, because the electromagnetic field coupling between two or multiple NPs can also lead to a significant SERS enhancement.[195] Different inorganic salts (NaCl, KCl, NaNO$_3$, KNO$_3$ and MgSO$_4$), surfactants and organic polyamines are normally experimentally employed to obtain the aggregations of NPs.[196-198] For example, the addition of KCl led to the great enhancement of Raman scattering by Brilliant green molecules due to the salt-induced formation of Ag aggregations.[199] MgSO$_4$ was shown to be more favorable than halide salts for the aggregation of citrate-coated Ag colloids and the following sensitive detection of DNA/RNA mononucleotides, because the strong affinity between Ag and halide ions might prevent the analytes getting closer to the surface of Ag NPs.[200] Spermine was employed as the aggregation agent for Ag colloids in the SERS detection of oligonucelotides showing that the protonated amine functional groups of spermine could not only be absorbed to the negatively charged surface of Ag NPs, but also interact with the phosphodioxygens of DNA, and thus bring the DNA in close affinity to Ag NPs.[197]

Metallic NPs, including spherical, sharp-edged, bimetallic and aggregated NPs, have been fabricated as SERS substrates. These nanosubstrate offers many advantages, such as size and shape-tunable properties, long-term stability and biocompatibility, which enable them to be applied for molecular detection in microorganisms, cells, tissues, and living animals.[201] In the future, SERS methodology will continue to be attractive for applications in sensing, environmental analysis and drug delivery tracing,[20, 201] therefore, there will be an increasing need for the development of novel SERS platforms with higher sensitivity and reproducibility.

1.2.4 Reactive Oxygen Species (ROS) Production

Metallic (Au, Ag, Cu), metal oxide, (CuO, ZnO), and semiconductor (TiO$_2$, CdS) nanomaterials have excellent antibacterial, genotoxic, cytotoxic and photocatalytic properties, and recent studies have demonstrated that these properties could be attributed to nanomaterial-induced generation of ROS,[202, 203] which refer to the highly oxidative species such as hydrogen peroxide (H$_2$O$_2$), superoxide anion (O$_2^{\bullet-}$) and hydroxyl radicals (OH$^\bullet$).[204]

The general principle for the photo-induced ROS production of semiconductor and metal oxide nanomaterials has been explained in 1.1.3 (Scheme 1.3) that the electrons and holes generated under light irradiation could react with oxygen and water leading to the formation of superoxide and hydroxyl radicals.[118, 205] Li and coworkers systematically investigated the photo-induced (UV light: 365 nm) ROS generation mechanism of a series of metal oxides NPs, including TiO$_2$, ZnO, Al$_2$O$_3$, SiO$_2$, Fe$_2$O$_3$ CeO$_2$ and CuO, which showed that their ROS

production redox potentials was strongly related to their band gap energy, and photogeneration of ROS could only occur when the energy of the incident light was higher than the band gap energy.[206] The ROS production ability of different TiO_2 crystallines (rutile, anatase and the mixture of both rutile and anatase) were utilized for the photocatalyzed degradation of organic dyes, and the mixture of rutile and anatase showed the best photocatalytic activity.[207] Photo-induced production of ROS by CdS quantum dots were employed for the activation of enzyme Cytochrome P450,[208] while the phototriggered ROS by TiO_2/Au hybrid NPs were employed for the light-controllable activation of peroxidase enzyme and the subsequent oxidation of nonfluorescent substrate Amplex Red to fluorescent resorufin (Scheme 1.6).[22]
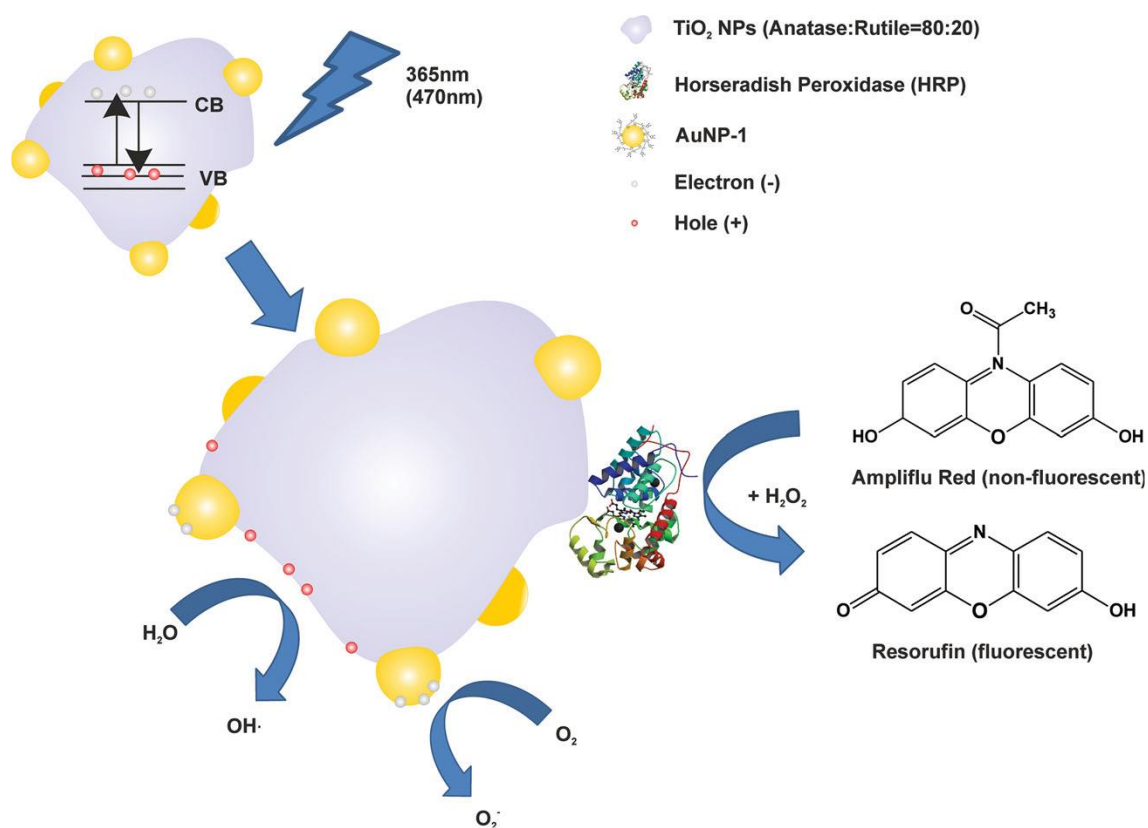
Scheme 1. 6 Photo-induced ROS generation by Au/TiO_2 hybrids for enzyme activation and subsequent substrate oxidation. Figure reprinted with permission from Ref 22. Copyright © 2013 WILEY-VCH Verlag GmbH & Co. KGaA, Weinheim

However, the mechanism for the ROS production ability of metallic and metal oxide nanomaterials in the absence of light irradiation remains unclear. It was proposed that the electron donor/acceptor active sites on the surface of nanomaterials could interact with oxygen to produce superoxide radicals, which could then trigger the generation of additional

ROS.[209] Metal ions, which are released through the dissolution of nanomaterials, can participate in the formation of such kind of active sites and trigger the production of ROS.[202, 210] He *et al.* studied the AgNP-induced ROS generation over a physiologically range of pH, and it was found that hydroxyl radical could be produced under acidic conditions and this process was accompanied by the dissolution of Ag NPs.[211] Cu^{2+} released from the dissolution of CuO NPs showed toxic effects towards *Escherichia coli* bacteria due to the DNA damage caused by CuO-induced ROS production.[212] The high redox activity of Cu NPs have also been shown to be cytotoxic due the formation of ROS, and the released Cu^{2+} ions could lead to the destruction of cell membrane or interact with proteins and DNA and cause the conformation and property changes.[213, 214]

Contrary to the above described findings, there were also evidences that the metal ions were not responsible for ROS generation by metal and metal oxide nanomaterials. ZnO NPs were shown to be cytotoxic due to ROS-induced oxidative stress in cells, while free Zn^{2+} ions and metal impurities did not contribute to ROS production and the cytotoxic effect.[215] Shi *et al.* employed a peroxidase activity assay to demonstrate that Cu^{2+} ions did not contribute to the excellent ROS generation ability of Cu NPs, and on contrary, the appearance of Cu^{2+} could cause the formation of oxide layer on the surface of Cu NPs, which significantly suppressed the ROS production.[76] Lee's group showed that Ag NPs could produce ROS and in turn cause the inactivation of the absorbed lactate dehydrogenase (LDH), which was proved by a fluorescent assay and a LDH leakage assay,[216] while in the control experiments where $AgNO_3$ was used for the ROS detection and LDH activity tests, no ROS was detected and no activity inhibition of LDH was observed, which indicated that the Ag^+ ions were not responsible for the ROS generation ability of Ag NPs.

Although the main reason for the ROS generation ability by metallic nanomaterial without light irradiation has not been fully understood and more efforts need to be put into understanding the mechanism, the ROS production ability of nanomaterials has already proven to be useful for applications in photocatalysis, phototherapy, cytotoxic and antibacterial studies.[203, 217, 218]

1.2.5 Catalytic Property

Catalysts are widely used in the treatment of environmental contaminants, industrial production of chemicals, pharmaceuticals, and design of solar fuels.[219, 220] Homogeneous catalysts are very efficient and selective, but they are difficult to be removed from the reaction media and cannot be recycled, which makes them at the same time contaminants and limits

their applications. Therefore, recyclable heterogeneous catalysts are referred for the green and environmental friendly catalytic applications.[221] Nanomaterials have emerged as attractive candidates for heterogeneous catalysis, as they are easily recyclable, and they have high surface area to volume ratios, which could provide more surface active sites for the catalyzed reactions.[222]

The use of metallic NPs as catalysts can be traced back to the 1970's when rhodium NPs were used for the dehydrogenation of olefins.[223] In 1987, small Au NPs were employed as very effective catalysts for the oxidation of carbon monoxide,[224] and later it was observed that the catalytic activity and selectivity of Au NPs could be significantly enhanced upon the decrease of the NPs' size.[225] Recently, Ag NPs (~5 nm) have been shown to have excellent catalytic activity towards the conversion of CO_2 to CO, and the conversion rate per unit surface area was 10 times higher in comparison to bulk silver.[226] When Cu NPs with an average diameter of 66 nm or 8 nm were used as catalysts for the conversion of iodobenzene into biphenyl, the conversion efficiencies were 88 and 95%, which were much higher than 43% when macrosized Cu was used.[21] The better catalytic activity of smaller NPs is caused by their higher surface area to volume ratios.[227]

Additionally, it has also been shown that nanomaterials with different morphologies have different catalytic properties. For example, different shaped Ag nanocrystals, including near spherical NPs, nanocubes and truncated triangular nanoplates, were used to catalyze the oxidation of styrene, and the results showed that the reaction rate catalyzed by Ag nanocubes was 14 and 4 times faster than the reactions catalyzed by Ag nanoplates and near spherical NPs (Figure 1.25d), respectively.[228] It was found that the exposed [100] crystal planes of Ag nanocubes played an important role for their higher catalytic activity (Figure 1.25c), while the truncated triangular nanoplates and near spherical NPs were less active because they exposed mainly the most-stable [111] crystal planes (Figure 1.25a and b). Similarly, CuO nanocrystals also displayed shape-dependent catalytic activity towards the oxidation of CO, the reaction rate catalyzed by CuO nanoplatelets was 6 and 3 times higher than the reactions catalyzed by CuO NPs and nanbelts, respectively, because the [01 $\bar{1}$] crystal planes exposed by CuO nanoplatelets were more active than the [111] and [001] crystal planes exposed by CuO NPs and nanbelts.[229] Au nanocubes with [100] crystal planes were also shown to be more active than the [111]-faced Au octahedral and [110]-faced Au rhombic dodecahedra nanocrystals towards the electrocatalytic oxidation of glucose.[230]
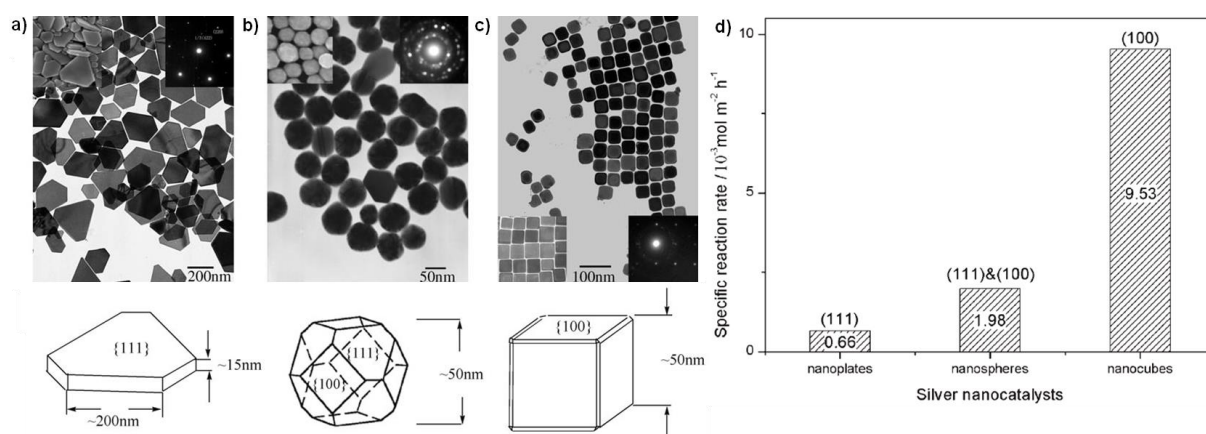
Figure 1. 25 TEM image of Ag nanocrystals: a) truncated triangular nanoplates, b) near spherical NPs, c) nanocubes, and their corresponding structural models with exposed crystal faces. The insets show the SEM images (left) and the selected area electron diffraction patterns (right). d) Specific reaction rate for styrene conversion over Ag truncated triangular nanoplates, near-spherical NPs, and nanocubes. Figure adapted with permission from Ref 228. Copyright © 2006 WILEY-VCH Verlag GmbH & Co. KGaA, Weinheim

Unlike metallic nanocatalysts, semiconductor nanomaterials have been widely used as photocatalysts for environmental and energy applications.[231-234] The mechanism for the photocatalytic properties of semiconductor nanomaterials, such as TiO_2, ZnO, ZnS and CdS, is that the photo-generated ROS species (Scheme 1.1.3) could interact with various kinds of molecules, such as carbon monoxide, nitrogen oxides, volatile organic compounds and fluorescent dyes.[235, 236]

As one of the most efficient and environmentally benign semiconductors, TiO_2 photocatalysts have been extensively used for the degradation of various pollutants, the design of solar cells, and cytotoxic studies, and there are many reviews comprehensively summarized the previous progress about the research and applications of undoped or doped TiO_2 photocatalysts.[117, 143, 237-241] Recently, Bian and coworkers designed an advanced Au/TiO_2 superstructure system by loading Au NPs onto TiO_2 mesocrystals *via* impregnation method, and it was observed that the lifetime of > 60% electrons in the obtained $Au/mesoTiO_2$ system was prolonged.[242] Due to the efficient charge separation of the $Au/mesoTiO_2$ system, its visible-light photocatalytic activity toward the degradation of organic dyes was significantly improved in comparison to conventional Au/TiO_2NP and Au/P25 (commercial TiO_2 NP) systems (Figure 1.26). Newly emerged pharmaceutical contaminants such as antibiotics could also be degraded by TiO_2 photocatalysts, and it was reported that the degradation efficiency of amoxicillin trihydrate, an antibiotic for the treatment of bacterial infections, over Sn-doped TiO_2 photocatalysts was higher than the pure TiO_2 due to the electron capture effect of Sn NPs.[243] TiO_2-Ag nanocomposites prepared by photodecomposition of Ag NPs on TiO_2

nanorods were used for the fabrication of solar cells, which showed higher photon-to-current conversion efficiency than pure TiO_2 nanorods.[244] TiO_2 nanotubes filled with Ag cores showed higher photocatalytic efficiency for water splitting than empty TiO_2 nanotubes.[245]
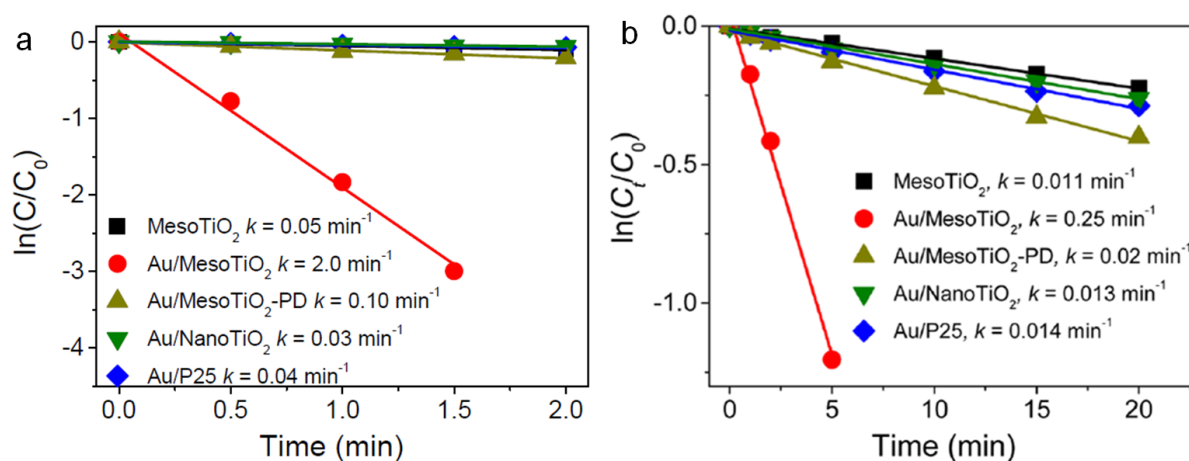
Figure 1. 26 Kinetic linear fitting curves for photocatalytic degradation of (a) rhodamine B and (b) methyelene blue and over different Au/TiO$_2$ nanocomposites under visible-light irradiation. Figure adapted with permission from Ref 242. Copyright © 2014 American Chemical Society

Numerous kinds of catalytic active nanomaterials with different sizes, shapes and compositions have been fabricated as powerful catalysts for chemical production, environmental applications and solar cell designs.[13, 144] However, challenges such as the development of multifunctional, robust, economical and many-times recyclable nanocatalysts with high activity, selectivity and efficiency still remain.[12] Further studies will be needed for optimizing the performance of nanocatalysts and tailoring them for different applications.

1.3 Biofunctionalization of Nanoparticles

Inorganic nanomaterials, such as metallic and semiconductor NPs, have similar dimensions to those of biomolecules, such as DNA oligonucleotides and proteins, so the construction of NP-biomolecule hybrids could integrate the excellent optical, electronic and catalytic properties of NPs and the unique recognition and selective catalytic features of biomolecules, and the novel hybrid materials might find applications in sensors, bioimaging, targeted drug delivery, catalysis, electronics and nanoscaled self-assembly.[246-248] The functionalization of NPs with biomolecules could be realized by several ways, including electrostatic adsorption,[249, 250] chemisorptions,[251] covalent binding,[252] and specific affinity

interaction.[253, 254] Herewith, a few of the most widely used methods for the biofunctionalization of NPs will be introduced.

1.3.1 Biofunctionalization of Nanoparticles through Electrostatic Adsorption

The biofunctionalization of NPs through electrostatic adsorption is a simple method, which only requires the mixing of NPs and biomolecules with different charges (Scheme 1.7).[255] Negatively charged NPs, such as those stabilized with carboxylic groups, citrate and lipoic acid, could be used for the immobilization of positively charged biomolecules i.e. proteins through electrostatic interaction, while positively charged NPs could be employed for the electrostatic binding of negatively charged biomolecules such as DNAs.[255]

For instance, immunoglobulin G (IgG) was attached to the surface of citrate-coated Au NPs through the electrostatic interaction between the positively charged amino acid side chains of IgG and the negatively citrate groups on the surface of Au NPs.[256] Positively charged spermine-stabilized Ag NPs were used for the attachment of dye-labeled DNA molecules, and the electrostatic binding ability between the dye-labeled DNA and Ag NPs were then utilized for DNA detection by SERS.[257] Coiled coil peptides (short chains of amino acid monomers involved in many biological processes, such as hormone regulation and intracellular transport[258]) were conjugated to the Au NPs through electrostatic interaction and facilitated the self organization of Au NPs.[259]

Scheme 1. 7 Electrostatic interaction

Although electrostatic adsorption is a very simple method, the obtained biomolecule-NP hybrid systems are unstable and can be influenced by the environmental conditions, such as pH and temperature.[260] The conformation of biomolecules might also change upon electrostatic adsorption, leading to the change of bioactivity and the orientations of i.e. proteins, which are very important for retaining their inherent functions, sometimes resulting in the deactivation of original biomolecules.[261]

1.3.2 Biofunctionalization of Nanoparticles through Chemisorption

Many kinds of chemical functional groups have certain affinity to the surface of inorganic NPs, for example, thiolated anchors, such as sulfides and disulfides could bind strongly to Au, Ag, and Pt,[262, 263] and catechol groups have affinity to metals (Au)[264] and metal oxides (TiO$_2$ and Fe$_2$O$_3$).[141, 265] These functional groups could be easily absorbed onto the surface of certain kinds of NPs and in turn stabilize them. Therefore, biomolecules containing different chemical functional groups could be directly used for the functionalization of NPs.

1.3.2.1 Biofunctionalization of Nanoparticles through Thiolated Anchors

Modification of Au NPs with DNA oligonucleotides was first reported by Mirkin *et al.* and Alivastos *et al.* in 1996,[266, 267] which opened up the new research area of DNA-NP conjugates. Due to the high affinity between thiol and noble metals, the most commonly used method so far for preparing the hybrids of DNAs and metallic NPs is the direct attachment of thiolated DNAs to the surface of NPs.[268, 269] Graham and coworkers prepared thiolated DNA oligonucleotides functionalized Ag NPs through salt aging method, and the obtained DNA-Ag conjugates were employed for the detection of target DNA by monitoring the plasmonic change of Ag NPs.[17] Mirkin's group reported the fabrication of heterofunctionalized Au NPs with both thiolated DNA and cysteine-terminated peptides.[270] Recently, a fast and efficient strategy was reported, in which the modification of gold nanorods (GNRs) with thiolated DNA was performed in a solution with low pH value (pH = 3) and high salt concentration.[268] The whole process took only five minutes, which was much faster compared to 2-3 days by employing the previously reported salt aging method (Figure 1.27).
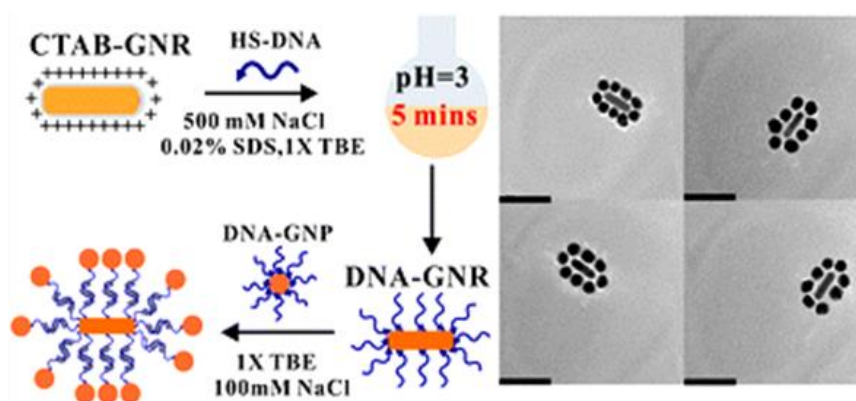
Figure 1. 27 (left) Schematic of the low pH strategy to modify GNRs and the formation of the GNR–GNP satellite structure; (right) TEM images of the GNR-GNP satellite structure (scale bar is 100 nm). Figure reprinted with permission from Ref 268. Copyright © 2013 the Royal Society of Chemistry

In the past years, proteins containing natural or genetically introduced cysteine residues have been employed in the design of functional bio-NP hybrids. For example, bovine serum albumin (BSA) protein was attached to Au NPs through the affinity between the free thiol of cysteine residue and Au, and the conformational stability of the protein on the surface of Au NPs were systematically studied under different pH conditions.[271] Elechiguerra *et al.* used BSA directly as a stabilizer for the one-pot synthesis of Ag NPs, which exhibited inhibition effects against HIV-1 virus *in vitro*.[272]

1.3.2.2 Biofunctionalization of Nanoparticles through Catechol Functional Groups

It has been reported that dopamine could bind to metals and metal oxides through the catechol functional groups.[264, 273] Taking advantage of this ability, Geiseler *et al.* reported the attachment of dopamine-modified peptide to the surface of TiO_2 NPs.[141] Paunesku and coworkers reported the functionalization of TiO_2 NPs with a dopamine-modified oligonucleotide DNA, and the obtained nanohybrids retained both the photocatalytic property of TiO_2 and the bioactivity of DNA.[274] Recently, metal oxide ($Fe_3O_4@TiO_2$) core-shell nanocomposites were modified with a dopamine-modified peptide, which was designed based on a DNA binding domain.[275] The DNA binding peptide enabled the cellular uptake of the NPs. The nanoconjugates entered into the cell nuclei and produced ROS under UV irradiation, which finally led to the cleavage of genomic DNA and cell death (Scheme 1.8). On contrary, bare nanocomposites could only cause damage to the cell membrane, because they did not have the DNA binding peptide on the surface and could not enter the nuclei.
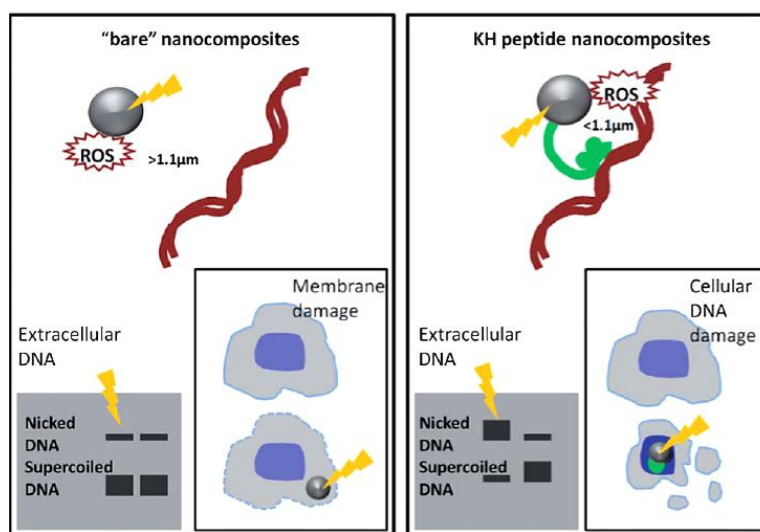
Scheme 1. 8 Schematic representation of apoptosis experiments performed with the peptide functionalized NPs. Figure reprinted with permission from Ref 275. Copyright © 2013 the Royal Society of Chemistry

Although the stability of the biomolecule-NP conjugates obtained by chemisorption is improved when compared to the conjugates obtained by electrostatic adsorption, sometimes this method could still induce the conformation and bioactivity change of biomolecules.[271, 276] Therefore, covalent attachment of biomolecules to NPs has been developed to improve the stability of biomolecules after conjugation.

1.3.3 Biofunctionalization of Nanoparticles through Covalent Binding

In order to solve the problems of instability and inactivity of biomolecules caused by physical or chemical adsorption onto nanoparticles, covalent binding methods through bifunctional linkers have been developed.[247] Different bifunctional linkers, which contain anchor groups for NP binding and additional functional groups to enable covalent attachment of the desired biomolecules, have been designed for the covalent functionalization of NPs with biomolecules.[277] Different types of reactions have been used to realize the covalent binding and some of them are described below.

1.3.3.1 Amide Coupling

One of the most versatile covalent binding methods is amide coupling, which involves the activation of carboxylates with an activation reagent, such as 1-Ethyl-3-(3-dimethylaminopropyl)-carbodiimide (EDC), for the further conjugation with primary amines (Scheme 1.9). The efficiency of this process can be increased by the addition of *N*-hydroxysuccinimide (NHS) or *N*-hydroxysulfosuccinimide (Sulfo-NHS) because the formation of amine reactive NHS esters could stabilize the amine reactive intermediates.[278] Due to its high conversion efficiency and excellent biocompatibility, it is widely used for the attachment of biomolecules to NPs.
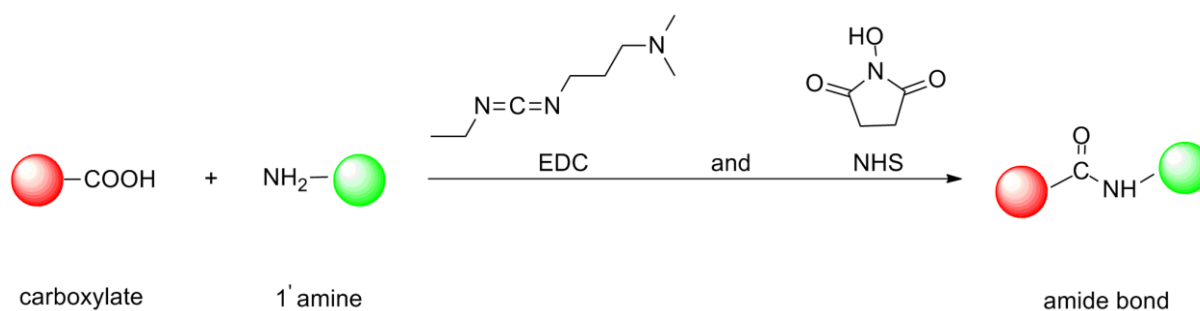
Scheme 1. 9 EDC/NHS cross linking between carboxylic acid and amine

For instance, it was reported that the immobilization of antibody immunoglobulin on to the surface of polyallylamine coated Au NPs could be realized through the EDC/NHS activation of the C-terminal carboxylic functional group of the antibody.[279] The antigen recognition ability of the antibody-AuNP conjugates was confirmed by an enzyme-linked immunosorbent assay. Li and coworkers employed amide coupling for the design of glucose oxidase-AuNP hybrids, which exhibited an enhanced thermal stability when compared to the free enzyme alone.[280] Lai *et al*. fabricated a LSPR nanobiosenser through the amide-coupling between anti-albumin antibody and mercaptoundecanoic acid (MUA)-coated Ag NPs on a glass substrate (Scheme 1.10), which was used for the detection of microalbuminuria by monitoring the LSPR change of Ag NPs.[281] The results showed that the antibody maintained its recognition ability, and the detection limit could reach to 1 ng/Ml, which indicated that the antibody-AgNP conjugates could serve as sensitive platform for the detection of antigens.
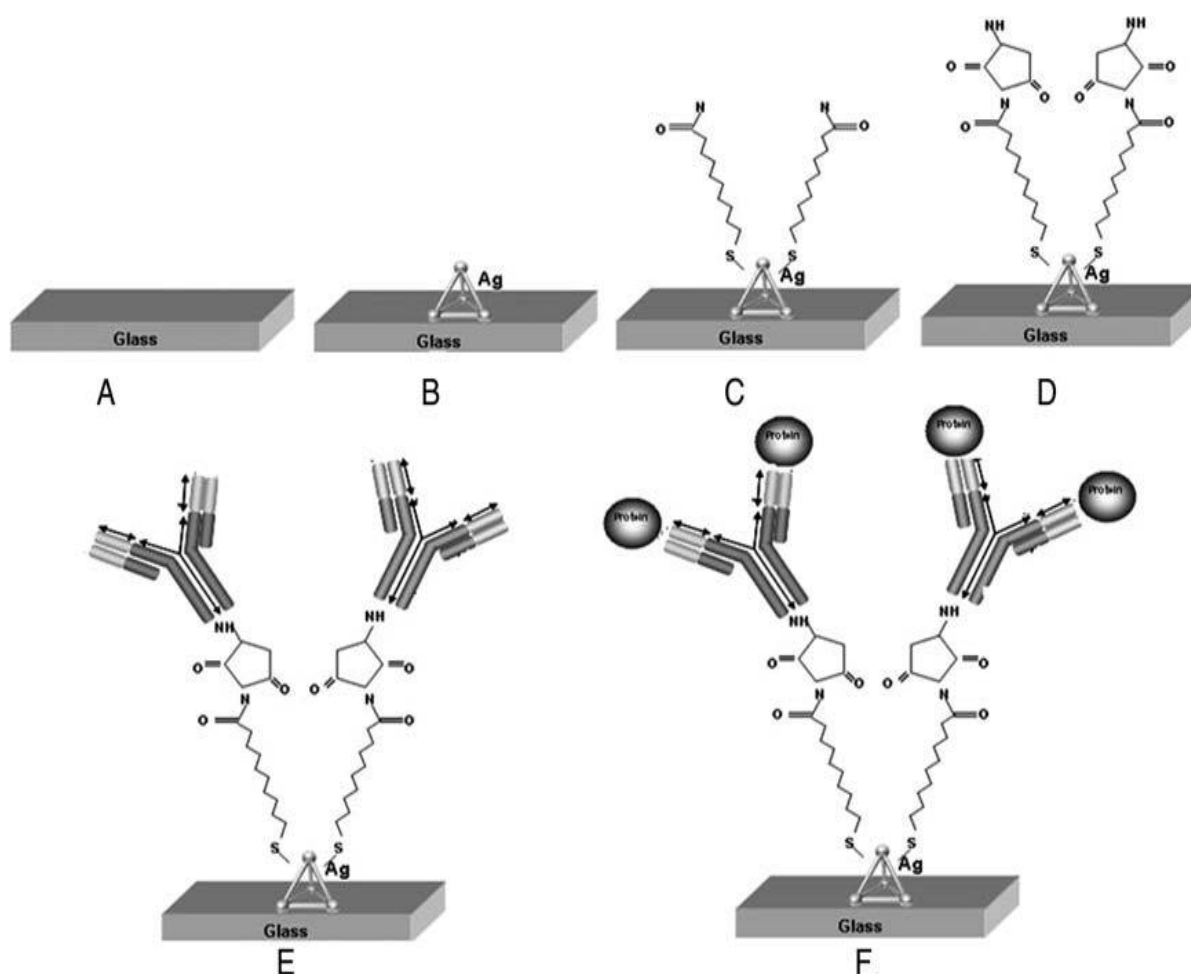
Scheme 1. 10 Design of LSPR nanobiosensor for the detection of microalbuminuria through EDC/NHS cross-linking between anti-albumin antibody and MUA-coated Ag NPs. Figure adapted with permission from Ref 281.

1.3.3.2 *Thiol-ene Click Chemistry*

Recently, click chemistry has emerged as a powerful strategy for the fabrication of bioconjugates, because it has many advantages compared with the conventional method, such as simple reaction conditions, short reaction time, high yields and compatibility with both organic and aqueous solvents.[282] As a representing click chemistry, thiol-ene click reaction (Scheme 1.11) has already been successfully applied in many fields, such as the modification of surfaces,[283] polymers[284] and design of dendrimer structures.[285] Because this reaction could be carried out at mild and biofriendly conditions, it has also been employed for the modification of proteins[286] and the conjugation of biomolecules and inorganic nanomaterials.[287, 288]
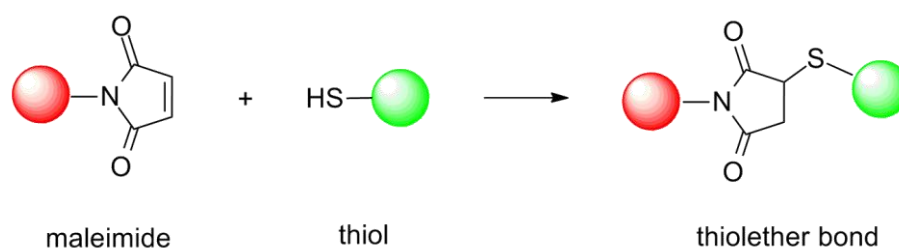
Scheme 1. 11 Click reaction between thiol and maleimide

Li and coworkers employed the combination of amide coupling and thiol-ene click chemistry for the design of targeting drug delivery system through the immobilization of an aptamer, which can specifically interact with nucleolin (NCL, an overexpressed protein on the plasma membrane of several kinds of cancer cells), to mesoporous silica NP (MSN)-based nanocarrier (Scheme 1.12).[287] The phosphonate-modified MSN (MSN-pho) nanocarrier was first reacted with 3-aminopropyltriethoxysilane (APTES) to afford amine-modified MSN (MSN-pho-NH$_2$). MSN-pho-NH$_2$ could undergo amide coupling with sulfosuccinimidyl-4-(N-maleimidomethyl) cyclohexane-1-carboxylate (sulfo-SMCC) to give maleimide-modified MSN, which was then used for the immobilization of thiolated DNA aptamer through the thiol-ene click reaction between the thiol and maleimide functional groups. The resulted drug delivery system was loaded with doxorubicin (DOX), which showed pH-dependent controlled release of DOX in MCF-7 breast cancer cells. This novel targeting strategy might be applied to other delivery systems and enable specific bindings to different cancer cells and increase the dosage efficiency of drugs.
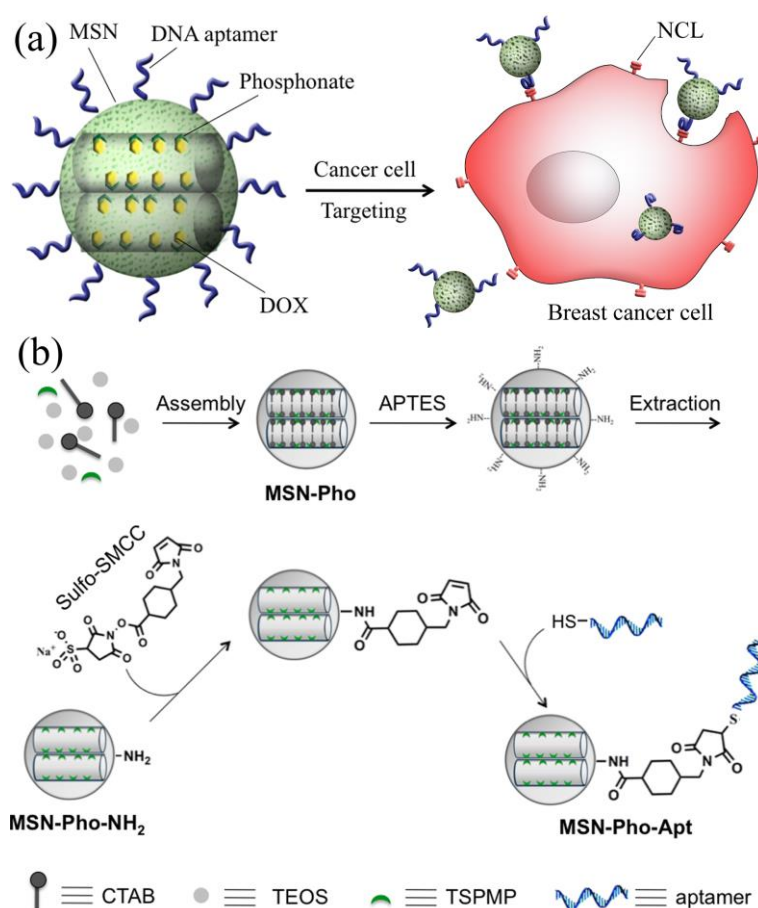
Scheme 1. 12 Schematic illustration of (a) the structure of the DNA aptamer functionalized MSN nanocarriers and the targeted delivery of DOX to breast cancer cells, and (b) the preparation procedure of the targeted delivery system. Figure reprinted with permission from Ref 287. Copyright © 2012 WILEY-VCH Verlag GmbH & Co. KGaA, Weinheim

Mattoussi's group described the preparation of thioctic acid (TA)-polyethylene glycol (PEG)-maleimide (TA-PEG-Mal) stabilized Au NPs, which were used for the conjugation with cysteine-terminated peptides through the click reaction between the thiol functional groups of cysteine and the maleimide on the surface of Au NPs.[289] Lee *et al*. employed maleimide-ethylene-glycol coated Au NPs for the immobilization of thiolated DNA.[288] The DNA strands in the DNA-AuNP conjugates maintained their hybridization ability, and were employed for the detection of target DNA in complex biological samples such as blood serum. Maleimide-functionalized Au NPs were immobilized on the membrane of living cells through the conjugation between maleimide and thiol-ended lipid, enabling the controlled delivery of NPs to the cell membrane, which might be useful for specific cell membrane labeling.[290]

1.3.3.3 Azide-Alkyne Cycloaddition

Azide-alkyne cycloaddition is another mostly used click reaction for the biomodification of NPs, which initially involves Cu(I)-catalyzed 1,2,3-triazole formation between azides and terminal alkynes (Scheme 1.13a).[291] Due to the toxicity of Cu(I) ions to cells and organisms and its ability to mediate protein modifications,[247] Cu(I)-free click reaction was promoted by Bertozzi's group, which involves the use of a highly strained cyclooctyne to react with azide (Scheme 1.13b).[292] Azide-alkyne cycloaddition has been successfully utilized in organic synthesis, polymer chemistry, and biochemistry, because it is a quantitative and robust reaction, it can be performed under mild conditions, and the resulted triazole is chemically stable.[293]
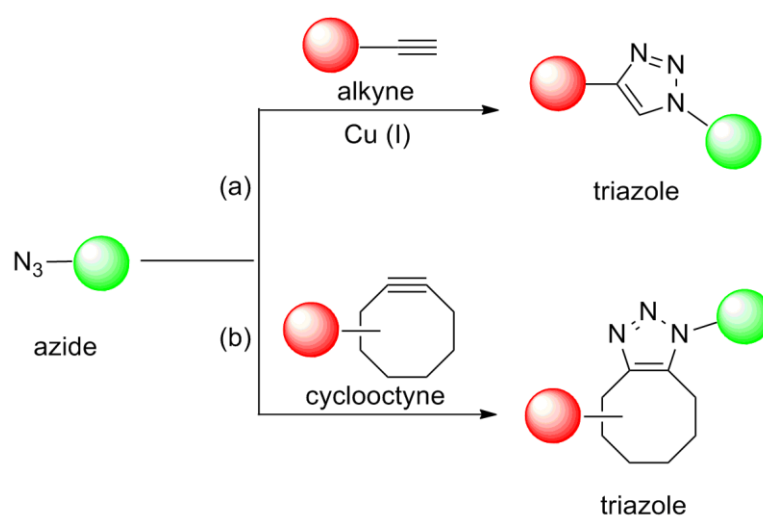
Scheme 1. 13 (a) Copper-catalyzed azide-alkyne cycloaddition; (b) copper-free azide-alkyne cycloaddition

The azide-alkyne cycloaddiction has also been employed for the attachment of biomolecules to the surface of inorganic NPs. For example, water soluble, azide-functionalized Au NPs were employed for the immobilization of acetylene-functionalized lipase through copper catalyzed azide-alkyne cycloaddiction.[294] Alkyne-functionalized DNA oligonucleotides were attached to the surface of azide-modified superparamagnetic iron oxide NPs in the presence of copper sulfate and ascorbic acid.[295] Protein-quantum dots hybrids were prepared through the copper free click reaction between azide-coated CdSe/ZnS quantum dots and cyclooctyne-modified transferrin, and the obtained hybrids retained both the bioactivity of the transferrin and the high fluorescence quantum yield of quantum dots.[296] Controlled assembly of Au NPs was realized through the copper free cycloaddition between azide-DNA-AuNP and dibenzocyclooctyne (DBCO)-DNA-AuNP conjugates (Scheme 1.14), and the yield of clicked Au NPs was 92%.[297] This strategy might be extended to the applications in nanostructure design and assembly of other nanomaterials.

S1: 5' – (C$_6$H$_{12}$S)AAAAAAAACGAGTGCTAAGGATCCGAA*X1*
S2: 5' – *X2*TTCACTGCAGATATCCATTCGAAAAAAAA (C$_6$H$_{12}$S)
S3: 5' – ACACACCGAATGGATATCTGCAGTGAATTCGGATCCTTAGCACTCGACACAC
S4: 5' – GTGTGTCGAGTGCTAAGGATCCGAATTCACTGCAGATATCCATTCGGTGTGT

X1: Azide
X2: Alkyne
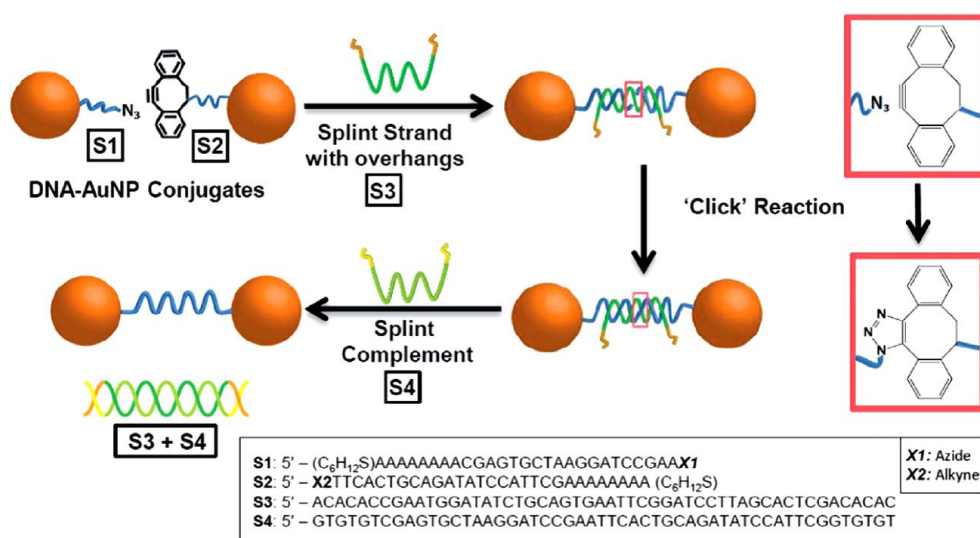
Scheme 1. 14 Illustration of dimer formation using the method of DNA-click chemistry. 3'-azide (S1) and 5'-DBCO (S2) DNA-AuNP conjugates are brought into close proximity through a templating splint strand (S3) with non-complementary overhangs (orange). 'Clicking' occurs immediately after hybridization. Addition of a single DNA strand (S4), fully complementary to S3, results in the removal of S3 through competitive hybridisation, leaving a NP dimer system connected via a single continuous DNA strand. Figure reprinted with permission from Ref 297. Copyright © 2013 the Royal Society of Chemistry

1.3.3.4 Diels-Alder Cycloaddition

Diels-Alder cycloaddition is a highly selective reaction between dienes and dienophiles (Scheme 1.15), which is one of the most useful reactions for organic synthesis. In 1980, Breslow's surprising discovery that aqueous solution could accelerate the reaction[298] had led researchers to utilize it for covalent modification of biomolecules. Diels-Alder bioconjugation of diene-oligonucleotide was first reported by Hill and coworkers in 2001,[299] and since then Diels-Alder reaction has been widely investigated for immobilization and modification of biomolecules.[300, 301]
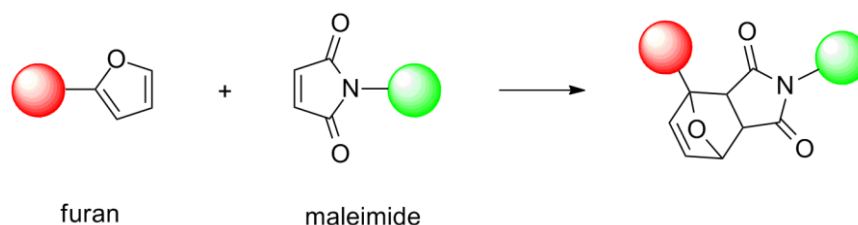
furan   maleimide

Scheme 1. 15 Diels-Alder cycloaddition

Perez *et al*. reported the modification of SiO$_2$-coated Au NPs with maleimide and their surface biofunctionalization with diene-modified DNA through the Diels-Alder cycloaddition

between maleimide and diene.[302] Shi *et al*. demonstrated the use of Diels-Alder cycloaddition for the preparation of immuno-polymeric NPs.[303] Amphiphilic, furan-functionalized copolymers, which could self-assemble to form micellar NPs in aqueous conditions, were employed to react with maleimide functionalized herceptin (anti-HER2) (Scheme 1.16), a therapeutic antibody for the treatment of human epidermal growth factor receptor-2 (HER2) in breast cancer cells. The HER2 targeting tests proves that the mild conditions for Diels-Alder cycloaddition was benefit for the preservation of the high selective binding ability of antibodies, which provide a novel alternative for immunotherapy and targeting delivery.
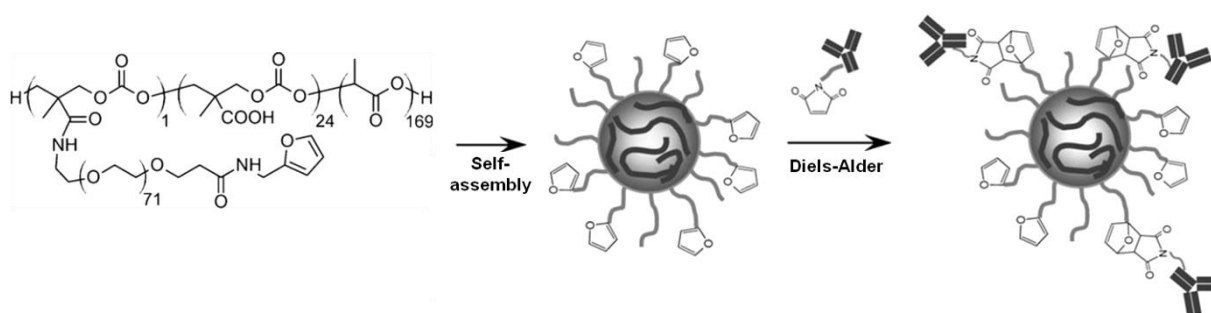
Scheme 1. 16 Schematic representation of the self-assembly of micellar nanoparticles from poly(2-methyl-2-carboxytrimethylene carbonate-*co-D,L*-lactide)-*graft*-poly(ethylene glycol)-furan and Diels–Alder reactions between the polymeric nanoparticles and maleimide-modified antibodies. Scheme adapted with permission from Ref 303. Copyright © 2007 WILEY-VCH Verlag GmbH & Co. KGaA, Weinheim

Besides the methods mentioned above, Staudinger ligation, native and chemoselectrive protein ligation have also been widely used for the biofunctionalization of NPs.[247] Covalent binding procedures can retain the stability and bioactivity of biomolecules after the formation of biomolecule-NP hybrids, which enables the hybrids to be used for the further biological applications or conjugation with other biomolecules.

1.4 Applications of Nanoparticles

As mentioned previously, NPs possess range of fascinating properties, including LSPR, SERS, fluorescence, ROS production and catalytic activity, which enable them to be useful for applications in optical property-based sensors, design of nanodevices and catalysis.[304, 305] In addition, the construction of biomolecule-NP hybrids could integrate the properties both components. The attachment of biomolecules might affect the optical, electrical and chemical properties of NPs, and in the meanwhile NPs might improve the activity and stability of biomolecules or make them robust in different chemical and biological environments, which

make the hybrids suitable materials for sensing, drug delivery, diagnostics, biocatalysis, and nanoassembly.[306, 307]

1.4.1 Biosensing
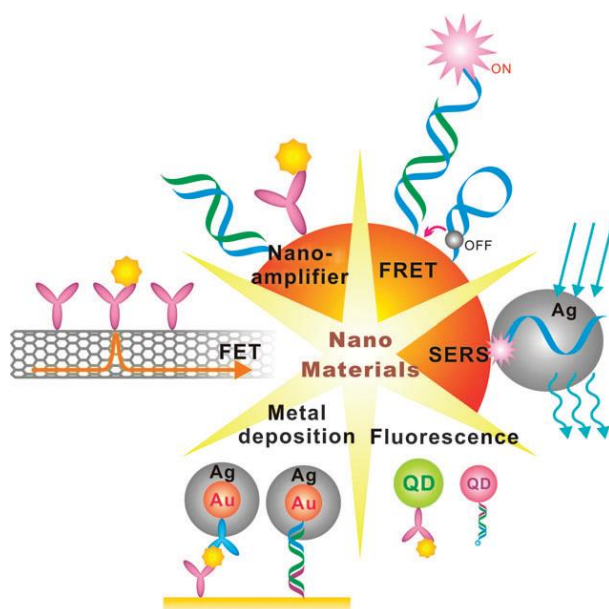
Scheme 1. 17 Schematic illustration for various ultrasensitive biodetection strategies by using biofunctionalized nanomaterials. Scheme reprinted with permission from Ref 309. Copyright © 2010 the Royal Society of Chemistry

Biosensor refers to a self-contained integrated device which is capable of providing specific quantitative or semi-quantitative analytical information using a biological recognition element which is in direct spatial contact with a transducer.[308] The optical properties of metallic NPs, such as LSPR, fluorescent and SERS, could be influenced by the addition of biomolecules or through biomolecule-mediated assembly, which in turn provide the information about the biological species and their interactions (Scheme 1.17).[309] Therefore, the optical properties of metallic NPs have been extensively applied in the design of biosensors for the identification and quantification of biomolecules.

Since the first reports about the modification of Au NPs with oligonucleotides in 1996,[266, 267] such kinds of bionanomaterials have been used as novel tools for the detection of low concentrations of target DNA oligonucleotides. In comparison to Au NPs, Ag NPs have higher molar extinction coefficients,[17] so the change of their optical property is more obvious, which could improve the detection sensitivity. By taking this advantage of Ag NPs, Graham and coworkers designed a sandwich assay to demonstrate that the conjugates of DNA oligonucleiotide and Ag NPs could be used for the detection of target DNA.[17] Ag NPs

modified with two different DNA sequences were used to hybridize with a target DNA which was fully complementary to these two sequences. The hybridization brought the Ag NPs really close and caused the aggregation of Ag NPs, which finally led to the change of the surface plasmon of Ag NPs (Figure 1.28). Due to the larger extinction coefficient of Ag NPs, the minimum detectable concentration of the target DNA was $50\times$ lower than that when Au NPs were used.
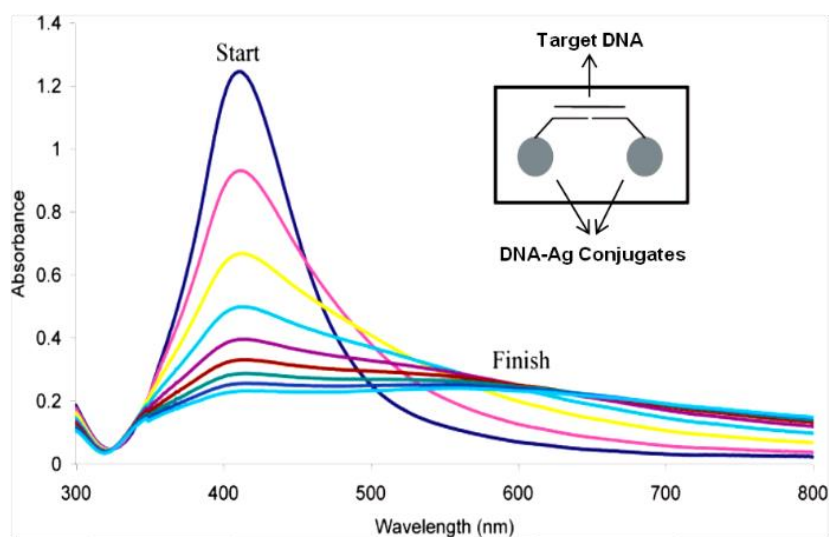
Figure 1. 28 UV-Vis spectra taken every 5 min of DNA-Ag conjugates hybridizing to a fully complementary target oligonucleotide. The inset shows that the conjugates are hybridizing in the "tail-to-tail" juxtaposition. Figure reprinted with permission from Ref 17. Copyright © 2008 American Chemical Society

Graham *et al.* also reported that Ag NPs exhibit much higher enhancement of Raman scattering than Au NPs,[186] thus sensitive detection of the attached molecules could be realized by using Ag NPs as SERS substrates. Figure 1.29 shows a SERS based diagnostic assay for the detection of specific DNA sequences.[310] A dye labeled DNA was used as the SERS primer, which had a self-complementary part. The self-hybridization of the SERS primer would occur in the absence of the target complementary sequence, so the dye molecules could not be absorbed to the surface of Ag NPs due to the electrostatic repulsion between negatively charged DNA and Ag NPs. While in the presence of target *c*DNA, which would form duplex with the SERS primer to prevent its self-hybridization, the dye labeled part of the SERS primer would be free to be absorbed to Ag NPs resulting in the enhancement of SERS signals. Therefore, the combination of SERS and DNA-AgNP conjugates afford a promising method for DNA analysis, which might found applications in single molecule detection and molecular diagnostics.
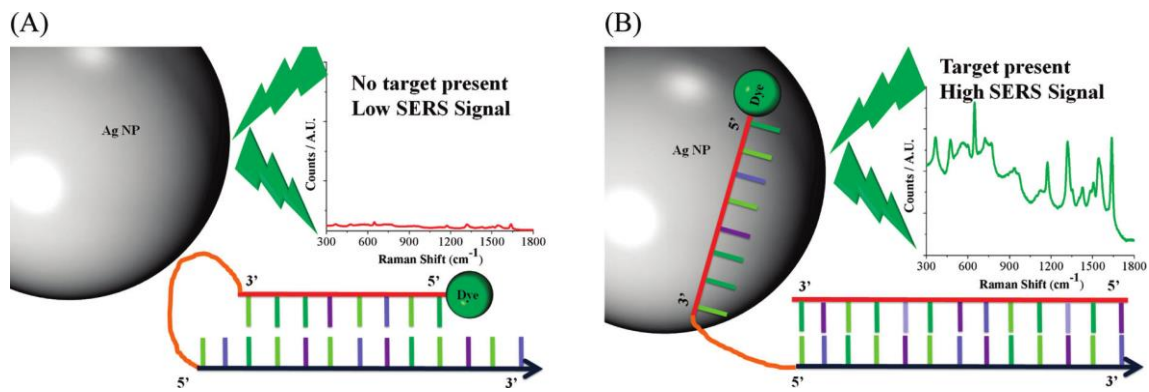
Figure 1. 29 (A) When the complementary target DNA is absent, the SERS primer is closed and predominantly *ds*DNA. The dye does not adsorb onto the negatively charged Ag NP, resulting in a low SERS response. (B) When the target DNA displaces the partly self-complementary region of the SERS primer, which is destabilized using mismatches and consists of a dye labeled DNA region which is then free to adsorb onto the negatively charged Ag NP's surface resulting in a high SERS response. Figure reprinted with permission from Ref 310. Copyright © 2011 American Chemical Society

Niemeyer's group employed difunctional DNA-AuNP (D$_2$-Au) conjugates for the sensitive detection of proteins.[311] Au NPs were functionalized by two different DNA sequences; one was tagged with streptavidin to capture biotinlate antibody immunoglobulin G, while the other was used for the attachment of additional layers of Au NPs through DNA hybridization (Figure 1.30a). The readout signals of the immunoassays for the detection of antigen were recorded by UV-Vis spectroscopy, and the SPR signals of Au NPs at 540 nm were dramatically amplified when additional layers of D$_2$-Au NPs were attached, and the detection limit was 0.1 fmol (Figure 1.30b), which was much sensitive than the controls without the additional layers of Au NPs or with monofunctional DNA-Au NPs (D$_1$-Au).
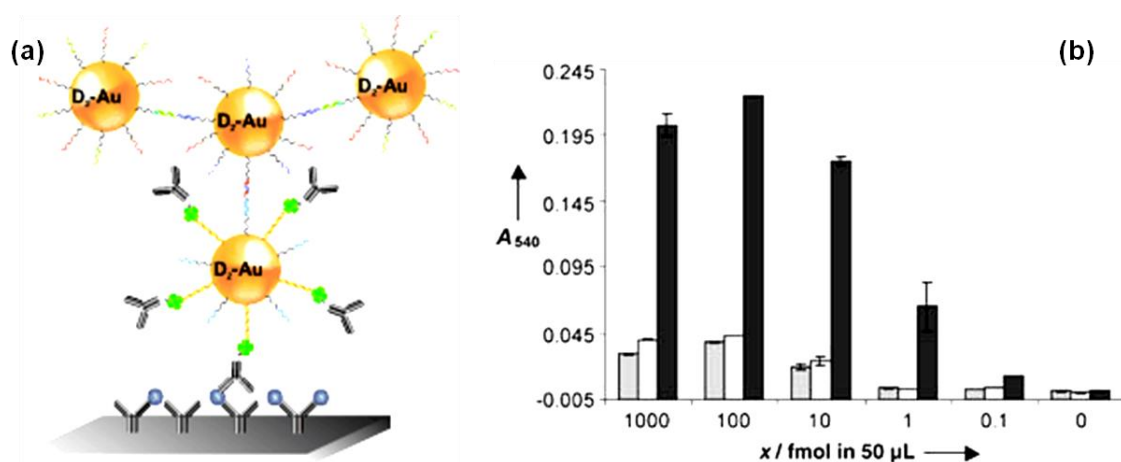
Figure 1. 30 (a) Design of antibody-D2-Au hybrid system for the detection of antigen, and (b) UV-Vis signal intensities of the immunoassays using D$_1$-Au (grey), D$_2$-Au (white) and multilayers of D$_2$-Au (black). Figure adapted with permission from Ref 311. Copyright © 2005 WILEY-VCH Verlag GmbH & Co. KGaA, Weinheim

In addition, Au NPs functionalized with a DNA detection sequence and horseradish peroxidase (HRP) were used for target DNA detection.[312] In the presence of target DNA, HRP confined at the surface of Au NPs could catalytically oxidize the additional substrate and generate optical signals that reflected the quantity of target DNA. Furthermore, Cu@Au core-shell NPs functionalized with DNA were used to detect the target DNA using an electronical assay.[313] The DNA hybridization process could cause the oxidative dissolution of Cu, and the amount of the released Cu^{2+} ions could be determined by sensitive anodic stripping voltammetry, which in turn enabled the quantification of target DNA. Recently, *ds*DNA-AuNP conjugates and conjugated polyelectrolytes (CPEs) with different fluorescent emissions and charges were employed to construct hybrid sensors for the detection of protein-DNA interactions, which was based on the emission change of CPEs upon the electrostatic interaction between DNA-AuNP, protein and CPEs.[314] Due to the highly fluorescence quenching ability of Au NPs, the hybrid sensors are highly sensitive and accurate in the determination of DNA-protein binding constant and stoichiometry.

Metallic NPs, with their unique optical and chemical properties, have been widely explored as sensor platforms, which have opened a new horizon for the development of novel diagnostic and therapeutic techniques and methodologies. However, more efforts are still needed to address the remained issues before using NPs for real clinical applications, for example, the massive production of NPs, the toxicity effects of NPs on cells, tissues, and organism, and the optimization of the sensitivity and compatibility of NP-based sensors.[315, 316]

1.4.2 Drug Delivery

Targeting drug delivery in disease-specific area such as cells and tissues is emerging as a novel and powerful technology for medical treatment.[317] Nanomaterials, whose sizes fall into the similar range as biomolecules, have been widely explored as carriers for the delivery of nucleic acids, proteins and drugs.[318, 319] In particular, gold nanomaterials have been studied extensively in biodiagnostics, gene regulation, and nanomedicine, because they are chemically inert and normally non-toxic, which make them suitable for clinical applications.[320-322]

Mirkin's group has been working on the design of polyvalent oligonucleotides Au NPs conjugates as delivery systems.[320, 323] For instance, paclitaxel (PTX), an active chemotherapeutic agent for the treatment of cancer, was attached to Au NPs through a fluorophore modified oligonucleotide (Figure 1.31).[320] The resulting drug delivery system enhanced the solubility of PTX in aqueous solution, and the drug efficiency of PTX-

DNA@Au conjugates was higher than that of free PTX, especially in PTX-resistant cell lines. In addition, the fluorophore labeled drug delivery system enabled the tracking of the conjugates and the visualization of intracellular drug uptake.
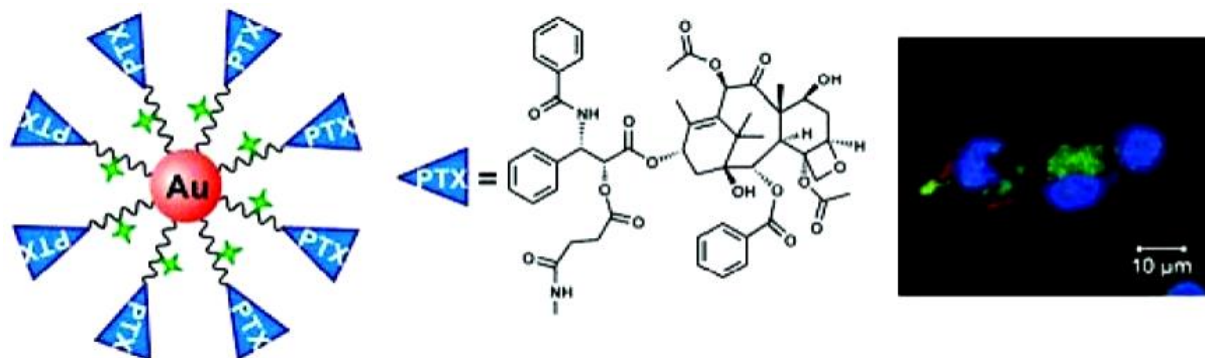
Figure 1. 31 Fluorophore labeled PTX-DNA@Au drug delivery system and the confocal image of intracellular uptake of the fluorescent PTX-DNA@Au conjugates. Figure reprinted with permission from Ref 320. Copyright © 2011 American Chemical Society

Recently a novel, efficient, pH-triggered targeting drug delivery method was reported by employing the conjugates of a proton-fuelled DNA (PF-DNA) and gold NPs (GNP) as drug nanocarrier.[324] pH responsive systems could be useful for targeting delivery is because the physiological pH of healthy tissues is ~7.4, while the pH value of disease parts, such as tumors, is often very low. This study investigated the controlled release of DOX by using PF-DNA-GNP nanocarrier, which revealed that PF-DNA could stably bind to DOX at pH 7.4 and only release DOX when the pH of the environment decreased to < 5.3 (Scheme 1.18). The intracellular uptake tests of the PF-DNA-GNP nanocarrier showed that no DOX was released in the cell culture media, and the drug release happened only in the acid environment of HeLa cells. It was also found that the PEGylation of the PF-DNA-GNP nanocarrier could reduce the non-specific serum protein adsorption, which facilitated the effective targeting delivery of DOX into cancer cells.
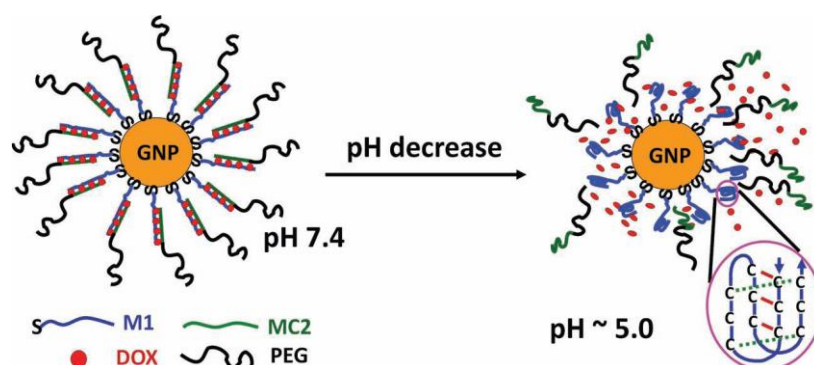
Scheme 1. 18 Principle of the PF-DNA-GNP for pH-triggered drug delivery: at normal physiological pH (7.4), DOX is intercalated stably in the M1/MC2 duplex on the GNP; only when the environment becomes weakly acidic (e. g. pH < 5.1), M1 forms i-motif which triggers the dissociation of MC2 and the consequent release of DOX. Inset showing the formation of i-motif by the M1 i-motif domain. Figure reprinted with permission from Ref 324. Copyright © 2013 WILEY-VCH Verlag GmbH & Co. KGaA, Weinheim

Khandelia et al. reported the fabrication of a versatile nanocarrier using agglomerates of Au NPs and protein, which was obtained by the electrostatic immobilization of positively charged lysozyme (Lyz), a low molecular weight protein targeting specifically to renal cancer cells, onto negatively charged citrate-Au NPs.[325] The Lyz-Au agglomerates were used for the loading of DOX, and the drug loaded nanocarriers were then coated with albumin to stabilize the whole system and to facilitate their uptake by cancer cells. Apoptosis tests showed that the drug-loaded nanocarriers could release DOX within cells and lead to cell death. After treading the cancer cells with the nanocarriers loaded with the highest concentration of DOX (0.84 μg/mL), the cell viability was reduced to 35%, which was more efficient than the cell viability of 74% when free DOX was used (Figure 1.32).
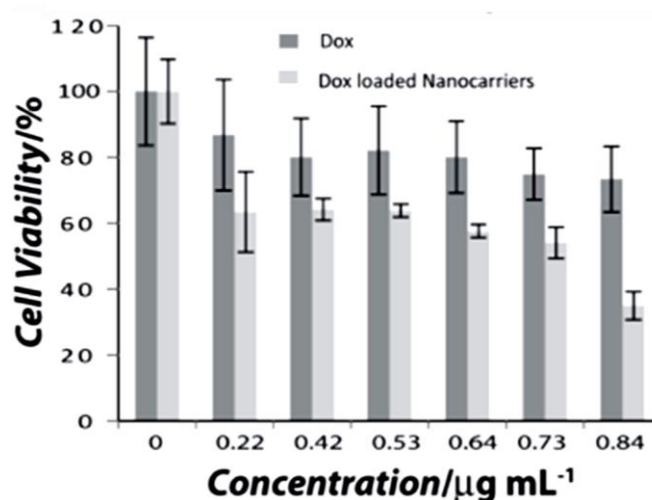
Figure 1. 32 Cell viabilities using free Dox and Dox-loaded nanocarriers at varying Dox concentrations. Figure adapted with permission from Ref 325. Copyright © 2013 WILEY-VCH Verlag GmbH & Co. KGaA, Weinheim

Polymer-coated Fe_3O_4 magnetic NPs were used for the immobilization of anticancer drug epirubicin and targeted to the brain parenchyma using the synergistic strategies of focused ultrasound and magnetic targeting.[326] Ag NPs were prepared using ciprofloxacin, a antibacterial drug, through a one-pot procedure, and the drug-coated Ag NPs demonstrated a time-dependent drug release ability.[327] Highly water soluble TiO_2 NPs were loaded with DOX through both non covalent interaction and covalent conjugation, and used for target drug delivery towards C6 glioma cells.[328] The tunable surface area of NPs enables the efficient loading of drugs, and the incorporation of drugs into NPs could prevent drugs from degradation.[329] In comparison to tradition drugs, NPs provide a more efficient, selective and controllable path for targeting drug delivery.

1.4.3 Enzyme Mimetics

In the past decade NPs have attracted lots of attention as potential enzyme mimetics due to their stability under different reaction conditions, large number of functional group on the surface and inherent catalytic properties.[330, 331] Particularly interesting is their use in bioinspired catalytic processes where they could act either as enzyme replacing catalytic species or as enzyme activators.

Fe_3O_4 magnetic NPs were discovered to possess an intrinsic enzyme-mimetic activity similar to that in natural peroxidases.[332] RuO_2 NPs have been shown to have strong catalase/peroxidase activity, which was even superior to some natural enzymes such as catalase from *A. niger*.[333] CeO_2 NPs with strong pH-dependent oxidase-like activity have been employed for the oxidation of a range of substrates.[334] Au NPs demonstrated catalase and superoxide dismutase activities, which could be utilized as enzyme mimetics to catalyze the decomposition of H_2O_2 and superoxide radicals.[335] Cu NPs were proved to have ROS generation ability, which could be employed for the activation of peroxidase enzymes and the following oxidation of nonfluorescent substrate 2, 7-dichlorodihydrofluorescein to fluorescent 2, 7-dichlorofluorescein.[76] Instead of serving as the activator for peroxidase enzymes, Cu nanocrystals (NCs) were also found to have intrinsic peroxidase-like activity, and could catalyze the oxidation of the organic substrate 3,3',5,5'-tetramethylbenzidine (TMB) by H_2O_2 into a blue dye.[336] As demonstrated in Scheme 1.19, the peroxidase-like activity of Cu NCs could be utilized for the colorimetric detection of glucose, which could turn oxygen into H_2O_2 in the presence of glucose oxidase. It was also found that the activity of Cu NCs was higher than that of horseradish peroxidase at neutral pH, which makes them favourable for biological applications.
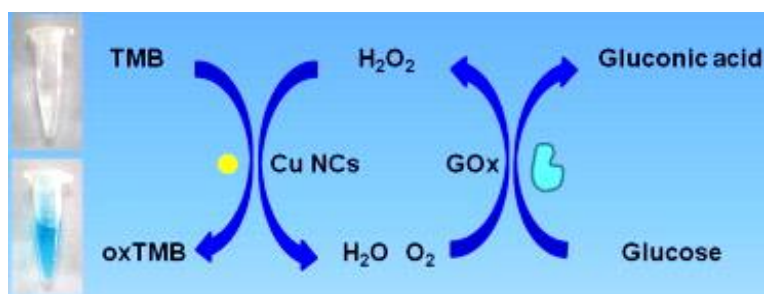
Scheme 1. 19 Schematic illustration of colorimetric detection of glucose by using glucose oxidase (GOx) and Cu NCs catalyzed colour reaction. Figure reprinted with permission from Ref 336. Copyright © 2013 Elsevier

Semiconductor NPs have also been used as enzyme mimetics. In an attempt to design novel enzyme-like catalysts, Slocik *et al.* prepared peptide coated CdS-Pt nanocomposite, which outperformed nitrate reductase enzyme by more than 23 fold.[337] CdS quantum dots and were used as photosensitive activators of P450[208] and peroxidase enzymes[338] enabling temporal and spatial control over enzymatic activity. TiO_2 nanorods exhibited ROS production ability, and were employed for the activation of horseradish peroxidase and the subsequent oxidation of nonfluorescent Amplex Red to fluorescent resorufin.[339] TiO_2 nanotube arrays were found to have peroxidase-like activity, and demonstrated catalytic activity towards the oxidation of different substrates (Figure 1.33), including TMB, 2,2'-azino-di(3-ethylbenzthiazoline-6-sulfonate (ABTS), and o-phenylenediamine (OPDA).[340]
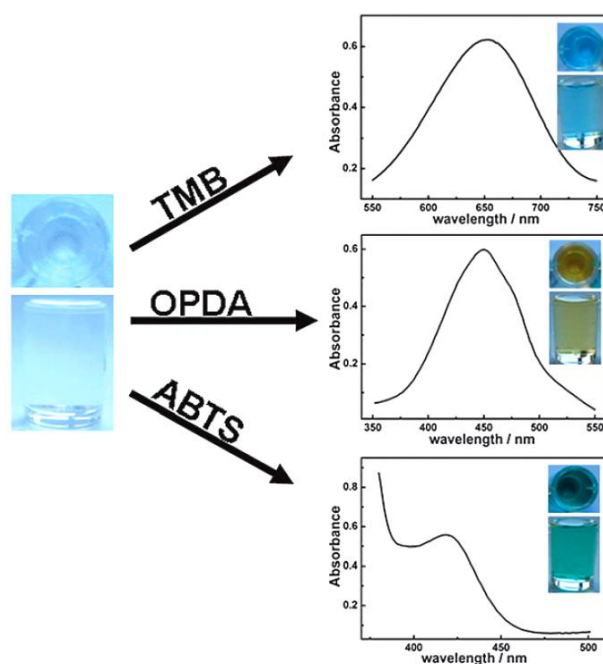
Figure 1. 33 The absorption spectra and digital photos of colorimetric reaction of TMB, OPDA and ABTS oxidation by H_2O_2 with TiO_2 nanotube arrays as the catalysts. Figure reprinted with permission from Ref 340. Copyright © 2013 the Royal Society of Chemistry

NPs as enzyme mimetics have exhibited higher stability than natural enzymes in many harsh conditions, such as different pH and temperatures.[330] In addition, in comparison to natural enzymes, NPs are easier to be prepared and purified, which overcome the disadvantages of the complicated separation and purification of enzymes.[341] Although works still need to be done to tailor the enzyme mimetic properties of nanomaterials and improve their specificity and selectivity, NP enzyme mimetics have great potentials to be applied in bioassays, catalysis and environmental detections.[341]

1.5 Research Objectives

Significant advances have been made in the research field of synthesis and application of metallic and semiconductor NPs as well as their hybrids with biomolecules, there will be an increasing need for the development of new, mild and efficient methods for their preparation, and the thorough exploration of their novel applications. In order to make the nanomaterials compatible and applicable in different chemical and biological environments, one of the most important things is to make them multifunctional and controllable.

Due to the ease of oxidation upon air exposure, the reproducible synthesis of stable and pure Ag and Cu NPs under aqueous conditions is still of great importance. One of the crucial factors to achieve this is the choice of proper capping agents for the protection and stabilization of NPs' surface, as bare Ag and Cu NPs can be oxidized and tend to aggregate to reduce their surface energy, which could severely influence their chemical, optical and catalytic properties. **Therefore, one of the focuses for this thesis is the surface modification and functionalization of Ag and Cu NPs in aqueous solutions employing different strategies and surface capping agents.**

Water-soluble, monodispersed and stable Ag NPs were successfully synthesized, and the plasmonic and fluorescent properties of the obtained Ag NPs were investigated. In addition, **the Ag NPs were used for the construction of DNA-AgNP conjugates through ligand exchange or mild Diels-Alder strategy, which was then employed for the assembly with Au NPs or the design of enzyme-AgNP hybrids through DNA-directed immobilization.** The activity of the obtained enzyme-AgNP hybrids have been compared with the free enzymes using a fluorescent enzymatic assay.

Unlike Au and Ag NPs, the potential applications of Cu NPs have not yet been fully tapped due to the ease of surface oxidation upon exposure to air. It is worthwhile to explore the applications of Cu NPs, because copper possess interesting properties such as SPR, catalytic activity and antibacterial properties, and it is much cheaper than Au and Ag, so it is

more suitable for large scale industrial production and applications. **Within this thesis, the preparation of stable Cu NPs in aqueous solutions using ascorbic acid and dopamine-based linkers was explored. The as-prepared Cu NPs have been found to possess ROS production ability, and could be employed as powerful enzyme mimetics**, **such as the activation of peroxidase enzyme or the mimicking of superoxide dismutase.** Due to the excellent ROS generation ability, the obtained Cu NPs could also be utilized as catalysts for the degradation of harmful fluorescent dyes and antibiotics.

Knowing that the obtained stable Cu NPs are able to produce ROS and have catalytic activity, we were interested in building the nanocomposites of Cu NPs with TiO$_2$ nanomaterials using clickable dopamine linkers, which have strong affinity to both Cu and TiO$_2$. As excellent photocatalysts, TiO$_2$ nanomaterials have already been proven to possess strong ROS generation ability under UV irradiation. Therefore, the combination of TiO$_2$ and Cu might afford novel, highly active and efficient nanomaterials that are useful for enzyme mimetics and environmental applications.

Chapter 2

Functionalization of Silver Nanoparticles

2 Functionalization of Silver Nanoparticles (Ag NPs)

Functionalization of NPs with appropriate molecules has become a useful way to improve their stability and compatibility, and facilitate their conjugation with drugs, polymers, organic compounds and biomolecules.[342] In particular, conjugation of biomolecules to the surface of NPs has made them applicable in sensing, delivery, catalysis, and nanostructure assemblies,[246-248] and there is an increasing need for novel, more efficient and milder methodologies for their preparation. Towards our goal of designing bio-AgNP hybrids, several different methods were attempted to prepare monodispersed, water soluble and stable Ag NPs, which could be used for the further immobilization of biomolecules.

2.1 Synthesis and Properties of Ag NPs

2.1.1 Oleylamine (OA)-Coated Ag NPs

As mentioned in chapter 1, a number of approaches, including citrate reduction, polyol method, thiol stabilization, seed-mediated growth and photo-induced strategy, have been developed for the preparation of Ag NPs with different sizes and morphologies.[29-33] Among all the methods, thermal decomposition is one of the most reproducible and efficient methods for the synthesis of monodispersed NPs with high crystallinity and uniform shapes.[83]
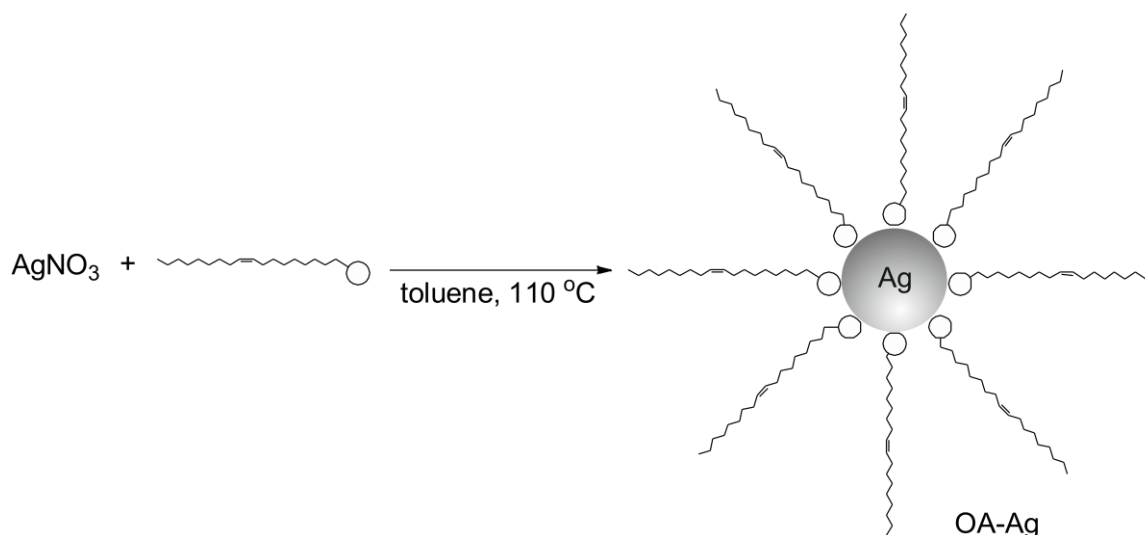
Scheme 2. 1 Schematic illustration for the synthesis of OA-coated Ag NPs

Herewith, in order to obtain monodispersed Ag NPs, a modified thermal decomposition method was first employed for the preparation Ag NPs.[343] Oleylamine (OA)-coated Ag NPs

were synthesized in toluene through the thermal decomposition of AgNO$_3$ at 110 $^{\circ}$C (Scheme 2.1). From the UV-Vis spectrum (Figure 2.1a), the plasmonic absorption of Ag NPs at 425 nm can be observed, and the TEM image (Figure 2.1b) shows that quasi-spherical Ag NPs with an average diameter of 14.9 nm were obtained. In order to use the Ag NPs for the further biofunctionalization with solvent-sensitive biomolecules such as DNAs and proteins, they need to be dispersible in aqueous solutions. To achieve that, ligand exchange was performed by ultrasonicating the mixture of OA-coated Ag NPs and 3-mercaptopropionic acid (MPA) for 30 min. After washing the NPs with cyclohexane and ethanol, they could be easily resuspended in water. However, TEM image shows that the ligand exchange process has led to the agglomeration of Ag NPs (Figure 2.1c), which was not desirable for the further uniform surface functionalization.
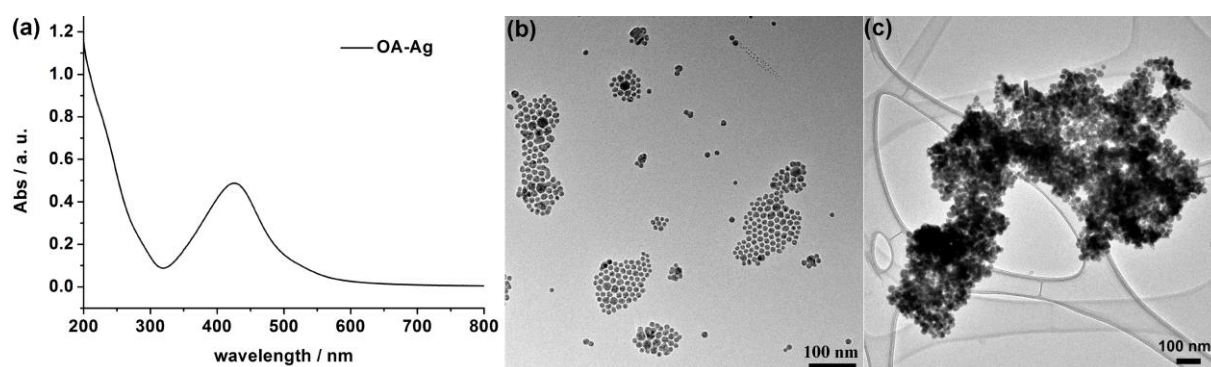
Figure 2. 1 (a) UV-Vis spectrum and (b) TEM image of OA-coated Ag NPs; (c) TEM image of MPA-coated Ag NPs after ligand exchange

2.1.2 Polyacrylic Acid (PAA)-Coated Ag NPs
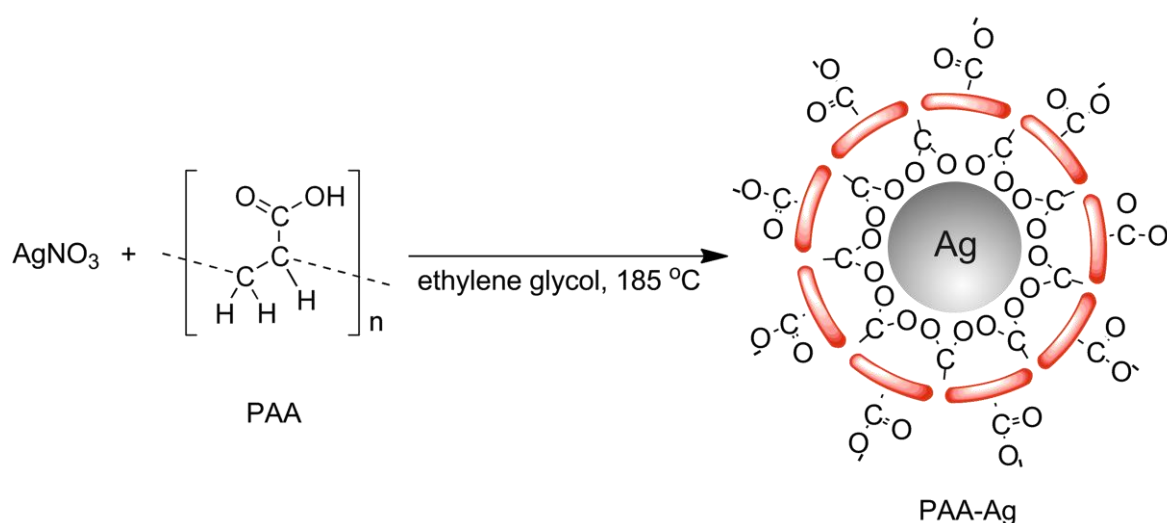
Scheme 2. 2 Schematic illustration for the synthesis of PAA-coated Ag NPs

Since it was observed that the phase transfer of Ag NPs from hydrophobic to hydrophilic phase through ligand exchange could lead to the aggregation of Ag NPs, we attempted to prepare Ag NPs directly in aqueous solutions. To achieve that, hydrophilic polyacrylic acid (PAA) was chosen as the surface stabilizer for Ag NPs, and ethylene glycol was used as both the solvent and the reducing agent (Scheme 2.2).[147] The reaction was performed at 185 °C, and aliquots were extracted from the main solution after 15 and 30 min to see if the reaction time would affect the size and optical properties of the obtained Ag NPs. After washing the NPs thoroughly and neutralizing the carboxylic groups on the NPs' surface, the NPs were finally redispersed in water.
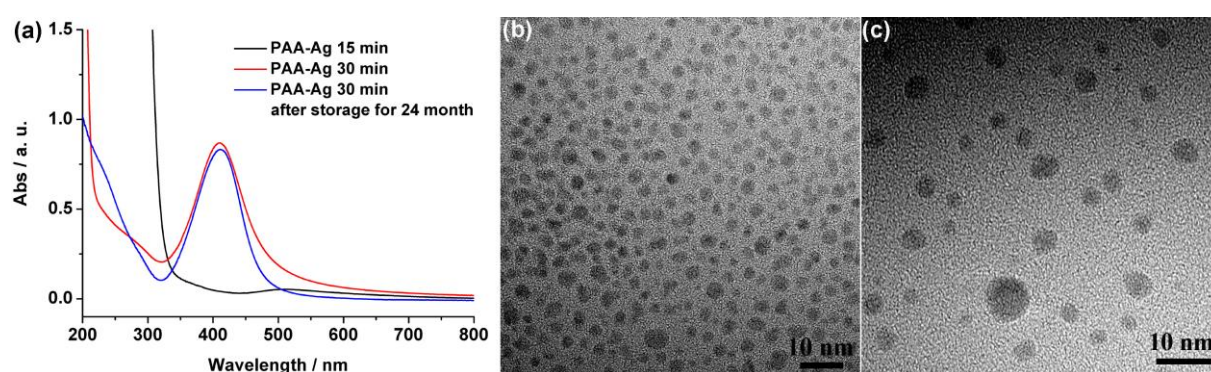
Figure 2. 2 (a) UV-Vis spectra of PAA-coated Ag NPs; (b) and (c) TEM images of PAA-coated Ag NPs obtained after 15 min and 30 min, respectively

As can be seen from the UV-Vis spectra (Figure 2.2a), the plamonic absorption for Ag NPs obtained after 15 min was really weak indicating that the NPs were very small. As mentioned before in 1.2.1, the absorption of NPs smaller than 5 nm could become weak and broad, and it could disappear completely when the size decreases to less than 2 nm.[154] The small size of Ag NPs (15 min) was also confirmed by the TEM image (Figure 2.2b), which showed that the average diameter of the Ag NPs obtained after 15 min was ~2.8 nm. However, Ag NPs extracted after 30 min, whose size was around 4.5 nm (Figure 2.2c), showed a well-defined absorption peak at 410 nm. The concentration of the PAA-Ag NPs (30 min) calculated using the extinction coefficient $\varepsilon_{410\ nm} = 7.1 \times 10^8$ M^{-1} cm^{-1} was ~67 nM,[251] and the NPs could be stable for 24 month as indicated by the UV-Vis spectrum in Figure 2.2a.

Following the successful preparation of stable spherical PAA-coated Ag NPs, the biofunctionalization of PAA-Ag NPs with DNA oligonucleotides would be performed, and the obtained DNA-AgNP conjugates were used for the assembly with Au NPs through DNA hybridization, which will be discussed in 2.2.1.

2.1.3 Benzotriazole (BT)-Coated Ag NPs

Benzotriazole with its complex forming triazole moiety, is considered to be one of the most effective corrosion inhibitors for copper and silver.[344, 345] Graham and colleagues have already successfully employed its Ag complexing ability to design a number of benzotriazole derivatives such as azo dyes to be used as excellent SERS labels.[346, 347]

2.1.3.1 *5-amino-benzotriazole (5-amino-BT)-Coated Ag NPs*
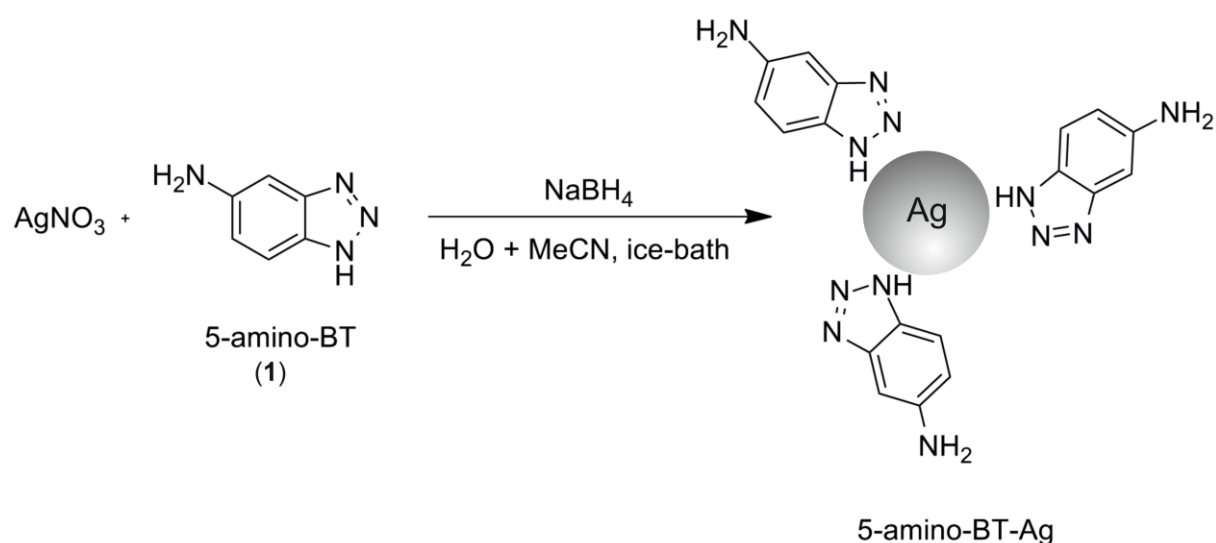
Scheme 2. 3 Schematic illustration for the synthesis of 5-amino-BT-coated Ag NPs

In order to investigate if benzotriazole derivatives could be directly employed for the preparation of Ag NPs, commercially available 5-amino-benzotriazole (5-amino-BT, **1**) was firstly used to synthesize Ag NPs through a simple one-pot procedure (Scheme 2.3). 5-amino-BT and AgNO$_3$ were dissolved in the mixture of H$_2$O and acetonitrile (MeCN) (V$_{H2O}$: V$_{MeCN}$ = 3: 2), and well mixed in an ice-bath for 1 h to ensure the chelating balance, following by the addition of the reducing agent NaBH$_4$. The reaction was stopped after 1 h, and the as obtained solution was directly used for UV-Vis (Figure 2.3a) and TEM characterization (Figure 2.3b). Due to the small size of the as-synthesized Ag NPs (~2.9 nm) (Figure 2.3c), there was no obvious absorption peak in the UV-Vis spectrum. The obtained Ag NPs were monodispersed, which proves that benzotriazole could well stabilize the surface of Ag NPs and prevent their aggregation.
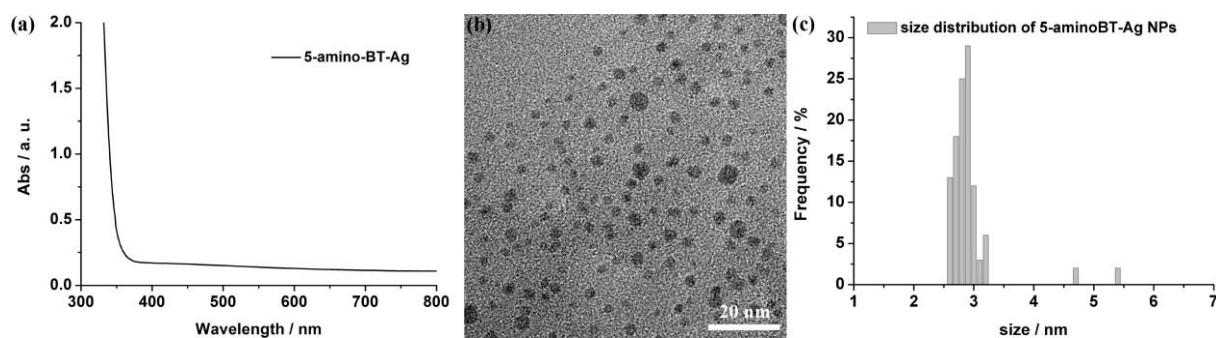
Figure 2. 3 (a) UV-Vis spectrum, (b) TEM image and (c) size distribution of 5-amino-BT-coated Ag NPs

2.1.3.2 *Benzotriazole-Maleimide (BTM)-Coated Ag NPs*

The above results proved that benzotriazole could be employed directly as a capping agent for the preparation of monodispersed Ag NPs. In order to facilitate the further surface functionalization of Ag NPs and avoid the use of additional coupling reagent, a bifunctional linker benzotriazole-maleimide (BTM, **4**) was designed. It has a triazole moiety on the one side, which could form stable complex with Ag, and on the other side a maleimide functional group, through which Ag NPs could be modified using bio-friendly, fast and mild methodologies, such as Michael addition and Diels-Alder cycloaddition.[303, 348]
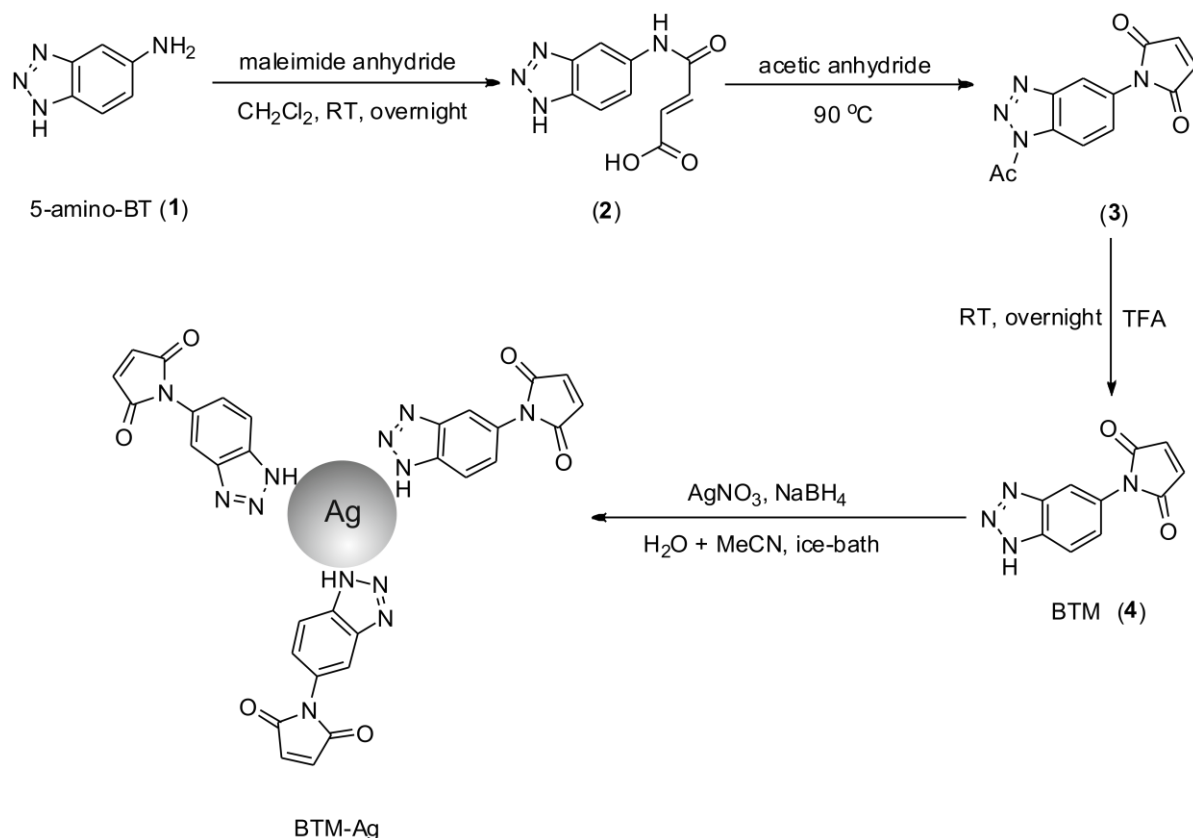
Scheme 2. 4 Schematic illustration for the synthesis of BTM (**4**) and the preparation of BTM-coated Ag NPs

BTM (**4**) was synthesized by the ring closure of 3-(1*H*-benzotriazol-5-ylcarbamoyl)acrylic acid (**2**) (Scheme 2.4) using the protocol reported by Graham *et al.*,[344] and then employed for the preparation of BTM-coated Ag NPs using the similar reaction conditions as that for the preparation of 5-amino-BT-coated Ag NPs (Scheme 2.4). TEM image shows that Ag NPs with average diameter of ~3.1 nm were obtained (Figure 2.4b and c), which resulted in the weak plasmonic band in the UV-Vis spectrum (Figure 2.4a).
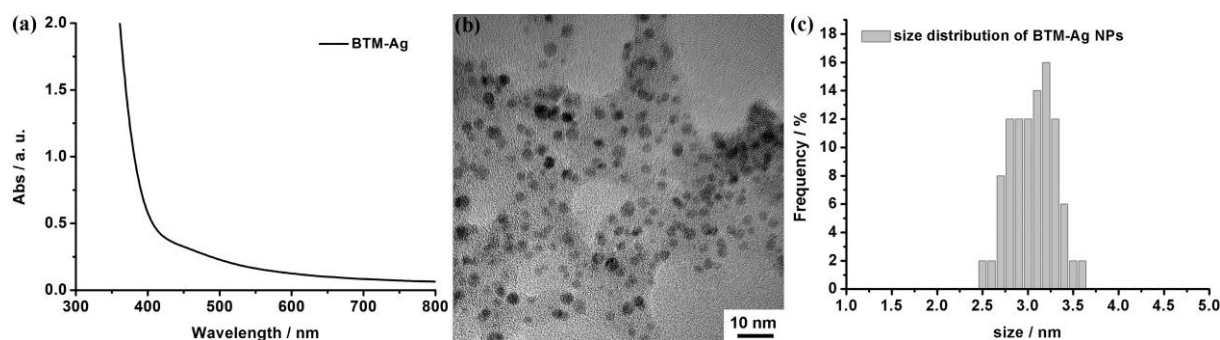
Figure 2. 4 (a) UV-Vis, (b) TEM image and (c) size-distribution of BTM-coated Ag NPs

Because there was no obvious absorption of Ag NPs, so it was difficult to calculate the concentration of Ag NPs according to the extinction coefficient. Therefore, we estimated the concentration of Ag NPs according to the amount of the precursor AgNO$_3$ and the size of the obtained NPs, which could be measured from the TEM images.[349] The following equations were used for the estimation of Ag NPs' concentration, where V stands for volume, N for number, R for radius, N$_A$ for Avogadro's constant, and c for concentration.

Equation 2.1 $\quad V_{cluster} = NV_{atom}$

Equation 2.2 $\quad \frac{4}{3} \pi (R_{cluster})^3 = N \frac{4}{3} \pi (R_{atom})^3$

From the TEM image the average radius of Ag NPs (~1.55 nm) could be known (Figure 2.4b and c), and the radius of Ag atom is 0.150 nm, so the number of Ag atoms per NP was:

Equation 2.3 $\quad N = (R_{cluster}/R_{atom})^3 = ((1.55 \times 10^{-9})/(0.150 \times 10^{-9}))^3 = 1215$

The amount of NPs produced by the reduction of 20 mL solution of AgNO$_3$ (0.1 mM) could be estimated as follows. First, the amount of the precursor AgNO$_3$ was:

$$\text{Moles of AgNO}_3 = 20 \times 10^{-3} \times 0.1 \times 10^{-3} = 2 \times 10^{-6} \text{ mol}$$

And the number of Ag atoms in the solution could be calculated by:

Equation 2.4 $\quad N_{atom} = \text{Moles of AgNO}_3 \times N_A = 2 \times 10^{-6} \times 6.022 \times 10^{23} = 1.20 \times 10^{18}$

So the number of Ag NPs produced by 2×10^{-6} mol AgNO$_3$ was:

Equation 2.5 $\quad N_{NP} = N_{atom}/N = 1.20 \times 10^{18}/1215 = 9.88 \times 10^{14}$

Therefore, the final concentration of the Ag NPs was 82 nM, which was estimated by：

Equation 2.6 $\quad c_{NP} = \dfrac{N_{NP}/N_A}{V_{Solution}} = \dfrac{9.88 \times 10^{14}/6.022 \times 10^{23}}{20 \times 10^{-3}} = 82 \times 10^{-9} \text{ mol} \cdot \text{L}^{-1}$
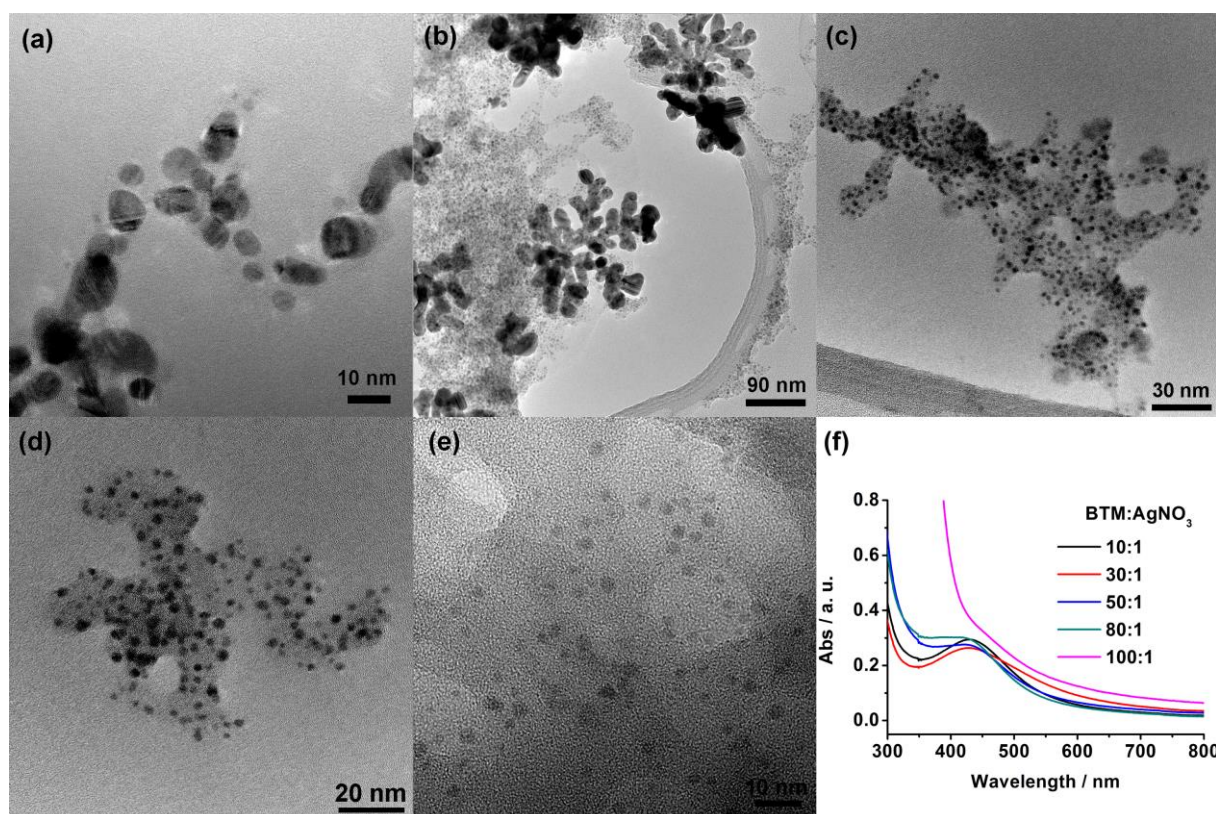
Figure 2. 5 (a-e) TEM images and (f) UV-Vis spectra of BTM-coated Ag NPs synthesized by using different molar ratios between BTM and AgNO$_3$: (a) 10:1, (b) 30:1, (c) 50:1, (d) 80:1 and (e) 100:1

In order to find out if the amount of the surface stabilizer would affect the morphology and the size of Ag NPs, different molar ratios between the capping agent BTM (**4**) and the

precursor $AgNO_3$ (10: 1, 30: 1, 50: 1, 80: 1 and 100: 1) were used for the synthesis of Ag NPs. As shown in the TEM images (Figure 2.5a-e), when n_{BTM}/n_{AgNO_3} was 10: 1, the average diameter of the obtained Ag NPs was around 10 nm, which was three times bigger than the Ag NPs obtained at ratio 100: 1 (~3.1 nm), because the existence of large amount of ligands could coat the surface of NPs and prevent their further growth.[350] Interestingly, when ratio 30:1 was used, dendrite nanostructures as well as spherical NPs could be observed in the TEM images, but the dendrites nanostructures disappeared upon the increase of the amount of BTM (**4**), leaving only spherical Ag NPs, which indicates that the larger amount of available ligands could stabilize the surface of Ag NPs, prevent them from agglomeration, and thus help to avoid the formation of dendrite nanostructures.[350] The morphology and size change of BTM-coated Ag NPs was also confirmed by their UV-Vis spectra (Figure 2.5f). Well-defined plasmonic bands of Ag NPs could be observed at 420 nm when the molar ratio between BTM and $AgNO_3$ was 10: 1 and 30: 1. However, when the ratio was increased to 50: 1 and 80: 1, the plasmonic peak of Ag NPs became broad and weak, and no plasmonic absorption of Ag NPs could be observed for ratio 100: 1 indicating the existence of very small NPs.

2.1.4 Fluorescence of Ag NPs

It has been reported that ultra-small metallic NPs have excellent fluorescent properties, and they have already been explored as fluorescent probes for bioimaging and therapeutic studies.[351, 352] Since the obtained PAA-Ag NPs and BTM-Ag NPs were very small, their fluorescent properties were explored.

2.1.4.1 Fluorescence of PAA-Coated Ag NPs
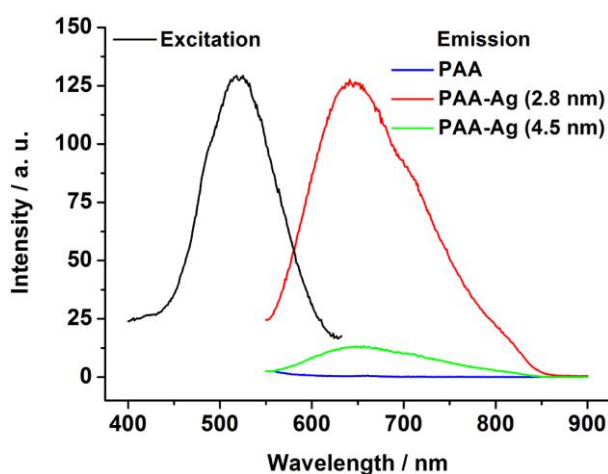
Figure 2. 6 Excitation and emission spectra of PAA-coated Ag NPs

As mentioned earlier in 2.1.2, the size of PAA-coated Ag NPs obtained after 15 min and 30 min were ~2.8 and 4.5 nm, respectively. The excitation spectrum in Figure 2.6 showed that the maximum excitation wavelength for PAA-Ag NPs was 520 nm, and the emission spectra of both Ag NPs were recorded at this excitation wavelength. As can be seen from Figure 2.6, the PAA-Ag NPs showed red emission bands from 625 to 850 nm, and the fluorescence intensity of the smaller Ag NPs (~2.8 nm) was higher than that of the bigger Ag NPs (~4.5 nm). The quantum yield of the smaller PAA-Ag NPs (3.52%) was also higher than that of the bigger PAA-Ag NPs (1.70%), which were calculated using Equation 2.7, and Φ stands for quantum yield, x is the unknown substance, s is the standard substance (here is rhodamine 101), A is the absorbance at the chosen excitation wavelengths, F is the fluorescence area recorded at the chosen excitation wavelengths, and n is the refraction index.

Equation 2.7 $\quad \Phi_x = \dfrac{A_S F_x n_x^2}{A_x F_S n_s^2} \Phi_S$

Such increase of fluorescence intensity and quantum yield observed with smaller NPs has also been observed for other kinds of NPs, for example, Au, CdS and Si NPs, and it has been understood that the decrease of photoluminescence lifetime with the increase of NPs' size is responsible for the weaker emission of bigger NPs.[353-355]

In addition, to eliminate any possible effects from the capping agent, the fluorescence spectrum of PAA was also recorded, which showed no emission signals, proving that Ag NPs were responsible for the detected fluorescence.

2.1.4.2 Fluorescence of BTM-Coated Ag NPs
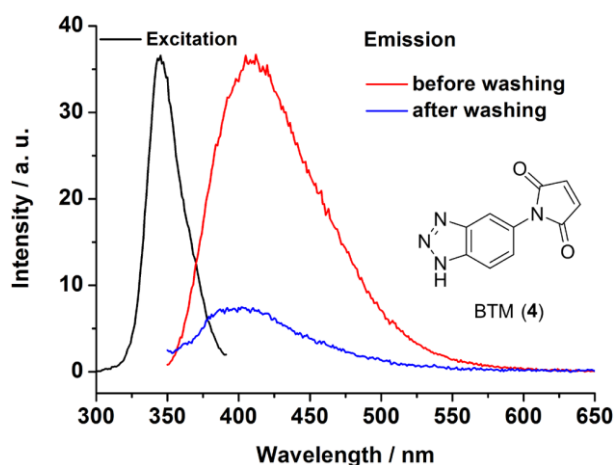
Figure 2. 7 Excitation and emission spectra of BTM-coated Ag NPs

The fluorescence property of BTM-coated Ag NPs (~3.1 nm) was also explored. The excitation spectrum (Figure 2.7) showed that the maximum excitation wavelength was 340 nm, and a violet emission at 410 nm with a quantum yield of 24.53% could be observed upon excitation at 340 nm (Figure 2.7). After the removal of excess BTM (**4**) by centrifugation and extensive washing with acetonitrile, the fluorescence intensity decreased sharply indicating that the fluorescence was caused by the capping agent BTM (**4**) rather than the Ag NPs themselves.

This phenomenon was explored further, as designing fluorescent NPs through the use of a proper linker could have further implications for the future screening of benzotriazole-based Ag NP hybrids. For that reason the fluorescence of BTM (**4**) was investigated and it was observed that its fluorescence could be influenced by the presence of water in the solvent system (Figure 2.8a), which might be caused by the fluorophore-solvent interaction expected from the Franck-Condon principle in solvation (Figure 2.8b).[356]
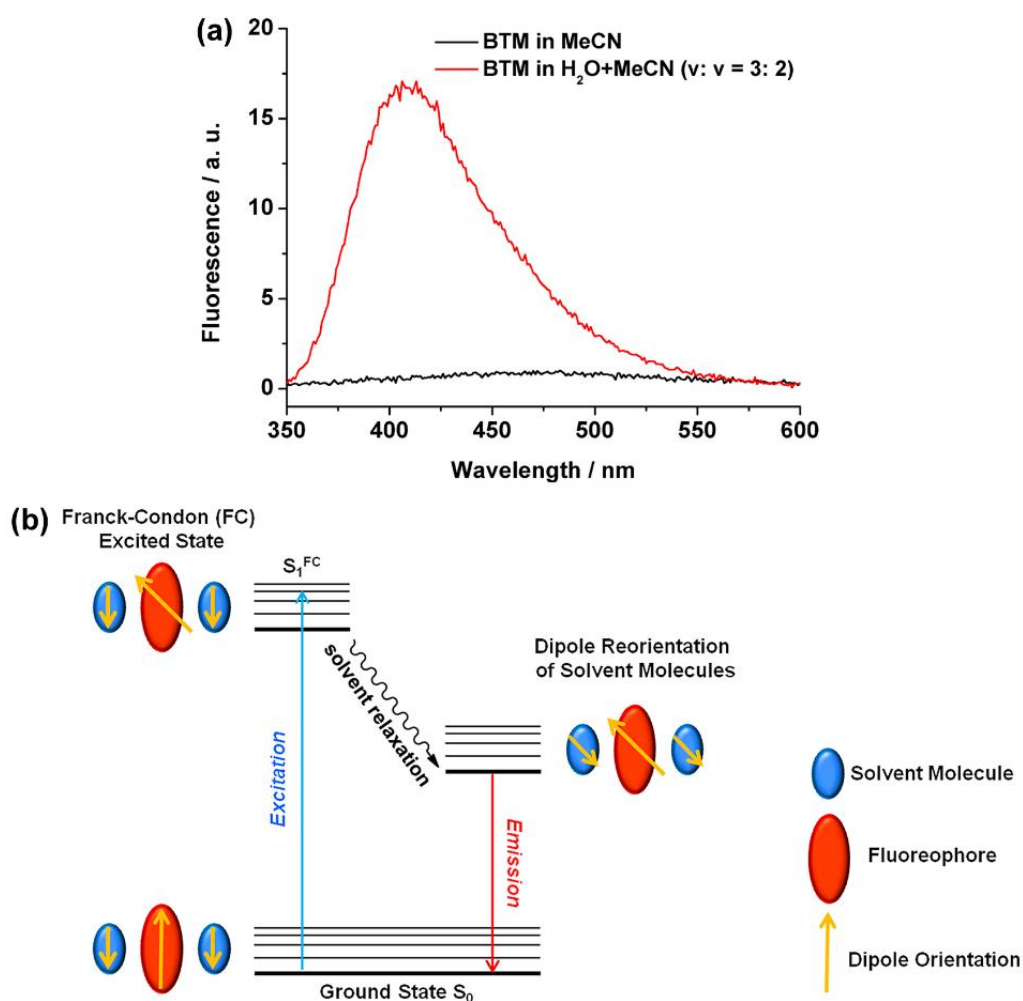
Figure 2. 8 (a) Fluorescence spectra of BTM (**4**) in different solvents (λ_{ex} = 340 nm) and (b) Illustration of Franck-Condon principle in solvation

The dipole moments of the polar solvent molecules could interact with the dipole moment of the fluorophore.[356] In the ground state, the solvent molecules are oriented in such a way that their dipole moments compensate for the dipole moment of the fluorophore in order to minimize the total energy of the whole system. After excitation, electronic transition to higher energy level leads to the change in the dipole moment of fluorophore, which ultimately induces the reorientation of the solvent molecules. The solvent relaxation around the excited fluorophore causes the decrease of the energy separation between the ground and excited states, which results in the increase of electronic transition probability and finally leads to the enhancement of the fluorescence intensity. Therefore, increasing the solvent polarity will correspondingly cause a decrease in the energy gap between the ground and excited states. Since the polarity of H_2O is higher than that of MeCN (polarity parameter: H_2O 10.2 and MeCN 5.8), so the fluorescence intensity of BTM (**4**) could be enhanced when H_2O appeared in the solvent system.
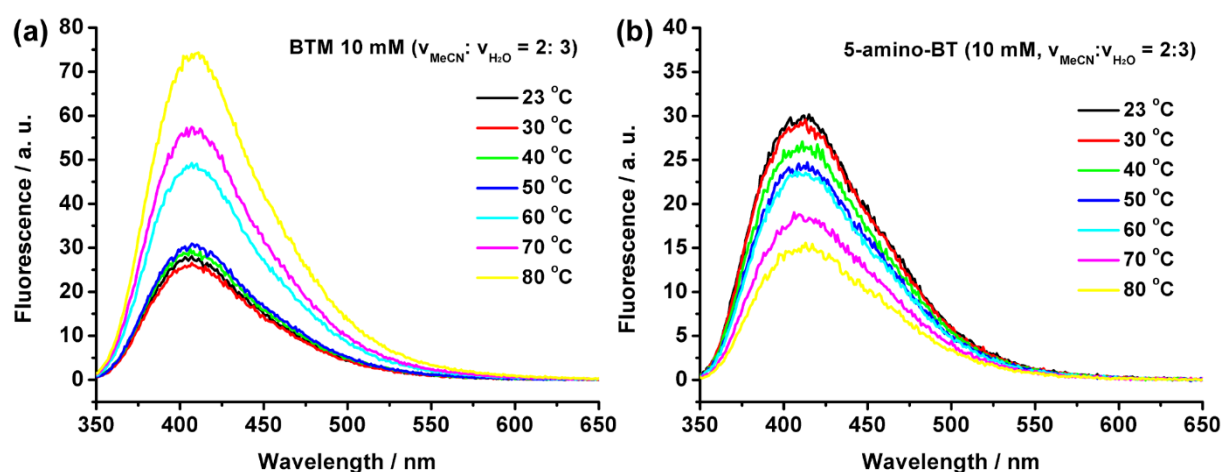
Figure 2. 9 Fluorescence spectra of (a) BTM (**4**) and (b) 5-amino-BT (**1**) in the mixture of MeCN and H_2O recorded at different temperatures (23 ~ 80 °C) (λ_{ex} = 340 nm)

In addition, it was observed that the fluorescence of BTM (**4**) increased with the increase of temperature, and a significant enhancement was observed when the solution of BTM (**4**) was heated to 60 °C (Figure 2.9a). On the other hand, the fluorescence of 5-amino-BT (**1**) slightly decreased when studied under the same conditions (Figure 2.9b).

To ensure that the fluorescence enhancement was not caused by the structural change of BTM (**4**) upon heating, BTM (**4**) was analyzed by NMR and MS after being heated at 60 °C overnight, and the results showed that no significant change of the molecular structure occurred, apart from the presence of traces of compound **2**, which indicate that maleimide could undergo ring opening hydrolysis when BTM (**4**) was heated to 60 °C in aqueous

solution. By comparing the fluorescence spectra of BTM (**4**) and compound **2** at the same concentrations (Figure 2.10), it could be seen that the emission intensity of compound **2** was not higher than that of BTM(**4**), so the appearance of traces of compound **2** should not lead to the increase of the fluorescence intensity.
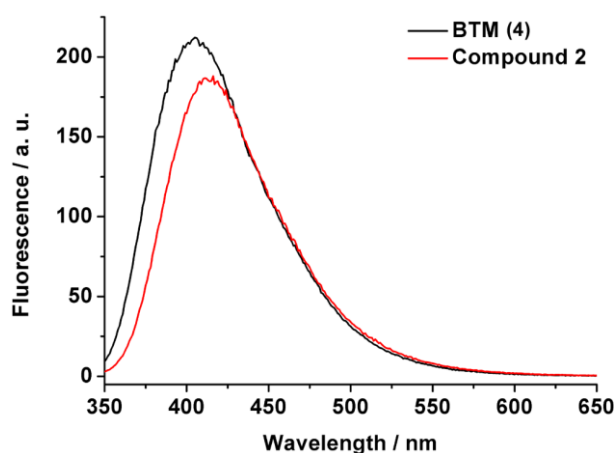
Figure 2. 10 Fluorescence spectra of BTM (**4**) and Compound **2** in the mixture of MeCN and H_2O (λ_{ex} = 340 nm)

In order to investigate further into the reasons for the significant fluorescence enhancement of BTM (**4**) after being heated at 60 °C, UV-Vis spectra of BTM (**4**) and 5-amino-BT (**1**) were measured at 23 and 60 °C (Figure 2.11). The absorption peak of BTM (**4**) (23 °C) at 300 nm could be attributed to the 2-*H* tautomer of BTM, while the other peak around 260 nm belongs to the 1-*H* tautomer of BTM (Figure 2.11a and Scheme 2.5).[357] After being heated at 60 °C, the peak at 300 nm decreased and the peak at 260 nm increased (Figure 2.11a), indicating that a fraction of 2-*H* BTM transformed to 1-*H* BTM. On the contrary, the ratio between the two absorption peaks of 5-amino-BT (**1**) did not change obviously (Figure 2.11b), which might be because there was no significant change in the ratio between its 1-*H* tautomer and 2-*H* tautomer.
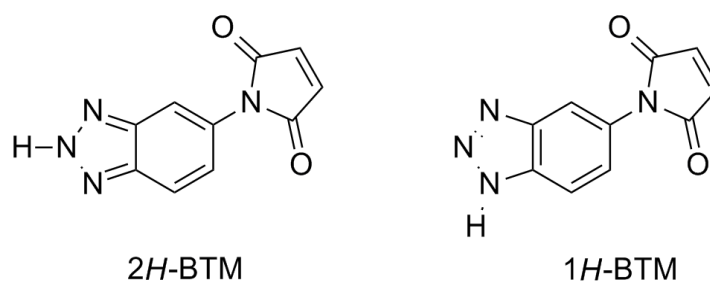
Scheme 2. 5 The 2*H*- and 1*H*- tautomers of BTM (**4**)
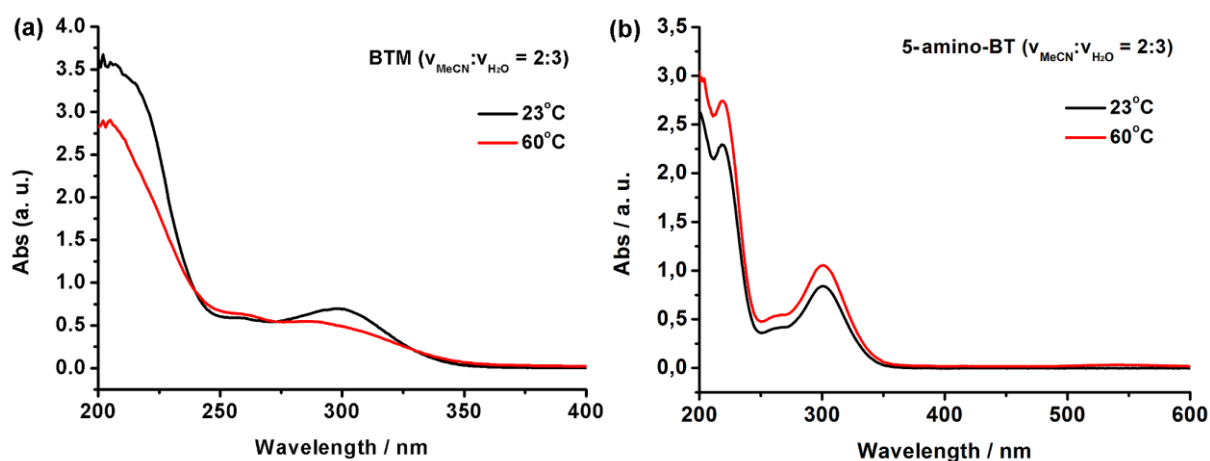
Figure 2. 11 UV-Vis spectra of BTM (**4**) and 5-amino-BT (**1**) at 23 ºC and 60 ºC

To further prove this, Fourier transform infrared spectroscopy (FTIR) was used to analyze the structures of BTM (**4**) and 5-amino-BT (**1**) before and after heating at 60 ºC (Figure 6.1 in the Experimental part). Compared with the FTIR spectrum of BTM (23 ºC) (Figure 6.1a), a new band appeared at 3507 cm^{-1} in the spectrum of BTM (60 ºC) (Figure 6.1b), which could be assigned to the N-H stretching vibration of the 1-*H* BTM (Table 2.1).[358] There was no obvious change in the FTIR spectra of 5-amino-BT (23 and 60 ºC) (Figure 6.1c and d). The structural information given by FTIR confirmed the results obtained by UV-Vis analyses that the fluorescence enhancement of BTM (**4**) upon heating might be caused by the tautomerization of BTM (**4**).

Table 2. 1 N-*H* stretching vibration band of BTM (**4**) and 5-amino-BT (**1**) in FTIR spectra

Compound	Wavenumber (cm^{-1})	N-*H* Stretching
BTM (23 ºC)	3468.9	2-*H*
BTM (60 ºC)	3506.7	1-*H*
5-amino-BT (23 ºC)	3373.5	2-*H*
5-amino-BT (60 ºC)	3374.0	2-*H*

2.2 Biofunctionalization of Ag NPs

Au NPs have been extensively studied for the construction of bio-NP conjugates,[267, 359] but only a few reports have demonstrated biofunctionalization of Ag NPs due to their lower chemical stability.[28] Most of the approaches employed thiol chemistry for the modification of Ag NPs because thiol anchors could bind to the metallic NPs strongly through the formation

of sulfur-metal covalent bond.[17, 251, 360] However, it has been reported that the energy of sulfur-Ag bond is 217 kJ/mol, which is lower than that of sulfur-Au bond (418 kJ/mol), so the affinity between thiol and Ag is weaker than the interaction between thiol and Au.[57] Since benzotriazole can form strong complex with metallic NPs through the triazole moiety,[344, 347] it is interesting to investigate if benzotriazole-based linkers such as BTM (**4**) could be used as an alternative anchor for the immobilization of biomolecules onto the surface of Ag NPs.

Two different strategies were employed for the biofunctionalization of Ag NPs with DNA, one was the direct attachment of benzotriazole-modified DNA to the surface of PAA-coated Ag NPs through ligand exchange, and the other was the covalent binding of diene-modified DNA to the surface of BTM-coated Ag NPs through Diels-Alder cycloaddition between the diene and maleimide functional groups.

2.2.1 Biofunctionalization of PAA-Coated Ag NPs with Benzotriazole-Modified DNA through Ligand Exchange

2.2.1.1 Preparation of Benzotriazole-Modified DNA

Two different DNA sequences, one was a 12-base oligonucleotide (DNA1: 5'-GGCGTATAACAA-3'), and the other was a 31-base oligonucleotide (DNA2: 5'-TTTTTTTTTGCTCTCAAGTGCGCAGCATCGA-3') were chosen as model DNA sequences for the modification of Ag NPs. Both DNA sequences were commercially supplied with alkane thiol groups at the 5'-ends, and then modified to contain benzotriazole using Michael addition between thiol groups and BTM (**4**).

DNA1: 5'-GGCGTATAACAA-3'
DNA2: 5'-TTTTTTTTTGCTCTCAAGTGCGCAGCATCGA-3'
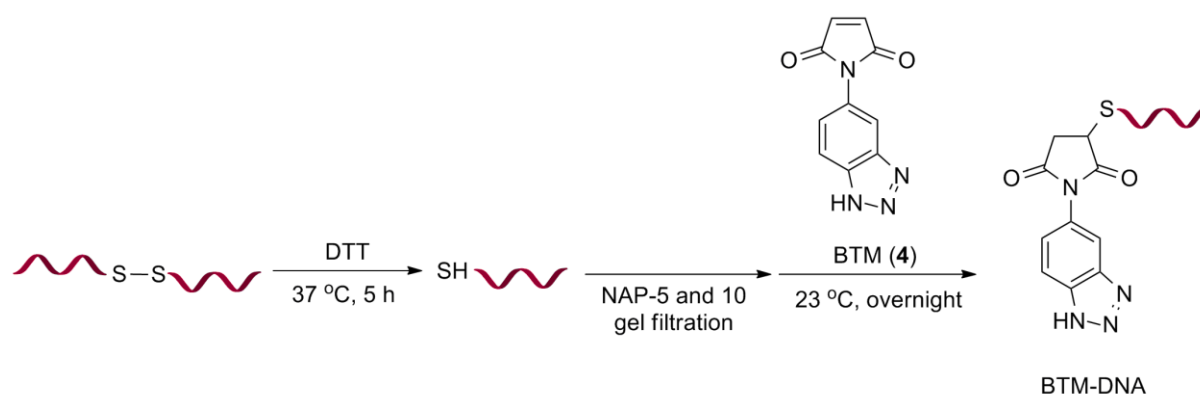
Scheme 2. 6 Modification of thiolated DNA with BTM

To achieve this, thiolated DNA sequences were first reduced with dithiothreitol (DTT) to ensure the cleavage of the disulfide bonds to thiols (Scheme 2.6). The freshly reduced SH-DNAs were incubated with BTM (**4**) at 23 °C overnight, and the ratio between BTM (**4**) and SH-DNAs was 10:1. The obtained products were purified by high-performance liquid chromatography (HPLC).
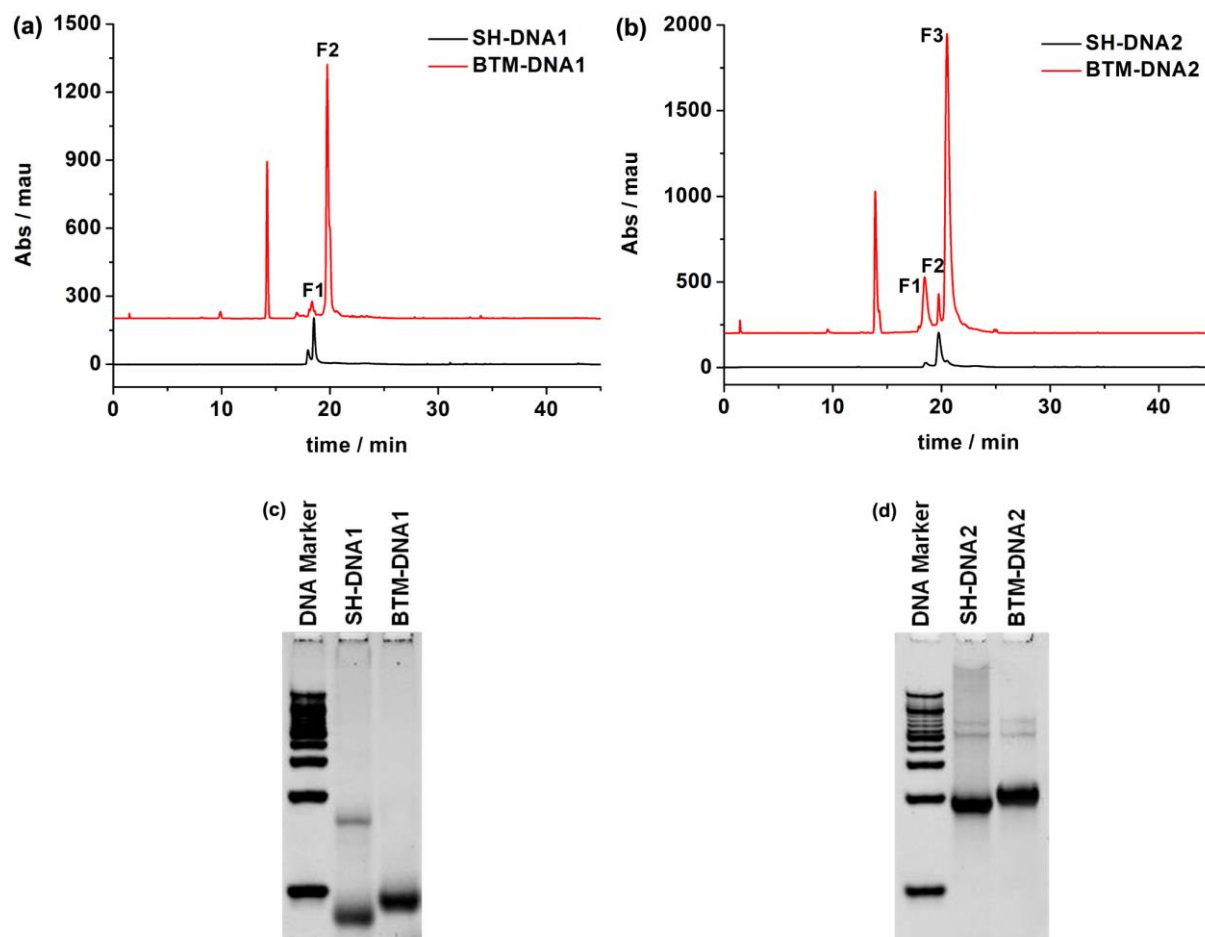
Figure 2. 12 (a and b) HPLC chromatogram of BTM-modified DNA1 and DNA2. (a) F1: SH-DNA1 and F2: BTM-DNA1; (b) F1 and F2: SH-DNA2 and F3: BTM-DNA2; (c and d) PAGE images for BTM-DNA1 and BTM-DNA2, respectively.

As can be seen from the HPLC chromatogram, unreacted SH-DNA1 (F1) (Figure 2.12a) and SH-DNA2 (F1 and F2) (Figure 2.12b) were eluted from the column at 18.5 and 18.5/19.8 min, and two new fractions were eluted at 19.7 and 20.5 min, respectively. The collected fractions were characterized by 21% polyacrylamide gel electrophoresis (PAGE), which showed that the electrophoretic mobility of the new fractions was different from that of the thiolated DNAs (Figure 2.12 c and d). The masses of the two new fractions detected by MALDI-TOF were 4090.5 g/mol and 9870.1 g/mol (Table 2.2), which matched the calculated

masses of BTM-modified DNA1 (4092) and DNA2 (9872), respectively. The yields of BTM-DNA1 and BTM-DNA2 were 30.3% and 32.0% indicating this modification method was efficient.

Table 2. 2 Calculated and detected mass of SH-DNAs and BTM-DNAs

DNA	Calculated Mass (g/mol)	Detected Mass by MALDI (g/mol)
SH-DNA1	3878	3876.9
BTM-DNA1	4092	4090.5
SH-DNA2	9658	9656.7
BTM-DNA2	9872	9870.1

After the successful preparation of BTM-modified DNAs, the next step would be the direct attachment of such DNAs to the surface of PAA-Ag NPs through ligand exchange.

2.2.1.2 Biofuctionalization of PAA-Ag NPs with BTM-DNAs through Ligand Exchange

DNA1: 5'-GGCGTATAACAA-3'

DNA2: 5'-TTTTTTTTTGCTCTCAAGTGCGCAGCATCGA-3'
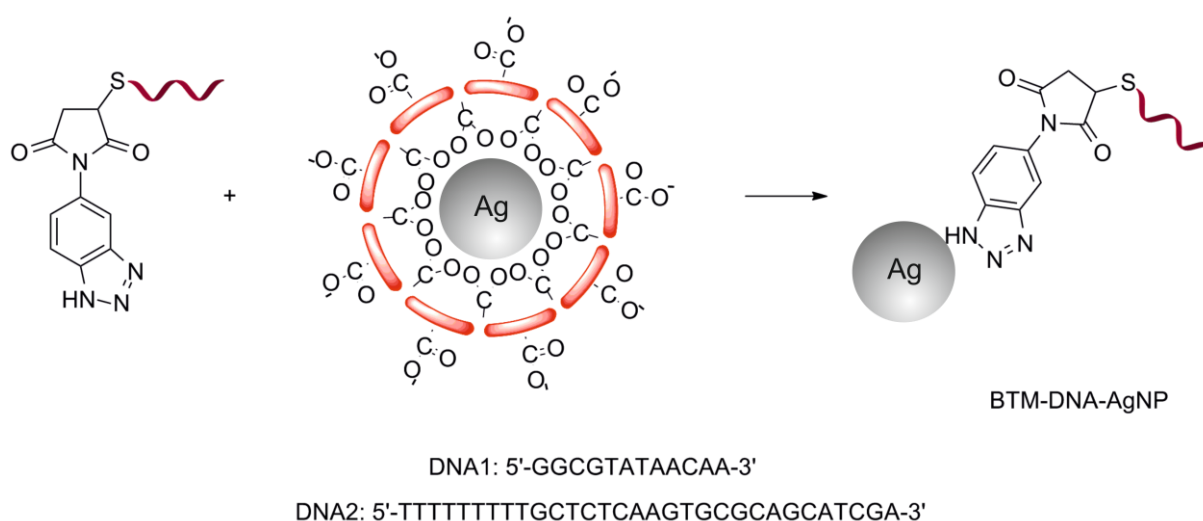
Scheme 2. 7 Biofunctionalization of PAA-Ag NPs with BTM-DNA through ligand exchange

The biofunctionalization of PAA-coated Ag NPs with both BTM-modified DNAs was realized using the conventional salt aging method with slight modification.[17] BTM-modified DNA was attached to the surface of PAA-coated Ag NPs through simple ligand exchange (Scheme 2.7). After incubating PAA-Ag NPs and BTM-DNA at room temperature for 24 h, PBS buffer and NaCl were added for several rounds of equilibration. Then the NPs were washed thoroughly to remove the excessive DNA, and redispersed in PBS buffer (1×). UV-

Vis spectra (Figure 2.13a) show that the plasmonic absorption of Ag NPs slightly shifted after DNA functionalization, but the plasmonic bands did not become broad, which indicated that the size distribution of Ag NPs did not change and no agglomeration was caused by the DNA modification process. The formation of BTM-DNA-AgNP conjugates was confirmed by the significant electrophoretic mobility shifts between unmodified PAA-Ag NPs and BTM-DNA-modified Ag NPs in the agarose gel (1%) (Figure 2.13b).
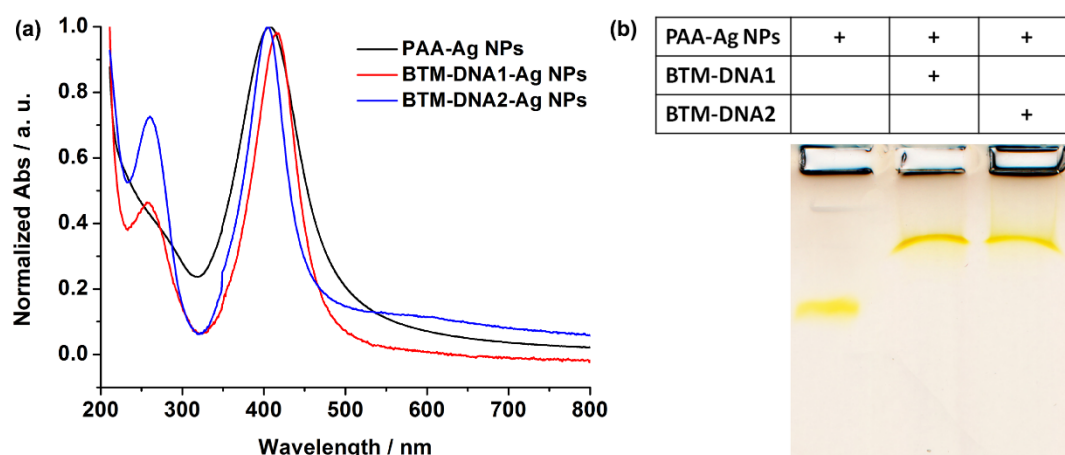
Figure 2. 13 (a) UV-Vis spectra and (b) agarose gel image for PAA-Ag NPs and BTM-DNA-AgNP conjugates

2.2.1.3 Stability of BTM-DNA-Functionalized Metallic NPs

To investigate the stability of BTM-DNA-AgNP conjugates, DTT displacement study was performed (Scheme 2.8), which has already been used for the stability tests of SH-DNA-AuNP conjugates by replacing the thiolated DNA with DTT on the surface of NPs and causing the irreversible aggregation of the NPs.[359] In such a way, the stability of the linkage towards the displacing small molecules in the environment could be explored.
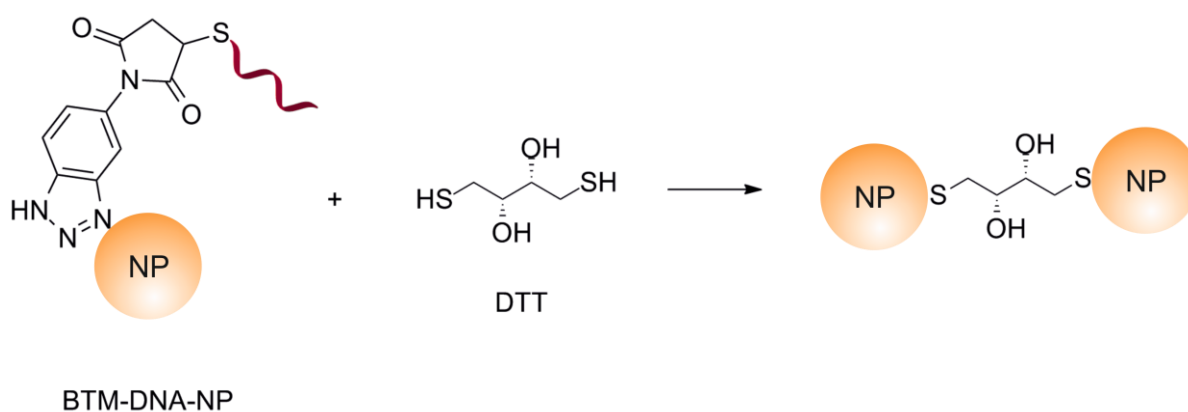
Scheme 2. 8 Stability tests of DNA-metallicNP conjugates using DTT displacement reaction

In order to estimate the stability of the interactions between BTM-DNA and Ag NPs, Ag NPs functionalized with SH-DNA1 as well as Au NPs modified with both BTM-DNA1 and SH-DNA1 were prepared using the same salt aging method, and the formation of the DNA-metallicNP conjugates was confirmed by agarose gel electrophoresis (1%) (Figure 2.14).
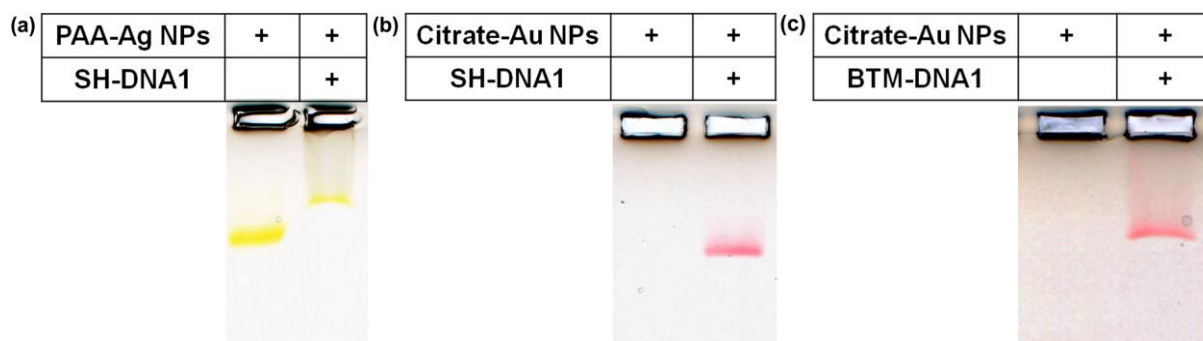
Figure 2. 14 Agraose gel image for (a) SH-DNA1-AgNP, (b) SH-DNA1-AuNP, and (c) BTM-DNA1-AuNP conjugates
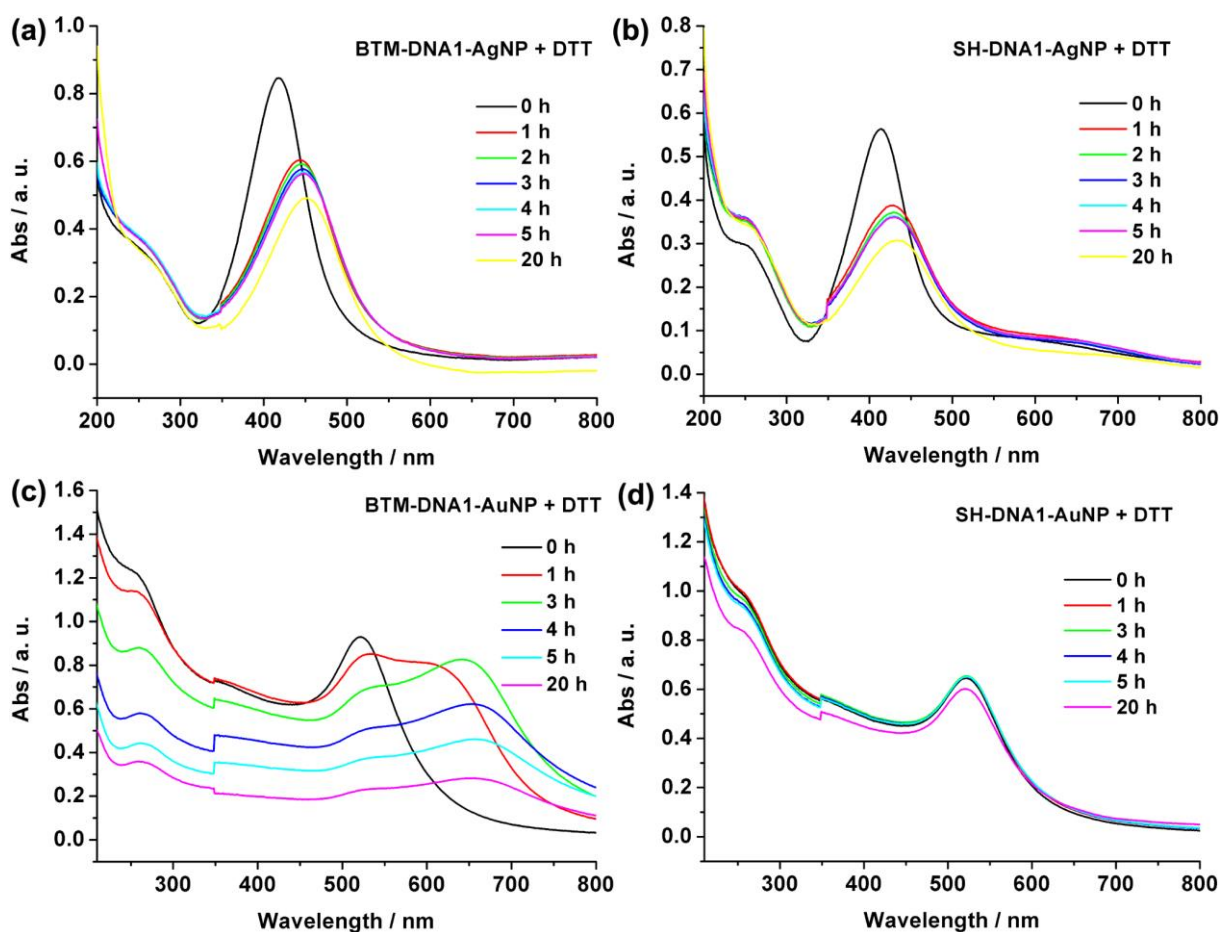
Figure 2. 15 Stability tests of (a) BTM-DNA1-AgNP, (b) SH-DNA1-AgNP, (c) BTM-DNA1-AuNP and (d) SH-DNA1-AuNP conjugates using DTT displacement reaction

For the stability tests, the displacement reagent DTT was added to DNA-modified metallic NPs in such way that the molar ratio between DTT and DNA1 was 10: 1. UV-Vis spectroscopy was used to monitor the absorbance changes of Ag and Au NPs after the addition of DTT. The UV-Vis spectra (Figure 2.15a and b) show that the plasmonic bands of Ag NPs became broad and red shifted after the treatment with DTT. In the case of BTM-DNA1-functionalized Ag NPs, the absorbance of Ag NPs decreased by 41.9% after 20 h incubation (Figure 2.15a), while it decreased by 45.6% in the case of SH-DNA1-functionalized Ag NPs (Figure 2.15b), which indicates that the stability of BTM-DNA1-AgNP was comparable with that of SH-DNA1-AgNP.

Contrary to Ag NPs, no obvious changes were observed for SH-DNA-functionalized Au NPs after incubation with DTT for 20 h (Figure 2.15d), proving the high stability of the SH-DNA1-AuNP conjugates. However, when the BTM-DNA1-functionalized Au NPs were treated with DTT, significant shifts and broadening of the plasmonic bands could already be observed after 1 h (Figure 2.15c), which indicated that the stability of SH-DNA-AuNP and BTM-DNA-AgNP was much higher than that of BTM-DNA-AuNP.

The results of the stability tests prove that benzotriazole has strong affinity to Ag NPs. This simple methodology for the functionalization of Ag NPs might be of particular interest to the scientists working on novel application of Ag NPs in biosensing and drug delivery, because the benzotriazole moiety is SERS active,[344, 347] and benzotriazole derivatives have already been used as drug precusors.[361, 362]

2.2.1.4 DNA Hybridization Using DNA-AgNPs Conjugates

To test if the DNAs were still functional after being attached to Ag NPs, DNA-AgNP conjuagtes were employed to hybridize with their complementary DNA stands (Scheme 2.9).
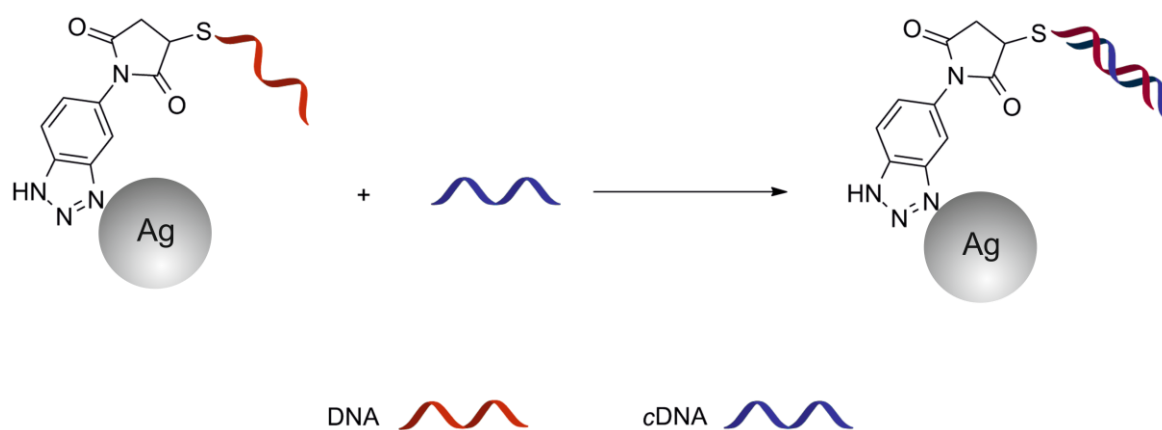
Scheme 2. 9 Hybridization of DNA and *c*DNA on the surface of Ag NPs

Firstly, the BTM-DNA1-AgNP conjugates were used to hybridize with its complementary strand cDNA1. Different conditions were attempted, such as incubation at room temperature, heating the solution up to 80 $^{\circ}$C and slowly cooling down, or the addition of MgCl$_2$ to stabilize the formation of DNA duplex.[363] However, the electrophoretic mobility of Ag NPs in the agarose gel did not change (Figure 2.16a), indicating that the hybridization of DNA1 with cDNA1 on the surface of Ag NPs was not successful.

(a) PAA-Ag NPs	+	+	+	+
BTM-DNA1		+	+	+
cDNA1			+	+
MgCl$_2$				+

(b) PAA-Ag NPs	+	+	+		+	+	+	
BTM-DNA2		+	+			+	+	
cDNA2			+	+			+	+
DNA2				+				+
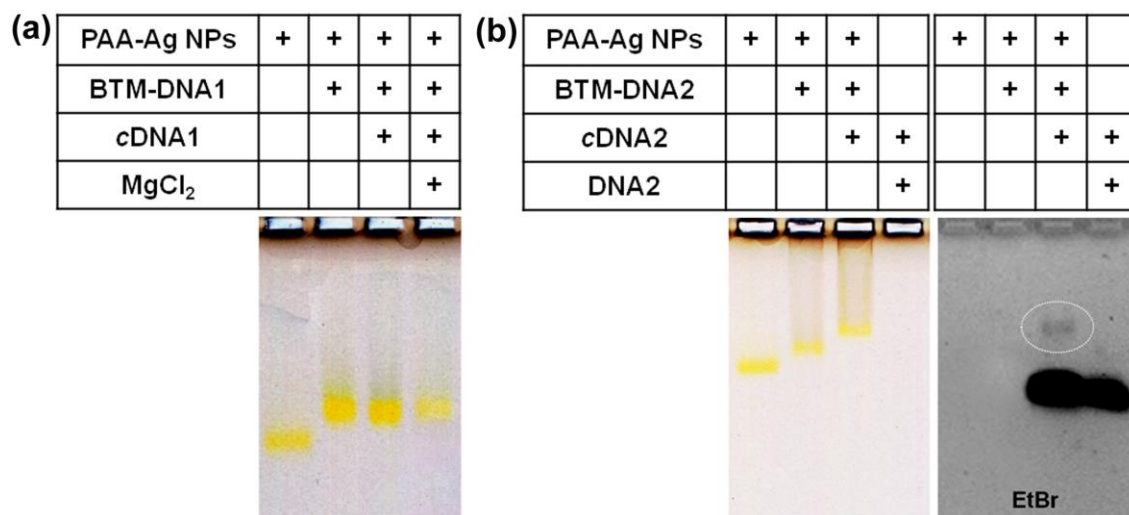
Figure 2. 16 Agraose gel image for the hybridization of (a) DNA1 and (b) DNA2 with their corresponding complementary strands cDNA1 and cDNA2 on the surface of Ag NPs. The black-white image in Figure 2.16b was taken under the UV-light mode of the gel imaging system after staining the gel with EtBr.

However, the successful hybridization of longer stranded DNA2 with cDNA2 was realized in such a way that BTM-DNA2-AgNP conjugates were first incubated with cDNA2 at 80 $^{\circ}$C to eliminate the DNA secondary structures, and then the solution was slowly cooled down to 37 $^{\circ}$C and incubated for 2 h. The NPs were then washed to remove excess cDNA2 strands and analyzed by agarose gel electrophoresis (1%). A clear band shift between Ag NPs before and after hybridization could be observed (Figure 2.16b), which indicates that the hybridization of longer DNA strands on the surface of Ag NPs was successful. The formation of dsDNA2-AgNP conjugates was further confirmed by staining the agarose gel with ethidium bromide (EtBr), a dsDNA staining agent (Figure 2.16b). The results proved that the DNA2 strands in the BTM-DNA2-AgNP conjugates maintained their hybridization ability, which enables the utilization of the conjugates for the further DNA-directed attachment of other molecules or assembly with other NPs.

2.2.1.5 Assembly of Au and Ag NPs through DNA Hybridization

The recognition property of DNA might be useful for the fabrication of promising nanocomposites with novel properties and functions. Such kind of nanocomposites could be used as building blocks for nano-assembly, structure design and the development of sensors and nanodevices.[364]

DNA2: 5'-TTTTTTTTTGCTCTCAAGTGCGCAGCATCGA-3'

cDNA2: 5'-GCACTTGAGAGCTTTTTTTTTTTTT-3'
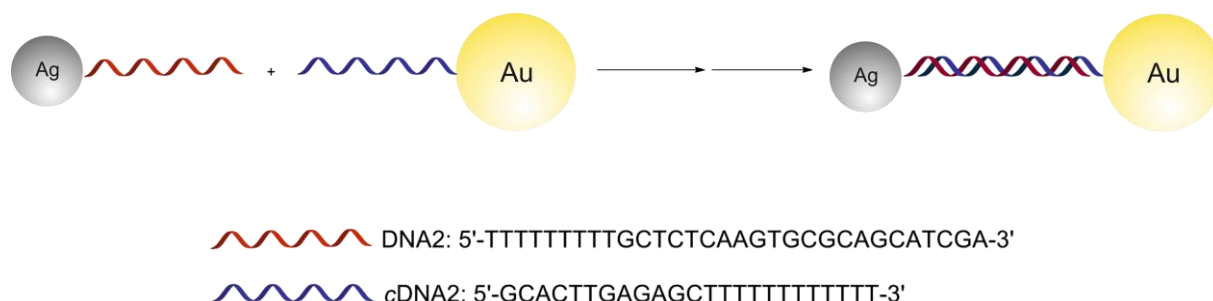
Scheme 2. 10 Assembly of Au and Ag NPs through DNA hybridization

The as-prepared DNA2-Ag NPs (~4.5 nm) were employed in the assembly with Au NPs (~10 nm) functionalized with the complementary sequence SH-cDNA2 (made by Dr. Dania Kendziora)[365] through DNA hybridization (Scheme 2.10), which was performed at similar reaction conditions as that for the preparation of dsDNA2-AgNP. The UV-Vis spectra (Figure 2.17a) show that the absorbance bands of the NPs became broad after the reaction indicating that Ag and Au NPs were brought close by assembly through the DNA hybridization. The formation of Au-dsDNA2-Ag nanostructure was confirmed by the mobility shift in 1% agarose gel electrophoresis (Figure 2.17b) and the TEM images in Figure 2.18.
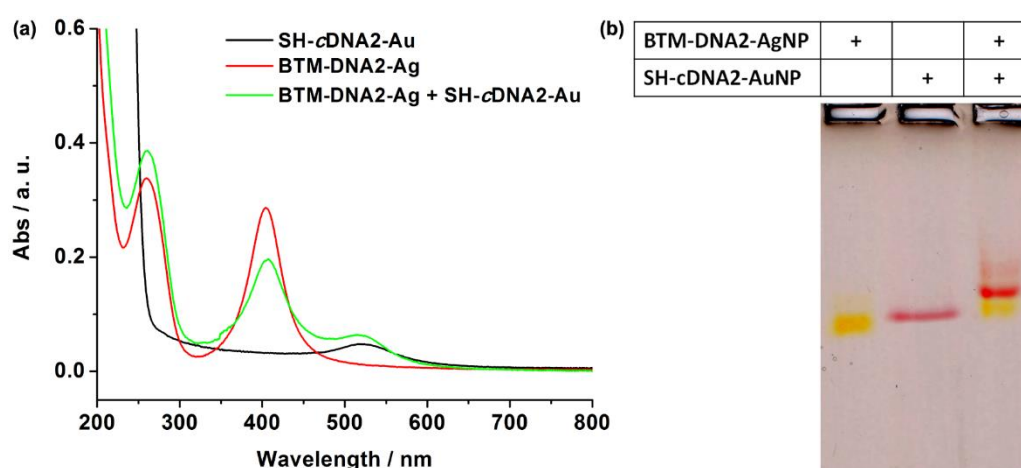
Figure 2. 17 (a) UV-Vis spectra and (b) agarose gel image for the assembly of Ag and Au NPs through the hybridization of BTM-DNA2 and SH-cDNA2 on the surface of Ag and Au NPs
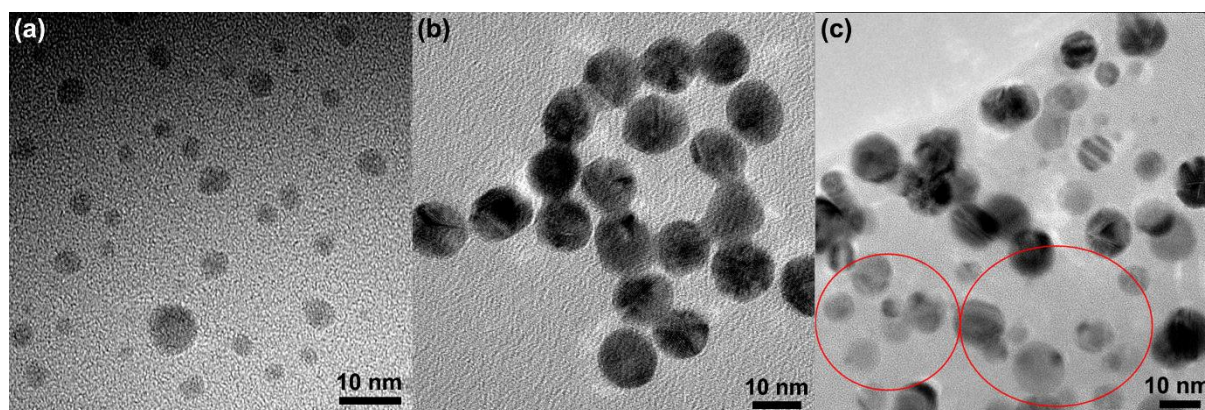
Figure 2. 18 TEM images of (a) PAA-Ag NPs, (b) citrate-Au NPs and (c) Ag-*ds*DNA-Au nanostructures

The obtained Ag-*ds*DNA2-Au nanocomposites have been employed as SERS substrates by Dr. Dania Kendziora for the detection enhanced yellow fluorescent protein, which was conjugated to Au NPs through another thiolated DNA strand.[365] The results showed that the Ag-*ds*DNA2-Au nanocomposites exhibited higher Raman enhancement ability than the Au NPs alone, which proved that the nanocomposites were more SERS active than Au NPs. Such kind of nano-assembly method might be expanded to the fabrication of different nanocomposites or the detection of other molecular species, and find applications in the design of plasmonic and SERS-based sensors.

2.2.2 Biofunctionalization of BTM-Coated Ag NPs with Furan-Modified DNA1 through Diels-Alder Cycloaddition

To increase the toolbox for the modification of Ag NPs, an additional mild and biofriendly chemical methodology for biofunctionalization was explored, namely Diels-Alder cycloaddition, which has already been used for the immobilization of DNA or protein onto NPs as introduced in 1.3.3.4.[302, 303] To achieve that, BTM-coated Ag NPs, which were synthesized through a simple one-pot method (described in 2.1.3.2), were employed to undergo Diels-Alder cycloaddition with furan-modified DNA.

2.2.2.1 Preparation of Furan-Modified DNA

Different strategies were attempted in order to obtain furan-modified DNA1 with a decent yield, which could be utilized for the further biofuntionalization of Ag NPs.

Method 1: Amide coupling between N-furan-2-ylmethyl succinamic acid (**5**) and NH$_2$-DNA1 on solid support

NH$_2$-DNA1 attached to the controlled pore glass (CPG) solid support was first employed for the amide coupling reaction, because it has been reported that solid phase reaction offers advantages than the conventional solution reaction. For example, it was reported that its incompressible rigid structure enables the free pass of reagents and solvents and makes the reaction proceed quickly,[366] and the solid support can easily be separated from the solvent, therefore the time-consuming purification procedures can be circumvented.[367] The solid phase strategy has already been successfully utilized for the synthesis or modification of DNA oligonucleotides.[368, 369]
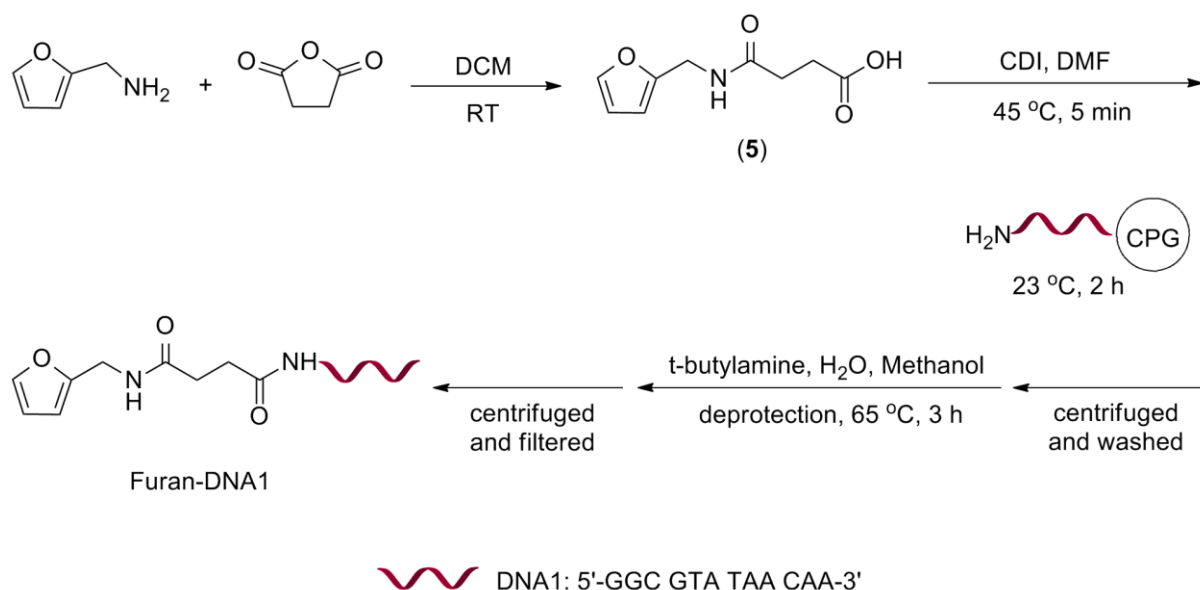
Scheme 2. 11 Synthesis of N-furan-2-ylmethyl succinamic acid (**5**) and its subsequent amide coupling with NH$_2$-DNA1 on solid support using CDI as a coupling reagent

The modification of NH$_2$-DNA1 on solid support with N-furan-2-ylmethyl succinamic acid (**5**), which was synthesized using furfurylamine and succinic anhydride, was first attempted by employing 1,1'-carbonyl diimidazole (CDI) as a coupling reagent (Scheme 2.11).[346] After the amide coupling reaction the DNA was cleaved from the solid support using *tert*-butylamine, and the obtained products were purified by HPLC. The chromatogram showed the presence of unreacted NH$_2$-DNA1 (F1) and three new fractions (F2, F3 and F4) (Figure 2.19a), which were then analyzed by PAGE (21%). Although the electrophoretic mobility of F2 and F3 was different from that of the starting NH$_2$-DNA1 (F1) (Figure 2.19b), no expected mass of the desired product (furan-DNA1) was obtained by the subsequent mass measurements using MALDI-TOF (Table 2.3), indicating that the amide coupling on solid support using CDI as a coupling agent was not successful.
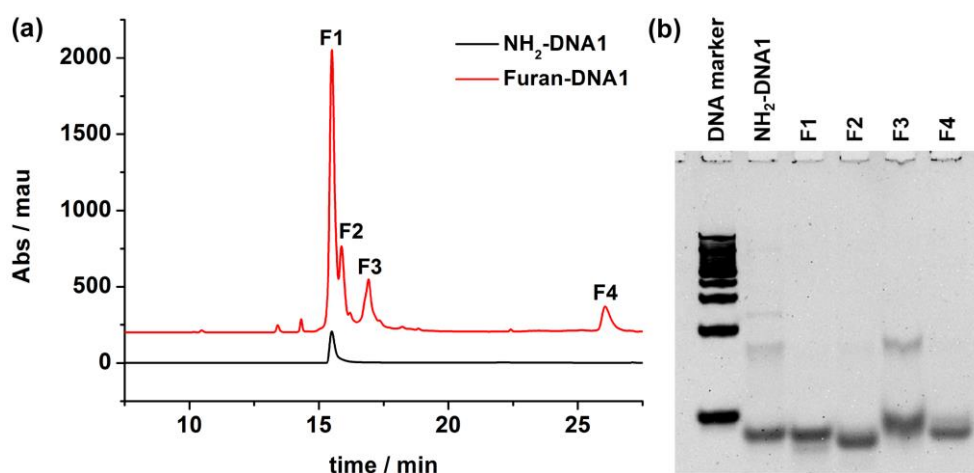
Figure 2. 19 (a) HPLC chromatogram and (b) PAGE image for NH$_2$-DNA1 and the products (F1 ~ F4) obtained by amide coupling of N-furan-2-ylmethyl succinamic acid (**5**) and NH$_2$-DNA1 on solid support using CDI as a coupling reagent

Table 2. 3 Calculated and detected masses of NH$_2$-DNA1 and F1 ~ F4 obtained by amide coupling of N-furan-2-ylmethyl succinamic acid (**5**) and NH$_2$-DNA1 on solid support using CDI as a coupling reagent

DNA	Calculated Mass (g/mol)	Detected Mass by MALDI (g/mol)
NH$_2$-DNA1	3861	3857.1
F1	3861	3857.1
F2	4041	3899.0
F3	4041	3962.0
F4	─	3862.3

To improve the amide coupling reaction, another set of reagents namely hydroxybenzotriazole (HOBT) and o-benzotriazole-N,N,N',N'-tetramethyl-uronium-hexafluoro-phosphate (HBTU) were employed (Scheme 2.12).[370] The obtained DNA products were purified by HPLC, and the chromatogram showed that 4 new peaks appeared between 20 and 30 min, which were different from the peak corresponding to the reactant NH$_2$-DNA1 (16.0 min) (Figure 2.20). However, the new peaks were not well separated, and the expected mass of furan-DNA1 could not be detected (Table 2.4) indicating that the amide coupling on solid support was again unsuccessful.
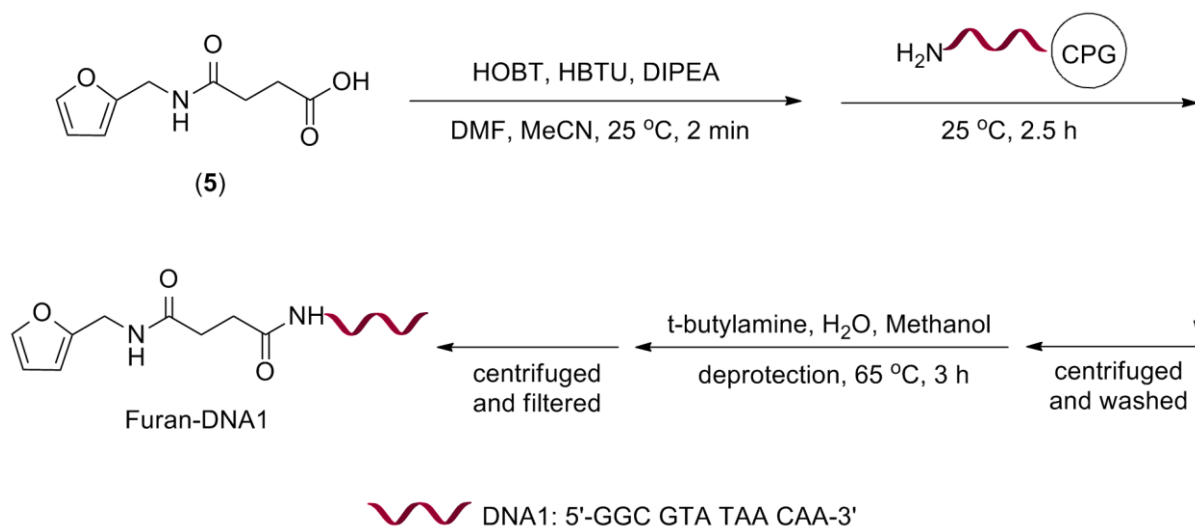
Scheme 2. 12 Amide coupling of N-furan-2-ylmethyl succinamic acid (**5**) and NH$_2$-DNA1 on solid support using HOBT/HBTU as coupling reagents
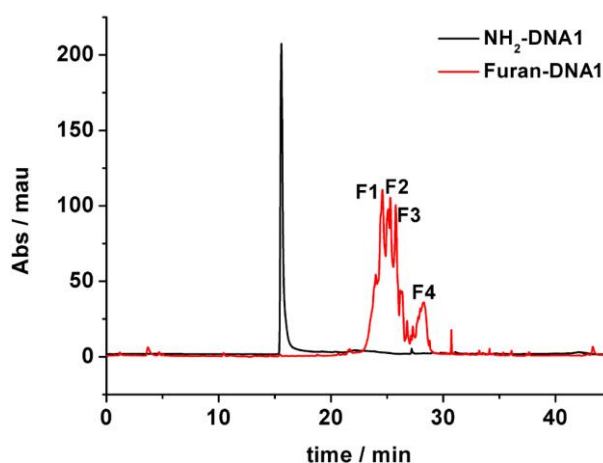
Figure 2. 20 HPLC chromatogram of NH$_2$-DNA1 and the products (F1 ~ F4) obtained by amide coupling of N-furan-2-ylmethyl succinamic acid (**5**) and NH$_2$-DNA1 on solid support using HOBT/HBTU as coupling reagents

Table 2. 4 Calculated and detected masses of NH$_2$-DNA1 and F1 ~ F4 obtained by amide coupling of N-furan-2-ylmethyl succinamic acid (**5**) and NH$_2$-DNA1 on solid support using HOBT/HBTU as coupling reagents

DNA	Calculated Mass (g/mol)	Detected Mass by MALDI (g/mol)
NH$_2$-DNA1	3861	3857.1
F1	4041	4453.4
F2	4041	4451.7
F3	4041	4502.0
F4	4041	4632.4

As shown above, no matter which kind of coupling reagents were used, the amide coupling reactions using NH$_2$-DNA1 immobilized on CPG solid supports did not afford the expected furan-modified DNA1. According to the masses of the obtained fractions, some unknown products were obtained, most probably a result from the reaction of the impurities on the CPG supports. Therefore, a new approach was taken, in which commercially available stock solution of NH$_2$-DNA1 was employed to under amide coupling with N-furan-2-ylmethyl succinamic acid (**5**) using CDI coupling approach (Scheme 2.13).

Method 2: Amide coupling between N-furan-2-ylmethyl succinamic acid (**5**) and NH$_2$-DNA1 in solution using CDI as a coupling reagent

DNA1: 5'-GGC GTA TAA CAA-3'
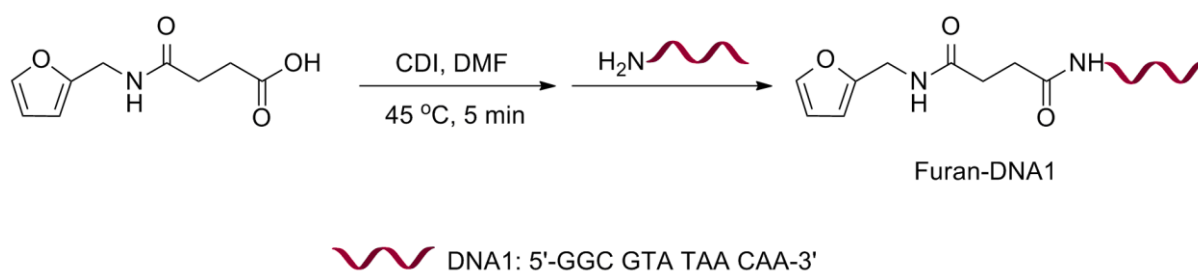
Scheme 2. 13 Amide coupling of N-furan-2-ylmethyl succinamic acid (**5**) and NH$_2$-DNA1 in solution using CDI as a coupling reagent

The reaction was first performed at 23 °C for 2 h, and the products were purified by HPLC (Figure 2.21a), which showed the peaks for the unreacted NH$_2$-DNA1 and a new fraction (F2) at 16.5 min and 17.9 min, respectively. PAGE (21%) analysis showed a clear mobility shift between the bands of NH$_2$-DNA1 and F2 (Figure 2.21b), and the MALDI-TOF measurements confirmed that F2 (4038.0 g/mol) was indeed the desired product furan-DNA1 (Table 2.5). However, the yield of furan-DNA1 was 3.0 %, indicating a rather inefficient reaction by which only a small amount of furan-DNA1 could be obtained.

To improve the yield, the same reaction was repeated at 37 °C overnight. After HPLC purification (Figure 2.21a) the masses of the obtained fractions were measured by MALDI-TOF (Table 2.5), which again confirmed that F2 was furan-modified DNA1. However, the yield of furan-DNA1 was increased to 26.2 %, indicating that the amide coupling reaction was more efficient at higher temperature.
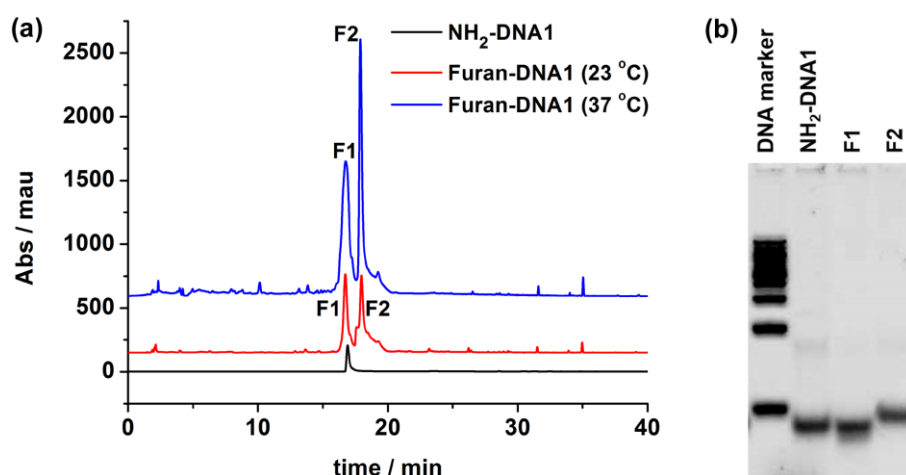
Figure 2. 21 (a) HPLC chromatogram and (b) PAGE image for furan-DNA1 obtained by amide coupling of N-furan-2-ylmethyl succinamic acid (**5**) and NH$_2$-DNA1 in solution using CDI as a coupling reagent

Table 2. 5 Calculated and detected masses of NH$_2$-DNA1, F1 and F2 obtained by amide coupling of N-furan-2-ylmethyl succinamic acid (**5**) and NH$_2$-DNA1 in solution using CDI as a coupling reagent

DNA	Calculated Mass (g/mol)	Detected Mass by MALDI (g/mol)
NH$_2$-DNA1	3861	3857.9
F1 (23 °C, 2 h)	3861	3858.0
F2 (23 °C, 2 h)	4041	4038.0
F1 (37 °C, overnight)	3861	3857.1
F2 (37 °C, overnight)	4041	4370.0

After the successful preparation of furan-DNA1 through the amide coupling of N-furan-2-ylmethyl succinamic acid (**5**) and NH$_2$-DNA1 in solution, the obtained furan-DNA1 would be utilized for the subsequent covalent biofuntionalization of BTM-coated Ag NPs through Diels-Alder cycloaddition.

2.2.2.2 Biofunctionalization of BTM-Ag NPs with Furan-DNA1 through Diels-Alder Cycloaddition

Different conditions were explored for the attachment of furan-DNA1 onto BTM-coated Ag NPs through Diels-Alder cycloaddition (Scheme 2.14).
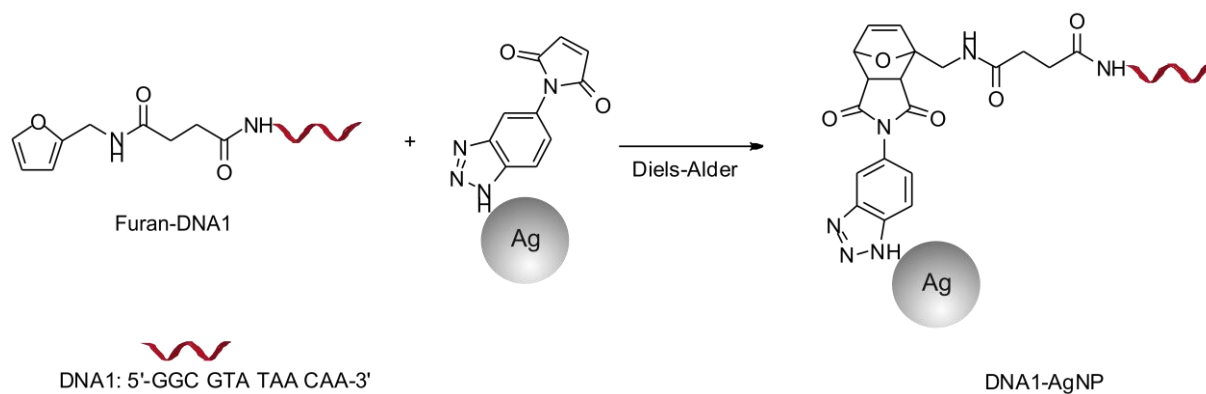
Scheme 2. 14 Formation of DNA1-Ag NP conjugates through the Diels-Alder cycloaddition between furan-modified DNA and BTM-coated Ag NPs

The reaction was first attempted in H_2O at room temperature or elevated temperature (45 °C), but the electrophorestic mobility of Ag NPs did not change after the reaction (Figure 2.22), which indicated that no DNA1-AgNP conjugates were obtained. However, it was reported previously that certain salts, such as LiCl and $CuNO_3$, which act as Lewis acids, could coordinate to the dienophile and consequently decrease its LUMO energy, facilitating its reaction with the diene HOMO and thus enhancing the efficiency of the Diels-Alder reaction.[298, 371] Indeed, when the reaction was performed in the presence of LiCl (0.3 M), the DNA1-AgNP conjugates were obtained after 2 h as indicated by the significant mobility shift in the agarose gel (1%) (Figure 2.22). Control experiment, in which unmodified DNA1 was used, has not resulted in the DNA1-AgNP conjugates, confirming that the attachment of DNA1 to Ag NPs occurred specifically through Diels-Alder cycloaddition.

BTM-Ag NPs	+	+	+	+	+
DNA1		+	+		
furan-DNA1				+	+
LiCl			+		+
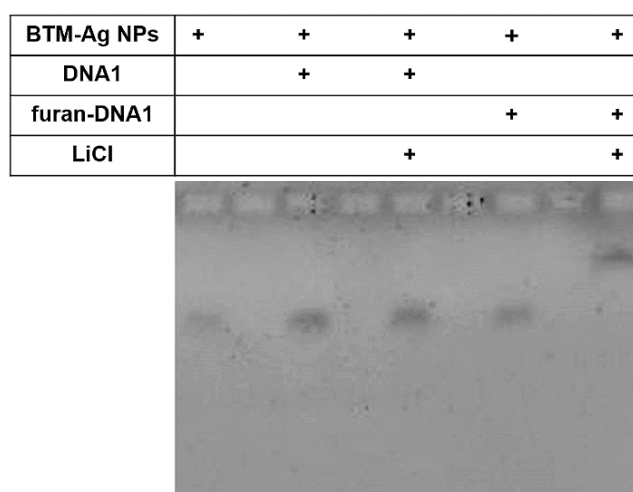
Figure 2. 22 Agarose gel image for DNA1-AgNP conjugates taken under the UV-light mode of the gel imaging system

2.2.2.3 Design of Protein-AgNP Hybrids through DNA-Directed Immobilization

To prove that DNA remains functional after being attached to Ag NPs, hybridization with *c*DNA1 was performed (Scheme 2.15), and the mobility shift observed in the agarose gel electrophoresis (1%) (Figure 2.23) indicated the hybridization was successful.

DNA1: 5'-GGC GTA TAA CAA-3'   *c*DNA1: 5'-TTG TTA TAC GCC-3'
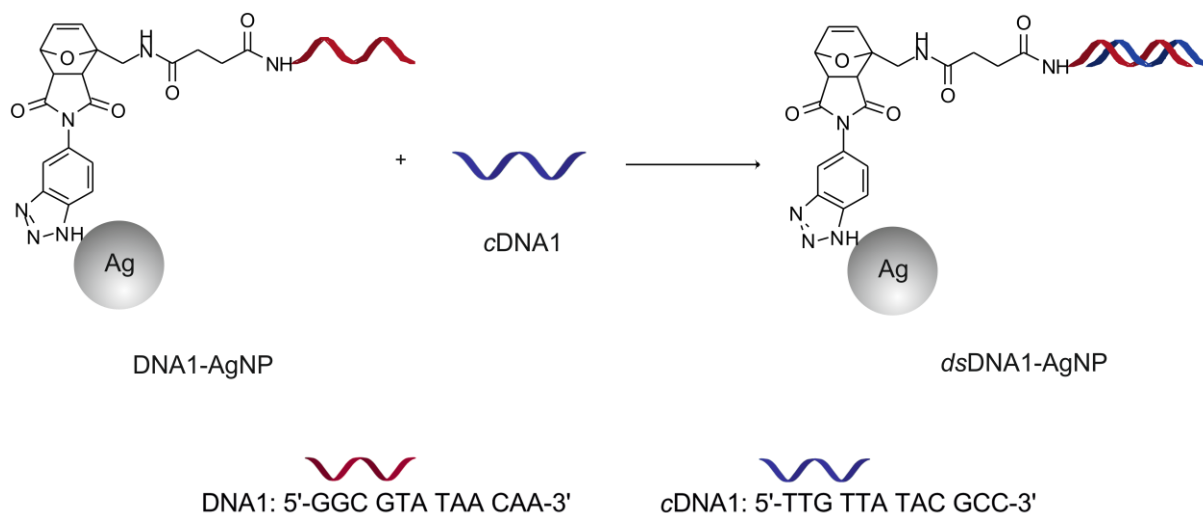
Scheme 2. 15 DNA hybridization on the surface of Ag NPs
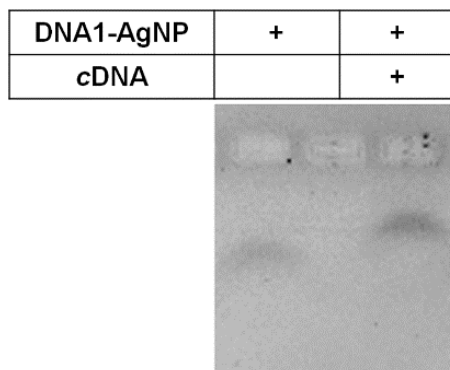
DNA1-AgNP	+	+
*c*DNA		+

Figure 2. 23 Agarose gel image for the hybridization of DNA1-AgNP and *c*DNA1 taken under the UV-light mode of the gel imaging system

The intrinsic hybridization ability of DNA has already been successfully utilized in nanotechnology, not only to prepare nanocomposites through the assembly of different NPs,[372] but also enable the attachment of different molecular species to the surface of NPs through DNA-directed immobilization. For example, Chen *et al*. studied the correlation between the fluorescent intensity of a fluorophore and the LSPR of Ag NPs through the DNA-directed attachment of fluorophore on Ag NPs.[373] Niemeyer's group reported the DNA-directed immobilization of antibody on Au NPs for the sensitive detection of antigen.[374]

To demonstrate that the as prepared DNA1-AgNP conjugates could also be used for the design of protein-AgNP hybrids, myoglobin (Mb), a heme-containing pseudo-peroxidase, was chosen as a proof of the attachment principle, as it belongs to the class of biologically important heme enzymes and its activity after immobilization can be directly studied by employing fluorescent enzymatic assays.
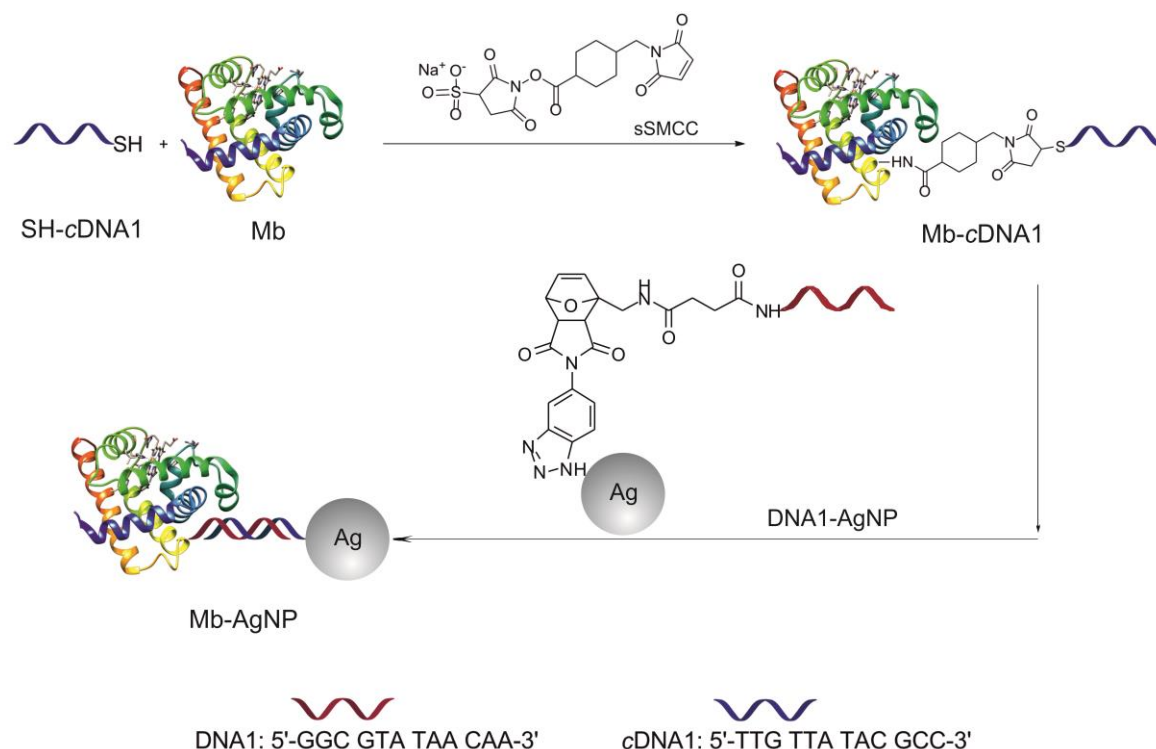
Scheme 2. 16 Preparation of Mb-*c*DNA1 conjugates and the subsequent immobilization of Mb on the surface of Ag NPs through DNA-directed immobilization

To achieve that, Mb first needs to be modified with *c*DNA1 to enable its subsequent attachment to Ag NPs (Scheme 2.16). Covalent Mb-*c*DNA1 conjugates were prepared using sulfosuccinimidyl-4-[N-maleimidomethyl]cyclohexane-1-carboxylate (Sulfo-SMCC) cross-linker. The products were purified by fast protein liquid chromatography (FPLC) (Figure 2.24), which showed that two fractions (I and II) were eluted shortly after 20 min, and their absorptions at 260, 280 and 410 nm indicated the existence of DNA1, protein and heme in both fractions. The formation of Mb-*c*DNA1 conjugates was further confirmed by PAGE (12%) analysis (Figure 2.25), which showed the significant mobility shift of both fractions in comparison to Mb and *c*DNA1 alone. The amounts of *c*DNA1 strands in both Mb-*c*DNA1 conjugates (I and II) were determined according to the absorbance at 280, 410 and 260 nm

(Figure 2.26), and the results indicated that Mb-*c*DNA1 (I) and (II) could be identified as conjugates containing one and two *c*DNA1 strands, respectively.
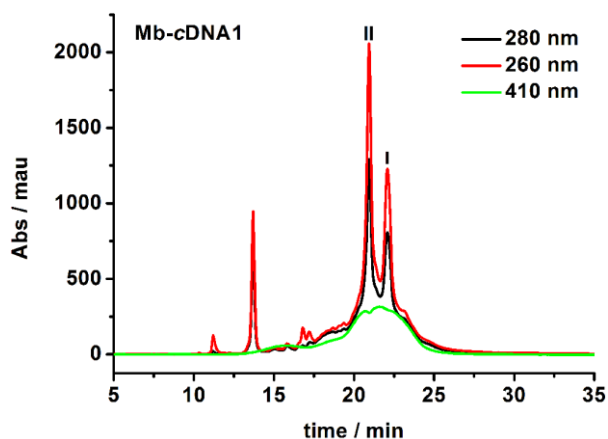
Figure 2. 24 FPLC chromatogram of Mb-*c*DNA1 conjugates
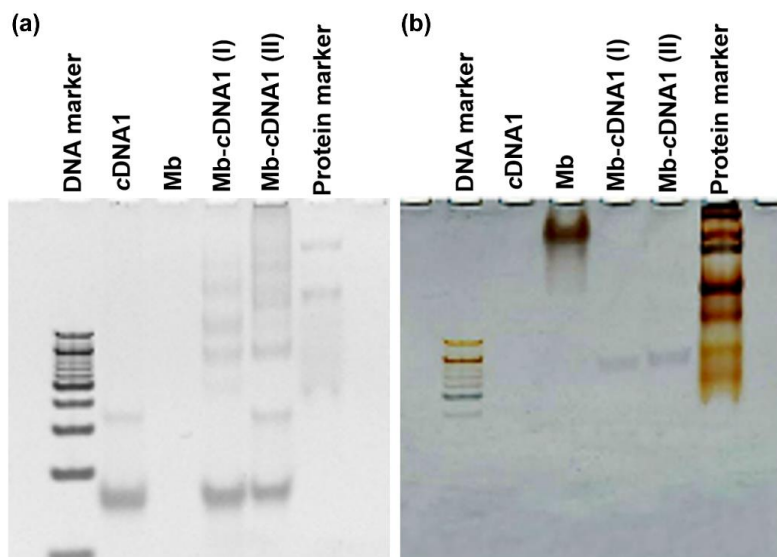
Figure 2. 25 PAGE images for Mb-*c*DNA1 (I and II) conjugates: (a) SYBR gold staining and (b) silver staining
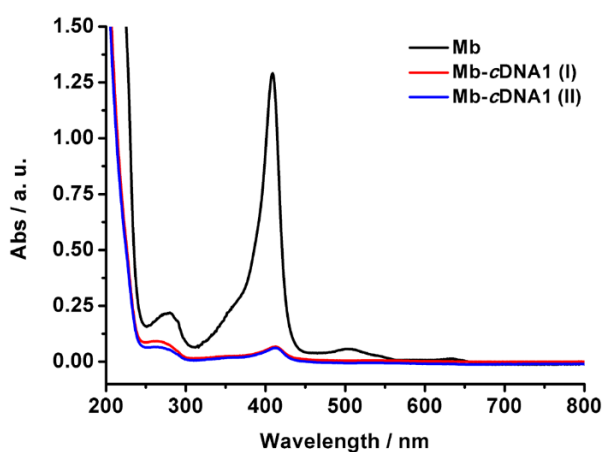
Figure 2. 26 UV-Vis spectra of Mb and Mb-*c*DNA1 (I and II) conjugates

103

Both Mb-*c*DNA1 (I) and (II) conjugates were then attached onto the surface of Ag NPs through DNA-directed immobilization, and the clear mobility shifts of Ag NPs after the hybridization process could be observed in the image for agarose gel electrophoresis (1%) (Figure 2.27), indicating the formation of Mb-AgNP hybrids.

DNA1-AgNP	+	+	+	+
*c*DNA		+		
Mb-*c*DNA1 II			+	+
Mb-*c*DNA1 I				+
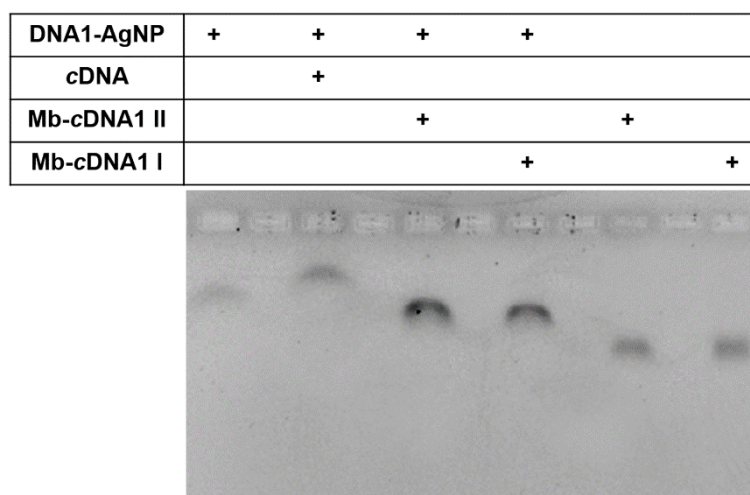
Figure 2. 27 Agarose gel image for Mb-AgNP hybrids taken under the UV-light mode of the gel imaging system

However, it is crucial to investigate the activity of the protein after the attachment to the surface of NPs, as undesired structural changes of protein might take place and in turn impair their activity.[271, 276]

Amplex Red (non-fluorescent)

Resorufin (fluorescent)
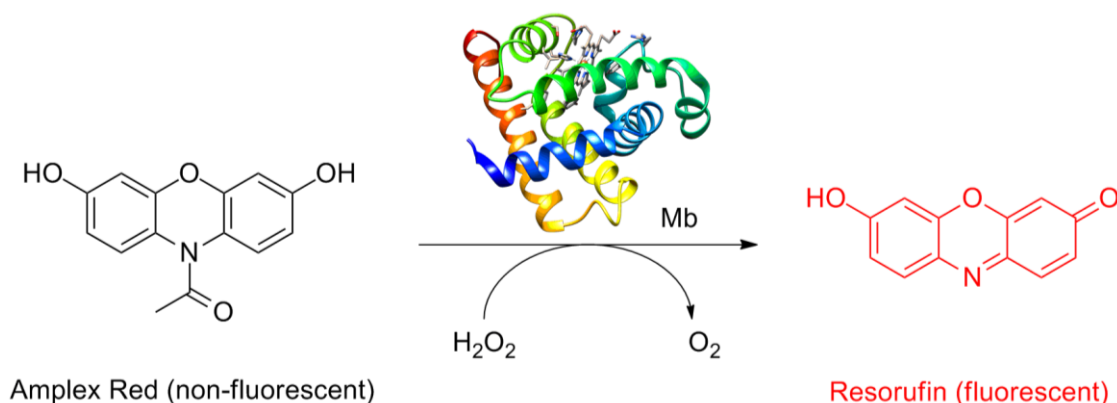
Scheme 2. 17 Schematic illustration for the peroxidase activity test of Mb-AgNP conjugates. Non-fluorescent Amplex Red could be oxidized into fluorescent resorufin by H_2O_2 in the presence of peroxidase enzyme.

In order to study the enzymatic activity of the Mb-AgNP hybrids, a reported peroxidase activity assay was employed,[338] in which non-fluorescent N-acetyl-3,7-dihydroxyphenoxazine (Amplex Red) could be oxidized into fluorescent resorufin (λ_{ex} = 540 nm, λ_{em} = 585 nm) by H_2O_2 in the presence of peroxidase enzymes (Scheme 2.17), so the activity of the enzyme

could be demonstrated by the detected fluorescence of resorufin. As can be seen from Figure 2.28, the peroxidase activity of Mb-cDNA1 (II) and Mb-AgNP (II) decreased significantly when compared to native Mb, while the enzyme remained fully active in Mb-cDNA1 (I) and Mb-AgNP (I) (a slight increase was even observed). The activity difference is most probably due to the differences in the orientation and position of cDNA1 strands on the surface of the proteins for two different protein-cDNA conjugates, as the sulfo-SMCC conjugation is not stereo- and regio-specific, and cDNA1 strands close to the heme active centre might impair the activity of the enzyme as in the case of Mb-cDNA1 (II).
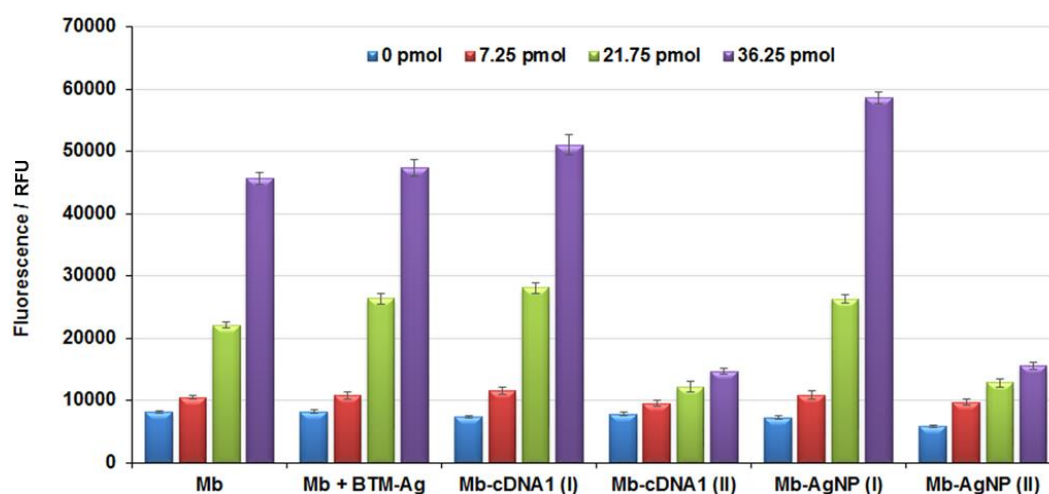
Figure 2. 28 Peroxidase activity of Mb, the simple mixture of Mb and BTM-Ag NPs, Mb-cDNA1 conjugates, and Mb-AgNP hybrids obtained through DNA-directed immobilization

2.3 Diels-Alder Cycloaddition for the Preparation of Polymer-AgNP Nanocomposites

After the successful preparation of protein-AgNP hybrids, we were also interested in checking if the Diels-Alder strategy could also be employed for the attachment of other molecular species onto BTM-coated Ag NPs. In particular, our interest lies in extending the application of such method to polymer materials.

Polymer-NP nanocomposites have attracted lots of attention recently and have been employed for applications in biolabelling, nanodevices and antibacterial studies, because they possess advantageous optical, mechanical and chemical properties,[375, 376] Especially, polymers can stabilize colloid NPs, and have been shown to be biostatic, and are able to control the release metal species.[376] One of the most used polymers for the modification of NPs is polyethylene glycol (PEG), which is an amphiphilic linear biocompatible polymer composed of repeated units of $-CH_2-CH_2-O-$.[350] The attachment of PEG to the surface of NPs (so

called PEGylation) could prevent the aggregation of NPs by stabilizing their surface, modify the size of NPs, and increase the biocompatibility and solubility of NPs, which facilitate the applications of NPs in imaging, drug delivery and therapy.[377] For instance, PEGylated superparamagnetic iron oxide NPs exhibited high performance at a relatively low dose in tumor imaging by magnetic resonance imaging.[378] PEG shell-coated colloidal mesoporous silica NPs exhibited higher biostability than the unfunctionalized NPs in a simulated body fluid.[379] PEGylated Au nanorods showed prolonged blood circulation and wider tissue distribution in an animal test than the non-PEGylated counterparts.[380]
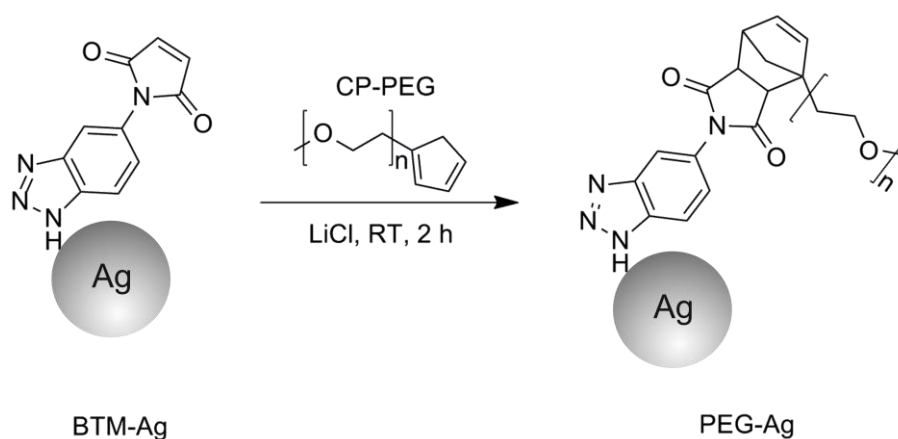
Scheme 2. 18 PEGylation of BTM-coated Ag NPs through Diels-Alder reaction

Herewith, to investigate if the PEGylation of BTM-coated Ag NPs could be realized by Diels-Alder strategy, cyclopenta-1,3-diene-modified polyethylene glycol (CP-PEG, Mw ~2000 g/mol, provided by Prof. Christopher Barner-Kowollik's group) was employed to functionalize Ag NPs (Scheme 2.18). Agarose gel electrophoresis (1%) showed a clear shift between the bands of BTM-coated Ag NPs and PEGylated Ag NPs (Figure 2.29a), indicating that PEG has been immobilized on the surface of Ag NPs. Interestingly, the fluorescence study of PEG-coated Ag NPs (Figure 2.29b) showed that the fluorescence intensity increased when the solution of PEG-AgNP was heated to 60 $^{\circ}$C, which proved that the intrinsic fluorescent property of BTM (**4**) was not affected by the PEG conjugation to the maleimide ring. This simple methodology for the preparation of fluorescent PEG-coated Ag NPs through the use of a fluorescent linker might be extended to the preparation of different fluorescent polymer-NP nanocomposites, which might be useful for applications in imaging and cell uptake studies.
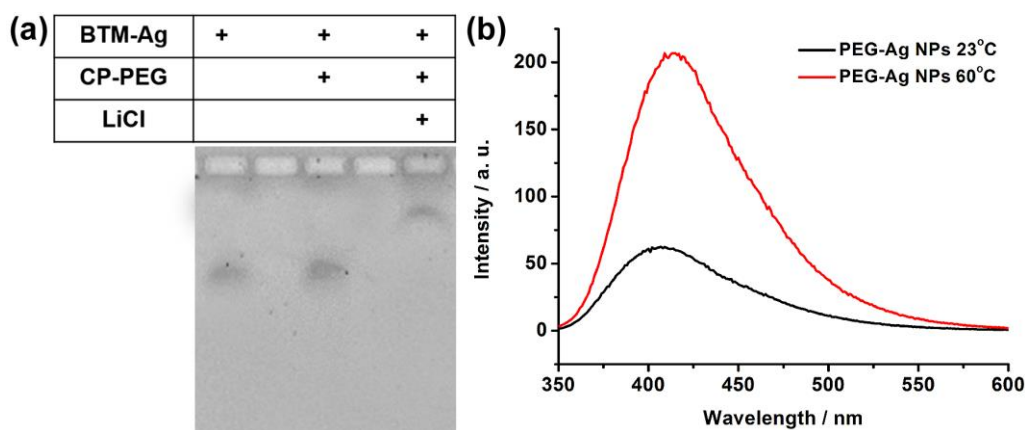
Figure 2. 29 (a) Agarose gel image for PEG-coated AgNP taken under the UV-light mode of the gel imaging system, and (b) fluorescence spectra of PEG-AgNP nanocomposites at 23 °C and 60 °C (λ_{ex} = 340 nm)

2.4 Conclusions

Different routes have been employed for the preparation of monodispersed and water soluble Ag NPs, including PAA- and BTM-coated Ag NPs. Both groups of NPs were found to be fluorescent, and the fluorescence of PAA-Ag NPs was resulted from their small size, while the fluorescence of BTM-Ag NPs was come from the fluorescent capping agent.

The subsequent surface biofunctionalization of Ag NPs with DNA oligonucleotides was realized through two different strategies: ligand exchange with BTM-modified DNA on PAA-coated Ag NPs and Diels-Alder cycloaddition between BTM-coated Ag NPs and furan-DNA. The as-prepared DNA-AgNP conjugates were employed for the assembly with Au NPs through DNA hybridization, and the obtained Ag-*ds*DNA-Au nanocomposites could be used as SERS substrates for the detection of fluorescent protein. Furthermore, the obtained DNA-AgNP conjugates were also employed for the design of protein (Mb)-AgNP hybrids through DNA-directed immobilization, and the enzymatic activity of Mb was retained after its immobilization on the surface of Ag NPs.

To extend the application of Diels-Alder strategy, the PEGylation of BTM-coated Ag NPs was performed using a diene-modified PEG, and the as-synthesized PEG-coated Ag NPs retained the intrinsic fluorescent property of BTM. The obtained fluorescent polymer-coated NPs might find applications in imaging and cell uptake studies.

Such kind of simple and efficient methodologies for the functionalization of NPs might be extended to the design and fabrication of other hybrid systems or nanocomposites with novel physical, chemical and biological characteristics, which might be useful for sensing, biocatalysis and imaging.

Chapter 3

Synthesis and Properties of Copper Nanoparticles

3 Synthesis and Properties of Copper Nanoparticles (Cu NPs)

Cu nanomaterials have been explored as essential candidates for catalysts, antibacterial agents, apoptosis, electronics and optical devices, because they possess many fascinating properties such as high catalytic potential, high conductivity and optical properties,[381-383] and in addition, the remarkably low cost of Cu compared to Au and Ag makes them more useful for scaled-up production.[384] However, the applications of Cu nanomaterials have been significantly limited by their instability against oxidation. In search for stable Cu nanomaterials, different synthetic methods have been developed up to date including thermal decomposition,[76] reverse micelle,[101] polyol method,[86] electrochemical approach,[95] and biotemplated strategy.[109] The stability and size of the obtained Cu nanomaterials vary greatly depending on the methods,[385, 386] and due to the ease of surface oxidation, the synthesis of stable Cu NPs under aqueous conditions still poses a significant challenge. In this thesis, different strategies have been attempted in order to get water-soluble and stable Cu NPs, which could be used for the further applications, such as enzyme mimetics and catalysis.

3.1 Synthesis of Cu NPs

3.1.1 Seed-Mediated Growth of Cu NPs
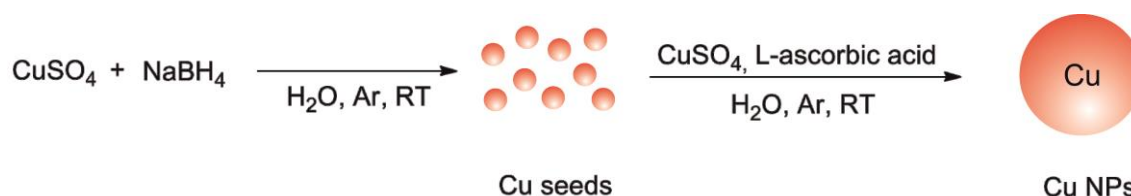
Scheme 3. 1 Schematic illustration for seed-mediated growth of Cu NPs at room temperature (RT) using salt reduction method

As introduced in 1.1.4, the synthesis of NPs through seed-mediated growth involves two separated steps: nucleation and growth.[61] Herewith, a reported seed-mediated growth method was employed for the preparation of Cu NPs (Scheme 3.1).[387] Firstly, Cu seeds with an average diameter of ~12.3 nm were prepared through the reduction of $CuSO_4$ with $NaBH_4$ under Ar protection. The TEM image (Figure 3.1a) shows that the as-synthesized Cu seeds were aggregated into chain-like structures, which were then employed for the preparation of Cu NPs.
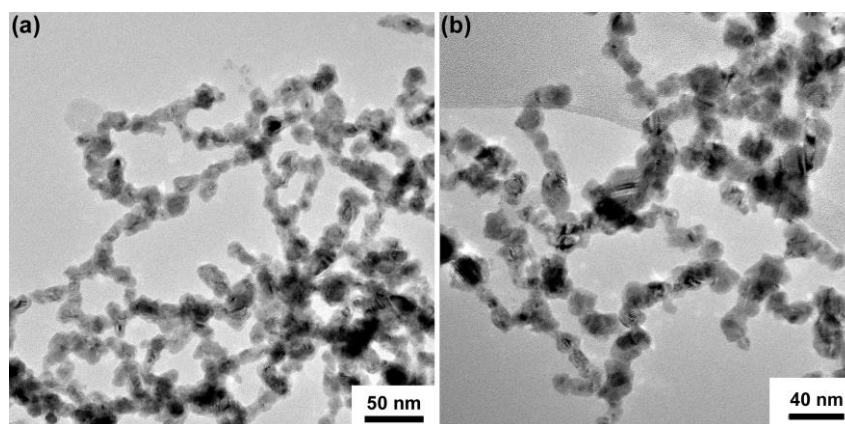
Figure 3. 1 TEM images of (a) Cu seeds and (b) Cu NPs obtained by seed-mediated growth method

After the addition of Cu seeds to the aqueous solution of $CuSO_4$, L-ascorbic acid was added to reduce $CuSO_4$ under Ar protection. The colour of the solution turned to brown after 5 min indicating the formation of Cu NPs. The obtained Cu NPs maintained the chain structures of Cu seeds (Figure 3.1b), and their average diameter was ~18.2 nm. However, the colour of the solution turned to blue after a couple of days indicating that the oxidation of Cu to Cu^{2+} occurred, as Cu^{2+} rich solution is normally blue or green, while Cu^+ in solution is colorless.[388] The instability of Cu NPs might be due to the lack of additional capping agents, and the direct exposure of NPs' surface to air could easily induce the oxidation of Cu NPs.

3.1.2 Polyvinylpyrrolidone (PVP)-Coated Cu NPs
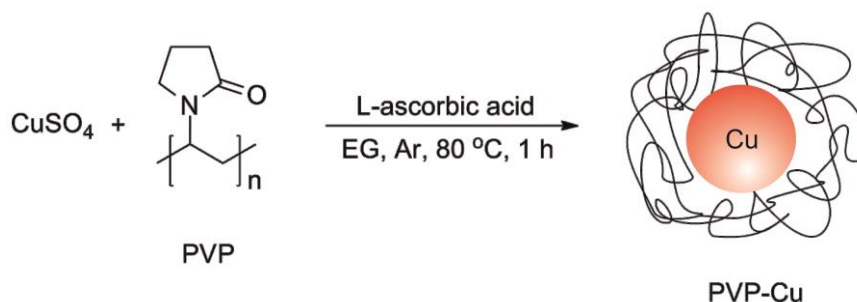
Scheme 3. 2 Schematic illustration for the preparation of PVP-coated Cu NPs

Polyvinylpyrrolidone (PVP) is a water-soluble polymer containing a polyvinyl backbone and polar amide groups.[389] Due to the complex formation ability of the N and O polar groups of PVP towards metals, it has already been widely used as surface coatings for colloid NPs such as Au, Ag and Pt.[112, 389, 390] Herein, PVP was employed as a capping agent and L-ascorbic acid as a reducing agent for the preparation of Cu NPs in ethylene glycol (EG) (Scheme 3.2).[77]

112
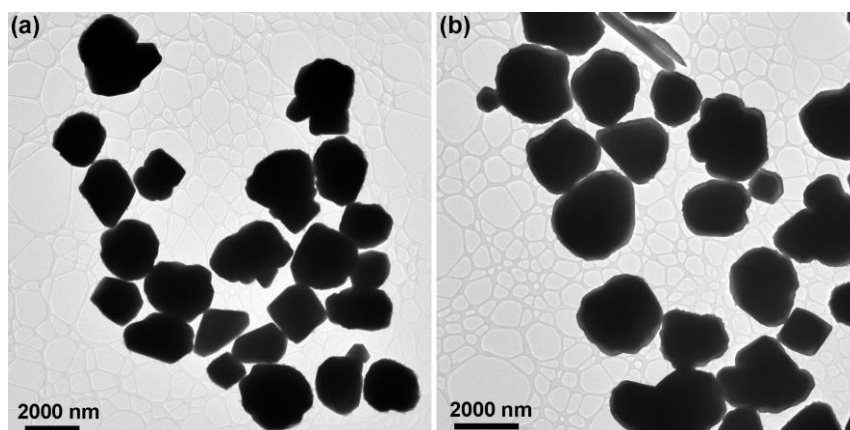
Figure 3. 2 TEM images of PVP-stabilized Cu NPs

The reaction was carried out at 80 ℃ for 1 h under Ar protection, after which the colour of the solution turned red, indicating the formation of Cu NPs. However, as can be seen from the TEM images (Figure 3.2), the obtained particles were really huge, and the average size was ~2 μm, which was not desirable for nanoscaled applications.

3.1.3 Citrate-Coated Cu NPs

Citrate has been extensively employed as a capping agent and a reducing agent for the preparation of Au and Ag NPs.[35, 29] Feldmann and co-workers have already employed citrate to prepared stable Cu NPs in diethylene glycol, which showed excellent stability even after months of storage or high temperature treatment.[86] Since the carboxylic groups of citrate have strong affinities to the surface of metals, it is interesting to know if citrate could be used as a good surface stabilizer for the synthesis of Cu NPs in aqueous solutions.
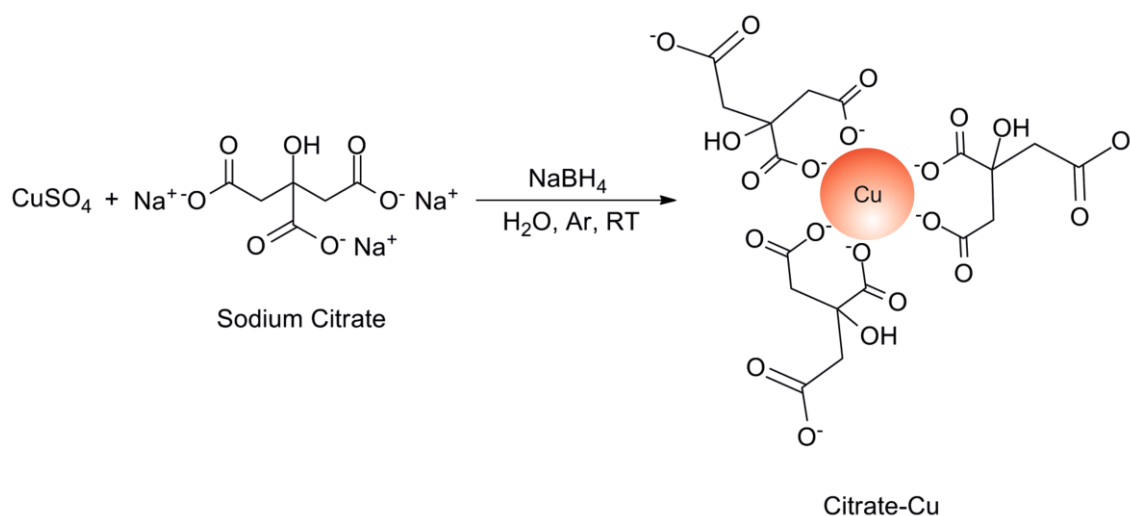
Scheme 3. 3 Schematic illustration for the preparation of citrate-coated Cu NPs

CuSO$_4$ was reduced by NaBH$_4$ in the presence of sodium citrate (Scheme 3.3), and the reaction was performed under Ar protection. The colour of the solution changed from blue to dark brown indicating the formation of Cu NPs.
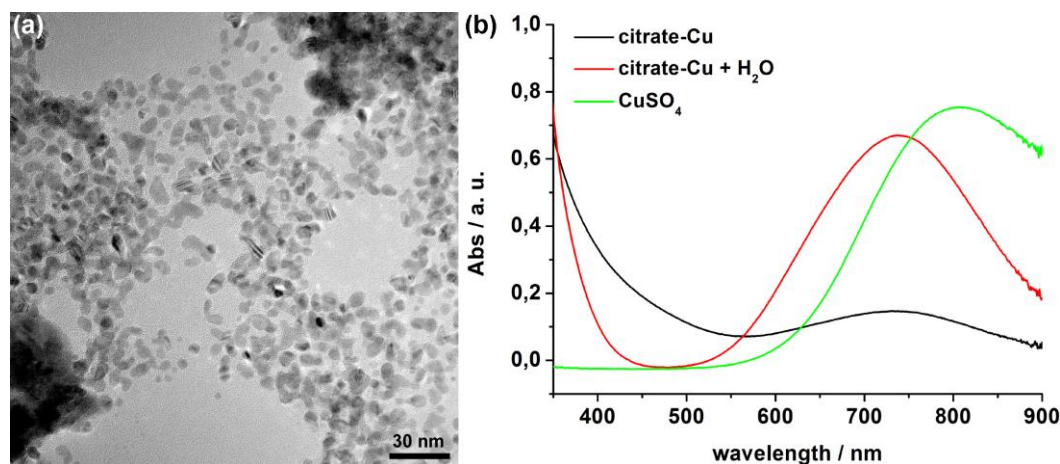
Figure 3. 3 (a) TEM image of citrate-coated Cu NPs, and (b) UV-Vis spectrum of CuSO$_4$ and citrate-coated Cu NPs (before and after the addition of extra H$_2$O)

As can be seen from the TEM image (Figure 3.3a), small NPs with an average diameter of 6.2 nm as well as a few agglomerated NPs could be observed. UV-Vis spectrum (Figure 3.3b) of the Cu NPs, which were washed thoroughly with ice-cold water, showed a broad absorption band between 550 and 800 nm indicating the existence of both Cu NPs and Cu^{2+}. When certain amount of H$_2$O (room temperature) was added to the solution of Cu NPs, the colour of the solution turned blue indicating that Cu NPs were oxidized by the dissolved oxygen in H$_2$O, which was confirmed by the absorption increase of Cu^{2+} at 740 nm in the UV-Vis spectrum (Figure 3.3b). The oxidation of Cu NPs upon the addition of H$_2$O indicates that citrate-coated Cu NPs were not stable enough and not suitable for the further applications in aqueous conditions.

3.1.4 Cetyltrimethylammonium Bromide (CTAB)-Coated Cu NPs

Cetyltrimethylammonium (CTAB) is a cationic surfactant, which has been extensively used for the stabilization of Au nanocrystals. By changing the ratio between the surfactant and the Au precursor, different shapes of the Au nanocrystals could be obtained, such as spherical NPs and nanorods.[391]
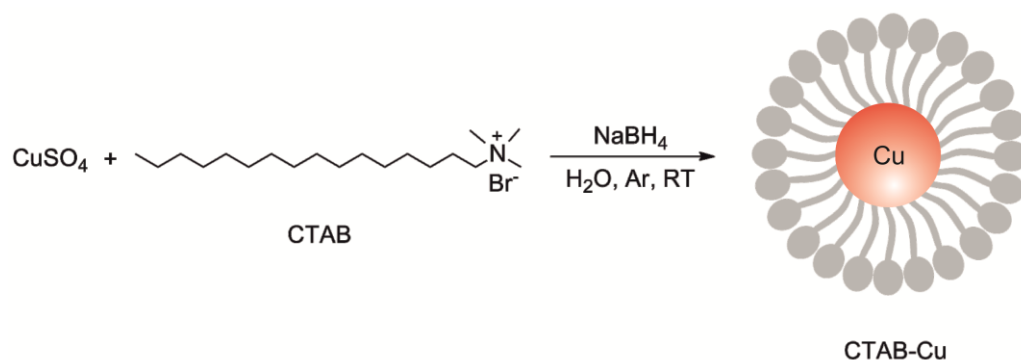
Scheme 3. 4 Schematic illustration for the preparation of CTAB-coated Cu NPs

In order to find out if CTAB could also be used as a capping agent for Cu, Cu NPs were prepared by reducing $CuSO_4$ with $NaBH_4$ in the presence of CTAB (Scheme 3.4). After the addition of the reducing agent $NaBH_4$, the colour of the solution changed from blue to brown, indicating the formation of Cu NPs. However, the colour of the solution turned back to blue after 30 min due to the oxidation of Cu NPs, indicating that Cu NPs coated by CTAB were even less stable than the NPs obtained by citrate reduction, which might be because that more CTAB is needed in order to stabilize the surface of Cu NPs.

3.1.5 Benzotriazole (BT) Derivatives-Coated Cu NPs

Benzotriazole (BT) is one of the most efficient corrosion inhibitors for Ag and Cu.[344, 345] In Chapter 2 it has already been demonstrated that BT could be used directly as capping agent for the synthesis of Ag NPs, therefore, it was interesting to know if 5-amino-BT (**1**) and BTM (**4**) could also be directly employed as stabilizers for the synthesis of Cu NPs.

R = NH₂ or maleimide
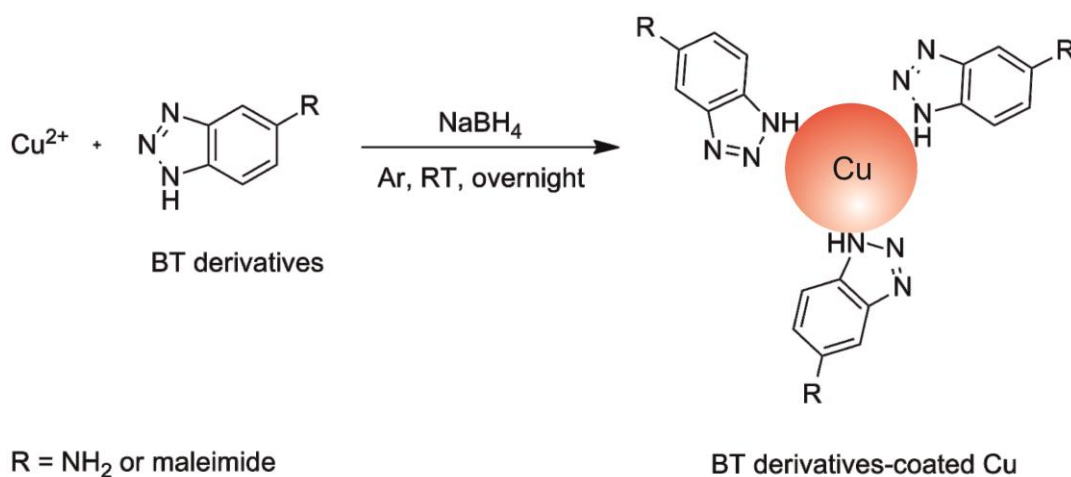
Scheme 3. 5 Schematic illustration for the preparation of BT derivatives-coated Cu NPs

It has been reported that the formation of Cu NPs was faster when $CuCl_2$ instead of $CuSO_4$ was used as the precursor due to the catalytic effect of chloride ions.[384] Therefore, $CuCl_2$ was used here to prepare BT-coated Cu NPs. The reduction of $CuCl_2$ with $NaBH_4$ was performed in the presence of 5-amino-BT (or BTM) under Ar protection (Scheme 3.5). After stirring the reaction at room temperature overnight, the color of the solution turned to black indicating the possible presence of nanostructured Cu. The products were washed thoroughly with MeCN and H_2O, and characterized by TEM. However, no NPs could be observed but rather an organic film as indicated by its sensitivity to electron beam (Figure 3.4).
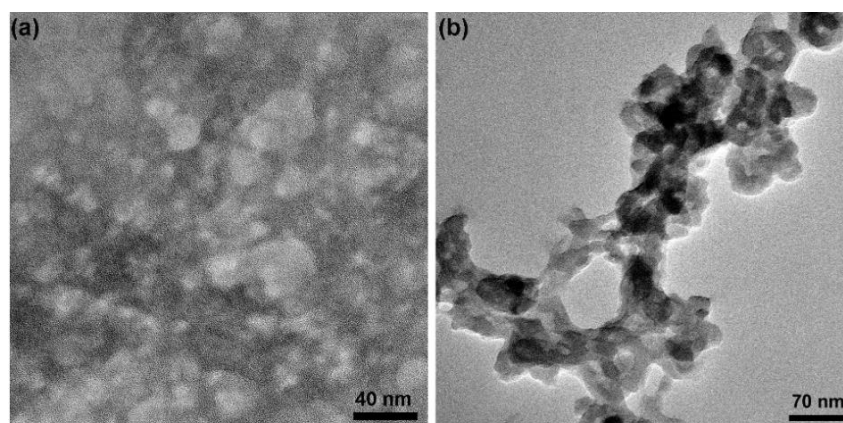
Figure 3. 4 TEM images of (a) BT-Cu NPs and (b) BTM-Cu NPs prepared using $CuCl_2$ as the precursor and the mixture of MeCN and H_2O as the solvent

It has been proposed that Cu(I)-halide complexes might form as intermidiates during the reduction process of Cu^{2+}, and the stability of Cu(I)-halide complexes is in the following order $CuCl < CuBr < CuI$.[392] To investigate if different halide ions could influence the formation of Cu NPs, the preparation of BT derivatives-coated Cu NPs was tried again using a reported procedure, in which $CuBr_2$ was used as the precursor.[393] $CuBr_2$ was mixed with BTM in methanol under Ar protection, and different molar ratios between BTM and $CuBr_2$ (1: 1 and 5: 1) were used in order to know if the amount of capping agent would affect the growth of NPs. After the addition of $NaBH_4$ and stirring at room temperature overnight, the solution became blurry, and the colour turned to pale green indicating the presence of Cu^{2+}. The products were characterized by TEM. However, same as above, no NPs could be found (Figure 3.5).
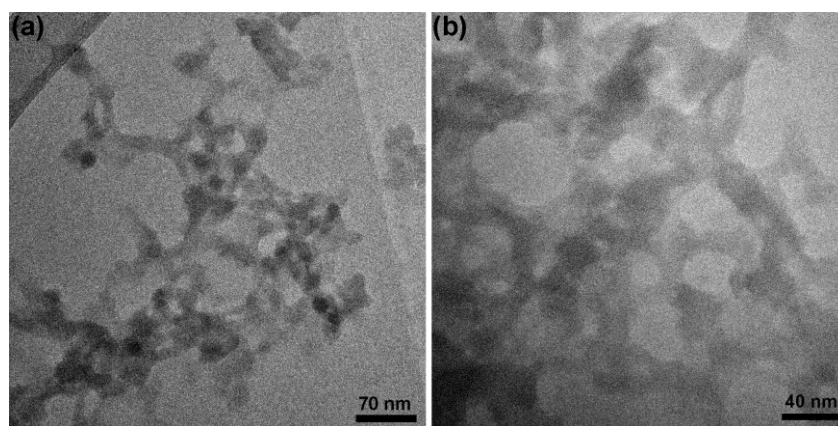
Figure 3. 5 TEM images of BTM-coated Cu NPs obtained when BTM: $CuBr_2$ was (a) 1: 1 or (b) 5 :1

The unsuccessful preparation of Cu NPs using BT derivatives as capping agents might be due to that the strong complex interaction between the triazole functional group and Cu^{2+} inhibited the reduction process. Thus, this synthetic method should be optimized by employing different ratios between BT ligands and Cu precursors, change of reaction temperature or solvent systems.

3.1.6 Iodide-Stabilized Cu NPs
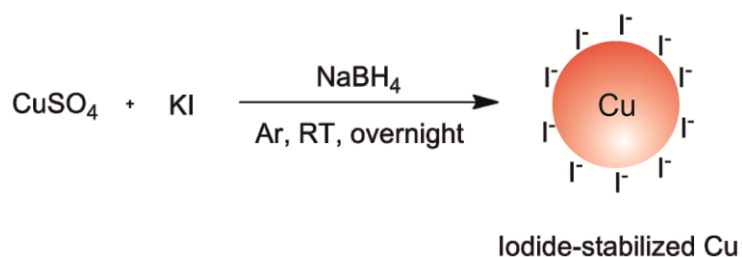
Scheme 3. 6 Schematic illustration for the preparation of iodide-stabilized Cu NPs

Since CuI is the most stable Cu(I)-halide complex, it might be possible to employ iodide directly for the stabilization of Cu NPs'surface. Kapoor *et al*. has reported that the presence of iodide anions during the reduction process of Cu^{2+} could lead to the formation of CuI, which then reprecipitated to afford Cu NPs.[392] Refering to this method, $CuSO_4$ and KI were first mixed together in H_2O and purged with Ar (Scheme 3.6). Then the reducing agent $NaBH_4$ was added, and the color of the solution turned wine-red immediately indicating the formation of Cu NPs.
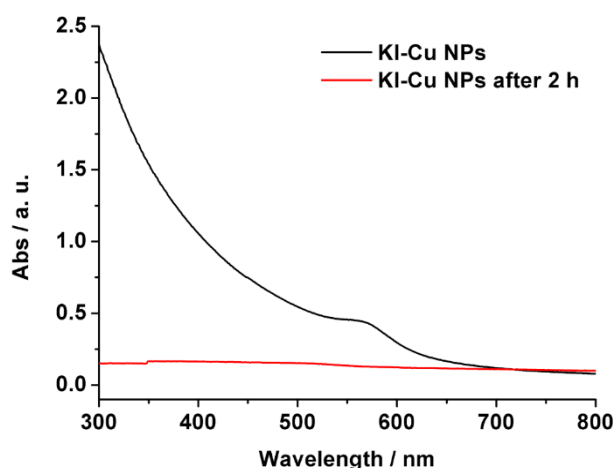
Figure 3. 6 UV-Vis spectra of KI-coated Cu NPs

However, after stirring at room temperature for another 2 hours, the color turned to yellowish green indicating that the oxidation of Cu NPs occurred. This was also confirmed by the UV-Vis spectra (Figure 3.6), which demonstrated that the plasmonic peak of Cu NPs at 575 nm disappeared when the wine-red solution turned to the yellowish green, indicating again that the iodide-coated Cu NPs were not stable.

3.1.7 DNA-Templated Synthesis of Cu NPs

DNA molecules have been employed as templates for the synthesis metallic NPs, such as Au and Ag.[394, 395] The phosphate groups of DNA are negatively charged, so they have strong affinity to the positively charged metal ions. The metal ions could then be reduced to form metallic NPs, which fit into the contour of the DNA templates.[396] Mokhir and co-workers have already reported the use of DNA duplex for the synthesis of Cu NPs, and the formation of Cu NPs was confirmed by the detected NPs' fluorescence at $\lambda_{ex} = 340$ nm and $\lambda_{em} = 580$ nm.[108] They have also demonstrated that the size of Cu NPs could be influenced by the length of the DNA strands, and longer DNA strands could lead to the formation of bigger Cu NPs and higher fluorescence intensity.
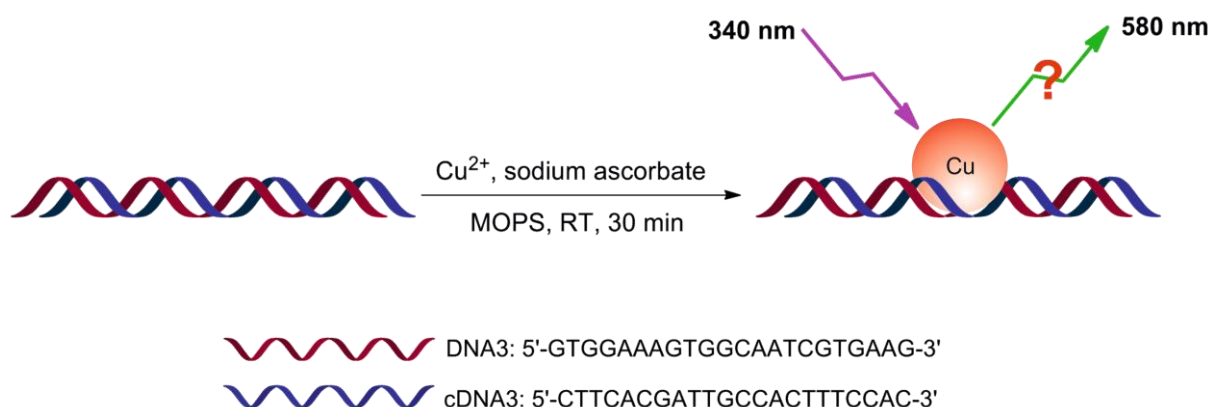
Scheme 3. 7 Schematic illustration for the *ds*DNA-templated synthesis of Cu NPs

In our approach, a 22-base oligonucleotide DNA3 was chosen to hybridize with its complementary strand *c*DNA3 in MOPS buffer (20 mM) containing 2 mM reducing agent sodium ascorbate. The formation of DNA3 duplex was confirmed by agarose gel electrophoresis (1 %) and the following gel staining with EtBr (Figure 6.2). Different types and amounts of Cu precursors ($CuSO_4$ or $CuCl_2$) (50-600 μM) were added to the solution of *ds*DNA3 templates (Scheme 3.7) in order to study if the concentrations of different precursors would affect the size and fluorescence of the obtained Cu NPs. After incubation at room temperature for 30 min, the fluorescence spectra of the obtained solutions were recorded at λ_{ex} = 340 nm. However, no matter how much Cu precursor or which Cu precursor was used, no fluorescence signals could be detected (Figure 3.7a) and no NPs could be observed by TEM characterization, indicating that there was no formation of small fluorescent Cu NPs, which might due to the weak reducing ability of sodium ascorbate.
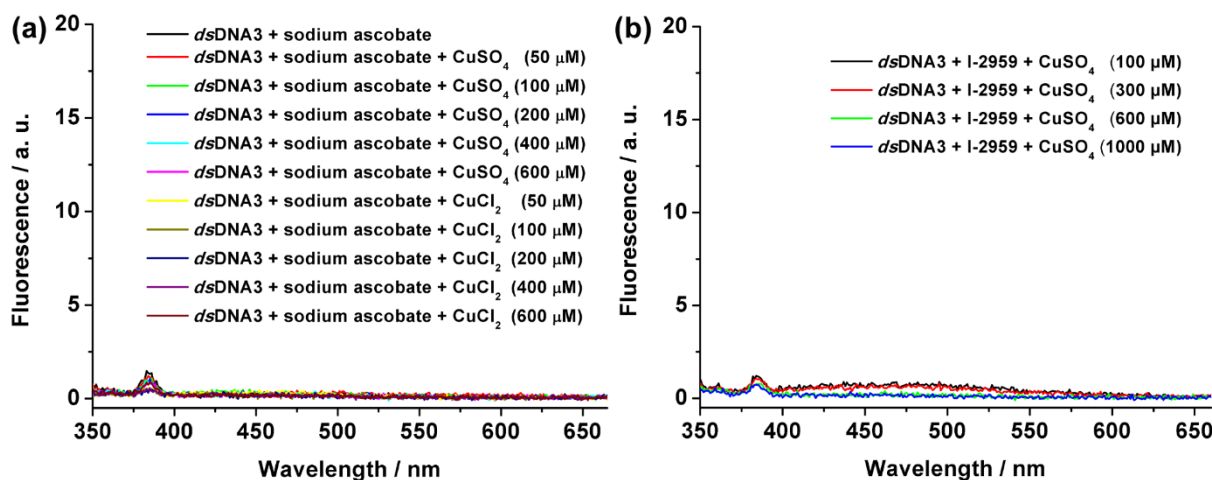
Figure 3. 7 Fluorescence spectra of the products obtained by *ds*DNA3-templated method using (a) sodium ascorbate and $CuSO_4$ (or $CuCl_2$); and (b) Irgacure-2959 and $CuSO_4$

To improve the reaction efficiency, the *ds*DNA-templated synthesis of Cu NPs was attempted again using a photo initiator Irgacure-2959 (I-2959, 2 mM),[384] instead of sodium ascorbate, as the reducing agent. The reactions using different amounts of Cu precursors were irradiated with a UV-lamp ($\lambda = 365$ nm) for 30 min, after which the fluorescence spectra of the solutions were recorded at $\lambda_{ex} = 340$ nm. However, the results were similar as above, no fluorescence signals could be detected (Figure 3.7b) indicating again that fluorescent Cu NPs were not formed.

3.1.8 Oleylamine (OA)-Coated Cu NPs
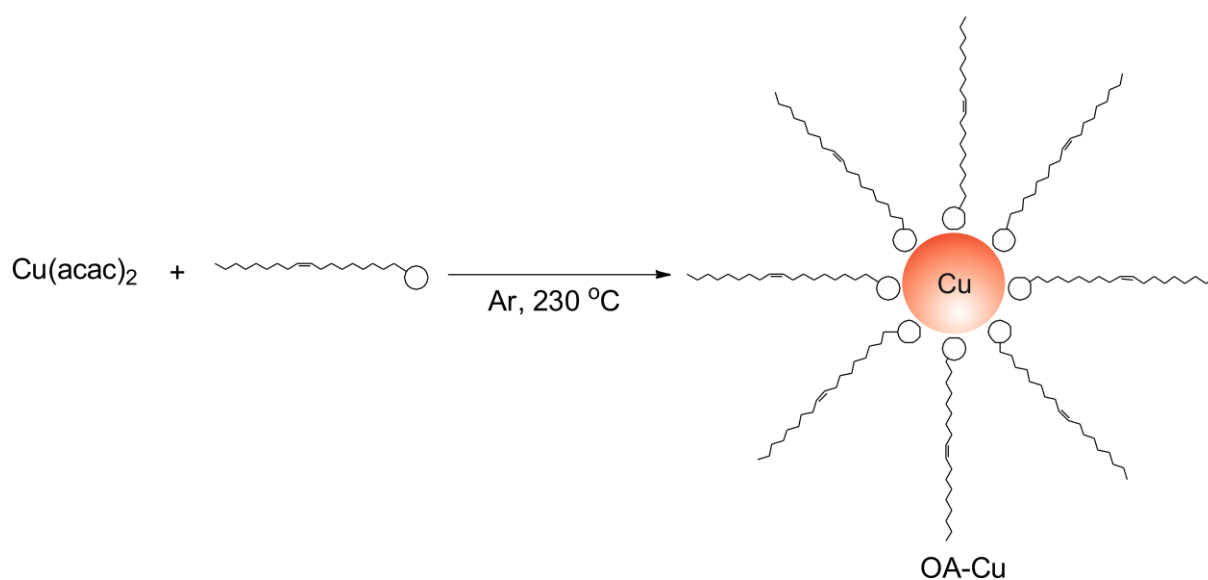
Scheme 3. 8 Schematic illustration for the synthesis of OA-coated Cu NPs

Oleylamine (OA)-coated Cu NPs were synthesized through the thermal decomposition of copper acetylacetonate in OA (Scheme 3.8) using a reported procedure.[76] The reaction was performed at 230 °C for 5 h under Ar protection. A sharp plasmonic absorption of Cu NPs at 585 nm could be observed in the UV-Vis spectrum (Figure 3.8a), and spherical Cu NPs with an average diameter of ~19.1 nm could be observed in the TEM image (Figure 3.8b).
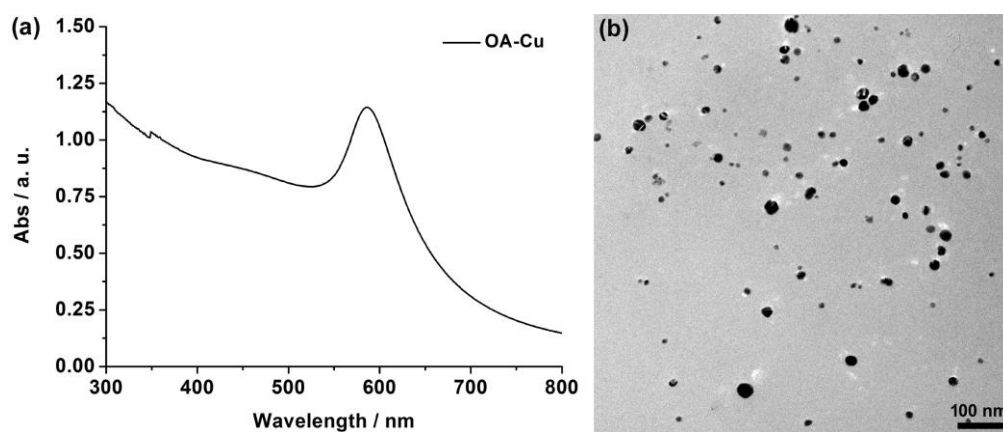
Figure 3. 8 (a) UV-Vis spectrum and (b) TEM images of OA-coated Cu NPs

In order to obtain water-soluble Cu NPs, ligand exchange was performed. The NPs were mixed with an ethanol solution of 11-mercaptoundecanoic acid (MUA). After being sonicated for 15 min and stirred at room temperature overnight, the NPs were washed thoroughly with ethanol and resuspended easily in the water, which indicated that the ligand exchange was successful. However, the MUA-coated Cu NPs precipitated at the bottom of the vial after 24 h indicating the agglomeration of Cu NPs occurred in water, which might because that Cu NPs were not well-coated by MUA after the ligand exchange process or the stabilizing ability of MUA was not as good as that of OA.

3.1.9 Polyacrylic Acid (PAA)-Coated Cu NPs

It has been described in 2.1.2 that hydrophilic polymer polyacrylic Acid (PAA) could be successfully used for the preparation of water-soluble and monodispersed Ag NPs. Since PAA possesses many carboxylic groups, which have strong affinity to metal surface, it has also been employed previously for the preparation of water-soluble Cu NPs, which were obtained through the reduction of Cu precursor by hydrazine in the presence of the capping agent PAA.[148]
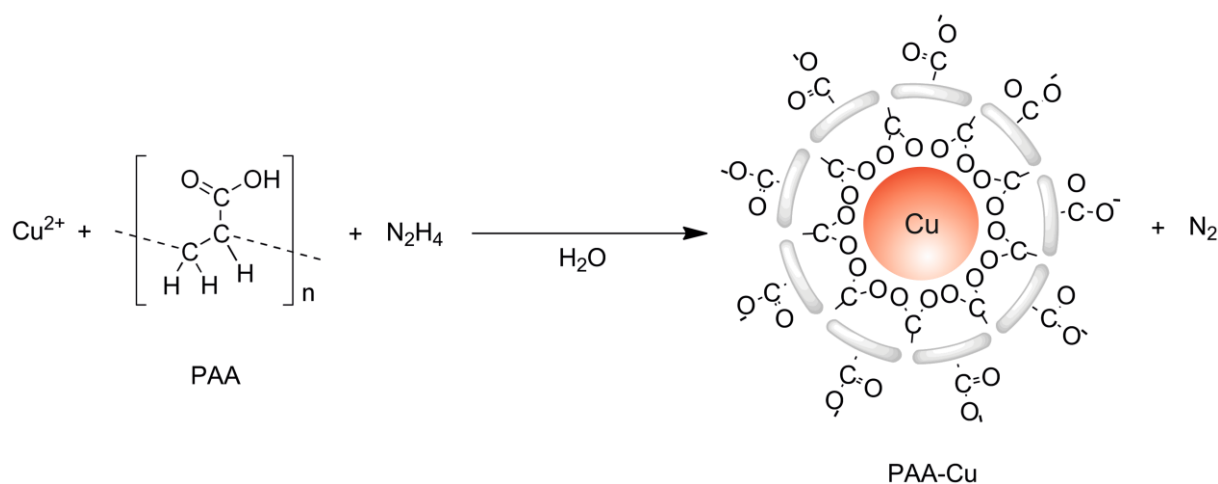
Scheme 3. 9 Schematic illustration for the synthesis of PAA-coated Cu NPs

Herewith, the preparation of PAA-Cu NPs was first attempted at 60 °C without any inert gas protection, because nitrogen could be produced during the reduction process of Cu^{2+} (Scheme 3.9), which could protect the Cu NPs from oxidation.[148] The obtained reddish brown solution was characterized by UV-Vis spectroscopy, which showed a broad plasmonic band of Cu at 585 nm as well as another absorption band at 450 nm (Figure 3.9a, black curve), which might because the existence of oxides in the solution. In addition, the colour of the solution turned from reddish brown to blue after overnight indicating that the oxidation of Cu NPs occurred, which might be due to that the surface of Cu NPs obtained at 60 °C was both very reactive and unstable.
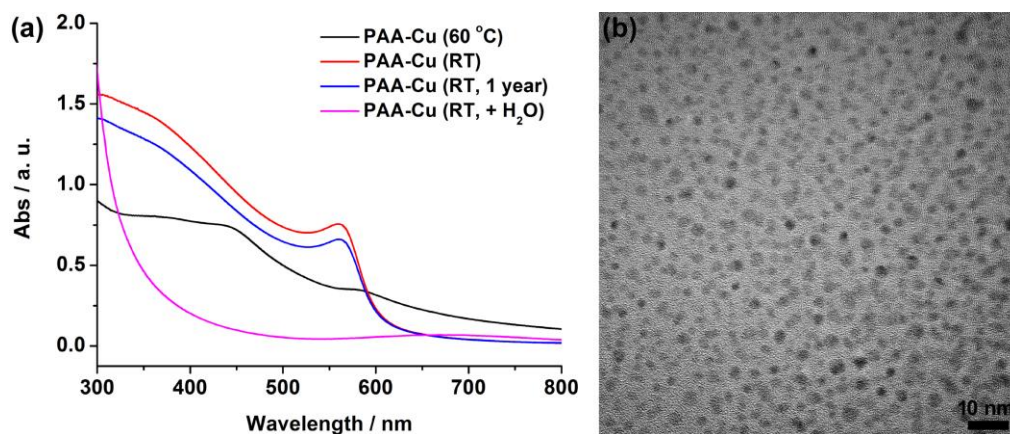
Figure 3. 9 (a) UV-Vis spectra of PAA-coated Cu NPs obtained at 60 °C or room temperature (RT); (b) TEM image of PAA-coated Cu NPs obtained at room temperature

To improve the stability of PAA-coated Cu NPs, the same reaction was performed again at room temperature, and a wine-red solution was obtained. The UV-Vis spectrum

(Figure 3.9a, red curve) showed a plasmonic band of Cu NPs at 575 nm, and the TEM image shows that monodispersed Cu NPs with an average diameter of ~3.0 nm were obtained (Figure 3.9b). Due to the existence of nitrogen in solution and large numbers of carboxylic groups on NPs' surface, the as-synthesized Cu NPs could be stable for over one year when stored at 4 °C as indicated by the plasmonic absorption of Cu recorded after one year (Figure 3.9a, blue curve).

However, when H_2O (20 μL) was additionally added to the solution of PAA-Cu NPs (100 μL), the colour of the solution turned from wine-red to blue overnight indicating the oxidation of Cu NPs ocurred, which was also confirmed by the disappearance of the plasmonic band in the UV-Vis spectrum (Figure 3.9a, violet curve). This might be due to the effect of the dissolved oxygen in the additional H_2O, which could both disturb the nitrogen balance around PAA-coated Cu NPs and oxidize the NPs, indicating that PAA-Cu NPs are not a good candidate for further applications due to their instability.

3.1.10 L-Ascorbic Acid (AA)-Coated Cu NPs
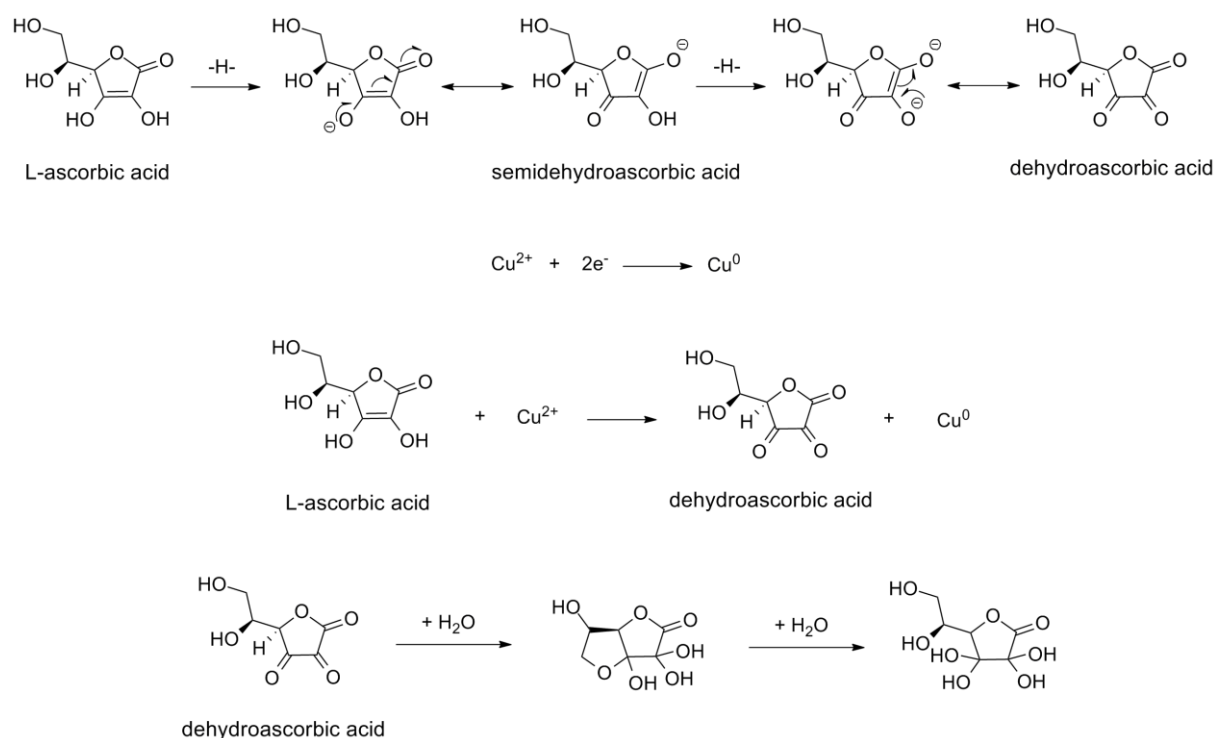
Scheme 3. 10 Mechanism for the reduction of Cu^{2+} by AA and the formation of polyhydroxyl structure for the surface stabilization of Cu NPs

L-ascorbic acid (AA) stabilized Cu NPs were synthesized using a previously reported method with slight modification.[383] $CuCl_2$ was reduced by AA at 80 °C, and the solution

became brown after 16 h indicating the formation of Cu NPs. The redox mechanism between AA and Cu^{2+} is demonstrated in Scheme 3.10.[383] AA could be oxidized to dehydroascorbic acid when Cu^{2+} is reduced to Cu^0.
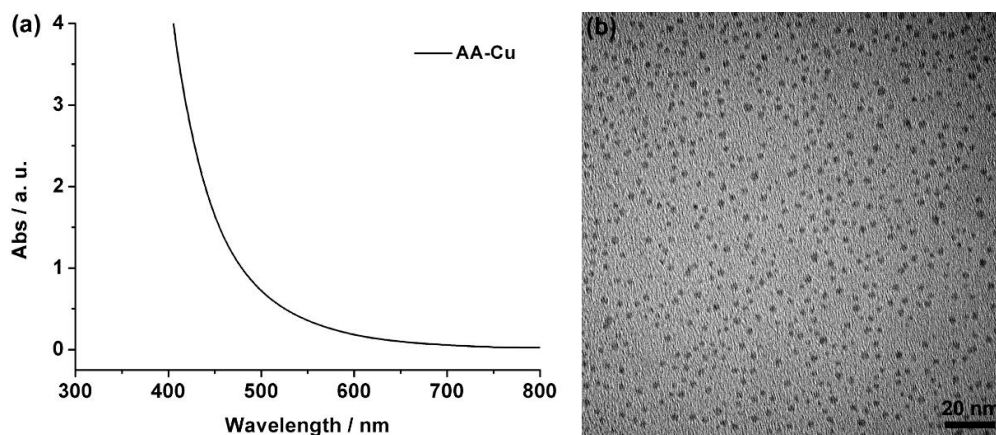
Figure 3. 10 UV-Vis spectrum and TEM image of AA-coated Cu NPs

No obvious plasmonic absorption of Cu NPs could be observed in the UV-Vis spectrum (Figure 3.10a) indicating the existence of small Cu NPs, which was further confirmed by the TEM image (Figure 3.10b). The average diameter of AA-coated Cu NPs was ~2.5 nm, and the as-synthesized Cu NPs could be stable for months.

A possible explanation for the stabilization effect of AA might lie in the formation of dehydroascorbic acid during its redox reaction with Cu^{2+}. Dehydroascorbic acid can undergo irreversible hydrolysis rapidly in aqueous solutions resulting in a polyhydroxyl structure (Scheme 3.10).[383] The hydroxyl groups could interact with NPs' surface, stabilize the NPs, and act as a protecting layer against oxidation.

3.1.11 Dopamine Derivatives-Coated Cu NPs

Dopamine (DA, **6**) is a water-soluble and easily available catechol containing biomolecule, and is a hormone and neurotransmitter that plays important roles in human brain and body.[397] DA possesses interesting properties such as the ability to undergo polymerization to afford bio-inspired glue,[398, 399] and it has already been employed as a reducing agent for the synthesis of Au NPs.[400] Since it has been mentioned above that the polyhydroxyl groups could stabilize the surface of Cu NPs through the formation of complex, we were interested in investigating the ability of the catechol groups of dopamine and dopamine-based linkers to act as stabilizing agents for Cu NPs in aqueous solutions.

Dopamine (DA)-Coated Cu NPs
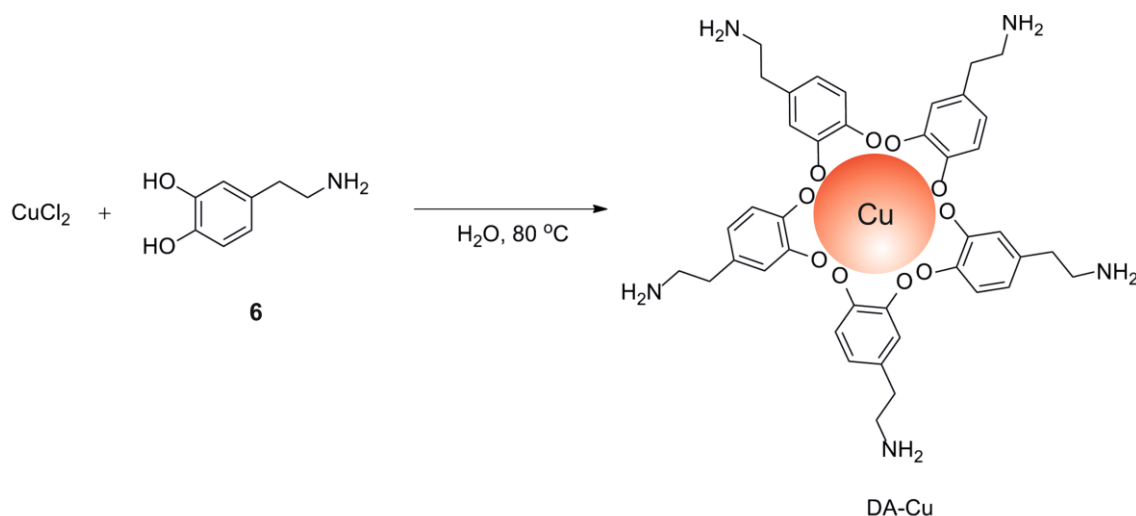
Scheme 3. 11 Schematic illustration for the synthesis of DA-coated Cu NPs

DA-coated Cu NPs was prepared by the reduction of CuCl$_2$ with DA (**6**) at 80 ºC without any additional reducing agent, capping agent and inert gas protection (Scheme 3.11). After 3 h the colour of the solution became dark brown, and the UV-Vis spectrum showed a broad absorption band of Cu NPs at 585 nm (Figure 3.11a).
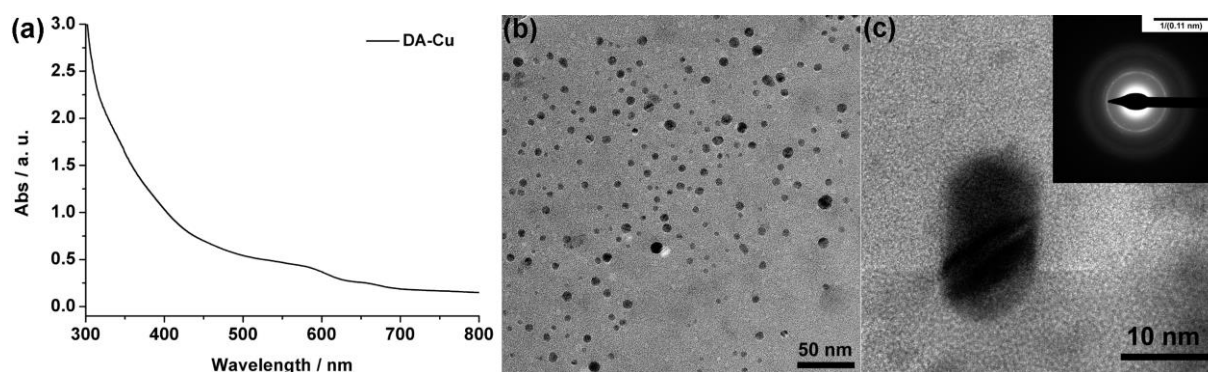
Figure 3. 11 (a) UV-Vis spectrum, (b) TEM image, and (c) SAED pattern of DA-coated Cu NP

TEM image (Figure 3.11b) shows that spherical NPs with an average diameter of ~7.0 nm were obtained. The selected area electron diffraction (SAED) pattern of Cu NPs was performed on an Au TEM grid (inset of Figure 3.11c). The interface distance d was 0.360 nm, which was calculated according to the SAED pattern using Equation 3.1, indicating that Cu NPs existed in face centered cubic (fcc) structures (d$_0$ of fcc Cu = 0.3613 nm).

Equation 3.1 $d = L\lambda/R$

L – the camera length given by the microscope

λ – the wavelength of the electron beam (which is fixed by the accelerating voltage)

R – the distance between the transmitted and diffracted spot
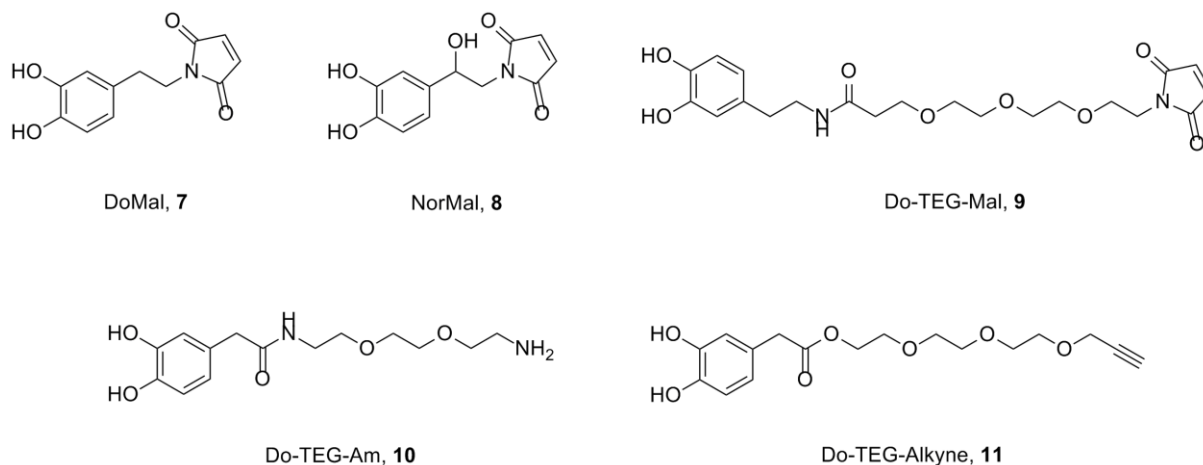
Scheme 3. 12 Molecular structures of the dopamine-based linkers

To introduce different functional groups to the surface of Cu NPs and in such a way facilitate further functionalization of the NPs, a series of dopamine-based linkers containing various functional groups was designed (synthesized by Dr. Ishtiaq Ahmed), including dopamine-maleimide (DoMal, **7**), norepinephrine-maleimide (NorMal, **8**), dopamine-triethylene glycol-maleimide (Do-TEG-Mal, **9**), DOPAC-triethylene glycol-amine (Do-TEG-Am, **10**), and DOPAC-triethylene glycol-alkyne (Do-TEG-Alkyne, **11**) (Scheme 3.12). All of the dopamine linkers-coated Cu NPs were prepared by heating the mixture of the capping agents and Cu precursor at 80 °C until the colour of the solution turned to dark brown (3 ~ 12 h). TEM images (Figure 3.12) show that spherical Cu NPs with different sizes were obtained (Table 1). The zeta potential analysis indicated that the most stable Cu NPs were those coated with DA (**6**) and Do-TEG-Am (**10**), which contained positively charged -NH$_2$ groups (Table 1) and prevented the aggregation of Cu NP.
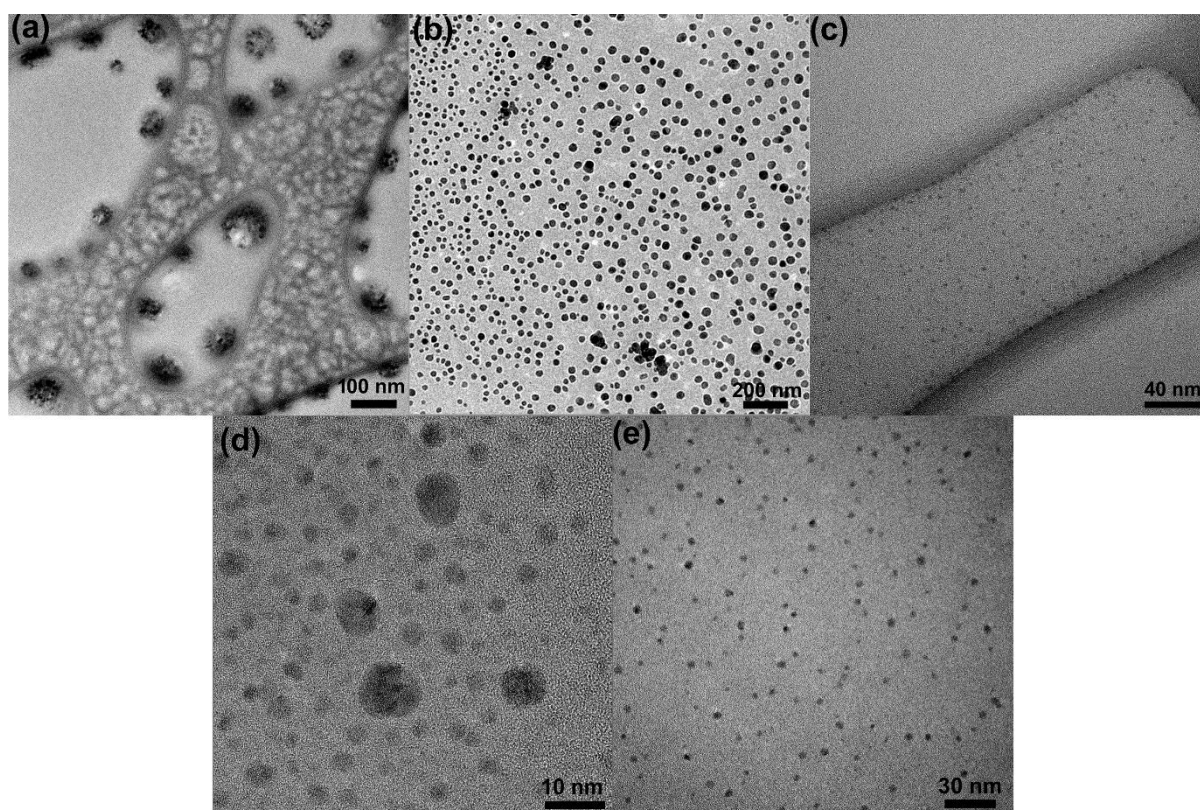
Figure 3. 12 TEM images of as-synthesized (a) DoMal-Cu, (b) NorMal-Cu, (c) Do-TEG-Mal-Cu, (d) Do-TEG-Am-Cu and (e) Do-TEG-Alkyne-Cu

Table 3. 1 Average diameter (d), zeta potential (ζ) of the as-synthesized dopamine linkers-coated Cu NPs, and ζ of the dopamine linkers-coated Cu NPs after 2 months of storage

	d / nm	ζ / mV	ζ (2 month) / mV
DA-Cu	7.0±2.7	40.2±2.6	32.1±0.5
DoMal-Cu	75.0±16.0	10.22±1.18	5.63±0.27
NorMal-Cu	41.7±4.1	2.83±0.86	1.91±0.32
Do-TEG-Mal-Cu	3.2±0.6	2.21±0.02	1.91±0.46
Do-TEG-Am-Cu	3.5±1.2	49.6±1.8	50.4±2.0
Do-TEG-Alkyne-Cu	3.8±1.1	-3.27±0.17	-4.38±0.31

In addition, no significant changes in the morphologies (Figure 3.13) and zeta potential values of Cu NPs (Table 3.1) were observed over months of storage at 4 ºC, which indicates that the as-synthesized dopamine linkers-coated Cu NPs were stable against air oxidation in aqueous solutions.
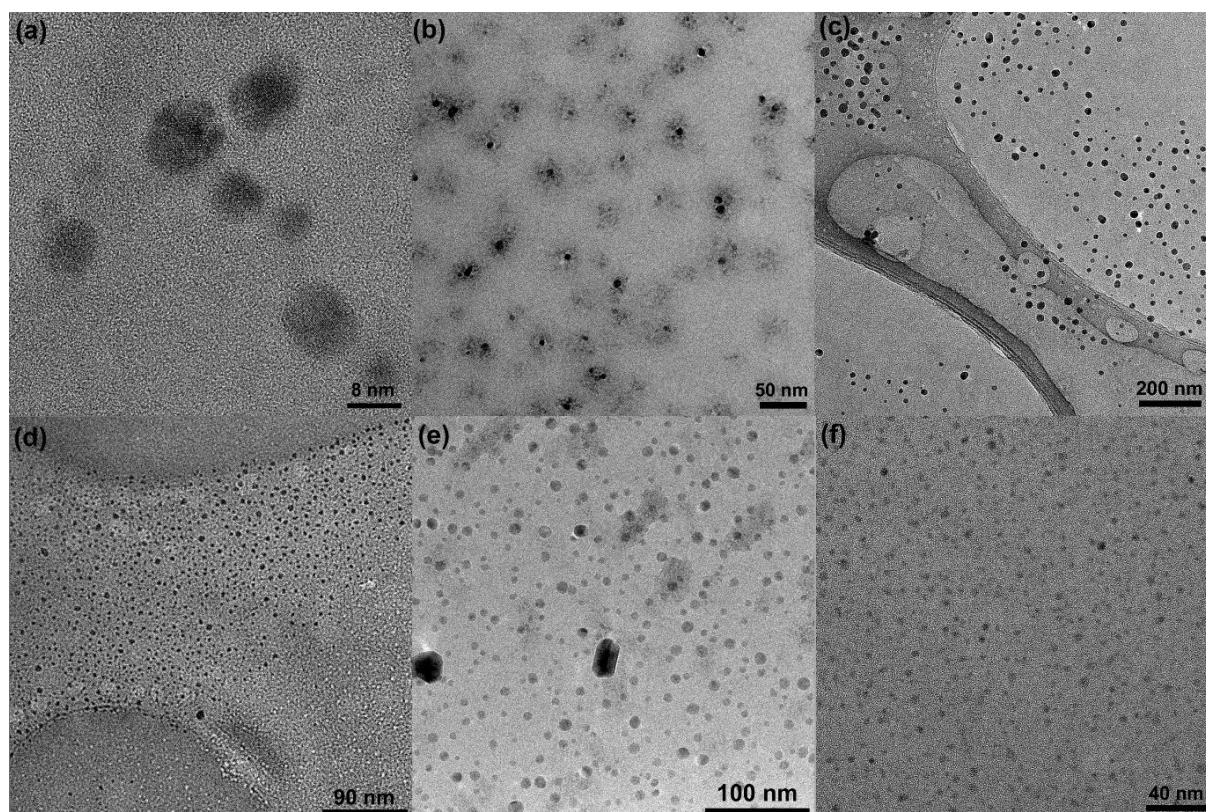
Figure 3. 13 TEM images of (a) DA-Cu, (b) DoMal-Cu, (c) NorMal-Cu, (d) Do-TEG-Mal-Cu, (e) Do-TEG-Am-Cu and (f) Do-TEG-Alkyne-Cu after two months of storage

In order to prove that the Cu NPs were stabilized by dopamine linkers through the catechol functional groups, which have strong affinity to metal surfaces due to the formation of stable complexes, representative FTIR spectra of the dopamine linkers DA (**6**), DoMal (**7**), and both linkers-stabilized Cu NPs were recorded (Figure 6.3), which showed that the stretching vibration bands of catechol groups (O-*H*) around 3300 ~ 3500 cm^{-1} disappeared after the synthesis of Cu NPs (Table 3.2) indicating that the dopamine linkers indeed stabilized the Cu NPs through the coordination between catechol groups and Cu.

Table 3. 2 O-*H* stretching vibration bands of DA (**6**), DA-Cu NPs, DoMal (**7**) and DoMal-Cu NPs in FTIR spectra

Sample	Wavenumber (cm^{-1})
DA (**6**)	3337.0
DA-Cu NPs	–
DoMal (**7**)	3458.2
DoMal-Cu NPs	–

As discussed above, although many methods have been attempted for the preparation of Cu NPs, only two kinds of water-soluble and stable Cu NPs have been obtained, and they were AA- and dopamine derivatives-coated Cu NPs. Both types of Cu NPs were synthesized using the same reaction conditions and the same concentrations of Cu precursors and capping agents, and they were all stabilized by the polyhydroxyl functional groups. Following the successful preparation and characterization of stable Cu NPs, their properties (such as ROS production ability and catalytic activity) and applications (enzyme mimetics, degradation of pollutants, and SERS activity) have been investigated.

3.2 Reactive Oxygen Species (ROS) Production by AA- and Dopamine Linkers-Coated Cu NPs

As mentioned previously in 1.2.4, ROS generation ability of metal, metal oxide and semiconductor nanomaterials has been proven to be responsible for their catalytic activities, antibacterial and cytotoxic properties.[207, 215] Shi and coworkers have employed a 2,7-dichlorodihydrofluorescein (DCFH) assay to demonstrated that Cu NPs also possess ROS generation ability, which was largely dependent on the composition of the NPs, i.e. the presence of the oxide layer and the type of the stabilizing ligands.[76] However, there are still many unknowns concerning the exact mechanism of ROS production as well as the factors influencing it, therefore it is of great importance to investigate the mechanism to enable the future design of CuNP probes which are useful in nanomedical and biocatalytic applications.

3.2.1 Peroxidase Activity Tests Using Amplex Red Assay

Different methods have been developed up to date for the detection of ROS, such as ferrous oxidation-xylenol orange (FOX) method based on the oxidation of Fe^{2+} to Fe^{3+} by H_2O_2 and the following complex formation between Fe^{3+} and xylenol orange, which absorbs at 550-600 nm,[401] and homovanillic acid (HVA) method based on the oxidation of non-fluorescent HVA to fluorescent HVA dimer by H_2O_2 in the presence of horseradish peroxidase (HRP).[402] Herewith, Amplex Red assay (Scheme 3.13), which has been used previously in Chapter 2 for the enzymatic activity study of Mb-AgNP hybrids, was first employed to assess the ROS production ability of Cu NPs as well as the ability to use such ROS for the activation of peroxidase enzymes.
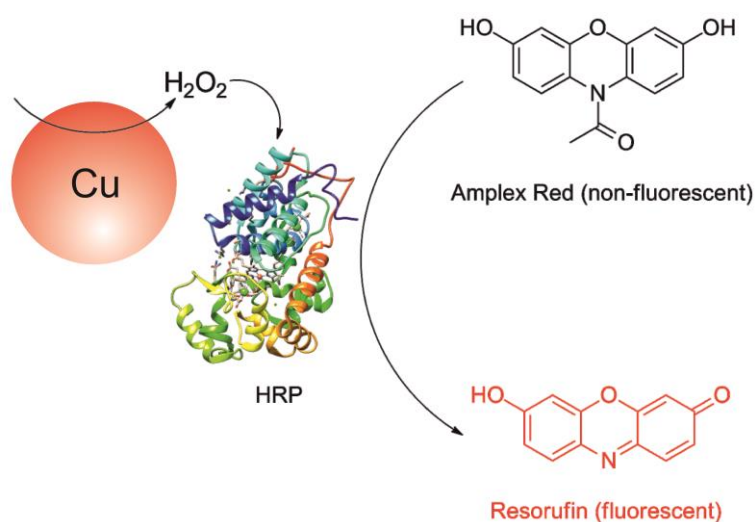
Scheme 3. 13 Schematic illustration for the peroxidase activity assay using Amplex Red, HRP and Cu NPs

Instead of using H_2O_2, AA- and dopamine linkers-stabilized Cu NPs were used as sources of ROS, which could be utilized for the activation of HRP and the subsequent oxidation of non-fluorescent substrate Amplex Red into fluorescent resorufin (Scheme 3.13).[338] In such a way, the ROS production by Cu NPs could be estimated by monitoring the fluorescence of resorufin on a microplate reader (BioTek Synergy H1, λ_{ex} = 540 nm, λ_{em} = 585 nm, sensitivity: 95).

As can be seen from Figure 3.14, the significant oxidation of Amplex Red and the formation of resorufin occurred only in the presence of both HRP and Cu NPs. To make sure that the effects observed were solely NP based, controls in the absence of Cu NPs and in the presence of ligands only (AA and dopamine linkers) were performed, which showed negligible activities indicating that Cu NPs were indeed the crucial factors for the successful activation of the peroxidase enzyme and the oxidation of Amplex Red (Figure 3.14). In addition, controls using Cu(II) salt precursor ($CuCl_2$) were also performed to dismiss any possible interfering effects of Cu^{2+} ions (Figure 3.14h).
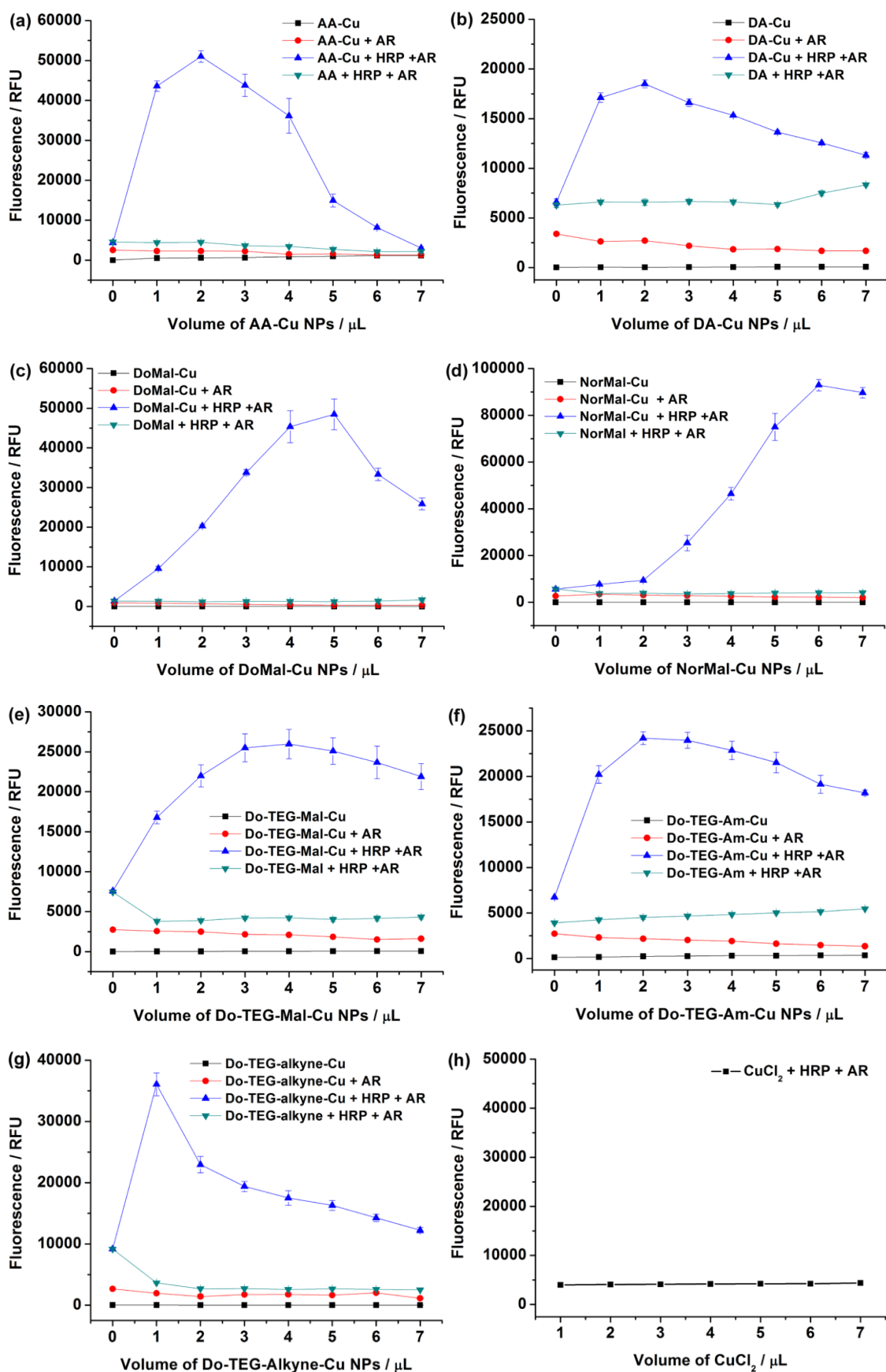
Figure 3. 14 Amplex Red (AR) assays using different volumes of (a) AA-Cu, (b) DA-Cu, (c) DoMal-Cu, (d) NorMal-Cu, (e) Do-TEG-Mal-Cu, (f) Do-TEG-Am-Cu, (g) Do-TEG-Alkyne-Cu, and the controls using the corresponding ligands or CuCl$_2$ (h) instead of Cu NPs

131

Interestingly, during the ROS study of AA- and dopamine linkers-coated Cu NPs, it was also observed that the fluorescence intensity of resorufin first increased and then began to decrease upon the addition of larger amount of Cu NPs (Figure 3.14a - g). We hypothesize that after the addition of certain amounts of Cu NPs a large amount of resorufin was produced, which could be further degraded by the continuously produced ROS.
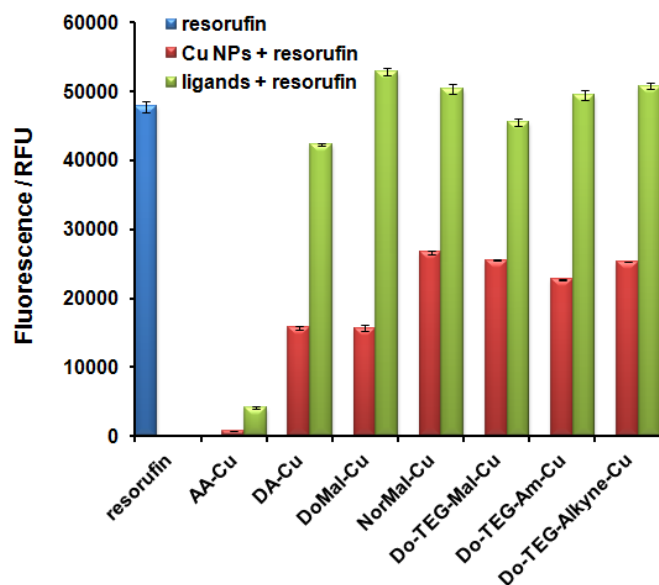
Figure 3. 15 Influence of AA- and dopamine linkers-coated Cu NPs (10 μL) on the fluorescence of resorufin, and the controls using the corresponding ligands instead of Cu NPs

This was additionally confirmed by experiments in which resorufin solution was exposed to different Cu NPs (Figure 3.15). The addition of Cu NPs to resorufin led to the decrease of its fluorescence intensity indicating that degradation of the fluorescent dye took place. Controls in which resorufin was exposed to the capping agents proved that all ligands with exception of AA did not affect the fluorescence of resorufin significantly. The effect of AA on resorufin has been reported previously showing that AA, which is a known antioxidant, is able to reduce fluorescent dyes.[349, 403]

3.2.2 Peroxidase Activity Tests Using DCFH Assay

To futher confirm the ROS production ability of AA- and dopamine linkers-coated Cu NPs, another ROS detection substrate 2,7-dichlorodihydrofluorescein (DCFH), which has been used previously by Shi *et al*. for the ROS study of OA-coated Cu NPs,[76] was employed for the peroxidase assay. Similar as Amplex Red, non-fluorescent DCFH could be oxidized to fluorescent 2,7-dichloro-fluorescein (DCF) by H_2O_2 in the presence of peroxidase enzymes (Scheme 3.14).
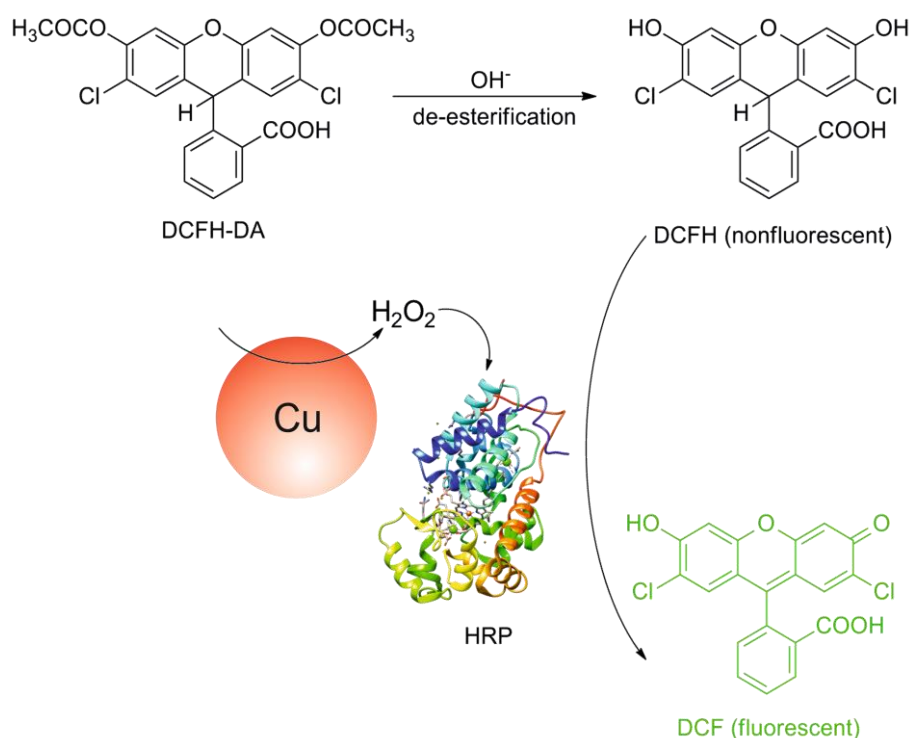
Scheme 3. 14 Schematic illustration for the de-esterification of DCFH-DA to DCFH, and the oxidation of non-fluorescent DCFH to fluorescent DCF in the presence of Cu NPs and HRP

DCFH was first prepared by the de-esterification of 2,7-dichlorodihydrofluorescein diacetate (DCFH-DA) with NaOH (Scheme 3.14), and then mixed with HRP and AA- or dopamine linkers-coated Cu NPs. The fluorescence of the resulted DCF was recorded at $\lambda_{ex} = 498$ nm and $\lambda_{em} = 535$ nm on a microplate reader (sensitivity: 80).
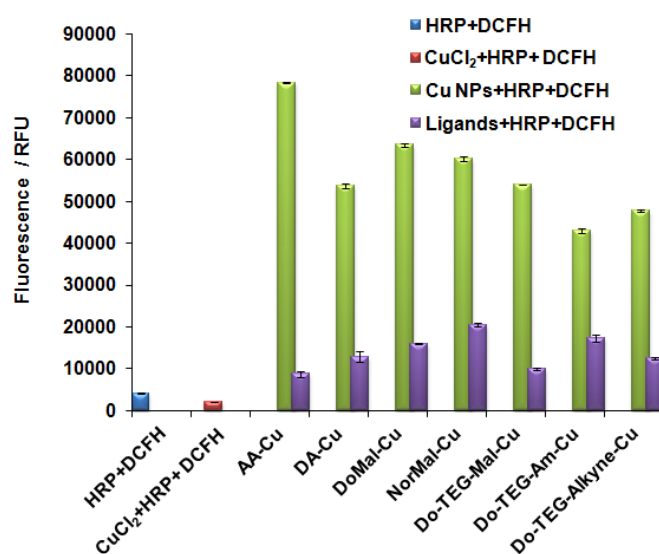
Figure 3. 16 DCFH assays using AA- and dopamine linkers-coated Cu NPs (3 μL), and the controls in the presence of corresponding ligands or CuCl$_2$ instead of Cu NPs

As shown in Figure 3.16, the activation of HRP and the oxidation of DCFH could only occur in the presence Cu NPs. Controls in the presence of $CuCl_2$ or the capping agents instead of Cu NPs showed negligible fluorescence, which again proved that AA- and dopamine linkers-coated Cu NPs possess ROS generation ability.

3.2.3 ROS Inhibition by Catalase

To confirm that Cu NPs really acted as a source of H_2O_2, the Amplex Red assays were performed again in the presence of catalase, an enzyme, which could catalyze the decomposition of H_2O_2 into H_2O and O_2 (Scheme 3.15).[404, 405]
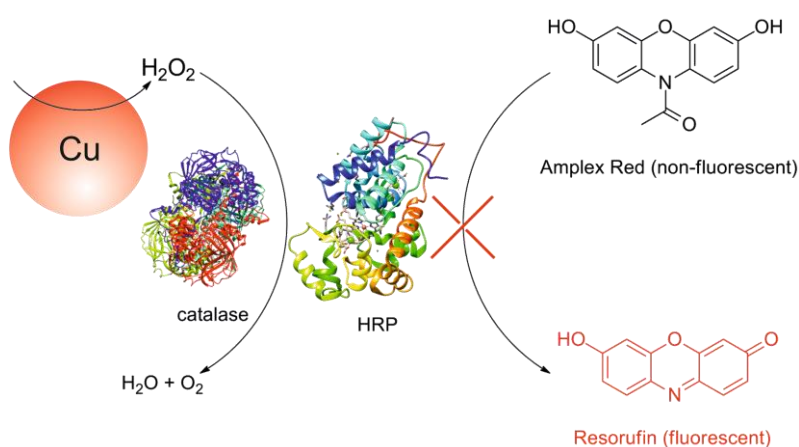
Scheme 3. 15 Schematic illustration for the ROS inhibition effect of catalase
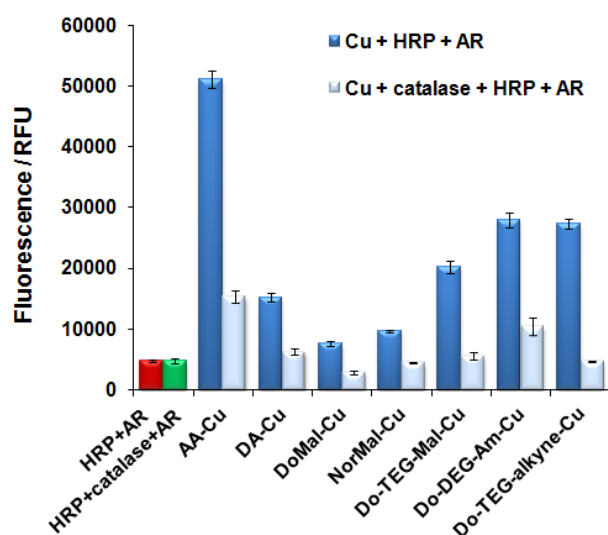
Figure 3. 17 Influence of catalase on the ROS production of AA- and dopamine linkers-coated Cu NPs (2 μL)

The influence of catalase on the formation of resorufin was monitored by fluorescence. As shown in Figure 3.17, the addition of catalase could lead to the dramatic decrease in the

134

production of resorufin as supported by the detecton of lower fluorescence, which indicated that Cu NPs-generated H_2O_2 was decomposed by catalase and in such a way interfered with the HRP activation and the subsequent resorufin production.

3.2.4 Quantification of Cu NPs-Generated ROS Using H_2O_2 Calibration Curve
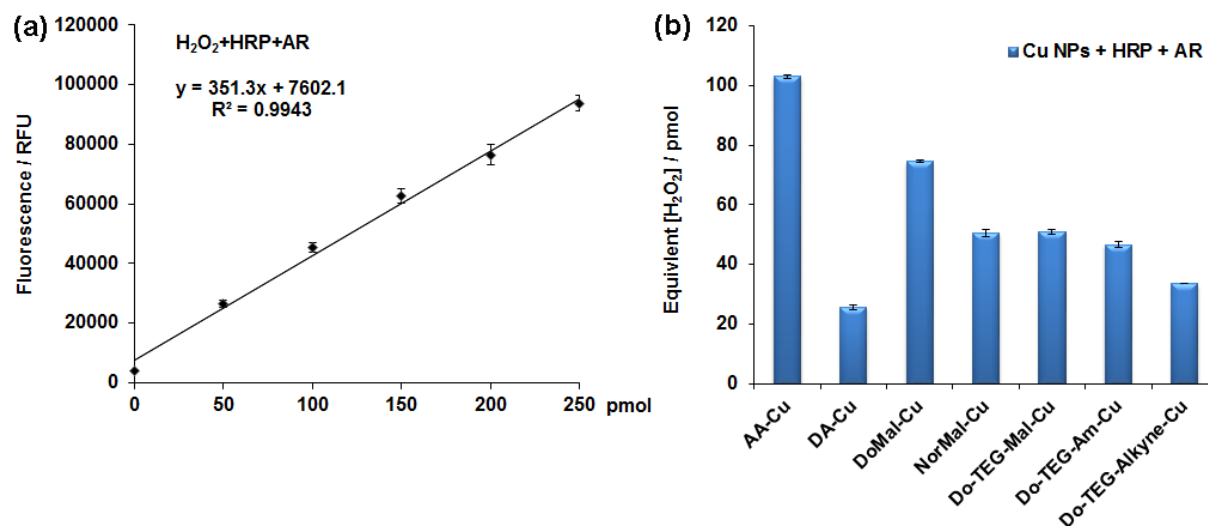
Figure 3. 18 (a) H_2O_2 calibration curve and (b) the ROS production ability of Cu NPs (3 μL) using Amplex Red assay

To assess the amount of H_2O_2 produced by AA- and dopamine linkers-coated Cu NPs, a calibration curve was made using H_2O_2 for the Amplex Red assay (Figure 3.18a). According to the calibration curve, the amounts of H_2O_2 produced by 3 μL of different Cu NPs were calculated (Figure 3.18b), and the results showed that the Cu NPs coated by AA and DoMal (3 μL) exhibited the highest ROS production capacity, which were equivalent to 103 and 75 pmol H_2O_2, respectively. The ROS production by Cu NPs coated with longer linkers was relatively lower, which might be because the longer linkers could form thicker layers on the surface of Cu NPs, thus limiting the defusion rate and the release of ROS. And the lower ROS production by DA-Cu NPs might be caused by the antioxidant and ROS scavenging effects of the amine-containing compound.[406]

3.2.5 Mechanism for the ROS Generation Ability of Cu NPs

3.2.5.1 Electron Paramaganetic Resonance Analysis of Cu NPs

In order to investigate the mechanism behind the ROS generation ability of AA- and dopamine linkers-coated Cu NPs and to determine which kind of ROS were produced by Cu NPs, electron paramagnetic resonance (EPR) measurements of Cu NPs were performed, which is a commonly used methodology for the detection of unpaired electrons and analyses of radicals and ROS.[407] EPR measures the resonant absorption of the microwave radiation by an unpaired electron of an atom or a molecule (paramagnetic species) when placed in a strong magnetic field, and the g value in EPR spectrum is the analog of the chemical shift in NMR, which could be used for the determination of different paramagnetic species.[407]
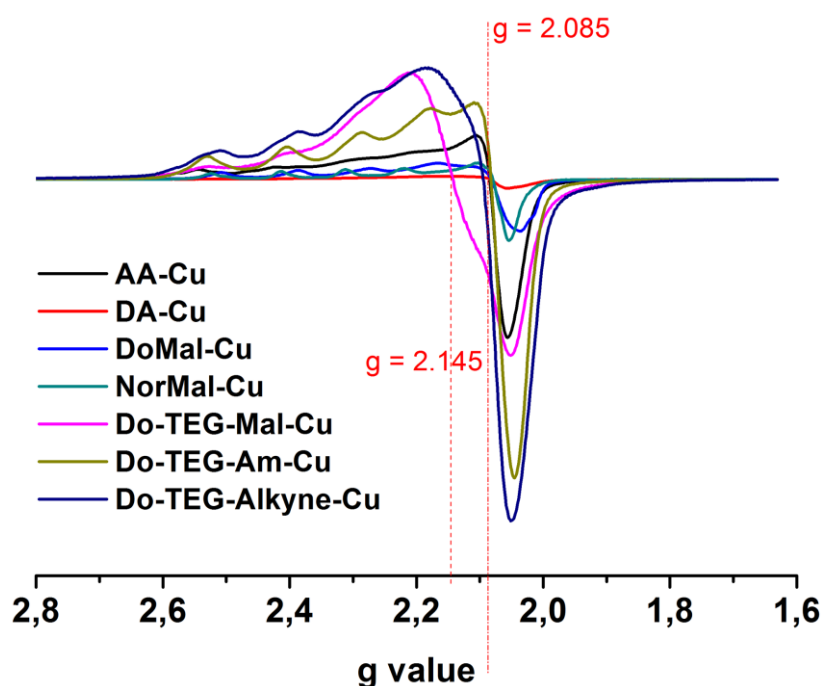
Figure 3. 19 EPR spectra of AA- and dopamine linkers-coated Cu NPs

As can be seen from Figure 3.19, all of the Cu NPs showed EPR signals at g = 2.085, which could be assigned to Cu^{2+}. As g values of transition metal ions could be affected by the chemical environments,[408] so different solvents and surface compositions might lead to different g values. It has been reported that the g values of $CuCl_2$ in H_2O and MeCN were 2.180 and 2.157, respectively,[409, 410] while they could shift to 2.0923 and 2.0897 when dopamine was added as a complex agent.[411] Therefore, it could be deduced that the observed EPR signals of Cu^{2+} at g = 2.085 was caused by the existence of catechol-Cu^{2+} complex on the surface of Cu NPs, and two possible complex structures (didentate bridging and catecholate chelating) are demonstrated in Scheme 3.16. In addition to the EPR absorption at g value 2.085, Do-TEG-Mal-Cu showed also another broad absorption at g value 2.145, which could be attributed to free Cu^{2+} ions.

didentate bridging   catecholate chelating

Scheme 3. 16 Formation of catechol-Cu(II) complex on the surface of Cu NPs

Figure 3. 20 (a) EPR spectrum of DoMal-Cu (insert is the magnification of the selected area of the spectrum), and (b) second derivative curves of the EPR spectrum of DoMal-Cu

EPR signals of radicals species, such as hydroxyl and superoxide radicals, normally appear at $g = 1.99 \sim 2.01$.[407] No obvious signals of hydroxyl or superoxide radicals could be observed in the EPR spectra of AA- and dopamine linkers-coated Cu NPs (Figure 3.19). However, when the EPR spectrum of DoMal-Cu NPs was magnified, a broad EPR signal at $g = 2.013$ could be observed, which was also confirmed by its second derivative curve (Figure 3.20). It has been reported previously that hydroquinone chemisorbs to the surface of metal oxides and forms semiquinone radicals, which are primarily oxygen-centered radicals and have high g values (up to 2.011 for some substitute quinones).[412] Therefore, we deduce that the broad EPR signal at $g = 2.013$ derived from the anion radicals of DoMal.

Figure 3. 21 EPR spectra of (a) DA-Cu NPs, (b) AA-Cu NPs, (c) NorMal-Cu NPs, (d) Do-TEG-Mal-Cu NPs, (e) Do-TEG-Am-Cu NPs, and (f) Do-TEG-Alkyne-Cu NPs. Inserts are the magnifications of the selected areas.

However, no obvious EPR signals of semiquinone radicals could be observed in the magnified spectra of the other Cu NPs (Figure 3.21 b-f) with exception of DA-Cu NPs (Figure 3.21a), which might be due to the fact that semiquinone radicals from the other Cu NPs have been mostly consumed by oxygen to form superoxide radicals (Scheme 3.17),[413] resulting in the production of H_2O_2.

3.2.5.2 Cu NPs as Superoxide Dismutase Mimetics

(a)
$$QH_2 + O_2 \longrightarrow Q^{\bullet -} + O_2^{\bullet -} + 2H^+$$
$$Q^{\bullet -} + O_2 \rightleftharpoons Q + O_2^{\bullet -}$$
$$QH_2 + Q \rightleftharpoons Q^{\bullet -} + Q^{\bullet -} + 2H^+$$
$$O_2^{\bullet -} + O_2^{\bullet -} + 2H^+ \xrightarrow{SOD} O_2 + H_2O_2$$

(b)
$$Cu^{2+} + QH_2 \longrightarrow Cu^+ + Q^{\bullet -} + 2H^+$$
$$Cu^+ + QH_2 \longrightarrow Cu + Q^{\bullet -} + 2H^+$$
$$Q^{\bullet -} + O_2 \rightleftharpoons Q + O_2^{\bullet -}$$
$$O_2^{\bullet -} + O_2^{\bullet -} + 2H^+ \xrightarrow{Cu\ complex} O_2 + H_2O_2$$
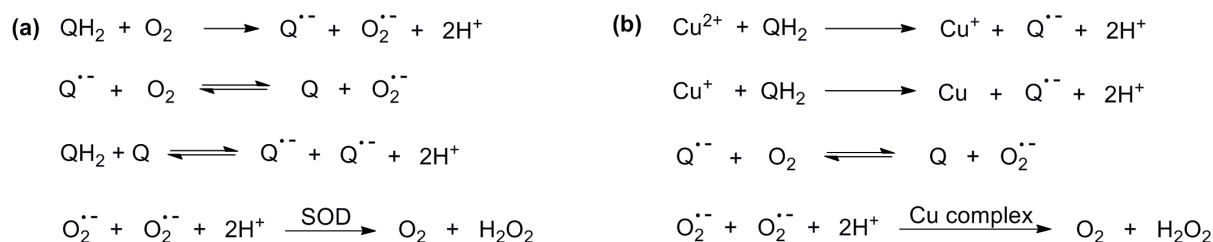
Scheme 3. 17 (a) Production of superoxide ($O_2^{\bullet -}$) and semiquinone radicals ($Q^{\bullet -}$) during the oxidation process of hydroquinones (QH_2) and the dismutation of superoxide radicals into H_2O_2 in the presence of SOD; (b) production of superoxide ($O_2^{\bullet -}$) and semiquinone radicals ($Q^{\bullet -}$) during the redox process between Cu^{2+} and QH_2 and the dismutation of superoxide into H_2O_2 in the presence of Cu complex

It has been reported that superoxide radicals could be produced during the oxidation of hydroquinone (Scheme 3.17a).[413] On the other hand, the addition of superoxide dismutases (SOD), enzymes containing metal ions such as copper and zinc as cofactors, could catalyze the dismutation of superoxide to O_2 and H_2O_2 (Scheme 3.17a).[414] Some reports demonstrated that Cu(II) complexes possess SOD-like activity and could act as superoxide scavengers.[415, 416] Therefore, we hypothesize that superoxide was produced during the redox process between dopamine linkers (or AA) and Cu^{2+} (Scheme 3.17b), and the complex formed between the hydroxyl groups and Cu^{2+} on the surface of Cu NPs might serve as SOD mimetics and catalyze the transformation of superoxide to H_2O_2. Therefore, no EPR signals of superoxide but only the signals of semiquinone radicals could be detected in the solution of Cu NPs.
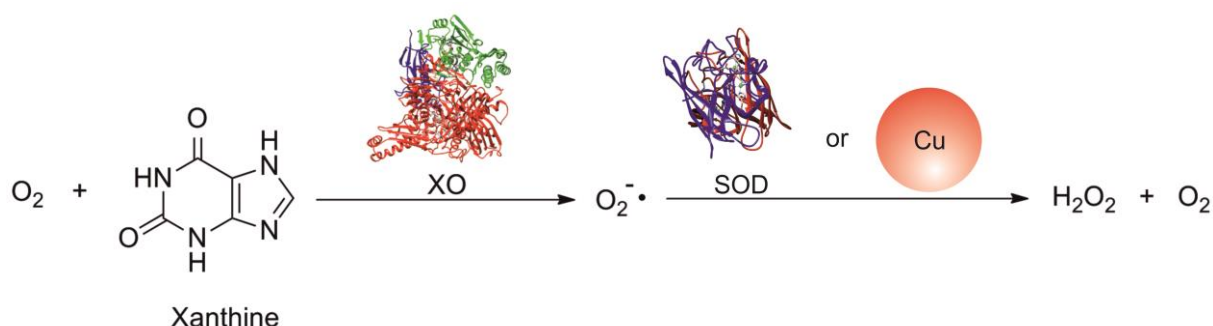
Scheme 3. 18 SOD activity assay using xanthine and XO as a source of superoxide, AA- and dopamine linkers-coated Cu NPs as SOD mimetics

To investigate the SOD-like activity of Cu NPs, a SOD activity assay was employed, in which xanthine and xanthine oxidase (XO) were used as a source of superoxide

(Scheme 3.18),[417] and commercially available superoxide detection reagent (Orange® Enzo Life Science) was used as a substrate. This non-fluorescent substrate is designed for the specific detection of superoxide and is not sensitive to any other ROS species including peroxide. It reacts with superoxide to afford a fluorescent product with an orange emission at 605 nm (λ_{ex} = 484 nm). If the AA- and dopamine linkers-coated Cu NPs acted as SOD substitutes, they would cause the dismutation of superoxide to O_2 and H_2O_2 (Scheme 3.18), and inhibit the reaction between superoxide and the substrate, which would in turn lead to the decrease of the fluorescence intensity.
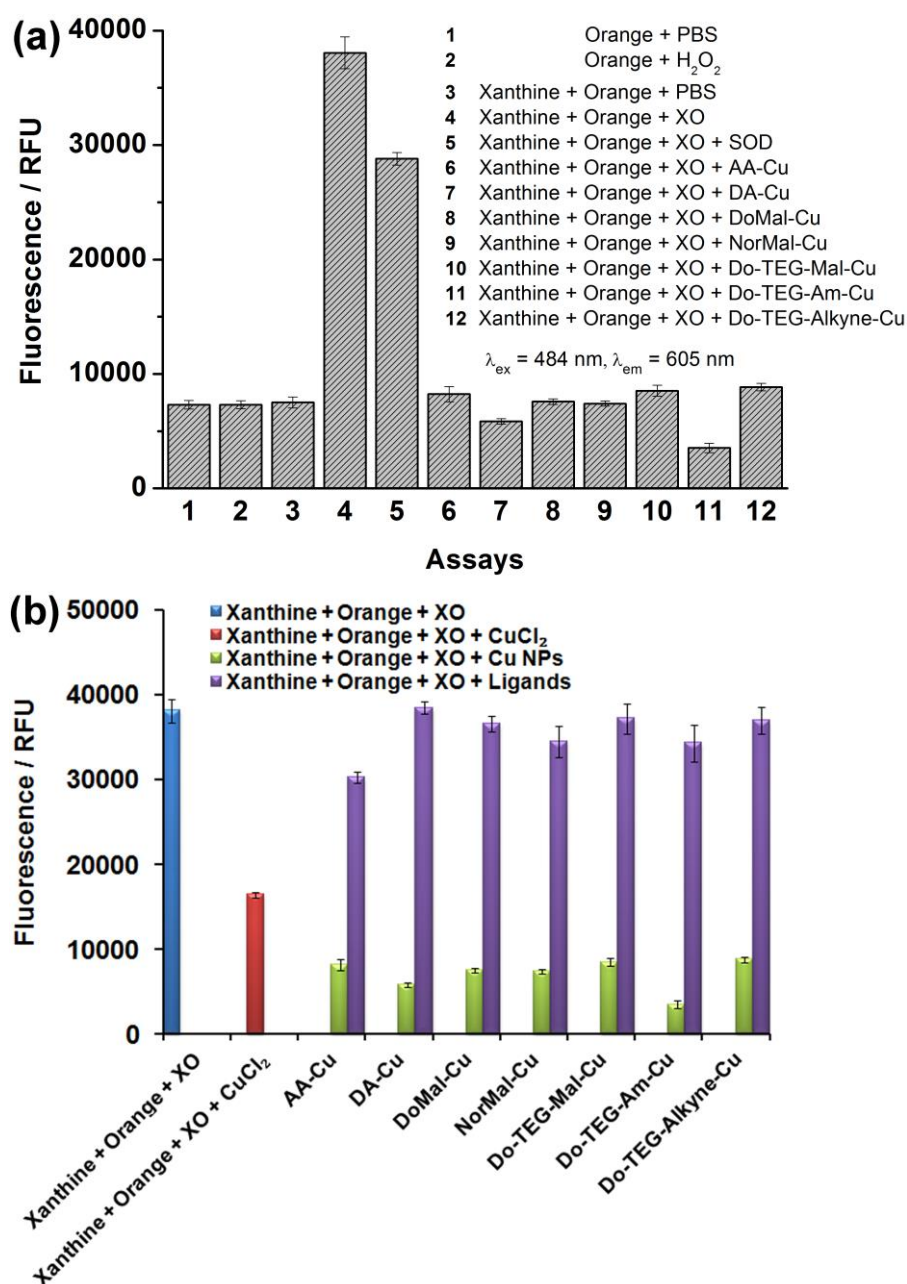
Figure 3. 22 (a) SOD activity assays using SOD, AA- and dopamine linkers-coated Cu NPs, and (b) the controls using corresponding ligands instead of Cu NPs

As shown in Figure 3.22a, the addition of Cu NPs could indeed inhibit the production of the fluorescent compound as supported by the decrease of fluorescence intensities, and the Cu NPs outperformed the natural SOD (from bovine erythrocytes) approximately two fold. The controls in the absence of Cu NPs and in the presence of the capping agents alone showed negligible influence on the fluorescence intensity (Figure 3.22b), indicating that they were not responsible for the observed SOD-like activity. However, fluorescence decrease was observed in the control where $CuCl_2$ instead of Cu NPs was used for the SOD activity assay (Figure 3.22b). It has been reported previously that under certain conditions Cu^{2+} ions could complex to XO and cause its structural and functional changes.[418] Therefore, the addition of $CuCl_2$ to XO might lead to the loss of XO's enzymatic activity and in turn inhibit the production of superoxide, which could finally result in the decrease in the production of the fluorescent compound. This means that if there was any Cu precursor left in the solution of Cu NPs, it might be responsible for the observed activity.
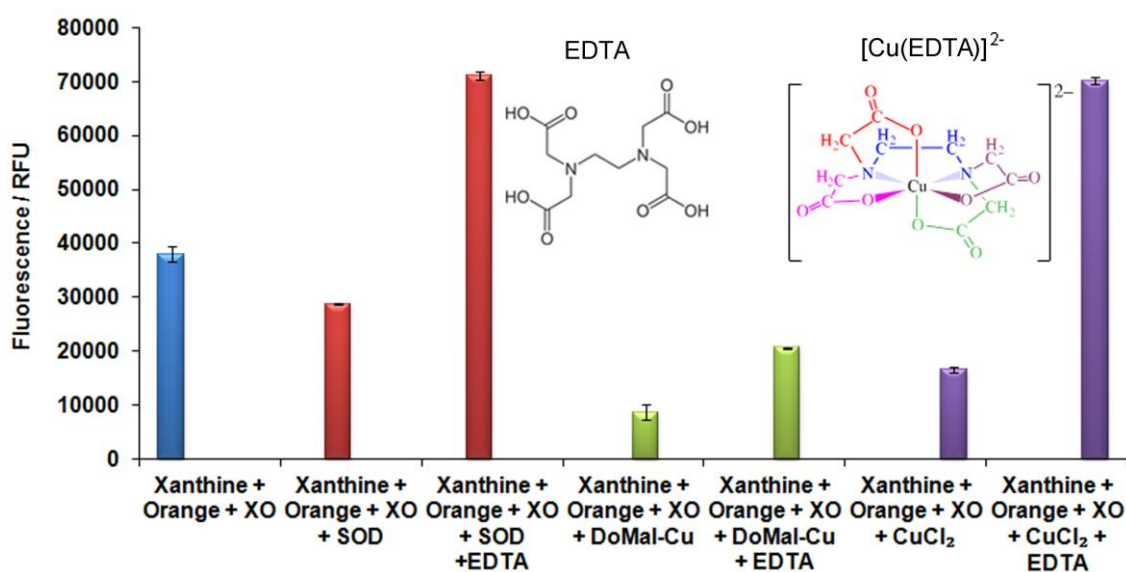
Figure 3. 23 SOD assay of natural SOD, DoMal-Cu and $CuCl_2$ in the presence of EDTA

(EDTA: SOD or Cu precursor or $CuCl_2$ was 1: 1). Insert: the structures of EDTA and $[Cu(EDTA)]^{2-}$ complex

However, this $CuCl_2$ effect could be removed by the addition of a chelate ligand ethylenediaminetetraacetic acid (EDTA) (Figure 3.23), which has already been used for the elimination of metal ions in chelation therapy or treatment of industrial waste,[419, 420] as it could form complex with Cu^{2+}, sequester the ions, and prevent them from interacting with XO. In order to determine the influence of Cu^{2+} ions on the observed SOD activity of Cu NPs, the SOD activity assays of natural SOD, DoMal-Cu NPs or $CuCl_2$ were performed again in the presence of EDTA, and the molar ratio between EDTA and natural SOD (or Cu precursor, or

CuCl$_2$) was 1: 1. As shown in Figure 3.23, natural SOD and CuCl$_2$ did not show any SOD activity in the presence of EDTA, and there was even a significant fluorescence increase. It was reported that EDTA-metal chelates could promote the reduction of oxygen to superoxide,[421] which might also be the reason for the observed fluorescence increase. On the other hand, although the activity of DoMal-Cu NPs has been suppressed slightly upon the addition of EDTA, the NPs remained active towards the dismutation of superoxide radicals. This additionally confirmed that Cu NPs not free Cu^{2+} were responsible for the inherent SOD-like activity and catalyzed the dismutation of superoxide to H$_2$O$_2$, which could be utilized for the activation of peroxidase enzymes.
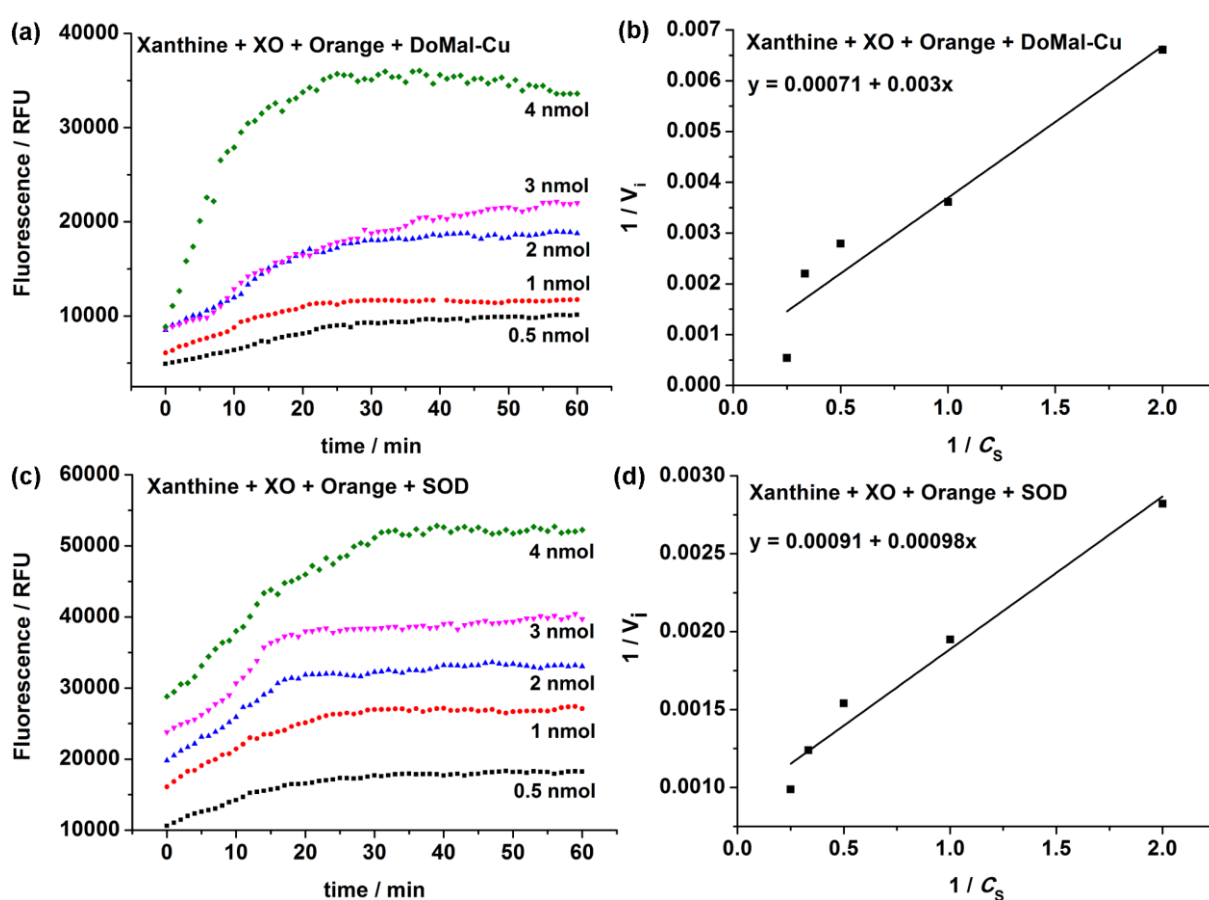
Figure 3. 24 (a) and (c) Enzyme kinetics, and (b) and (d) Lineweaver-Burk plots of DoMal-Cu and SOD

To study the SOD mimicking ability of Cu NPs, the enzyme kinetics of DoMal-Cu and SOD were performed using different amounts of superoxide detection agent (Orange® Enzo Life Science, 0.5 ~ 4 nmol), and the fluorescence was recorded every minute for 1 h (Figure 3.24a and c). An enzyme-catalyzed reaction could be expressed by the Michaelis-Mention equations (Equation 3.2 and 3.3),[422] according to which, the initial reaction velocity (V_i) could be determined by the slope of the kinetics curves in the first few minutes of the reactions

142

(Figure 3.24a and c), and the Michaelis constants K_m of both DoMal-Cu and SOD could be calculated by plotting the corresponding $1/V_i$ vs. $1/C_S$ (Lineweaver-Burk plots, Figure 3.24b and d). K_m reveals how easily an enzyme can be saturated by the substrate, and the larger the value of K_m, the more substrate the enzyme can handle before its saturation. According to Equation 3.3 and Figure 3.24b and d, the K_m values of DoMal-Cu and SOD were 4.17 and 1.08, respectively, indicating that it is easier for the natural SOD enzyme to get saturated.

Equation 3.2 $\quad V_i = \dfrac{V_{max}C_s}{K_m + C_s}$

Equation 3.3 $\quad \dfrac{1}{V_i} = \dfrac{K_m}{V_{max}}\left(\dfrac{1}{C_s}\right) + \dfrac{1}{V_{max}}$

V_i and V_{max} — initial and maximum reaction velocity

C_s — the initial concentration of substrate

K_m — Michaelis constant

The enzymatic assays and kinetics studies showed that such kind of CuNP-based enzyme mimetics exhibited higher activity in comparison to the natural enzymes. In addition, Cu NPs mimetics could survive harsh conditions, such as different temperatures and pH (the solutions of Cu NPs are acidic, pH values are 2~5), which makes them potential materials to be applied in catalysis and environmental detections as well as bioassays.

3.3 Catalytic Property of Cu NPs towards the Degradation of Water Pollutants

As mentioned previously in 3.2.1, the production of excessive ROS by AA- and dopamine linkers-coated Cu NPs could lead to the degradation of resorufin, so it is interesting to explore if Cu NPs, apart from being enzyme mimetics, could also be utilized as catalysts for the degradation of water pollutants, such as harmful fluorescent dyes and antibiotics.

3.3.1 Degradation of Fluorescent Dyes by Cu NPs

As two representative water-soluble dyes, rhodamine B (RB) and methylene blue (MB) are widely used as colorants in textile and printing industry.[423, 424] They pose a considerable threat to the environment as they are found to be harmful to humans and animals, and there is an ongoing search for new methodologies for their removal. Photocatalysis using nanomaterials such as TiO_2 and CdS has already shown considerable success,[423, 425, 426] as they

can produce highly reactive radicals under light irradiation. Since the AA- and dopamine linkers-coated Cu NPs possess ROS generation ability, it is interesting to explore the use of such Cu NPs for the degradation of RB and MB.
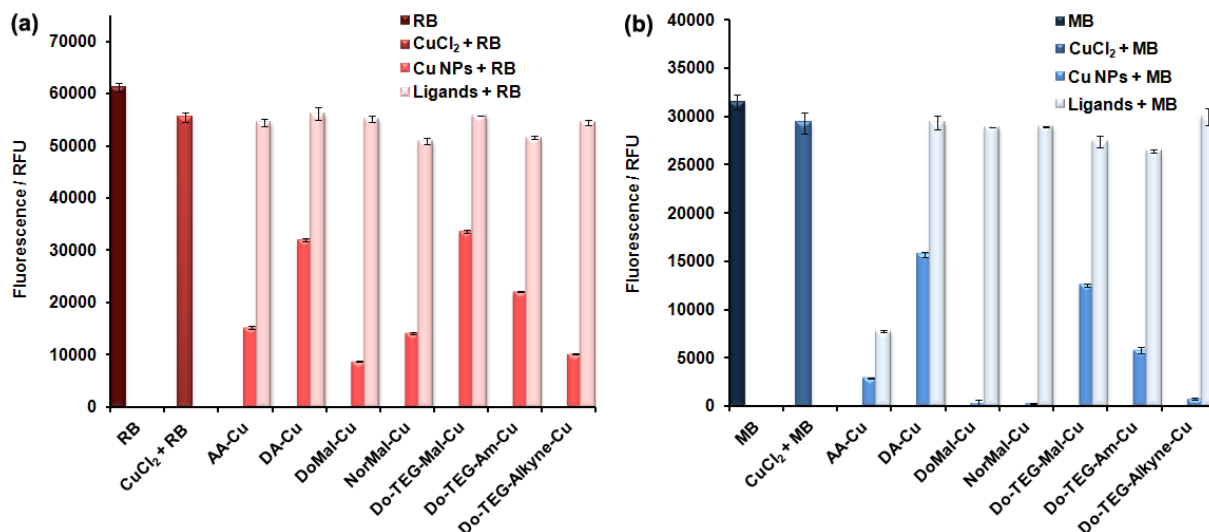
Figure 3. 25 Degradation of (a) RB and (b) MB by AA- and dopamine linkers-coated Cu NPs, and the controls using the corresponding ligands or $CuCl_2$ instead of Cu NPs

AA- and dopamine linkers-coated Cu NPs have been explored as catalysts for the degradation of RB and MB. As can be seen from Figure 3.25, strong degradation ability can be observed, and the most effective Cu NPs were DoMal-Cu with degradation efficiencies of 85.8% and 99.2% for RB (20.8 μM) and MB (31.2 μM), respectively (Table 3.3). Negative controls using Cu(II) salt or the capping agents instead of Cu NPs did not show any catalytic activity except again the strong influence of AA on MB (Figure 3.25b), indicating that the presence of Cu NPs was crucial for the degradation fluorescent dyes.

Table 3. 3 Degradation efficiencies (η) of RB and MB in the presence of 10 μL of Cu NPs

	η_{RB} / %	η_{MB} / %
DoMal-Cu	85.8	99.2
NorMal-Cu	76.9	99.1
Do-TEG-Alkyne-Cu	83.4	97.5
AA-Cu	75.2	90.8
Do-TEG-Am-Cu	63.9	81.5
Do-TEG-Mal-Cu	45.1	60.2
DA-Cu	47.8	50.2

3.3.2 Degradation of Fluorescent Antibiotics by Cu NPs

Recently, pharmaceutical compounds such as antibiotics have emerged as a new group of water pollutants. The continuous and inappropriate release of these compounds into the environment might cause resistance in bacterial populations, and make them ineffective for the treatment of certain diseases.[427] Different methods have been developed up to date for the removal of antibiotics, for example, ozonation has been employed for the treatment of sulphamethoxazole with a 99.24% degradation effciency[428], and the ROS production ability of TiO_2 nanomaterials has been utilized for the fully degradation of amoxicillin.[429]

Considering their ROS generation ability, AA- and dopamine linkers-coated Cu NPs were employed as catalysts for the treatment of two different fluorescent antibiotics, one was chromomycin A3 (CMA, 20 μM), an anti-bacterial, anti-fungal, and antitumor antibiotic, and the other was doxorubicin (DOX, 20 μM), a drug widely used in clinical anticancer chemotherapy. All of the Cu NPs showed excellent catalytic activity towards the degradation of CMA and DOX as indicated by the significant fluorescence decrease (Figure 3.26), while the controls in the absence of Cu NPs and in the presence of capping agents did not have obvious influence on the fluorescence of CMA and DOX.
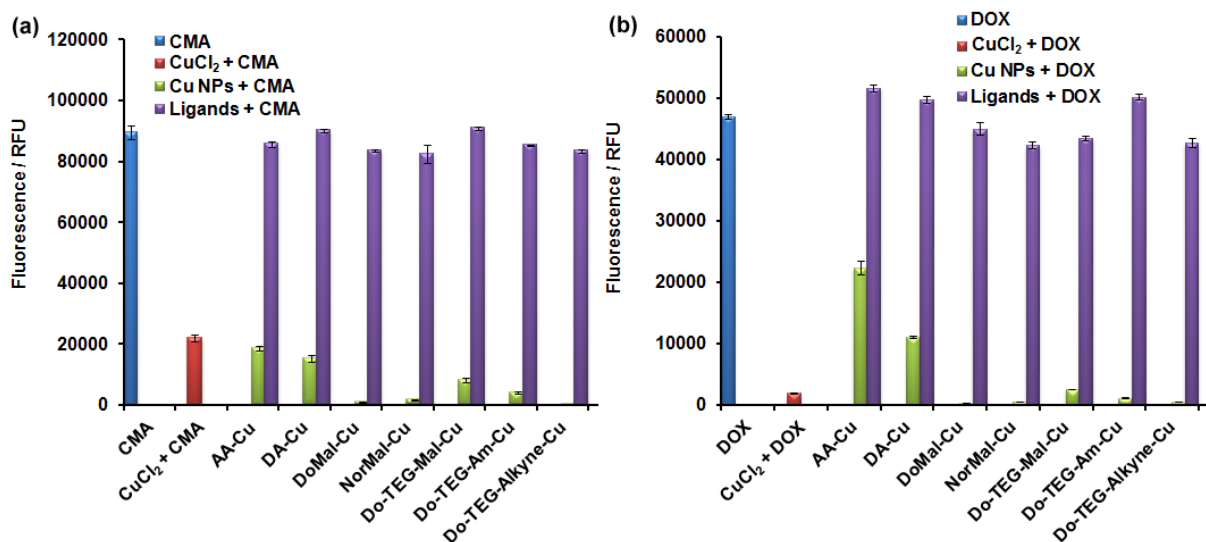
Figure 3. 26 Degradation of CMA and DOX by AA- and dopamine linkers-coated Cu NPs, and the controls using the corresponding ligands or $CuCl_2$ instead of Cu NPs

However, in the control where $CuCl_2$ was used instead of Cu NPs, the decomposition of antibiotics also occurred (Figure 3.26), indicating that Cu^{2+} could also cause the degradation of antibiotics. It has been reported that some antibiotics could be decomposed by divalent

metal ions through the formation of antibiotic-metal complex intermediates during the hydrolysis process of antibiotics.[430, 431]
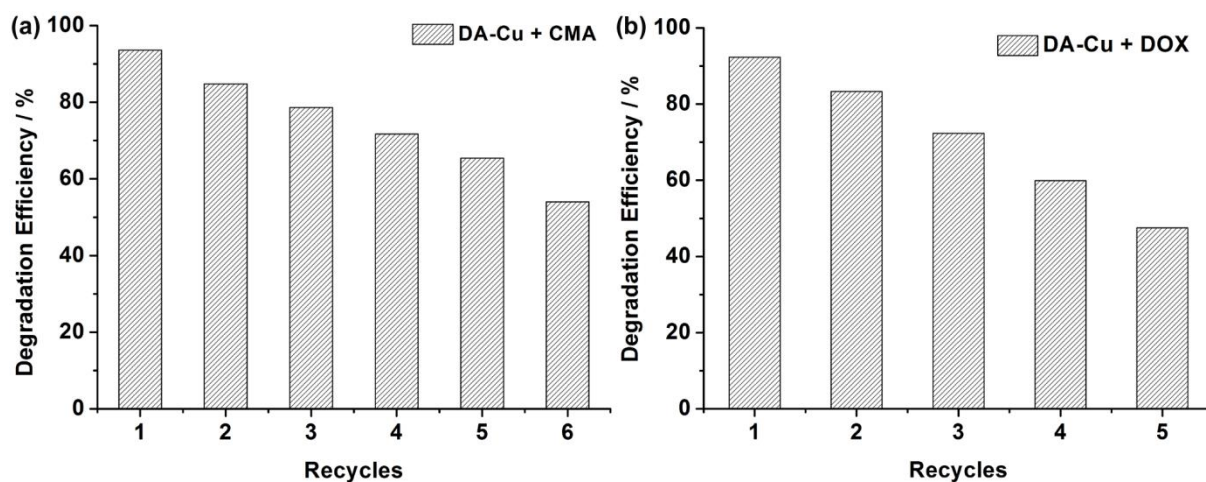
Figure 3. 27 Recycles of DA-Cu NPs for the degradation of CMA and DOX

However, Cu NPs possess an advantage over Cu^{2+} ions for the degradation of water pollutants, which is that the NPs could be recycled and reused, and this was demonstrated by recollection of DA-coated Cu NPs by centrifugation after each degradation cycle and their reuse in a new cycle. Such procedures were repeated several times, and as can be seen from Figure 3.27, the degradation efficiencies of CMA and DOX by Cu NPs were still higher than 50% after recycling for 5 and 6 times, respectively.

As shown above, Cu NPs exhibited excellent catalytic activities towards the degradation of fluorescent dyes and antibiotics. The heterogeneous metallic NP catalysts can be recycled, which can help to avoid the contamination problem caused by conventional homogeneous catalysts. Therefore, they might find potential applications in the preparation of active surfaces or coatings that are useful for environmental applications.

3.4 Cu NPs as SERS Substrates

It has been mentioned in 1.2.3 that noble metallic nanomaterials are suitable substrates for SERS as they are excellent plasmonic materials.[182] In particular, Au and Ag NPs have already been widely applied as building blocks for the design of SERS-based sensors,[188, 189] while only a few reports have explored the SERS property of Cu NPs due to their instability upon air exposure. Raman scattering occurs only when the plasmon oscillations are perpendicular

to the surface of the substrates, therefore, rough surfaces or arrangements of NPs are needed for SERS measurements.[181]

To investigate if the obtained stable Cu NPs could be used as SERS substrates, DA-coated Cu NPs were employed for the detection of a series of SERS active compounds. Since the enhancement of Raman scattering signals could be realized when the frequency of incident light is in resonance of the plasmon frequency, two different lasers with wavelengths 532 and 633 nm were chosen to excite the localized surface plasmon of DA-Cu NPs, which has a maximum absorption at 585 nm (Figure 3.11 in Part 3.1.11). First, a negatively charged dye Eosin (Figure 3.28a) was chosen to study the SERS property of positively charged DA-Cu NPs (zeta potential: 40.2 mV).
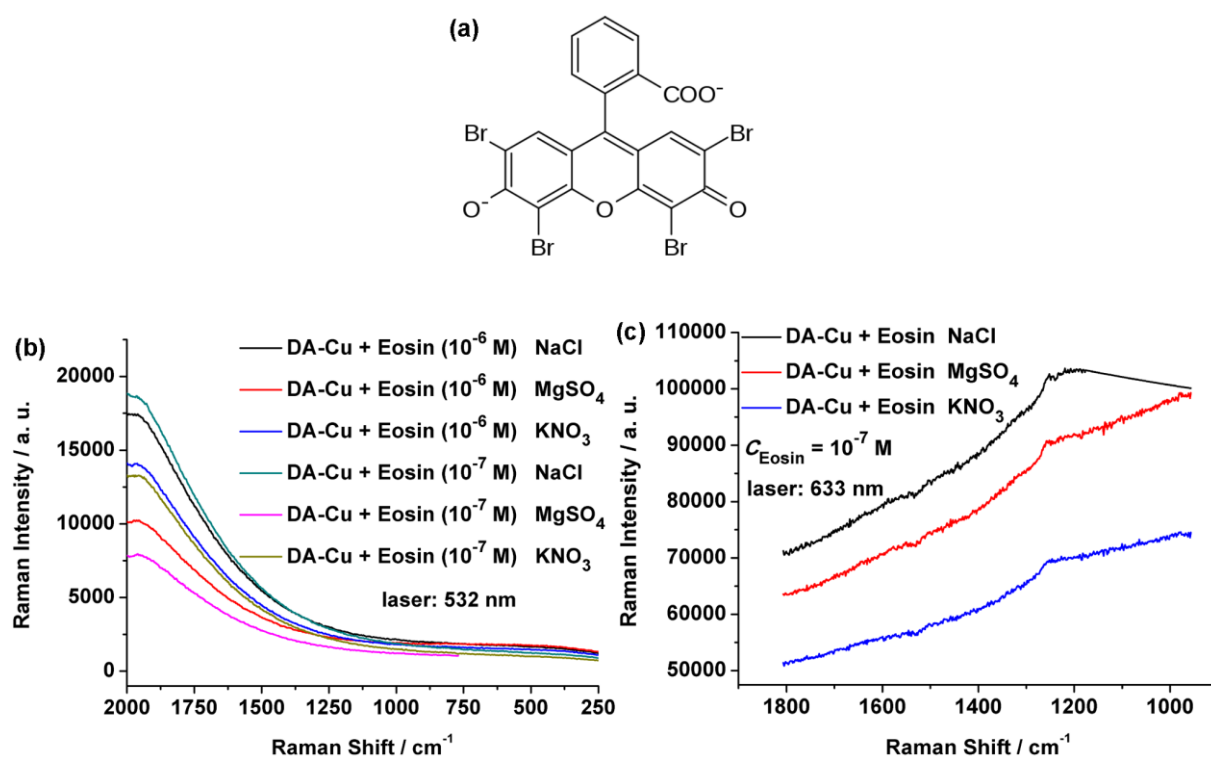
Figure 3. 28 (a) Molecular structure of Eosin, and SERS spectra of Eosin recorded using a (a) 532 nm or (b) 633 nm laser and different aggregation agents (NaCl, MgSO$_4$ or KNO$_3$);

As can be seen from Figure 3.28b, no SERS signals could be observed when the spectra of Eosin were recorded using a 532 nm laser, no matter how much Eosin or which kind of aggregation agent was used. When the wavelength of the laser was changed to 633 nm, only really weak SERS signals could be observed (Figure 3.28c), probably due to a very weak electrostatic interaction between.
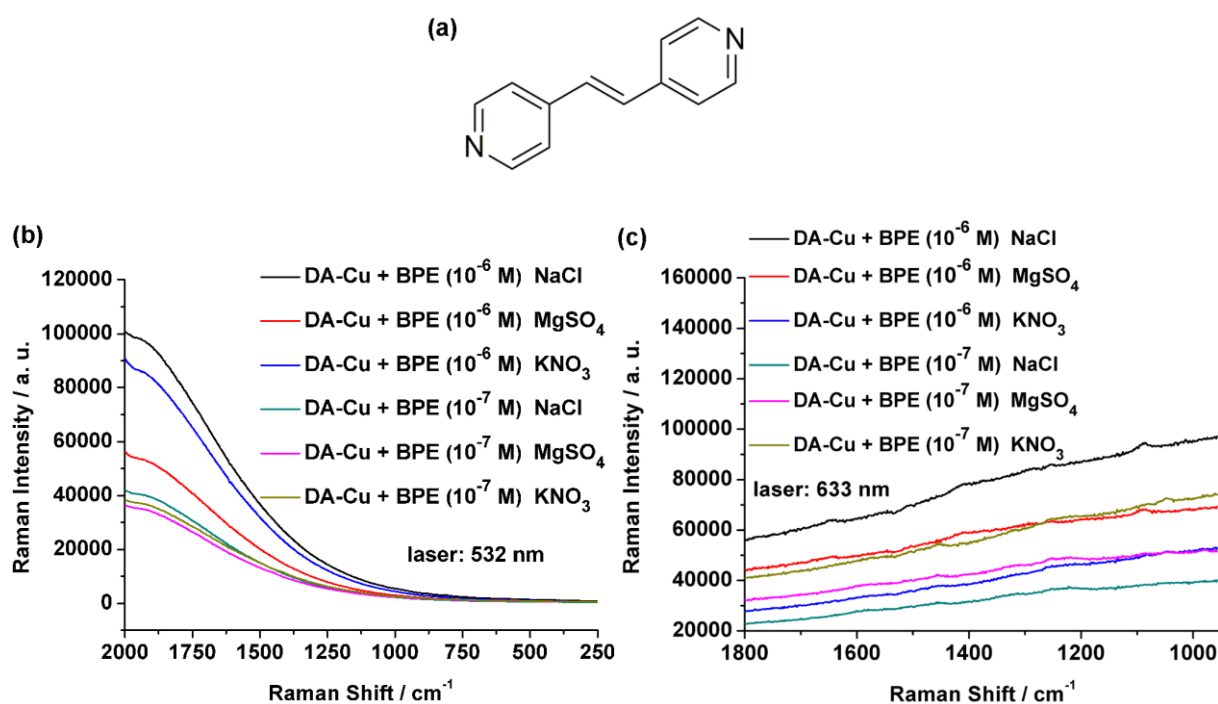
Figure 3. 29 (a) Molecular structure of BPE; and SERS spectra of BPE recorded using a (a) 532 nm or (b) 633 nm laser and different aggregation agents (NaCl, MgSO$_4$ or KNO$_3$);

In order to improve the interaction between the DA-Cu NPs and the SERS active compounds, 1,2-bis(4-pyridyl)ethylene (BPE), a molecule containing metalphilic nitrogen (Figure 3.29a), was chosen to investigate if it can be chemi-absorbed onto the surface of DA-Cu NPs and give better SERS signals. Unfortunately, no SERS signals were obtained when the solution was excited by a 532 nm laser (Figure 3.29b), while only really weak signals were observed when the wavelength of the laser was changed to 633 nm (Figure 3.29c). No obvious improvents of the SERS signals were realized even when different aggregation agents were used or the concentration of BPE was increased from 10^{-7} to 10^{-6} M.
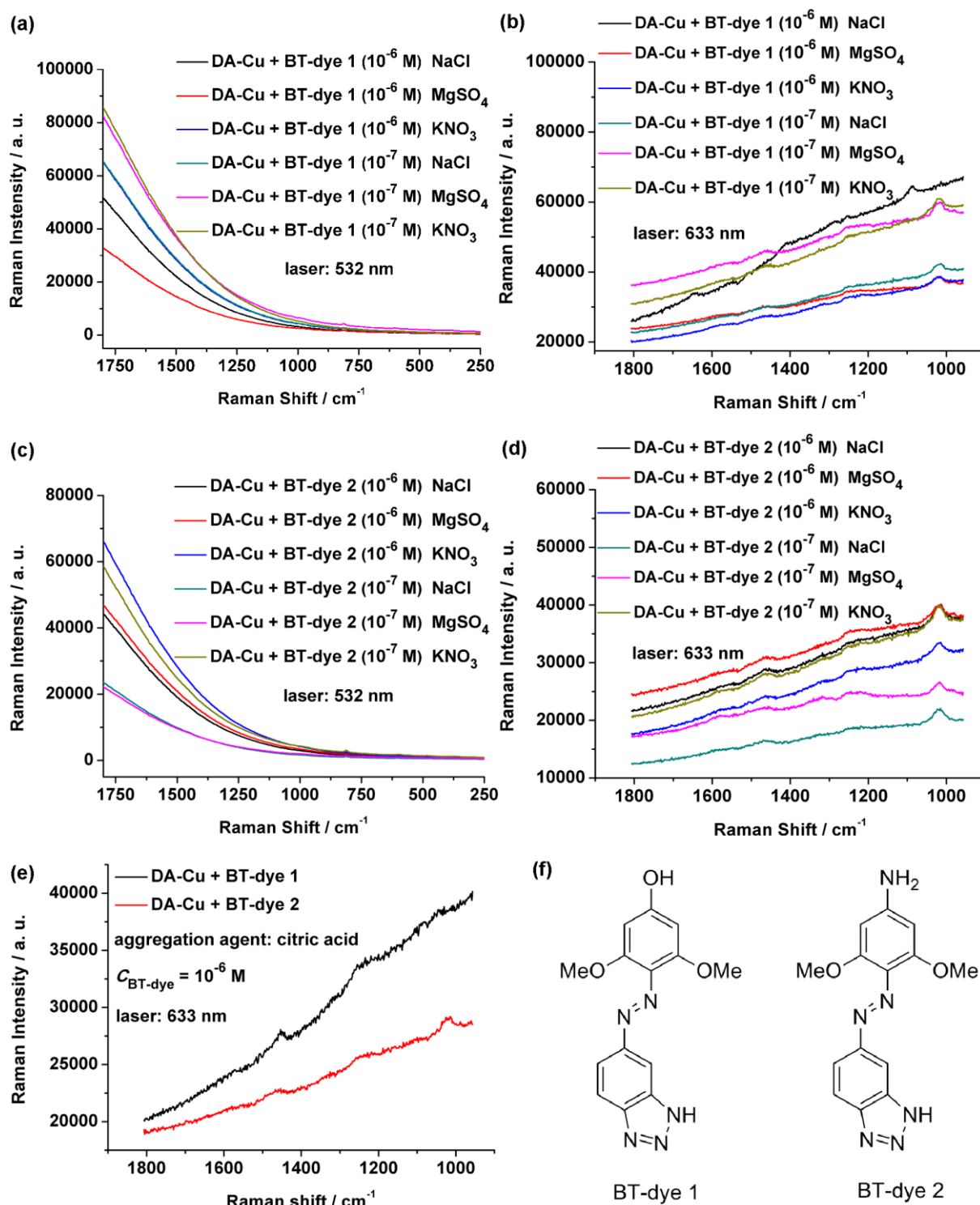
Figure 3. 30 SERS spectra of BT dye 1 and 2 recorded using different lasers (a and c) 532 nm or (b, d, e) 633 nm and different aggregation agents (NaCl, MgSO$_4$, KNO$_3$ or citric acid); (f) molecular structures of BT dyes

To further investigate if the chemisorption of SERS active labels on DA-Cu NPs could help to improve the SERS signals, benzotriazole dyes (BT-dye 1 and 2, Figure 3.30f) were employed for the SERS measurements because the triazole moiety has the strong affinity to metals. However, similar to the aforementioned results, no SERS signals could be obtained

149

when a 532 nm laser was used for the excitation (Figure 3.30a and c), while weak signals could be observed when a 633 nm laser was used (Figure 3.30b and d). In addition, other than NaCl, MgSO$_4$, and KNO$_3$, citric acid was also used as an aggregation agent, because it is negatively charged due to the existence of three carboxylic groups, thus it should be able to bring the positively charged DA-Cu NPs to close affinity and cause their agglomerations, which would finally lead to better SERS signals. However, as can be seen from Figure 3.30e, the SERS signals of both BT dyes were not improved.
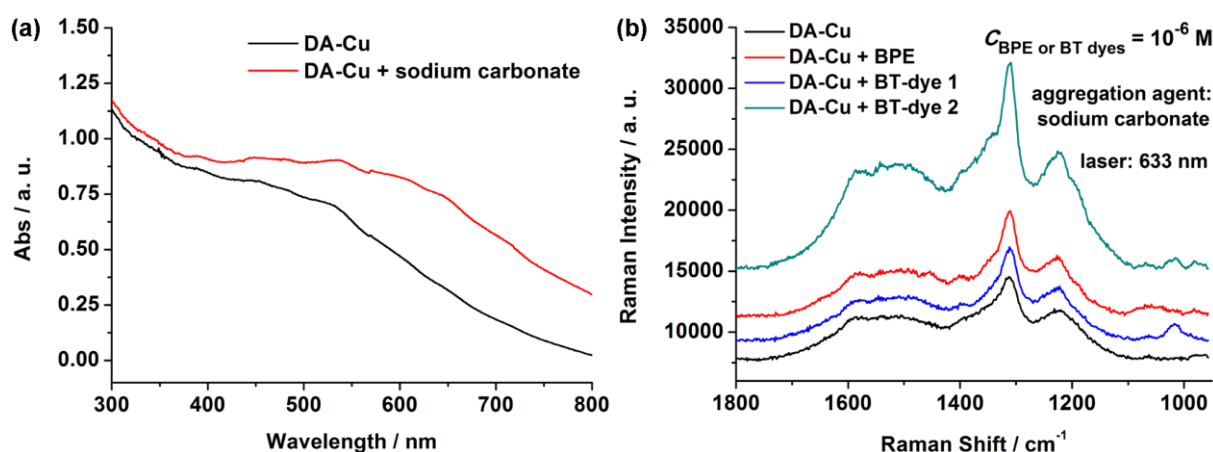
Figure 3. 31 (a) UV-Vis spectra of DA-Cu NPs before and after the pH adjusting with sodium carbonate, and (b) SERS spectra of DA-Cu NPs alone, BPE and BT dyes recorded using a 633 nm laser, and the pH of the solutions was adjusted by sodium carbonate

The similar results obtained from different SERS active compounds above might indicate that the DA-Cu NPs might not be properly aggregated, so there were not enough rough surfaces for Raman scattering to occur. Therefore, instead of the addition of salts, a different strategy, pH adjusting, was used to induce the aggregation of DA-Cu NPs. As can be seen from the UV-Vis spectra (Figure 3.31a), the plasmonic band of DA-Cu NPs red shifted after adjusting the pH to 8 by the addition of sodium carbonate, and indeed SERS signals could be observed clearly from DA-Cu NPs themselves (Figure 3.31b). However, when BPE or BT dyes were added to DA-Cu NPs, which was followed by the aggregation of Cu NPs through pH adjusting, no SERS signals of BPE or BT dyes could be observed except the signals from DA-Cu NPs themselves (Figure 3.31b), which might because that the suface of Cu NPs were well-coated by DA and the interaction between DA and Cu was so strong that BPE or BT dyes could not reach to the surface of Cu NPs.

From the results above, we can know that the aggregation of Cu NPs could be achieved by pH adjusting. However, the surface capping agent DA inhibited the interaction between Cu NPs and the SERS active compounds. Therefore, the conditions for using Cu NPs as SERS substrates still need to be systematically optimized, such as ligand exchange at elevated temperatures or longer incubation time.

3.5 Conclusion

Different methods, such as chemical reduction, seed-mediated growth, DNA-template method and thermal decomposition, have been employed in order to obtain water-soluble and stable Cu NPs. Various capping agents have also been used as stabilizers for the synthesis of Cu NPs, such as PVP, citrate, CTAB, KI, BT derivatives, OA, and PAA. However, the obtained Cu NPs could be stable for only a few hours to a couple of days or could be easily oxidized, which make them not suitable for the further applications in aqueous systems.

However, use of molecules containing polyhydroxyl groups, such as AA, DA and DA derivatives, which have strong affinity to the surface of Cu NPs, resulted in Cu NPs that are stable over months of storage. Interestingly, the AA- and dopamine linkers-coated Cu NPs possess ROS generation ability, which could be utilized for the activation of peroxidase enzymes and the subsequent oxidation of ROS detection substrates. To understand the mechanism behind the ROS production ability, EPR measurements were performed, which showed that semiquinone radicals was produced in the solution of Cu NPs. During the oxidation process of hydroquinone to semiquione and then to quinone, superoxide radiacals were also generated. The ligand-Cu(II) complexes on the surface of Cu NPs could behave like superoxide dismutase (SOD), and catalyze the dismutation of superoxide radicals to H_2O_2, and this hypothesis was confirmed by the SOD assays.

Apart from being effective enzyme mimetics, AA- and dopamine linkers-coated Cu NPs could also be used as catalysts for the degradation of pollutants in waste water, such as fluorescent dyes (RB and MB), and antibiotics (CMA and DOX).

Furthermore, the SERS property of DA-coated Cu NPs was investigated using different SERS active dyes and different aggregation agents. It was found that pH adjusting was more effective than the addition of salts for the aggregation of Cu NPs. However, no SERS signals of the dyes but only the signals of DA-Cu NPs themselves could be observed, which might because that the surface of Cu NPs were well-coated by DA and the interaction between them was so strong that other molecules could not come close to the surface of Cu NPs. Therefore, optimization of the SERS conditions still needs to be explored.

The stable Cu NPs coated with AA and dopamine linkers exhibited excellent enzyme mimetic property and catalytic activity, which makes them excellent candidate to be utilized in bioassays, catalysis, and environmental applications.

Chapter 4

Preparation and Properties of Hybrid Titanium Dioxide Nanomaterials

4 Preparation and Properties of Hybrid Titanium Dioxide (TiO₂) Nanomaterials

As one of the most important semiconductor nanomaterials, TiO_2 has been extensively explored for applications in solar cells, water splitting, paints, photocatalysis and the degradation of contaminants.[117] As mentioned in 1.1.3, TiO_2 nanomaterials are able to generate electron-hole pairs under UV light irradiation (Scheme 1.3), and these electrons (e^-) and holes (h^+) could then react with oxygen and water to produce ROS, such as superoxide and hydroxyl radicals, which have strong redox potential and are responsible for the excellent photoactivity of TiO_2.[118] However, due to the large band gaps of TiO_2 (3.20 and 3.02 eV for anatase and rutile) and the easy recombination of electron-hole pairs, the application of TiO_2 has been limited.[117] Different strategies, such as dye sensitization and doping with metallic ions or NPs,[117] have been developed to reduce the energy gap or to prevent the electron-hole recombination,[118] which can help to improve the photoactivity of TiO_2.

Within presented thesis, the photo-induced ROS production ability of both self-prepared and commercial TiO_2 nanomaterials were investigated and compared. In addition, the functionalization of TiO_2 NPs with DNA sequences has been attempted using different linkers. Furthermore, it was shown in Chapter 3 that dopamine linkers-coated Cu NPs could also produce ROS; therefore, methods were explored to prepare hybrid TiO_2-Cu nanocomposite, which might influence the photocatalytic activity of TiO_2 nanomaterials.

4.1 Synthesis of TiO₂ NPs
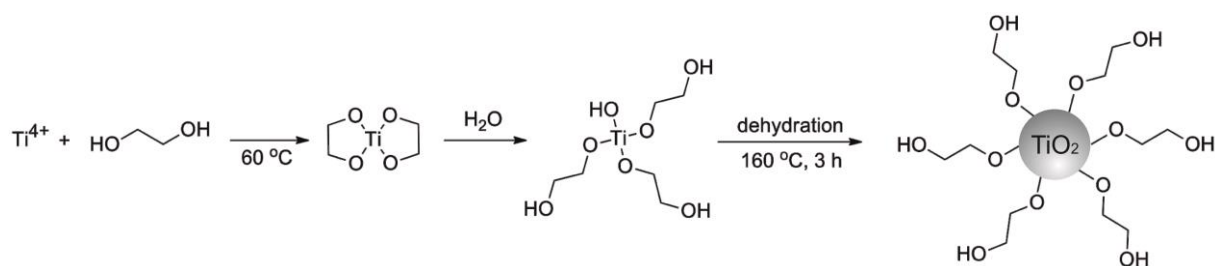
Scheme 4. 1 Schematic illustration for the synthesis of TiO_2 NPs through polyol method

TiO_2 NPs was synthesized by a polyol method with slight modification, in which ethylene glycol (EG) was used as both the solvent and the capping agent for the NPs (Scheme 4.1).[432] The reaction mechanism has been explained as follows:[432] titanium precursor first reacts with EG to afford titatium glycolate, which can reduce the hydrolysis rate of titanium precursor

(Scheme 4.1). After the addition of water, hydroxyl groups can partially replace the coordinated EG, and then the dehydration between the hydroxyl groups and the formation of EG-coated TiO_2 NPs begin to take place when the temperature is increased to 160 ^{o}C.
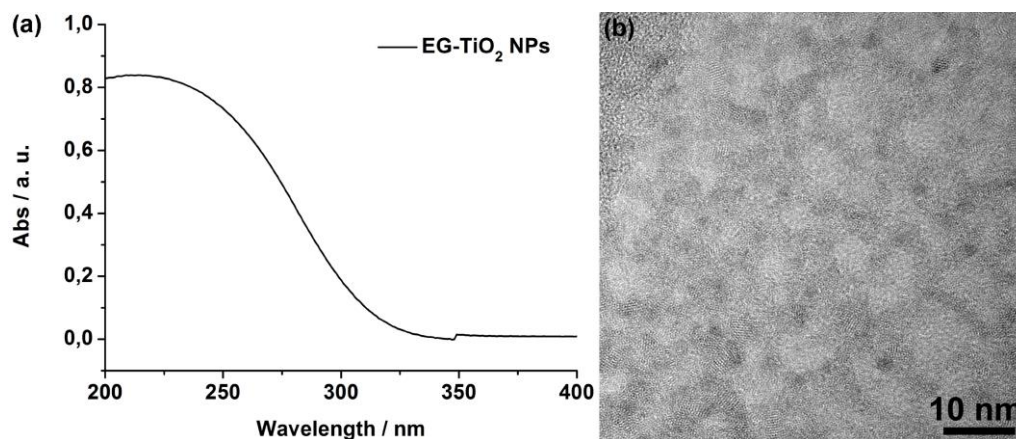
Figure 4. 1 (a) UV-Vis and (b) TEM image of EG-coated TiO_2 NPs

The reaction was stirred at 160 ^{o}C for 3 h, after which the NPs were collected by precipitation with acetone and washed 3 times with acetone. As can be seen from Figure 4.1a, EG-coated TiO_2 NPs showed a broad absorption band in the UV region between 200 and 350 nm, and TEM image shows that small NPs with an average diameter of ~3.4 nm were obtained. Due to the hydrophilic property of the capping agent EG, the obtained NPs could be easily dispersed in water, which makes them applicable in aqueous systems. After the preparation of TiO_2 NPs, the biofunctionalization of TiO_2 NPs was performed.

4.2 Biofunctioanlization of TiO_2 Nanomateirals

It has been mentioned previously in Chapter 1.4 that the construction of biomolecule-NP hybrids could integrate the optical, electrical and chemical properties of NPs and the biocatalysis and recognition properties of biomolecules.[306, 307] Due to the high stability and biocompatibility of TiO_2,[433, 434] conjugates of biomolecules (DNA oligonucleotides, proteins or peptides) and TiO_2 have been already designed for applications in delivery, biodiagnostics, and biocatalysis. For example, Levina and coworkers designed TiO_2-DNA nanocomposites through a polylysine linker for cell penetration studies, which showed that it was much easier for polylysine-modified DNA oligos to enter the cells when they was conjugated to TiO_2 NPs (~5 nm).[435] Thurn *et al.* employed dopamine as a linker for the preparation of DNA-TiO_2 conjugates, which might have potentials for sequence specific intracellular DNA cleavage.[436] Shimizu's group demonstrated the preferential uptake of avidin-conjugated TiO_2 NPs by

cancer cells, and the hydroxyl radicals produced by the NPs could cause cell injury under ultrasonic treatment.[437] However, unlike in the case of metallic NPs, only a few methods have been used for the preparation of bio-TiO$_2$ conjugates, and they are mainly based on electrostatic interaction and amide coupling. [435, 437, 438] Therefore, novel efficient methods for the biofunctionalization of TiO$_2$ nanomaterials still need to be developed.

4.2.1 Biofunctionalization of TiO$_2$ NPs using Benzotriazole Linker

It has been reported recently that the heterocyclic triazole could be used for the surface modification of TiO$_2$, and it could enhance the photogenerated electron-hole pair and in turn increase the photocurrent of TiO$_2$-based solar cells.[439] Thus the triazole-TiO$_2$ interaction might provide another opportunity for the biofunctionalization of TiO$_2$ nanomaterials.

The traizole moiety of benzotriazole (BT) has already been used in Chapter 2 to stabilize the surface of Ag NPs, so it was available for the modification of TiO$_2$ NPs and their further biofunctionalization. Therefore, bezotriazole-maleimide (BTM)-modified DNA1 (preparation procedures are in 2.2.1.1) was employed for the functionalization of water-soluble EG-coated TiO$_2$ NPs as shown in Scheme 4.2.

DNA1: 5'-GGCGTATAACAA-3'
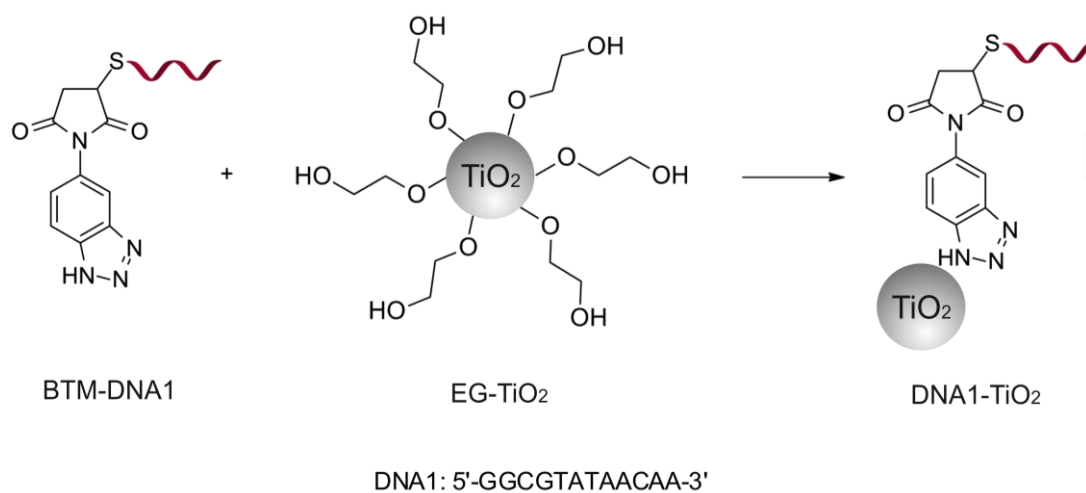
Scheme 4. 2 Biofunctionalization of EG-TiO$_2$ NPs with BTM-DNA1

20 μL EG-coated TiO$_2$ (20 μg/mL) was mixed with 2 nmol BTM-DNA1 in water, and incubated at room temperature for 1 d, The NPs after modification were characterized by agarose gel electrophoresis (1%), and the image of the gel was taken under UV light mode of the imaging system as BTM-DNA1 is visible under UV light due to the fluorescence of BTM. However, as shown in Figure 4.2, the mobility of BTM-DNA1 did not change after incubation

with EG-coated TiO$_2$ NPs, indicating that the DNA was not attached to TiO$_2$ NPs through the BTM linker.
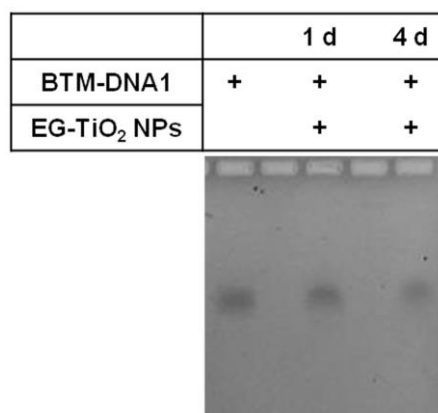
Figure 4. 2 Agarose gel image for BTM-DNA1-TiO$_2$NP conjugates taken under the UV light

The incubation time was then prolonged to 4 d, however, the electrophoretic mobility of BTM-DNA1 still did not change. The reason for the unsuccessful functionalization of EG-TiO$_2$ with BTM-DNA1 might be that the interaction between titanium and EG (bond energy of Ti-O is 109 kcal/mol) is stronger than that between triazole and titanium (bond energy of Ti-N is 78 kcal/mol),[440] so the triazole functional group of BTM could not replace the hydroxyl groups of EG on the surface of TiO$_2$ NPs. Other attempts using BTM directly for the synthesis of TiO$_2$ or ligand exchange using BT molecules were not performed due to the time constrains, but are the subjects of another ongoing project.

4.2.2 Biofunctionalization of TiO$_2$ NPs using Doapmine Linkers

As a robust linker for the immobilization of functional molecules, dopamine not only has strong affinity to metals, but can also coordinate to metal oxides, such as Fe$_2$O$_3$ and TiO$_2$.[436, 441] In addition to the example mentioned at the beginning of 4.2, bifuntional dopamine linkers, i.e. dopamine-lipoic acid and dopamine-maleimide, have also been successfully employed by our group for the construction of TiO$_2$-Au nanocomposites and the attachment of peptide to TiO$_2$ NPs, respectively.[22, 141]

In this thesis, two different dopamine linkers, dopamine-maleimide (DoMal, **7**) and dopamine-triethylene glycol-maleimide (Do-TEG-Mal, **9**), were employed for the biofunctionalization of EG-coated TiO$_2$ NPs (Scheme 4.3), as both linkers have catechol groups for the surface modification of TiO$_2$ NPs and maleimide functional groups for the further covalent attachment of furan-modified DNA1 through Diels-Alder cycloaddition. In

addition, Do-TEG-Mal (**9**) has a hydrophilic TEG chain between catechol and maleimide, thus its solubility in water should be better than DoMal (**7**), which might facilitate its reaction with furan-modified DNA1 in water.
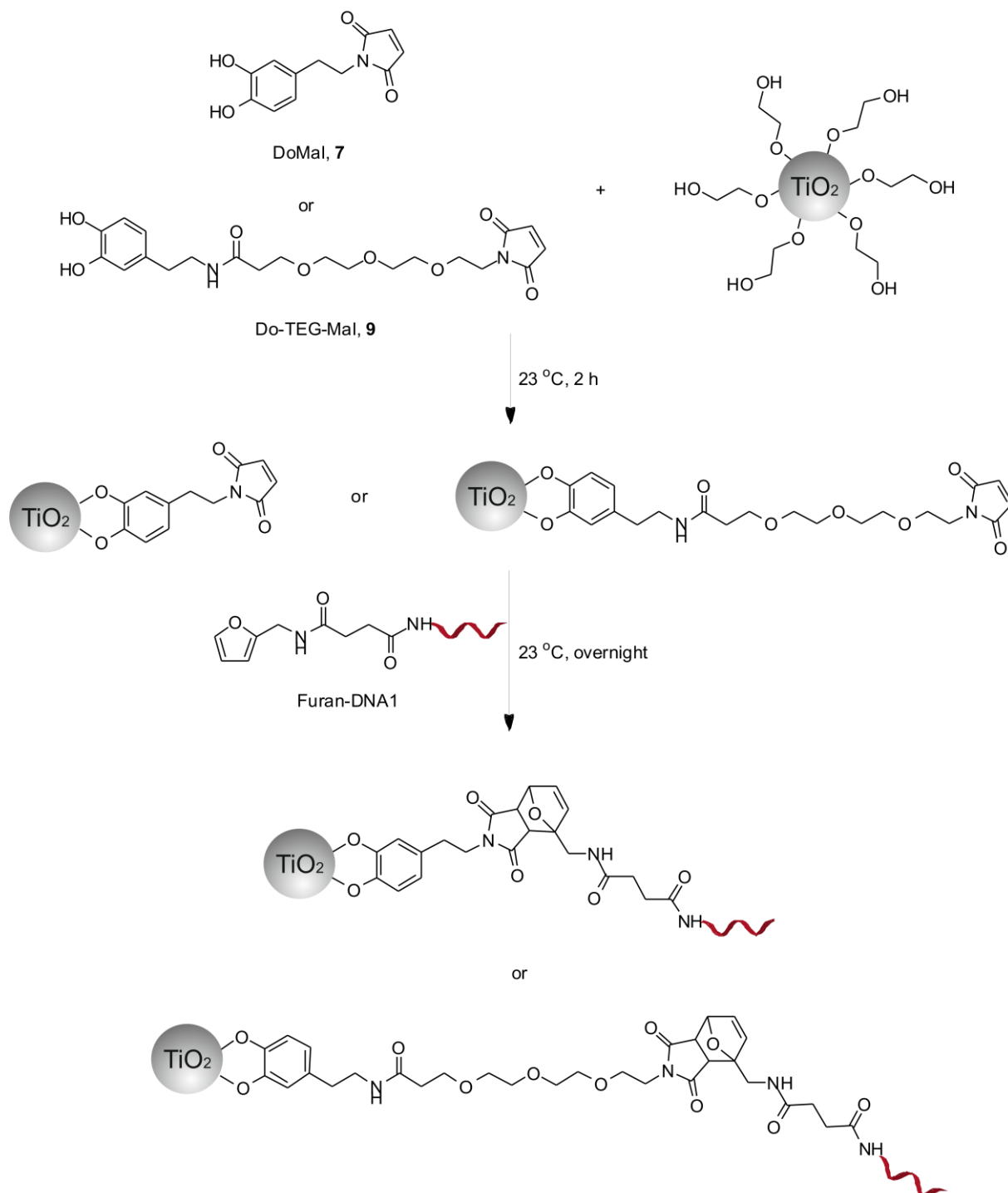
Scheme 4. 3 Modification of EG-TiO$_2$ NPs with dopamine linkers and the following attachment of furan-DNA through Diels-Alder cycloaddition

EG-coated TiO_2 NPs were first incubated with DoMal (**7**) and Do-TEG-Mal (**9**) at room temperature for 2 hours (Scheme 4.3), and the colour of the solution turned orange due to the charge transfer between TiO_2 and dopamine linkers,[141] indicating the successful surface modification of TiO_2 NPs, which was also confirmed by the increased absorption of TiO_2 NPs in the visible light region (400~600 nm) after the modification (Figure 4.3).
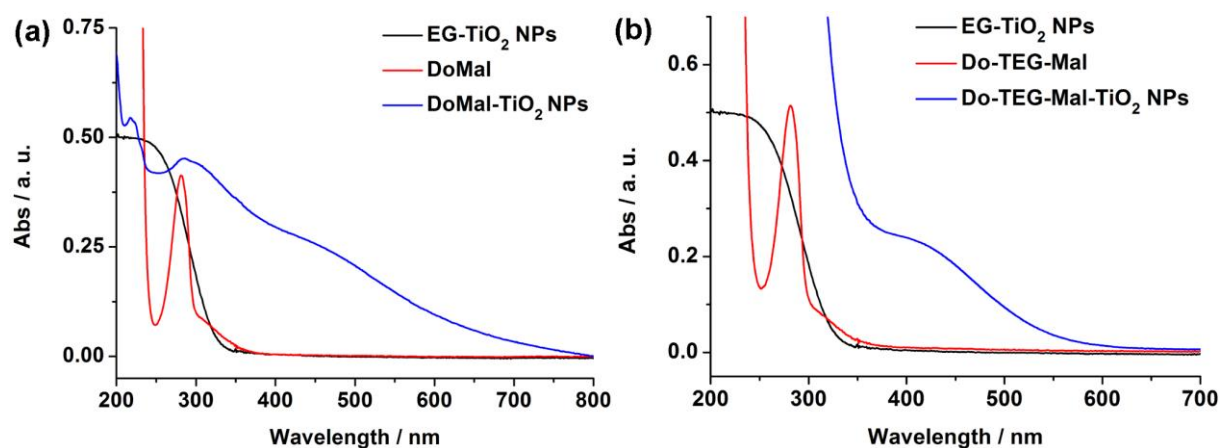
Figure 4. 3 UV-Vis spectra of (a) DoMal-modified TiO_2 NPs and (b) Do-TEG-Mal-modified TiO_2 NPs

The obtained DoMal- and Do-TEG-Mal-modified TiO_2 NPs were then incubated with furan-DNA1 at room temperature overnight (Scheme 4.3). After washing the NPs with water three times, the NPs were characterized by gel electrophoresis. As can be seen from Figure 4.4a, no obvious mobility shift of the TiO_2 NPs could be observed in the agarose gel (1%). The agarose gel was then stained with SYBR gold to visualize the DNA in the gel, and the image taken under UV light showed a single band for furan-DNA1 and smearing bands of DNA1-functionalized TiO_2 NPs (Figure 4.4b), indicating that some of the furan-DNA1 strands have been attached to TiO_2 NPs, but they were not well separated from the free furan-DNA1.
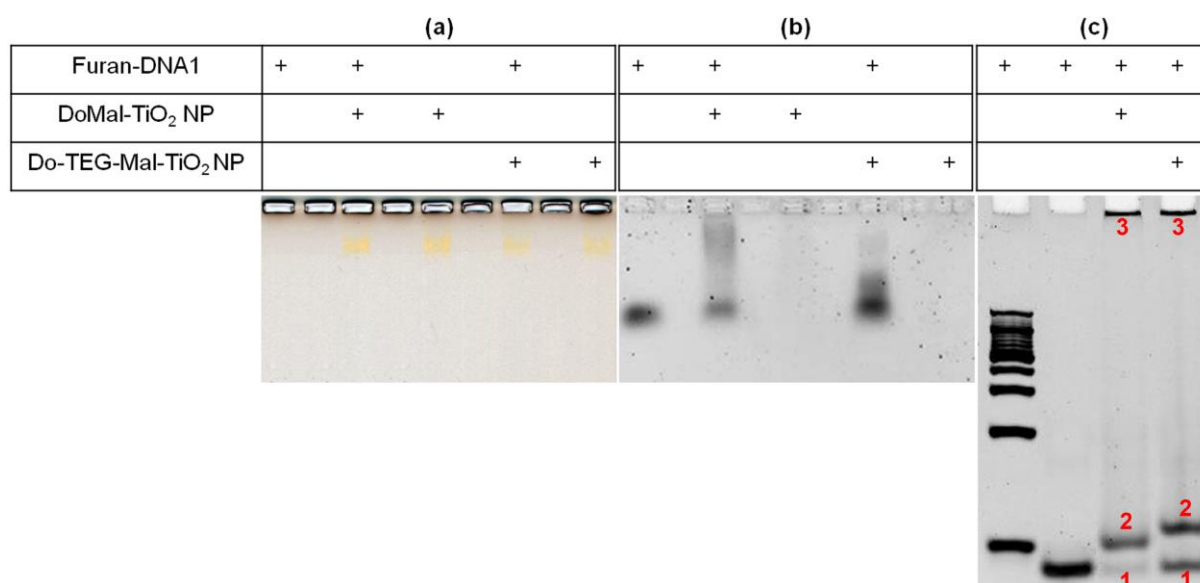
Figure 4. 4 Agarose gel images of DNA1-TiO$_2$NP conjugates taken under (a) visible and (b) UV light, respectively; (c) native PAGE image of DNA1-TiO$_2$NP conjugates taken under UV light

Therefore, 21% PAGE was then used for the separation and stained with SYBR gold, and as shown in Figure 4.4c, DNA1-functionalized TiO$_2$ NPs, which were obtained using both dopamine linkers, showed three different bands. The mobility of the first band was the same as that of furan-DNA1, the second one above the first might be attributed to the products of furan-DNA1 and free linkers in the solution, and the third band in the gel pockets should be DNA1-functionalized TiO$_2$ NPs, which did not enter the gel probably due to the size effect of DNA1-TiO$_2$NP conjugates. To further confirm that the bands in the gel pockets were DNA1-functionalized TiO$_2$ NPs, the gel bands 3 were cut out, and the samples were extracted by ultrafiltration (Millipore) and characterized by TEM. As shown in Figure 4.5, TiO$_2$ NPs could be observed in the samples extracted from the gel bands 3, proving that the DNA1-functionalization-TiO$_2$ NPs were obtained using both linkers.
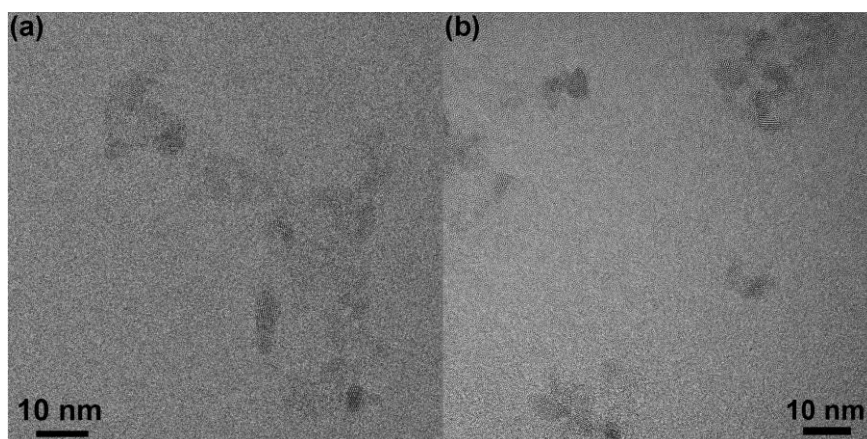
Figure 4. 5 TEM images of DNA1-TiO$_2$NP conjugates prepared using (a) DoMal (**7**) and (b) Do-TEG-Mal (**9**) and recollected from the PAGE gel band 3

The successful preparation of DNA-TiO$_2$NP conjugates using dopamine linkers through Diels-Alder cycloaddition offers another mild methodology for the biofunctionalization of TiO$_2$ nanomaterials, which might be useful for biocatalysis, controlled cell uptake of TiO$_2$ NPs and cytotoxicity studies.

4.3 ROS Production by TiO$_2$ Nanomaterials

After the successful preparation and fucntionalization of TiO$_2$ NPs, the photo-induced ROS generation ability of the EG-coated TiO$_2$ NPs was investigated using the Amplex Red assay (Scheme 4.4), which has already been used previously in Chapter 2 and 3 for the study of the enzymatic activity of Mb-AgNP hybrids and the ROS production ability of Cu NPs.
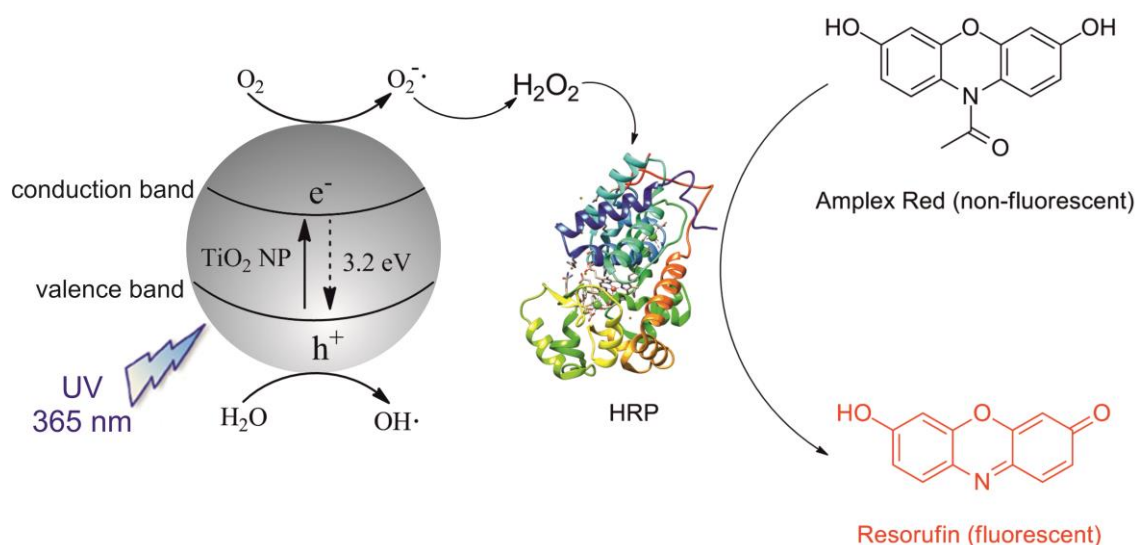
Scheme 4. 4 ROS production by TiO$_2$ NPs under UV light irradiation, and the use of such ROS for the activation of HRP and oxidation of nonfluorescent substrate Amplex Red to fluorescent resorufin

Different amounts (1~7 μL) of EG-TiO$_2$ NPs (1 mg/mL) was mixed with phosphate buffer and irradicated by UV light (365 nm) for 20 min, after which HRP and Amplex Red were added, and the ROS production by EG-TiO$_2$ NPs was estimated by monitoring the fluorescence of resorufin on a microplate reader (λ_{ex} = 540 nm, λ_{em} = 585 nm, sensitivity: 80).
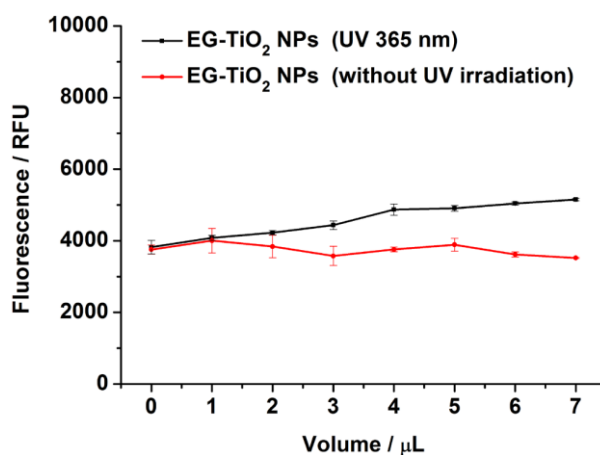
Figure 4. 6 ROS production by different amounts of EG-TiO$_2$ NPs under UV light (365 nm) irradiation and the controls without UV light irradiation

As shown in Figure 4.6, the ROS production of EG-coated TiO$_2$ NPs under UV light irradiation (365 nm) increased when the amounts of NPs increased as supported by the increased fluorescence intensity, and no ROS production was detected in the controls without UV light irradiation. However, the difference between the ROS productions by EG-TiO$_2$ NPs under UV light irradiation and without UV light irradiation was not significant, indicating that the UV light has not been used efficiently by EG-coated TiO$_2$ NPs. Most probable reason for this lies in the crystallinity and the size of the EG-TiO$_2$ NPs obtained by the polyol method, namely in such small and not highly crystalline NPs, the recombination of photo-generated electrons and holes might occur easily and thus decreasing the activity of TiO$_2$ NPs.
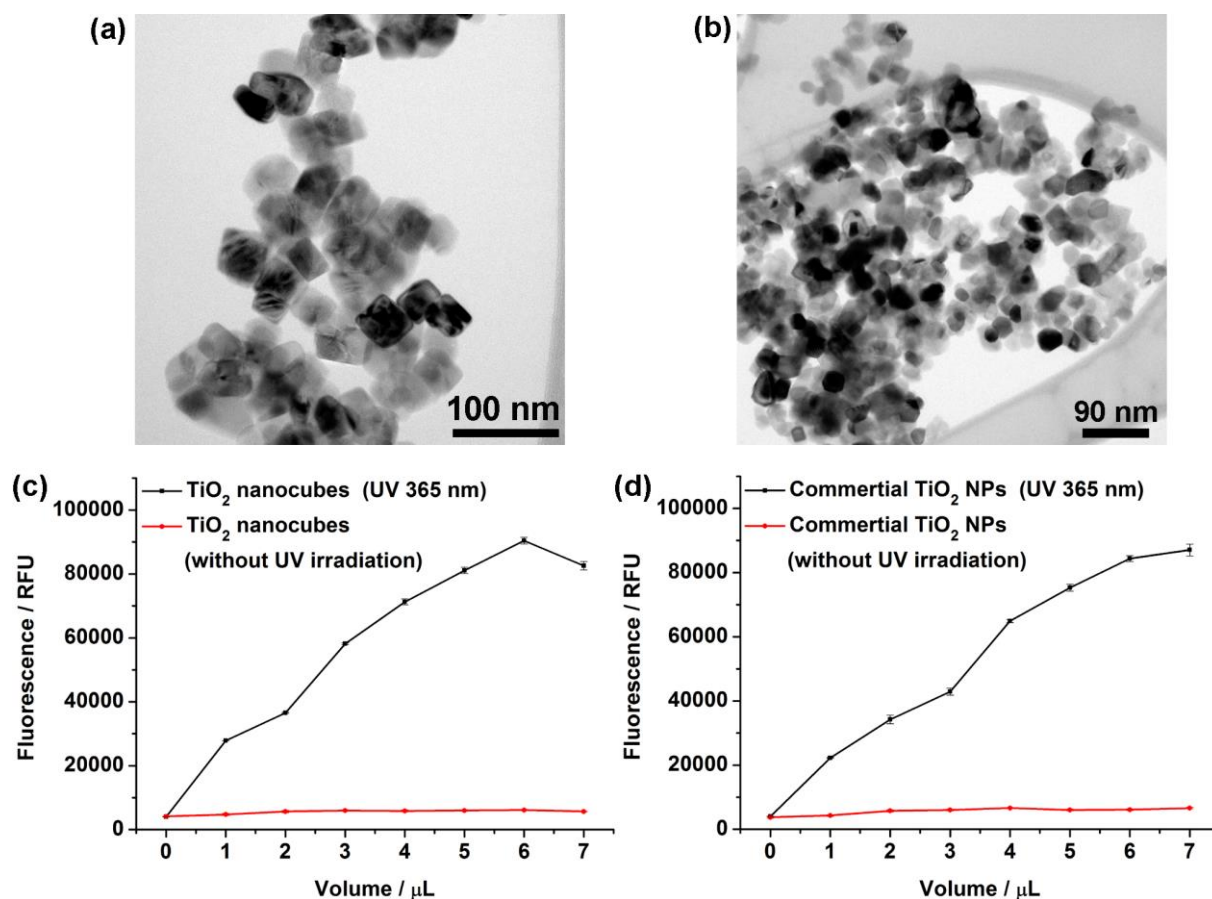
Figure 4. 7 TEM images of (a) TiO_2 nanocubes and (b) commercial TiO_2 NPs; and ROS production by different amounts of (a) TiO_2 nanocubes and (b) commcercial TiO_2 NPs under UV light (365 nm) irradiation and the corresponding controls without UV light irradiation

To investigate if the TiO_2 nanomaterials with bigger size and better crystallinity would be more efficient in UV light-induced ROS production, TiO_2 nanocubes (Figure 4.7a, 20-50 nm, supplied by Prof. Dr. Jun Zhang's group in Inner Mongolia University, China) and commercial TiO_2 NPs (Figure 4.7b, 20-40 nm) were employed for the Amplex Red assays, which were performed at the same conditions to the assays for EG-TiO_2 NPs.[442] As can be seen from Figure 4.7c and d, the fluorescence increased significantly with the increase of the amount of TiO_2 nanocubes or commercial TiO_2 NPs, while the controls without UV irradiation did not show any ROS production.

From the fluorescence intensities obtained after the irradiation of EG-TiO_2 NPs (Figure 4.6), TiO_2 nanocubes (Figure 4.7c) or commercial TiO_2 NPs (Figure 4.7d) followed by the addition of HRP and Amplex Red, it can be concluded that TiO_2 nanocubes or commercial TiO_2 NPs were more efficient than EG-TiO_2 NPs in ROS production under UV irradiation. Therefore, TiO_2 nanocubes and commercial TiO_2 NPs were chosen for the following preparation of the hybrid TiO_2-Cu nanocomposites.

4.4 Preparation of TiO₂-Cu Nanocomposites Using Clickable Dopamine Linkers

The above results showed that TiO$_2$ nanocubes and commercial TiO$_2$ NPs were able to produce ROS under UV light irradiation, and it has been demonstrated in Chapter 3 that Cu NPs also possess ROS generation ability. Furthermore, plasmonic NPs such as Au and Ag were shown to act as electron sinks to prolong the longevity of the charge speration of TiO$_2$ and therefore lead to the enhanced ROS production even when irradiated at wavelength close to the plasmonic absorption of the attached NPs.[22] Therefore, we would like to investigate the preparation of hybrid TiO$_2$-Cu nanocomposites in order to prevent the recombination of the photo-induced electrons and holes, reduce the band gap of TiO$_2$ nanomaterials, and thus improve their photocatalytic activity.

As dopamine has strong affinity to both TiO$_2$ and Cu NPs, two clickable dopamine-based linkers (Scheme 4.5) were designed to facilitate the preparation of TiO$_2$-Cu nanocomposites. One of the linkers was dopamine-coumarin-azide (DCA, **12**) and the other was dopamine-cyclooctyne (DCO, **13**) (Synthesized by Dr. Ishtiaq Ahmed). The azide and cyclooctyne functional groups of the linkers can undergo strain promoted copper-free click reaction,[292] which can afford a fluorescent product (**14**).[141] Thus such increase of fluorescence after the click reaction could be used as a self-reporting system to indicate the successful reaction between both linkers.

4.4.1 Click Reaction between Dopamine-Coumarin-Azide and Dopamine-Cyclooctyne

dopamine-coumarin-azide (DCA, **12**)   dopamine-cyclooctyne (DCO, **13**)

14
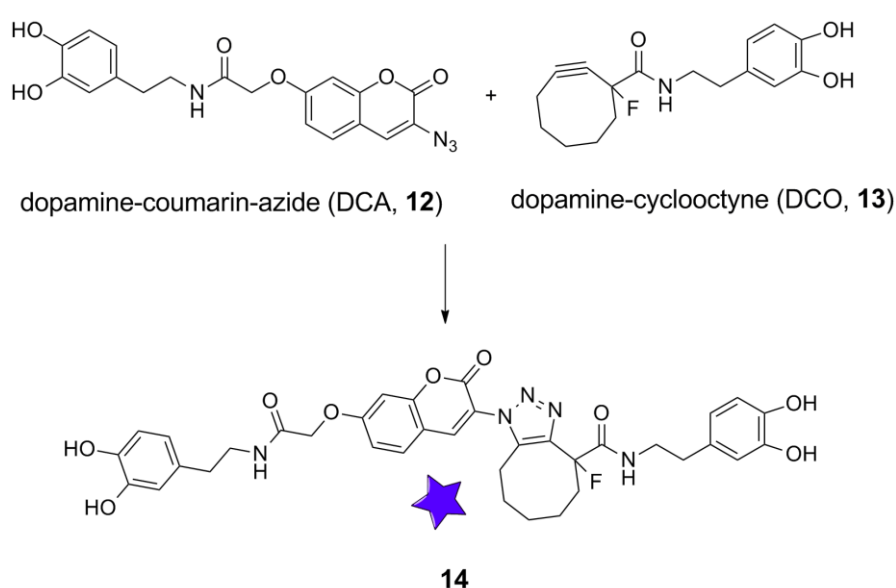
Scheme 4. 5 Copper-free click reaction between DCA (**12**) and DCO (**13**), which would be used later for the preparation of TiO₂-Cu Nanocomposites

To investigate the proper conditions, under which the click reaction between DCA (**12**) and DCO (**13**) can occur to afford the expected fluorescent product (**14**), the reaction between these two linkers was first performed in solution instead of on the surface of NPs (Scheme 4.5). Both linkers were dissolved in ethanol and incubated at room temperature for 2 h, after which the fluorescence of the product was recorded (λ_{ex} = 340 nm). As shown in Figure 4.8a, the obtained product was not fluorescent, indicating that the reaction was not successful. Therefore, the reaction time was then prolonged to overnight, but unfortunately no fluorescence could be detected after the reaction, and the mass of the expected product (**14**) (701.25 g/mol) could not be detected, which indicated that the reaction failed.
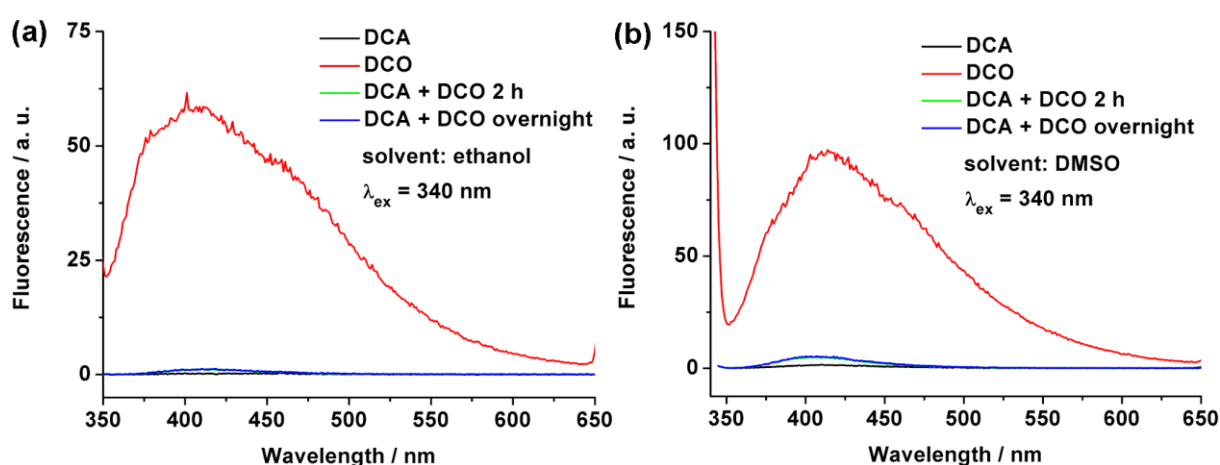
Figure 4. 8 Fluorescence of DCA (**12**), DCO (**13**), and the product (**14**) of the click reactions between DCA and DCO in (a) ethanol and (b) DMSO

It has been reported previously that the click reaction between DCA (**12**) and alkyne was successful when DMSO was used as a solvent.[141] To investigate if the unsuccessful click reaction above was caused by some kind of solvent effects, the reaction was performed again in DMSO instead of ethanol. However, as can be seen from Figure 4.8b, the product was non-fluorescent, indicating again that the reaction did not work.
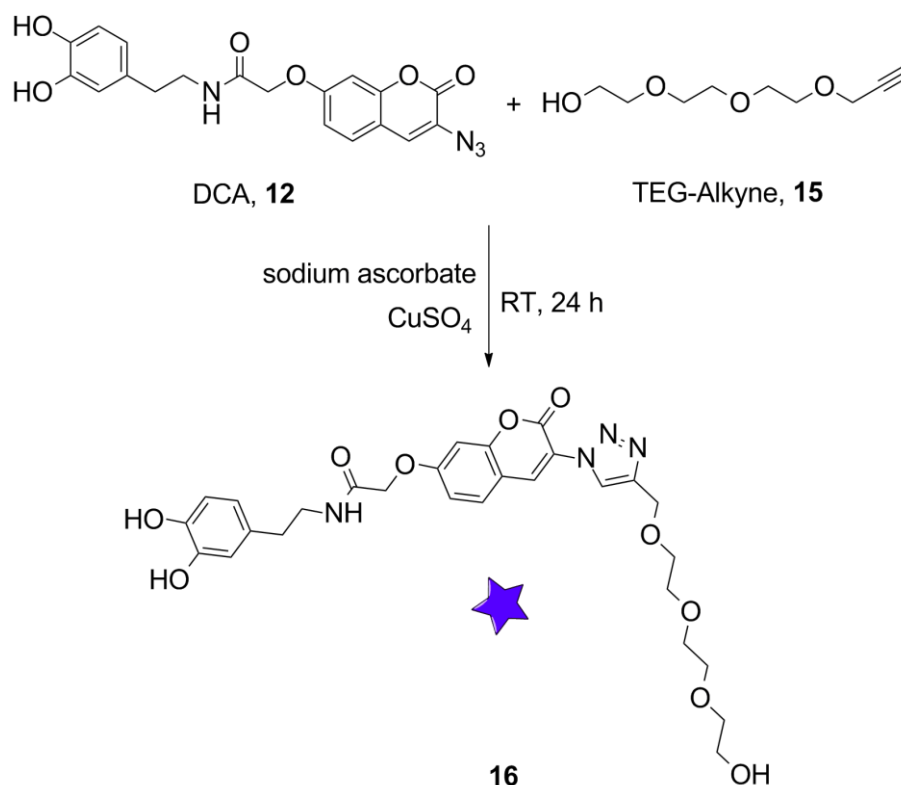
Scheme 4. 6 Copper-catalyzed click reaction between DCA (**12**) and TEG-Alkyne (**15**)

To further understand the reason for the failure of what is considered a fast and reliable click reaction, triethylene glycol-alkyne (TEG-Alkyne, **15**, prepared by Dr. Ishtiaq Ahmed) instead of DCO (**13**) was used to undergo copper-catalyzed click reaction with DCA (**12**) in the presence of $CuSO_4$ and sodium ascorbate (Scheme 4.6).[141]
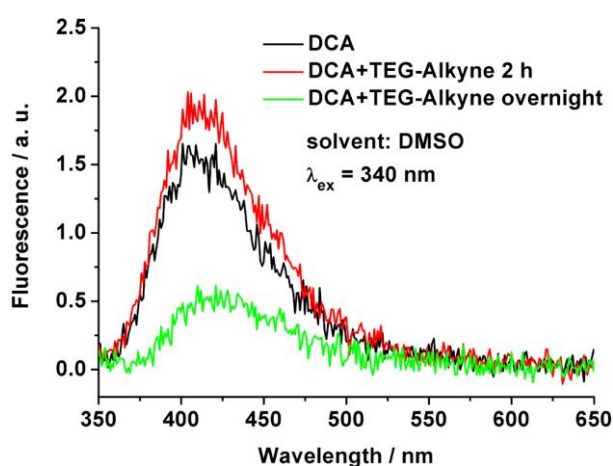
Figure 4. 9 Fluorescence spectra of DCA (**12**), TEG-Alkyne (**15**), and the product (**16**) of the click reaction between DCA and TEG-Alkyne in DMSO

However, no fluorescence could be detected after the reaction (Figure 4.9), and no expected mass (584.21 g/mol) could be found, indicating again the click reaction between DCA (**12**) and TEG-alkyne (**15**) was not successful, which might indicate the inherent problem with one of the reagents, and in this case the DCA (**12**). Thus the NMR of DCA was recorded, showing the signals of DCA as well as the peaks of dopamine impurity, which might have affected the click reaction. Therefore, freshly prepared pure DCA (**12**) was then used in the following click reaction with DCO (**13**) in DMSO at room temperature for 24 h. Interestingly, the freshly prepared DCA (**12**) was no longer soluble in ethanol, indirectly proving that the DCA used in the previous experiments was not pure.
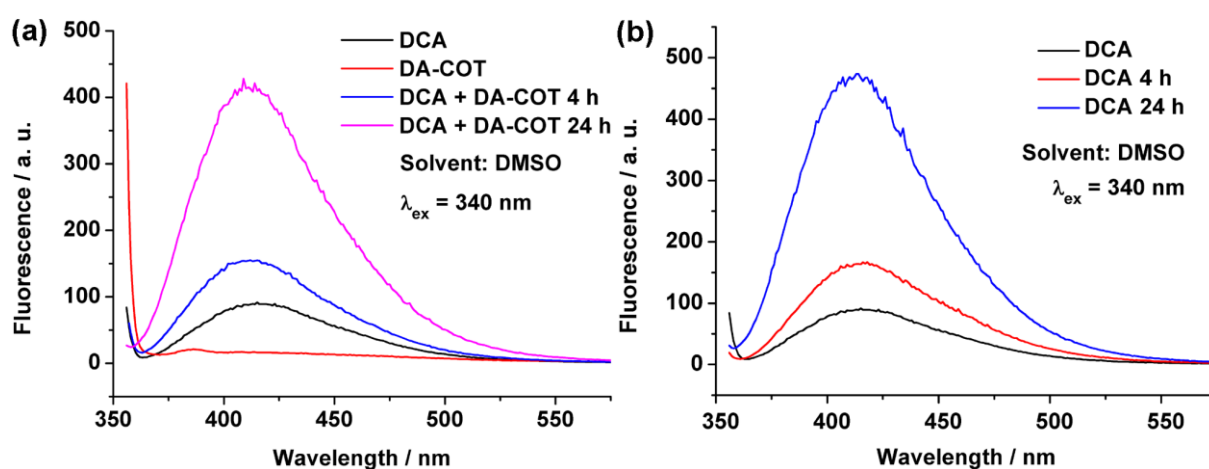
Figure 4. 10 (a) Fluorescence of DCA (**12**), DCO (**13**), and the product (**14**) of the click reactions between fresh DCA and DCO at room temperature for 24 h; (b) Fluorescence of fresh DCA (**12**) alone in DMSO after incubation at room temperature for 24 h

As shown in Figure 4.10a, the fluorescence increase could already be observed after 4 h, and a significant increase occurred after 24 h, which might indicate that the click reaction between the freshly prepared DCA (**12**) and DCO (**13**) was successful. However, when the fluorescence of DCA (**12**) alone was also measured after incubation at room temperature for 24 h, a fluorescence increase was also observed (Figure 4.10b), which was not expected but might be assigned to the solvation of DCA in highly polar solvent,[443, 444] indicating that fluorescence measurement might not be a proper way to monitor the click reaction between DCA (**12**) and DCO (**13**). Therefore, NMR and MS of the product were recorded, which showed that the product (**14**) with the expected mass ([M+H]$^+$: 702.3) was obtained.

The above results showed that freshly prepared pure DCA (**12**) must be used for the click reaction with DCO (**13**) in order to obtain the desired product (**14**). Since the right conditions for the reaction of both linkers in solution have been found, the next step was the use of both

linkers for the modification or preparation of TiO₂ and Cu NPs, which could further be employed for the construction of TiO₂-Cu nanocomposites as shown in Scheme 4.7.
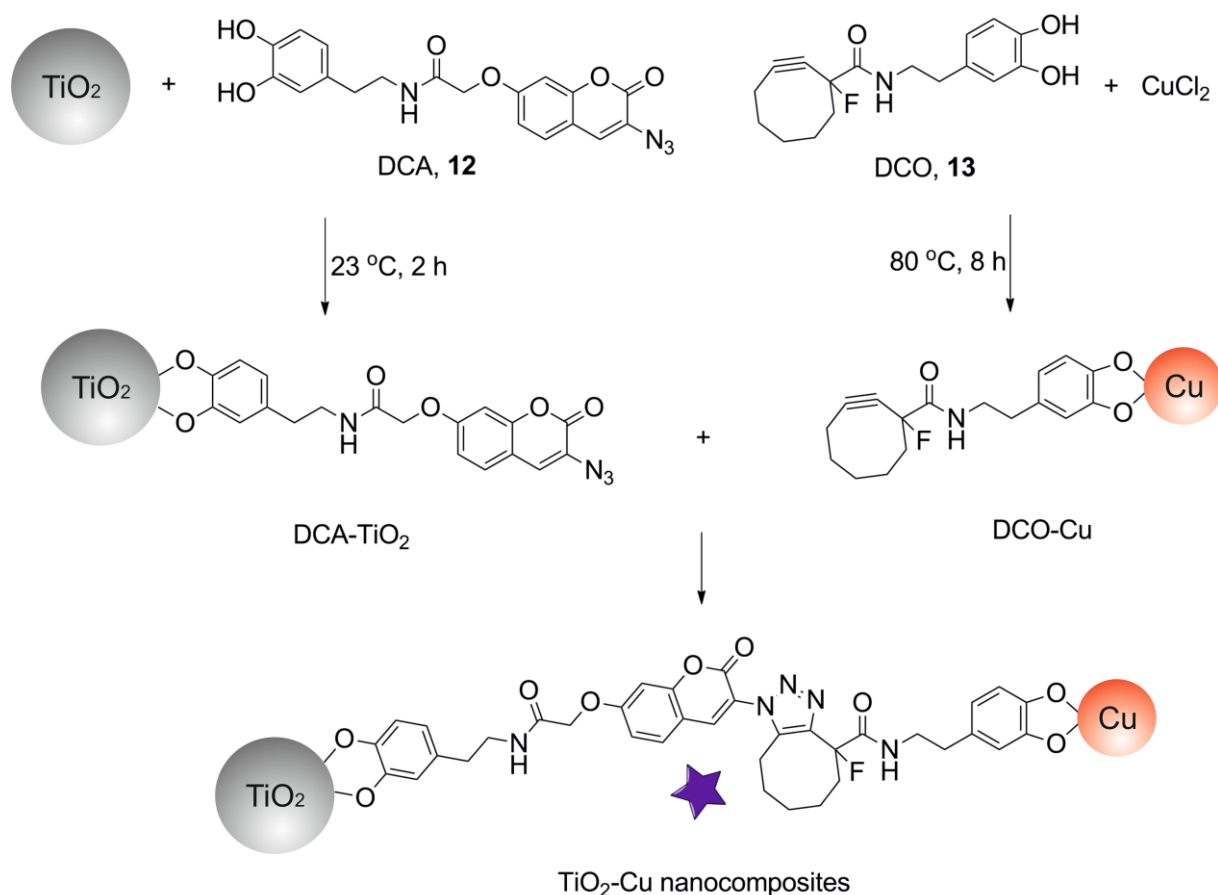
Scheme 4. 7 Prepration of DCA-TiO₂, DCO-Cu, and the following construction of TiO₂-Cu nanocomposites through the click reaction between DCA (**12**) and DCO (**13**)

4.4.2 Modification of TiO₂ Nanomaterials with Dopamine-Coumarin-Azide (DCA)
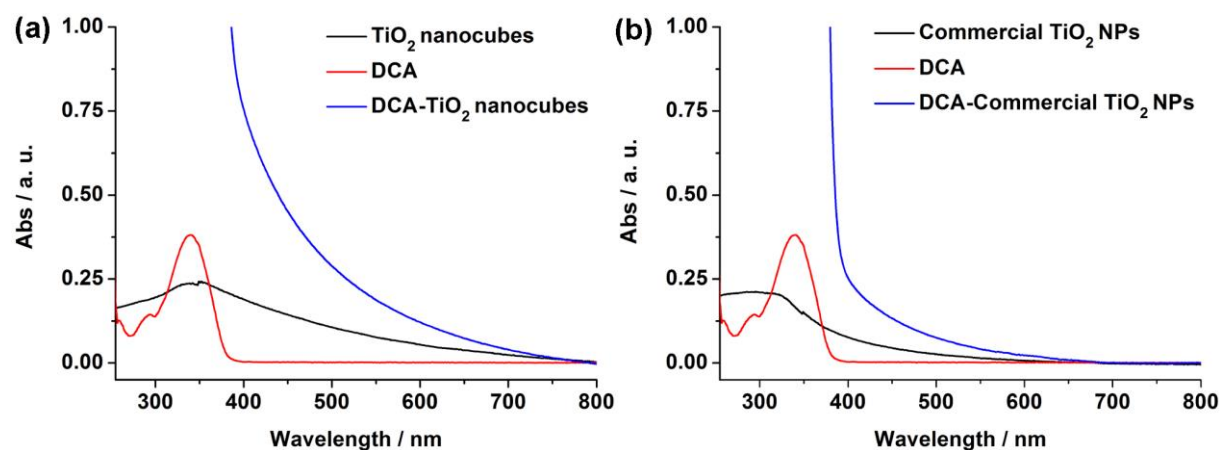
Figure 4. 11 UV-Vis spectra of (a) TiO₂ nanocubes and (c) commercial TiO₂ NPs before and after surface modification with DCA (**12**)

DCA-coated TiO_2 nanomaterials were prepared by incubating TiO_2 nanocubes or commercial TiO_2 NPs with DCA (**12**) in DMSO at room temperature for 2 hours (Scheme 4.7). After incubation the colour of the solution turned yellow indicating the successful surface modification of TiO_2 with DCA (**12**), which was also confirmed by the increased absorption of TiO_2 in the visible light region after the modification (Figure 4.11).

4.4.3 Synthesis of Dopamine-Cyclooctyne (DCO)-Coated Cu NPs
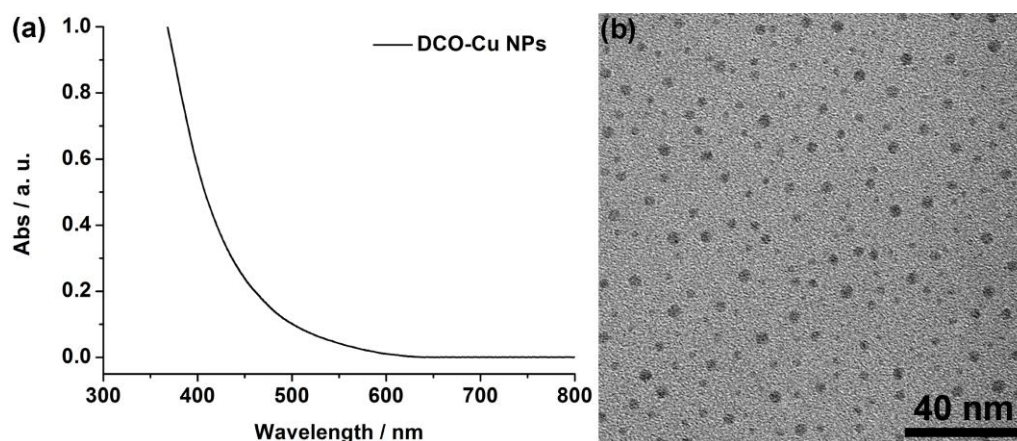
Figure 4. 12 UV-Vis spectrum and TEM image of DCO-coated Cu NPs

DCO-coated Cu NPs were prepared in ethanol using the similar method as that for the preparation of DA-Cu NPs. DCO (**13**) and $CuCl_2$ were mixed in ethanol and refluxed at 80 $^\circ$C for 8 h under vigorous stirring (Scheme 4.7). As shown in Figure 4.12a, no obvious plasmonic absorption of Cu NPs could be observed in the UV-Vis spectrum of DCO-Cu NPs, indicating the existence of small Cu NPs, which was confirm by the TEM characterization (Figure 4.12b), showing that Cu NPs with an average diameter of ~3.8 nm were obtained.

After the successful preparation of DCA-TiO_2 and DCO-Cu NPs, the next step would be the preparation of TiO_2-Cu nanocomposites through the click reaction between the two dopamine linkers on top of the NPs.

4.4.4 Preparation of TiO₂-Cu Nanocomposites

The click reaction between DCO-coated Cu NPs (in ethanol) and DCA-modified TiO_2 nanocubes or commercial anatase TiO_2 NPs (in DMSO) was perfomed at room temperature for 24 h (Scheme 4.7), after which the NPs were collected by centrifugation and washed three times with DMSO.
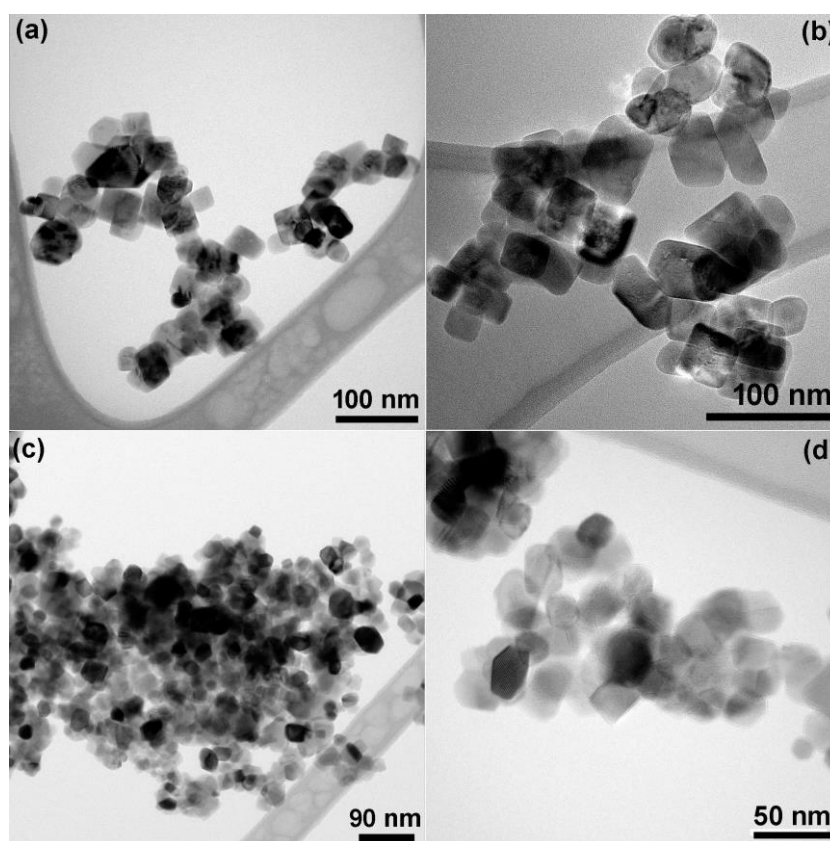
Figure 4. 13 TEM images of (a) TiO$_2$ nanocubes, (b) TiO$_2$ nanocube-CuNP nanocomposites, (c) commercial TiO$_2$ NPs, and (d) commercial TiO$_2$NP-CuNP nanocomposites (The click reaction was performed in the mixture of ethanol and DMSO).

As can be seen from the TEM images of the NPs obtained after the click reaction (Figure 4.13b and d), only TiO$_2$ nanocubes or commercial TiO$_2$ NPs could be observed, but no traces of smaller Cu NPs, indicating that the preparation of TiO$_2$-Cu nanocomposites through the click reaction between the two linkers on the surface of NPs was not successful. This might partially be due to the solvent issues - DCO-Cu NPs were in ethanol and used as prepared for the click reaction with DCA-TiO$_2$, and the existence of ethanol in the solvent system might influence the dispersity of DCA-modified TiO$_2$ nanomaterials as DCA (**12**) was not soluble in ethanol, thus the reaction between DCA-TiO$_2$ and DCO-Cu NPs might be affected.
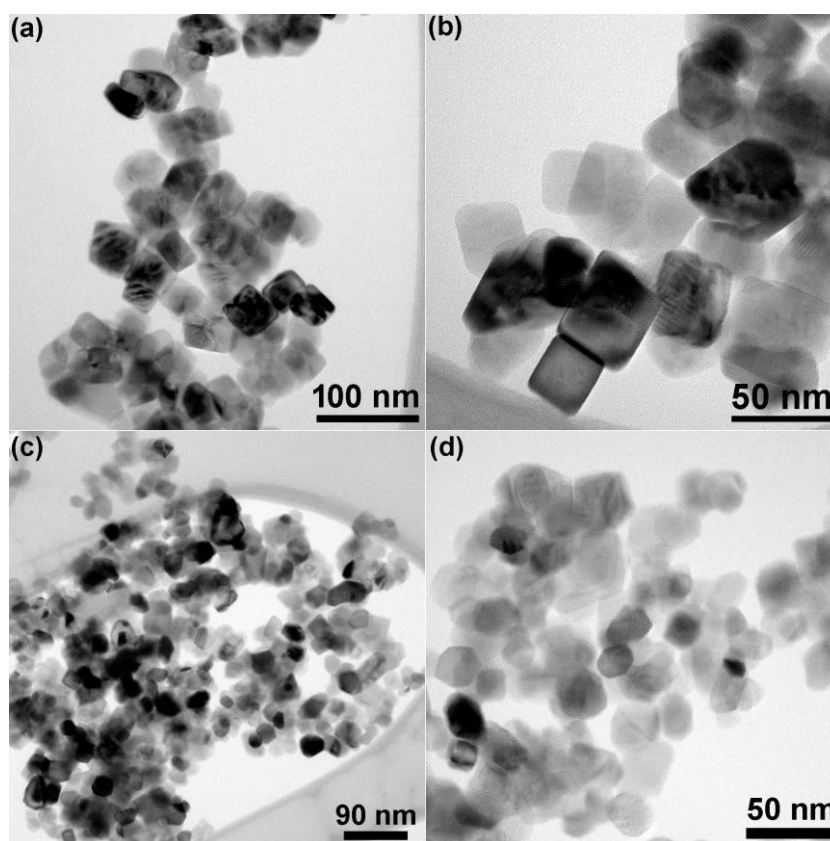
Figure 4. 14 TEM images of (a) TiO$_2$ nanocubes, (b) TiO$_2$ nanocube-CuNP nanocomposites, (c) commercial TiO$_2$ NPs, and (d) commercial TiO$_2$NP-CuNP nanocomposites (The click reaction was performed in DMSO).

Therefore, the click reaction was performed again only in DMSO. The solvent (ethanol) of DCO-coated Cu NPs was evaporated in speed vacuum. The dried DCO-Cu NPs were redispersed in DMSO and then mixed with the DMSO solutions of DCA-modified TiO$_2$ nanomaterials. After incubation the mixture at room temperature for 24 h, the NPs were centrifuged and washed with DMSO before TEM characterization. However, there were again only TiO$_2$ nanocubes or NPs in the TEM images, and no Cu NPs could be observed (Figure 4.14), indicating that TiO$_2$-Cu nanocomposites were not obtained.

Another possible reason for the failure of the click reaction on NPs might lie in the full or partial removal of the cyclooctyne functional group in the case of Cu NPs, as the preparation of DCO-Cu NPs was performed under refluxing at 80 °C, which might affect the stability of DCO (**13**). Therefore, the ethanol solution of DCO was heated at 80 °C for 8 h, and then dried for NMR and MS analysis, which did not show any structural change, proving that the high temperature treatment was not responsible for the failure of the click reaction on NPs.

Obviously, the reaction conditions for the click reaction in the presence of NPs were not the same as the conditions for the reaction in solution, which might be due to some unknown effects from the NPs. Therefore, in order to obtain the TiO$_2$-Cu nanocomposites through the

172

click reaction between the dopamine linkers, the optimization of the reaction conditions still needs to be systematically explored, such as increasing the reaction temperature or adjusting the ratios between DCA-TiO$_2$ and DCO-Cu NPs.

4.5 Conclusions

Small ethylene glycol (EG)-coated TiO$_2$ NPs (~3.4 nm) were synthesized by polyol method. The EG-coated TiO$_2$ NPs was then modified with dopamine-based biofuctional linkers, dopamine-maleimide (DoMal) and dopamine-TEG-malemide (Do-TEG-Mal), as the catechol groups have strong affinity to TiO$_2$, and the maleimide functional groups were employed for the further attachment of furan-modified DNA strands through Diels-Alder cycloaddition.

However, the peroxidase activity assays showed that the photo-induced ROS production ability of EG-coated TiO$_2$ NPs was very weak in comparison to the commercial TiO$_2$ NPs and TiO$_2$ nanocubes. Therefore, commercial TiO$_2$ NPs and TiO$_2$ nanocubes were chosen for the following preparation of TiO$_2$-Cu nanocomposites, as the incorporation of Cu to TiO$_2$ nanomaterials might be able to reduce the band gap of TiO$_2$ nanomaterials and inhibit the recombination of photo-genetated electrons and holes by TiO$_2$. In addition, Cu NPs also possess ROS generation ability, thus the construction of TiO$_2$-Cu nanocomposites might also influence the photocatalytic activity of TiO$_2$ NPs.

To achieve that, two dopamine-based linkers, dopamine-coumarin-azide (DCA) and dopamine-cyclooctyne (DCO) were designed, as the catechol groups could be utilized for the modification or preparation of TiO$_2$ and Cu NPs, and the azide and cyclooctyne mioeties could undergo click reaction, through which the TiO$_2$ and Cu NPs could be linked to afford the TiO$_2$-Cu nanocomposites. The conditions for the successful click reaction between DCA and DCO in solution have been found, however, the click reaction on the surface of NPs was not successful. Therefore, the optimized conditions for the preparation of TiO$_2$-Cu nanocomposites still need to be systematical investigated.

Chapter 5

Summary and Outlook

176

5 Summary and Outlook

This thesis has demonstrated the reproducible synthesis, modification and funtionalization of metallic (Ag and Cu) and semiconductor (TiO_2) NPs employing different strategies and surface capping agents, and the potential applications of the obtained NPs have been explored, such as their use as SERS substrates, as enzyme mimetics, and as catalysts for the degradation of pollutant dyes and antibiotics.

One of the focuses for this thesis is the surface modification and functionalization of Ag and Cu NPs in aqueous solutions. Due to the ease of oxidation upon air exposure, the reproducible synthesis of stable and monodispersed Ag and Cu NPs under aqueous conditions is still of great importance. One of the crucial factors to achieve this is the choice of proper capping agents for the protection and stabilization of NPs' surface, as bare Ag and Cu NPs can be oxidized and tend to aggregate to reduce their surface energy, which could severely influence their chemical, optical and catalytic properties.

Firstly, water-soluble, monodispersed and stable Ag NPs were successfully synthesized using polyacrylic acid (PAA) or benzotriazole-based linkers such as benzotriazole maleimide (BTM) as capping agents, and the plasmonic and fluorescent properties of the obtained Ag NPs were investigated. In addition, the Ag NPs were used for the construction of DNA-AgNP conjugates through ligand exchange or Diels-Alder cycloaddition, which was then employed for the further assembly with Au NPs or the design of enzyme-AgNP hybrids through DNA-directed immobilization. Such kind of simple, mild and efficient methodologies for the functionalization of NPs might be extended to the design and fabrication of other nanocomposites or hybrid systems with novel physical, chemical and biological characteristics, which might be useful for sensing, biocatalysis and imaging.

Secondly, stable Cu NPs were prepared in aqueous solutions using ascorbic acid (AA) and dopamine-based linkers as capping agents. Interestingly, the as-prepared Cu NPs possess excellent ROS production ability, which could be employed for the activation of peroxidase enzymes or the catalytic degradation of harmful fluorescent dyes and antibiotics. During the investigation of the ROS generation mechanism, it was found that AA- and dopamine linkers-coated Cu NPs could behave like superoxide dismutase (SOD), and catalyze the dismutation of superoxide to H_2O_2. The SOD assays showed that the activity of Cu NPs outperformed the natural SOD for about twice fold, and the Cu NPs were more tolerant to the chlating agent EDTA than SOD was. Such kind of CuNP enzyme mimetics might be useful for catalysis, bioassays, as well as the design of surface coatings for environmental applications.

In addition, the SERS property of DA-coated Cu NPs was investigated using different SERS active dyes and different aggregation agents. It was found that pH adjusting was more effective than the addition of salts for the aggregation of Cu NPs. However, no SERS signals of the dyes but only the signals of DA-Cu NPs themselves could be observed, which might be because the strong interaction between DA and Cu NPs prevented the interaction between SERS active dyes and Cu NPs. Therefore, optimization of the SERS conditions still needs to be explored for Cu NPs, as they might be an potential alternative for applications in sensing, where Au and Ag NPs can be used.

At last, small ethylene glycol (EG)-coated TiO_2 NPs were synthesized using a polyol method and successfully functionalized with DNA through bifunctional dopamine linkers. However, the peroxidase activity assays showed that the photo-induced ROS generation ability of EG-TiO_2 NPs was weaker in comparison to TiO_2 nanocubes and commercial TiO_2 NPs. Therefore, TiO_2 nanocubes and commercial TiO_2 NPs were chosen for the preparation of TiO_2-Cu nanocomposites, as the incorporation of Cu to TiO_2 nanomaterials might be able to reduce the band gap of TiO_2 nanomaterials and inhibit the recombination of photo-genetated electrons and holes by TiO_2. However, the preparation of TiO_2-Cu nanocomposites through two clickable dopamine linkers (dopamine-coumarin-azide and dopamine-cyclooctyne) was not successful, which still needs to be systematically investigated by the other collegues in our group, as the combination of TiO_2 and Cu might afford novel, highly active and efficient nanomaterials that are useful for catalysis, enzyme mimetics and environmental applications.

Chapter 6

Experimental Part

6 Experimental Part

6.1 Chemicals and Materials

6.1.1 Chemicals

All the chemicals, except 5-amino-benzotriazole (Alfa Aesar), were purchased for Sigma-Aldrich or Carl Roth and used directly without further purification. Milli-Q water was used throughout the experiments. DNA marker (O'Range Ruler™ 10 bp DNA ladder, ready to use) was purchased from Thermo Scientific. Protein markers (Precision Plus Protein™ Unstained Standards) and Silver Stain Plus Kit were purchased from Bio-Rad. Superoxide detection reagent (Orange) was purchased from Enzo Life Science.

6.1.2 DNA Oligonucleotides

Table 6. 1 DNA oligonucleotides used in this dissertation (purchased from Sigma-Aldrich)

DNAs	Sequences (5' ⟶ 3')	Modification
DNA 1	GGCGTATAACAA	5'-SH-C6 or 5'-NH$_2$-C6
cDNA 1	TTTTTTTGTTATACGCC	5'-NH$_2$-C6
DNA 2	TTTTTTTTTGCTCTCAAGTGCGCAGCATCGA	5'-SH-C6
cDNA 2	GCACTTGAGAGCTTTTTTTTTTTT	5'-SH-C3
DNA 3	GTGGAAAGTGGCAATCGTGAAG	5'-NH$_2$-C6
cDNA 3	CTTCACGATTGCCACTTTCCAC	5'-SH-C6 or none

6.1.3 Proteins

Table 6. 2 Proteins used in this dissertation (purchased from Sigma-Aldrich)

Proteins	Type	Molecular Weight
Myoglobin	From equine skeletal muscle	~17 kDa
Horseradish Peroxidase	Type VI-A, 250-330 units/mg	~44 kDa
Xanthine Oxidase	From bovine milk, $\geq$ 0.4 units/mg	~270 kDa
Catalase	From bovine liver, 2000-5000 units/mg	~250 kDa (tetramer)
Superoxide Dismutase	From bovine erythrocytes, $\geq$ 3000 units/mg	~32.5 kDa

6.1.4 Buffers

Table 6. 3 Buffers and the corresponding recipes

Buffers	Compositions
TBE (5×)	450 mM Tris, 450 mM boric acid, 10 mM EDTA, pH = 8 ~ 8.3
Anion exchange buffer A	20 mM Tris, pH = 8.3
Anion exchange buffer A	20 mM Tris, 1 M NaCl, pH = 8.3
HPLC elution buffer	0.1 M NH$_4$OAc
Phosphate buffer (0.1 M)	A: 1 M NaH$_2$PO$_4$, B: 1 M Na$_2$HPO$_4$, the mixure of 88 mL A and 12.0 mL B was diluted to 1 L with H$_2$O, pH = 6
PBS buffer (10×)	137 mM NaCl, 2.7 mM KCl, 10 mM Na$_2$HPO$_4$·7H$_2$O, 2 mM KH$_2$PO$_4$, pH = 7.4
Loading buffer (6×) for DNA and Protein	10 mM Tris, 60 mM EDTA, 0.03% bromophenol blue, 0.03% xylene cyanol, 60% glycerin, pH 7.6
NP-loading buffer (6×)	10mM Tris, 60 mM EDTA, 60% glycerine, pH = 7.6
MOPS	20 mM 4-Morpholinepropanesulfonic acid, pH = 7.5
MALDI Matrix	5 mg 3-hydroxypicolinic Acid, 100 μL H$_2$O, 100 μL acetonitrile, 12.5 μL ammonium citrate

6.2 Instruments and Methods

6.2.1 UV-Vis and Fluorescence Spectroscopy

Quartz-cuvettes were used for UV-Vis absorption and fluorescence spectra measurement. UV-Vis absorption spectra were recorded on a Cary 300 spectrophotometer (Varian) in the wavelength region 200 ~ 800 nm, and the background of the solvents, which were used for dissolving the substances, were recorded and subtracted before the measurements of corresponding samples. Fluorescence spectra were recorded on a CARY Eclipse fluorescence spectrophotometer (Varian).

6.2.2 Nuclear Magnetic Resonance (NMR)

The NMR spectra were recorded on the following instruments.
^{1}H-NMR 250 MHz: Bruker AC 250

All of the NMR spectra were recorded at room temperature using tetramethylsilane (TMS) as internal standard. The spectra were calibrated using the residual solvent signal as internal standard. The chemical shift δ is expressed in "ppm", and the coupling constant J is in "Hz". Splitting patterns in the NMR spectra are identified as: s, singlet; d, doublet; t, triplet; q, quartet; m, multiplet; br s, broad singlet; and dd, doublet of doublets.

6.2.3 Mass Spectrometry (MS)

The mass of the compounds were measured by fast atom bombardment mass spectrometry (FAB-MS). FAB mass spectra were recorded on a Finnigan MAT 95 mass spectrometer. Generally, positive FAB produces protonated molecular ions $[M+H]^+$. Fragments can be identified according to their mass-to-charge ratios (m/z), and the intensity of the signals represents the relative abundance of the ions. The most intense signal is the base peak, which is assigned an abundance of 100.

6.2.4 Matrix-Assisted Laser Desorption Ionization - Time of Flight Mass Spectrometry (MALDI-TOF)

MALDI-TOF measurements were performed on an Autoflex III MALDI-TOF mass spectrometer equipped with 200 Hz Smartbeam II laser beam (Bruker Daltonik). The DNA oligonucleotides samples were prepared by co-crystallization of the corresponding matrix, 3-hydroxypicolinic acid, on a Bruker ground-steel sample target with 384 spots.

6.2.5 Infrared Spectroscopy (IR)

IR spectra were recorded by the DRIFT mode using a Bruker IFS-88 Fourier transform infrared spectrometer. Solid samples were analyzed using potassium bromide (KBr) as matrix. The absorption bands of functional groups in IR spectra are expressed in wavenumbers (cm^{-1}).

6.2.6 High-Performance Liquid Chromatography (HPLC)

DNA purifications were performed on an Agilent 1200 series HPLC system.

Degasser: G1311A

Autosampler: G1329A ALS,

Thermostated column compartment TCC,

Pump: quaternary Pump G1311A

Fluorescence Detector: FLD G1321A

Diode-array detector: DAD G4212A/B,

Fraction collector: Analyt. FC G1364C

Column: RP C18, 250×4.0 mm, Hypersil ODS 5μm

Running Buffers: A: 0.1M ammonium acetate; B: acetonitrile

Flow rate: 1 mL/min

Table 6. 4 Stand Gradient for the Purification of DNA Oligonucleotides by HPLC

t/min	0	10	15	20	15	32	40	45
B%	0	5	10	15	30	80	100	0

6.2.7 Fast Protein liquid chromatography (FPLC)

Protein purifications were performed on a *GE Healthcare* Äkta Explorer 900 FPLC System. Prepacked chromatography column for ÄKTA™ systems was used.

Pumpe: P-900

Detectors: Monitor UV-900 and Monitor pH/C-900

Fraction collector: Frac-950

Anion exchange column: MonoQ 5/50 GL

Running buffer: A: 20 mM Tris, pH = 8.3; B: 20 mM Tris, 1 M NaCl, pH = 8.3

Flow rate: 1 mL/min

6.2.8 Transmission Electron Microscopy (TEM) and Selected Area Electron Diffraction (SAED)

TEM images and SAED patterns were taken on a Philips CM200FEG/ST electron microscopy and operated at an acceleration voltage of 200 kV.

6.2.9 Zeta potential

The surface charge of nanoparticles was determined by Zeta potential measurements on a Malvern Zetasizer Nano range instrument.

6.2.10 Microtiterplate Reader

The peroxidase activity tests and the degradation of fluorescent dyes and antibiotics were performed on a Synergy^{TM} H1 hybrid multi-mode microplate reader (BioTek) using a 96-well microtiterplate.

6.2.11 Centrifugation

The centrifugation of nanoparticles and buffer exchange with viva spins were performed on Centrifuge 5415 R and 5804 R.

6.2.12 Polyacrylamide Gel Electrophoresis (PAGE)

Native PAGE was used for the separation of DNA or proteins according to their size. 10 mL gel solution was prepared following the recipes below (Table 6.5). After polymerization of the gel solution, the glass plates were put into an electrophoresis system (Bio-Rad). Then 1 μl of loading buffer (6×) was added to 5 μL of DNA or protein samples and loaded into the wells. Gels were run in 1× TBE buffer at 100 V.

Table 6. 5 Recipes for PAGE

Gel components	Gel Percentage	
	21%	12%
5×TBE	2 mL	2 mL
30% acrylamide and bis-acrylamide solution, 37.5:1	7 mL	4 mL
H_2O	1 mL	4 mL
Ammonium Persulfate (APS, 10%)	100 μL	100 μL
Tetramethylethylenediamine (TEMED)	4 μL	4 μL

6.2.13 Agarose Gel Electrophoresis

Agarose gel was prepared by dissolving certain amount of agarose in 0.5× TBE buffer in a microwave oven. After cooling down the solution slightly, the solution was casted in an electrophoresis system. After the formation of polymerized gel, 0.5× TBE buffer was added to the chamber. Then 3 μl of loading buffer (6×) was added to 15 μL samples and loaded into the wells. Gels were run in at 100 V.

6.2.14 Gel Staining and Imaging

When the gel running was completed, the gel was carefully transferred into a staining chamber. The staining solution for *ss*DNA or *ds*DNA was prepared by dissolving 3 µL SYBR gold or ethidium bromide in 30 mL 1× TBE buffer. Bio-Rad Silver staining kit was used for protein staining.The images of the stained gels were taken under UV-irradiation by using a Bio-Rad Gel Doc^{TM} XR imaging system.

6.2.15 Electron Paramagnetic Resonance (EPR)

EPR spectra of the nanoparticles were measured in Prof. Angelika Brueckner's group in the University of Rostock. EPR spectra were recorded on a Bruker EMX CW-microspectrometer at 100 K using liquid nitrogen stream. g values were calculated using the equation $h\nu = g\beta B_0$ with B_0 and ν being the resonance field and frequency (9.433 Hz), respectively.

6.2.16 Surface Enhanced Raman Spectroscopy (SERS)

SERS property of DA-Cu NPs was investigated in Prof. Duncan Graham's group in the University of Strathclyde. Typically in a disposable cuvette or a microtiterplate, 100 µL of DA-Cu NPs were mixed with 10 µL of different aggregation agents, such as NaCl (2 M), KNO_3 (2 M), $MgSO_4$ (2 M), citric acid (2 M), or sodium bicarbonate (1 M), and different SERS active molecules (Eosin, 1,2-Bis(4-pyridyl)ethylene, and benzotriazole dyes) with different concentrations (10^{-6} or 10^{-7} M). SERS property of Cu NPs under the excitation of a 532 nm laser was studied on an Avalon spectrometer equipped with a 532 nm laser and Raman station R3. Raman spectra were recorded between 250 and 2000 cm^{-1} Raman shift at a resolution of 2 cm^{-1}. SERS property of Cu NPs under the excitation of a 633 nm laser was measured on a Renishaw InVia Raman microscope equipped with a 633 nm laser. Raman spectra were recorded between 800 and 1800 cm^{-} Raman shift for 10 or 20 seconds at 1% of the laser power corresponding to 35 µW for the 633 nm laser.

6.3 Synthesis of Linkers

6.3.1 Synthesis of Benzotriazole-Maleimide (BTM, 4)

3-(1H-Benzotriazol-5-ylcarbamoyl)acrylic acid (**2**)
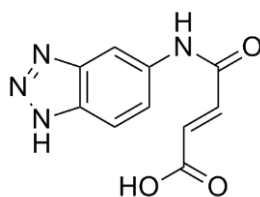
(**2**)

10 mmol 5-amino-benzotriazole (5-amino-BT, **1**) was partially dissolved in 50 mL dichloromethane (DCM). Maleic acid anhydride (20 mmol) was dissolved in 10 mL DCM and added to the above solution portionwise over half an hour. The reaction mixture was stirred at room temperature overnight. The grey precipitate was collected by filtration, washed with DCM and dried to give the title compound **2** (BT-maleamic acid) in 88% yield. ^{1}H NMR (DMSO-d$_6$, 250 MHz) δ: 6.34 (1H, d, J = 12.5, CHCHCO$_2$H), 6.53 (1H, d, J = 12.5, CHCHCO$_2$H), 7.41 (1H, br s, H-7), 7.92 (1H, br s, H-4), 8.36 (1H, br s, H-6), 10.6 (1H, s, CO$_2$$H$); m/z (FAB) for C$_{10}H_8N_4O_3$ [M+H]$^+$: 233.2.

1-(1H-Benzotriazol-5-yl)pyrrole-2,5-dione (BTM, 4)

(**4**)

Anhydrous sodium acetate (7.5 mmol) was dissolved in 125 mL acetic anhydride and compound **2** (6.3 mmol) was added. The mixture was refluxed and stirred at 90 ℃ for 4 h. After removing the acetic anhydride by rotary evaporator, the residue was dissolved in 10 mL trifluoroacetic acid (TFA) and the mixture was stirred at RT overnight. After the removal of TFA in rotary evaporator, cold H$_2$O was added and the precipitate was collected by filtration, washed with ethanol and dried. The product was purified by column chromatography eluting with EtOAc in hexane (10–70%) to give the title compound **4** as a yellow powder in 50.7% yield. R$_f$ (DCM-MeOH 9:1) 0.18; ^{1}H NMR (DMSO-d$_6$, 250 MHz) δ: 7.23 (2H, s, CH=CH), 7.40 (1H, d, J = 7.5, H-7), 7.89 (1H, s, H-4), 8.01 (1H, d, J = 7.5, H-6); m/z (FAB) for C$_{10}$H$_6$N$_4$O$_2$ [M+H]$^+$: 215.1.

6.3.2 N-Furan-2-ylmethyl succinamic acid (5)

(5)

Succinic anhydride (17 mmol) was dissolved in DCM (10 mL) and added to furfurylamine (1.0 mL, 10 mmol) dropwise and the reaction mixture was stirred for 3 h at RT. The title compound **5** was collected by filtration, washed with DCM and dried. R_f (DCM-MeOH 9:1) 0.12; ^{1}H NMR (DMSO-d_6, 250 MHz) δ: 2.34 (2H, t, J = 5.0, COCH_2), 2.43 (2H, t, J = 5.0, CH_2CO$_2$H), 4.22 (2H, d, J = 5.0, CH_2NH), 6.21 (1H, s, Fur-H), 6.36 (1H, s, Fur-H), 7.55 (1H, s, Fur-H), 8.29 (1H, s, CO$_2$$H$), 12.07 (1H, br s, N$H$CO); m/z (FAB) for $C_9NO_4H_{11}$ [M+H]$^+$: 198.1.
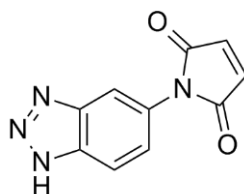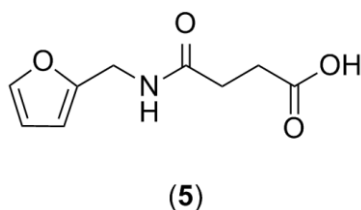
6.4 Synthesis and Functionalization of Ag NPs

6.4.1 Synthesis of Oleylamine (OA)-Coated Ag NPs

OA-Coated Ag NPs were synthesized using a thermal decomposition method with slight modification.[343] 50 mL toluene was added in a 100 mL flask and heated to 110 ^{o}C under Ar protection. 0.5 mmol AgNO$_3$ in 2 mL OA were injected to the flask under vigorous stirring. The reaction was kept at 110 ^{o}C for 6 h before it was cooled down to room temperature. During this procedure, the color of the solution changed from colorless to light yellow, light brown and finally to dark brown. 40 mL ethanol was added into the solution to precipitate the Ag NPs. The suspension was centrifuged at 5000 rpm for 5 min and the supernatant was discarded. The precipitate was washed three times with ethanol and redispersed in cyclohexane to give a brownish yellow dispersion.

Phase transfer of the Ag NPs from cyclohexane to H$_2$O was realized by ligand exchange. 1 mL 3-mercaptopropionic acid was mixed with 1 mL cyclohexane and added to 5 mL cyclohexane suspension of Ag NPs. The solution was sonicated for 30 min. The precipitation was collected by centrifugation, washed with cyclohexane and ethanol, and finally resuspended in H$_2$O.

6.4.2 Synthesis of Polyacrylic Acid (PAA)-Coated Ag NPs

In a typical synthesis, 0.45 mmol PAA was dissolved in 15 mL ethylene glycol (EG) and heated to 185 °C in an oil bath under Ar protection.[147] 0.1 g AgNO$_3$ was dissolved in 3 mL EG at room temperature and quickly injected into the above boiling solution under vigorous stirring. Aliquots were extracted using a syringe after 15 and 30 min. After cooling down to room temperature, the NPs were collected by precipitation with excessive acetone and centrifugation at 5000 rpm for 15 min. The precipitate was washed with acetone three times, and finally redispersed in distilled water by neutralizing the carboxylic acid groups on the NPs' surface with 0.5 M NaOH solution.

6.4.3 Synthesis of Benzotriazole (BT) Derivatives-Coated Ag NPs

BT derivatives (5-amino-BT (**1**) and BTM (**4**)) were used as capping agents to synthesize Ag NPs through a simple one-pot route. Typically, 0.2 mmol BT derivatives and 0.002 mmol AgNO$_3$ were dissolved in the mixture of 12 mL H$_2$O and 8 mL MeCN (V$_{H2O}$: V$_{MeCN}$ = 3: 2). The solution was stirred in ice-bath for 1 h to achieve a chelating balance, after which 2 mL freshly prepared NaBH$_4$ solution (5 mM) was added drop wise. The reaction was stirred in ice-bath for 1 h.

Different molar ratios between BTM and AgNO$_3$ (10:1, 30:1, 50:1, 80:1 and 100:1) were also tried to synthesize BTM-coated Ag NPs using the same procedures.

6.4.4 NMR and MS Analysis of BTM after Heating at 60 °C

BTM was analyzed by NMR and MS after heating at 60 °C overnight. ^{1}H NMR (DMSO-d$_6$, 250 MHz) δ: 6.34 (0.14 H d, J = 12.5, C*H*CHCO$_2$H), 6.52 (0.07 H d, J = 12.5, CHC*H*CO$_2$H), 7.21 (2H, s, C*H*=C*H*), 7.41 (1H, d, J = 10.0, H-7), 7.89 (1H, s, H-4), 8.01 (1H, d, J = 5.0, H-6), 8.34 (0.07 H, br s, H-6), 10.6 (0.07 H, s, CO2*H*). m/z (FAB) for C$_{10}$H$_6$N$_4$O$_2$ [M+H]$^+$ 215.25 and C$_{10}$H$_8$N$_4$O$_3$ [M+H]$^+$ 233.17. The comparison of the NMR and MS results with compounds **2** and **4** in Part 6.3.1 showed that there was no significant change of the molecular structure of BTM (**4**) occurred, apart from the presence of traces of compound **2.**

6.4.5 FTIR Analysis of BTM and BT before and after Heating at 60 °C

The FTIR spectra of BTM (**4**) and 5-amino-BT (**1**) were recorded before and after heating at 60 °C overnight (Figure 6.1).

(a)

(b)

(c)
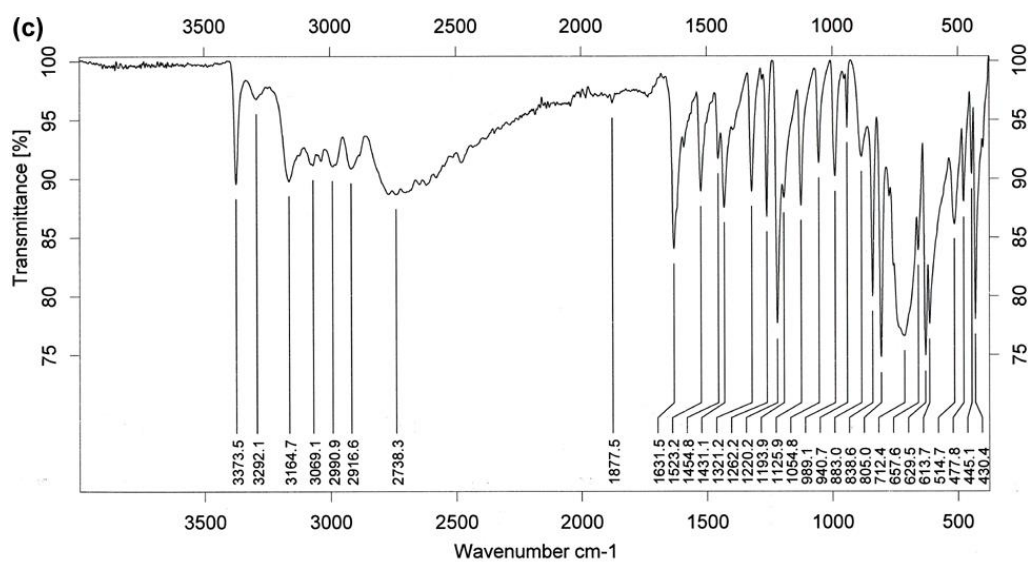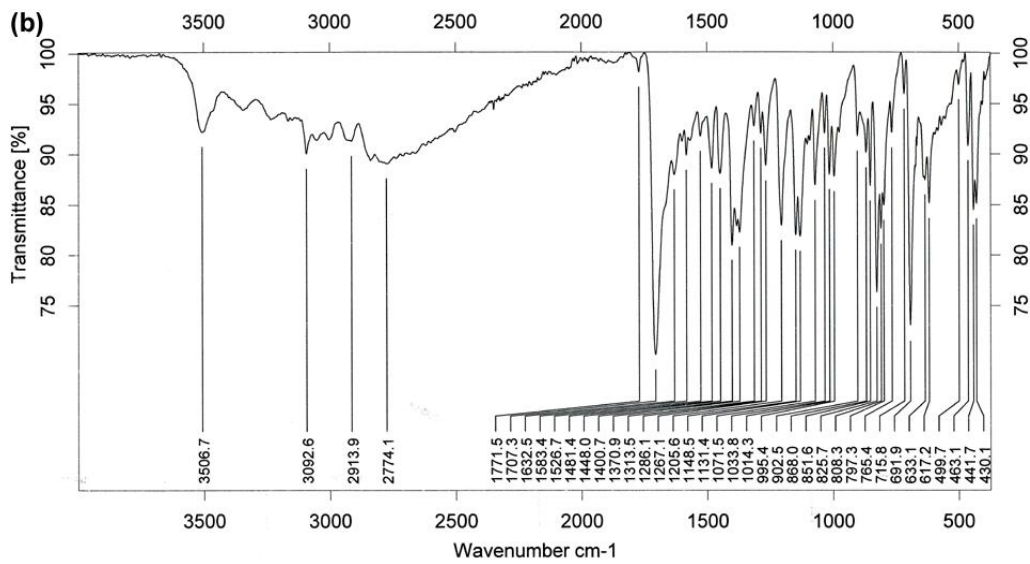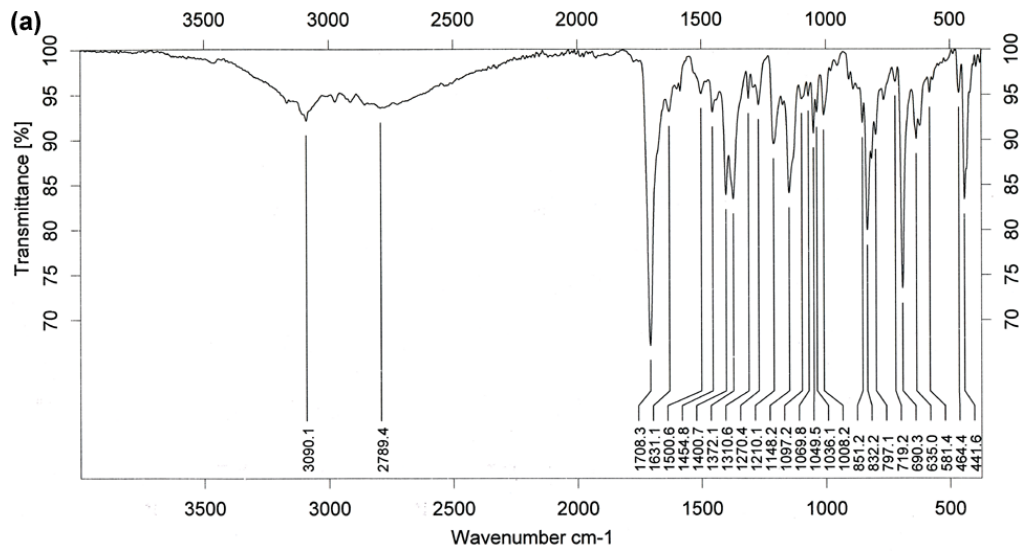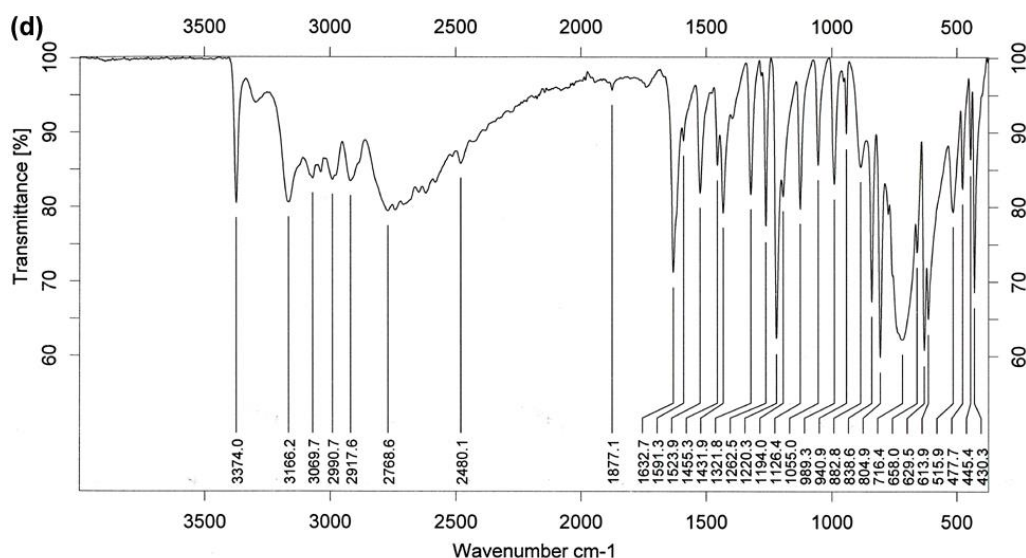
Figure 6. 1 FTIR spectra of (a) BTM 23 ºC, (b) BTM 60 ºC, (c) 5-amino-BT 23 ºC and (d) 5-amino-BT 60 ºC

6.4.6 Preparation of BTM-Modified DNA
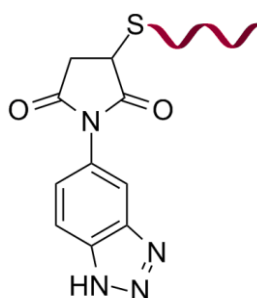
BTM-DNA

BTM-DNA1

100 μL aqueous solution of 12-base thiol-modified DNA1 (SH-DNA1, 100 μM) was first incubated with 60 μL dithiothreitol (DTT, 1M) to cleave the disulfide bond to thiols. After incubation at 37 °C for a certain period 5 h, the solution was purified by NAP-5 and NAP-10 columns (*GE Healthcare*) to remove excessive DTT and impurities. Freshly reduced DNA solution was eluted directly to 10 μL acetonitrile (MeCN) solution of BTM (10 mM) and incubated at 23 °C overnight. The obtained products were purified by HPLC using linear gradient of buffer B over 45 min (buffer A: ammonium acetate, buffer B: acetonitrile). The masses of the collected fractions were measured by MALDI-TOF.

BTM-DNA2

191

BTM-modified DNA2 was synthesized by using similar procedures for BTM-DNA1, except that 100 μL aqueous solution of 31-base thiol-modified DNA2 (SH-DNA2, 100 μM) was used. The products were purified by HPLC and the masses of the collected fractions were measured by MALDI-TOF.

6.4.7 Biofunctionalization of PAA-Ag NPs with BTM-DNA through Ligand Exchange

BTM-DNA-AgNP
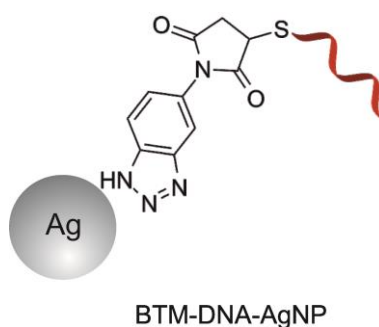
The functionalization of PAA-coated Ag NPs with BTM-modified DNA (1 or 2) was realized by ligand exchange using the conventional salt aging method with slight modification.[17] 100 μL aqueous solution of PAA-Ag NPs (67 nM) was mixed with 3 nmol BTM-modified DNA. After incubation at room temperature for 24 h, PBS buffer was added and its final concentration was 10 mM. The solution was left to equilibrate at room temperature for 24 h. Then NaCl solution (0.02 M) was added twice for another two rounds of equilibration, and the final concentration of NaCl was 0.1 M. At last Ag NPs were collected by centrifugation, washed thoroughly with PBS buffer (1×) to remove the excessive free DNA, redispersed in 100 μL PBS buffer (1×), and analyzed by 1% agarose gel electrophoresis.

6.4.8 Biofunctionalization of Citrate-Au NPs with BTM-DNA1

BTM-DNA-AuNP
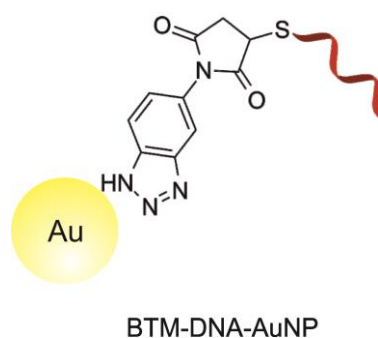
The conjugates of citrate-Au NPs and BTM-DNA1 were prepared by using the similar method as above. 100 μL aqueous solution of citrate-Au NPs (28 nM) was mixed with 2 nmol

BTM-modified DNA1. After salt-assisted equilibration with PBS buffer and NaCl, Au NPs were collected by centrifugation, washed, and redispersed in 100 μL PBS buffer (1×).

6.4.9 Biofunctionalization of PAA-Ag NPs and Citrate-Au NPs with SH-DNA1
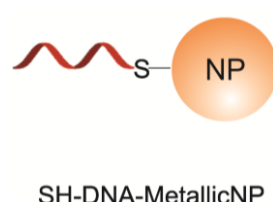
SH-DNA-MetallicNP

100 μL aqueous solution of 12-base thiol-modified DNA1 (SH-DNA1, 100 μM) was first incubated with 60 μL dithiothreitol (DTT, 1M) to cleave the disulfide bond to thiols. After incubation at 37 °C for a certain period 5 h, the solution was purified by NAP-5 and NAP-10 columns to remove excessive DTT and impurities. Freshly reduced DNA was eluted directly to 50 μL aqueous solution of PAA-Ag NPs (67 nM) or 100 μL aqueous solution of citrate-Au NPs (28 nM). After salt-assisted equilibration with PBS buffer and NaCl, Ag NPs were collected by centrifugation, washed, and redispersed in 100 μL PBS buffer (1×).

6.4.10 Stability Tests of BTM-DNA-MetallicNP Conjugates

The stability of BTM-DNA-metallicNP conjugates was tested using DTT displacement reaction. 1 μL DTT (1 mM) was added to certain amount of aqueous solution of BTM-DNA1-AgNP (or BTM-DNA1-AuNP, SH-DNA1-AgNP, SH-DNA1-AuNP) conjugates, and the molar ratio between DTT and DNA1 was 10: 1 in all the reactions. Both solutions were incubated at 23 °C for 20 h, and the UV-Vis spectroscopy was used to monitor the absorption change of the Ag and Au NPs.

6.4.11 Hybridization of BTM-DNA-AgNP with *c*DNA

*ds*DNA-AgNP
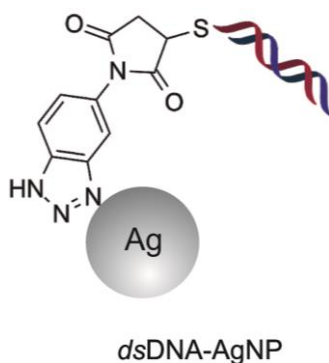
20 μL PBS solution of BTM-DNA1-AgNP conjugates was incubated with its complementary DNA (cDNA1, 1 nmol) at room temperature for 2 h. The NPs were then centrifuged, washed three times with PBS buffer ($1\times$) to remove the complementary strands which were not hybridized, and finally redispersed in PBS buffer ($1\times$). However, the agarose gel electrophoresis (1%) showed that the hybridization was not successful. To promote the hybridization, the mixture of BTM-DNA1-AgNP and cDNA1 was first incubated at 80 °C for 30 min to eliminate the secondary structure of the DNA strands, and then slowly cooled down (5 °C/min) to 23 °C and incubated for 2 h. The similar hybridization procedures were attempted also in the presence of Mg^{2+} (50 mM). However, the hybridization was still unsuccessful.

On the contrary, the successful hybridization of longer stranded DNA2 with cDNA2 was realized in such a way that 20 μL PBS solution of BTM-DNA2-AgNP conjugates was mixed with cDNA2 (1 nmol). The mixture was first incubated at 80 °C for 30 min to eliminate the secondary structure of the DNA strands. Then it was cooled down slowly (5 °C/min) to 37 °C and incubated at 37 °C for 2 h, after which the solution was cooled down to room temperature. The NPs were then collected by centrifugation, washed three times with PBS buffer ($1\times$) to remove the unhybridized complementary strands, redispersed in PBS buffer ($1\times$), and analyzed by 1% agarose gel electrophoresis.

6.4.12 Assembly of Au and Ag NPs through DNA Hybridization

Ag-dsDNA-Au
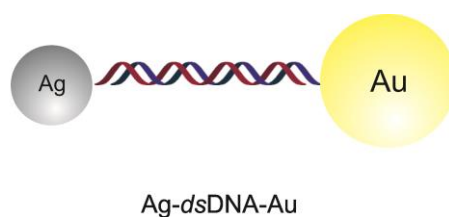
10 μL PBS solution of BTM-DNA2-modified Ag NPs (c_{AgNP} = 32 nM) were mixed with 16.8 μL TETBS solution of SH-cDNA2-modified Au NPs (c_{AgNP} = 19 nM). The molar ratio between Ag and Au NPs were 1: 1. The mixture was first incubated at 80 °C for 30 min, and then cooled down slowly (5 °C/min) to 37 °C and incubated at 37 °C for 5 h, after which the solution was cooled down to room temperature and characterized by UV-Vis spectroscopy, agarose gel electrophoresis (1%) and TEM.

6.4.13 Preparation of Furan-Modified DNA1
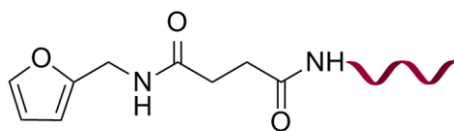
Furan-DNA1

Method 1: Amide coupling between N-furan-2-ylmethyl succinamic acid (**5**) and NH$_2$-DNA1 on solid support

N-furan-2-ylmethyl succinamic acid (compound **5,** 0.12 mmol) was activated with 1,1'-carbonyl diimidazole (CDI, 0.22 mmol) in anhydrous dimethylformamide (DMF, 1 mL) at 45 ^{o}C for 5 min. The activated compound **5** was added to the controlled pore glass (CPG) solid support carrying 314 nmol amino-modified 12-base DNA1 (NH$_2$-DNA1) and incubated at 23 ^{o}C for 2 h, after which the solid support was centrifuged, and washed with 100 μL DMF, 100 μL MeCN and dried with nitrogen. The oligonucleotide was then deprotected from the solid support using t-butylamine. Solid support carrying modified DNA1 was placed in an Eppendorf tube, the deprotection solution (100 μL t-butylamine, 100 μL H$_2$O and 200 μL methanol) was added and the mixture was heated at 65°C for 3 h. Finally, the solution containing the deprotected oligonucleotide was recovered by centrifugation and filtered to remove the left solid. After removing the solvent in *vacuo*, the oligonucleotide was redissolved in distilled water and purified by HPLC. However, no mass of the expected product (furan-DNA1) was detected by MALDI-TOF.

To improve the reaction, another set of coupling reagents Hydroxybenzotriazole (HOBT), o-benzotriazole-N,N,N',N'-tetramethyl-uronium-hexafluoro-phosphate (HBTU), and N,N-diisopropylethylamine (DIPEA) were used. 33 μmol N-furan-2-ylmethyl succinamic acid (**5**) was dissolved in 150 μL DMF and 150 μL MeCN, and activated by 33 μmol HOBT, 33 μmol HBTU, and 10 μL DIPEA at 23 ^{o}C for 2 min. The activated compound **5** was added to the solid support carrying 314 nmol NH$_2$-DNA1 and incubated at 23 ^{o}C for 2 h. The rest procedures were the same as above.

Method 2: Amide coupling between N-furan-2-ylmethyl succinamic acid (**5**) and NH$_2$-DNA1 in solution using CDI as a coupling reagent

0.06 mmol N-Furan-2-ylmethyl succinamic acid was activated with 0.12 mmol CDI in anhydrous DMF (0.4 mL) at 45 ^{o}C for 5 min. Then 100 μL aqueous solution of NH$_2$-DNA1 (100 μM) was added. The solution was mixed thoroughly and incubated at 23 ^{o}C for 2 h.

After removing DMF by speed vacuum, the product was redissolved in 100 μL H_2O and purified by HPLC. The mass of the products were measured by MALDI-TOF, which showed that the desired product furan-DNA1 was obtained, but its yield was really low (3.0%). However, when the same reaction was performed again at 37 °C overnight, the yield of furan-DNA1 was increased to 26.2%.

6.4.14 Biofunctionalization of BTM-Ag NPs with Furan-DNA1 through Diels-Alder Cycloaddition
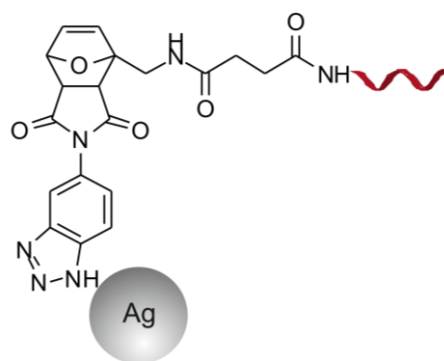
DNA1-AgNP

The Diels-Alder reaction of BTM-coated Ag NPs and furan-modified DNA1 was first attempted at room temperature. 100 μL solution of as-synthesized Ag NPs were centrifuged, washed with the mixture of H_2O and MeCN, and redispersed in 100 μL mixture of H_2O and MeCN (v_{H2O}: v_{MeCN} = 3: 2). 200 μL aqueous solution containing 2 nmol furan-modified DNA1 was added to the BTM-Ag NPs and incubated at 23 °C for 2 h. After the reaction, the NPs were again centrifuged, washed and redispersed in the mixture of H_2O and MeCN for agarose gel electrophoresis (1%) analysis. However, the mobility of the Ag NPs in the agarose gel didn't change, indicating the cycloaddition wasn't successful. Then the reaction was performed again at the similar conditions, except that the reaction temperature was increased to 45 °C, but the results were still the same.

However, it was reported previously that certain salts, such as LiCl and $CuNO_3$, could promote the rate of Diels-Alder cycloaddition in aqueous solutions.[298, 371] Therefore, the same reaction was performed again in the appearance in 0.3 M LiCl. After incubating the mixture at 23 °C for 2 h, the DNA1-functionalized Ag NPs were collected by centrifugation, and the obtained product was analyzed by agarose gel electrophoresis (1%), which showed an obvious mobility shift in comparison to the BTM-coated Ag NPs.

6.4.15 Hybridization of Furan-DNA1-Functionalized Ag NPs with *c*DNA1
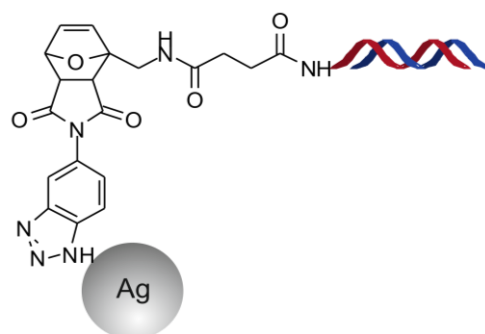
*ds*DNA1-AgNP

The hybridization ability of furan-DNA1-AgNP conjugates was tested by using its complementary strand *c*DNA1. 100 μL aqueous solution of DNA1-AgNP conjugates was incubated with 1 nmol *c*DNA at 23 °C overnight. The product was collected by centrifugation, washed three times with water to remove the unhybridized complementary strands, redispersed in water, and characterized by agarose gel electrophoresis (1%).

6.4.16 Preparation of Mb-*c*DNA1 Conjugates
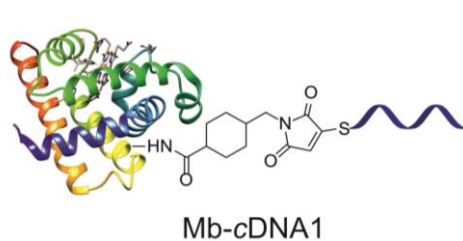
Mb-*c*DNA1

100 μL thiol-modified *c*DNA1 (100 μM) was first reduced with DTT (1 M) at 37 °C for 2 h. 200 μL Myoglobin (Mb) solution (200 μM) was incubated with sulfosuccinimidyl-4-[N-maleimidomethyl]cyclohexane-1-carboxylate (Sulfo-SMCC) crosslinker at 23 °C for 2 h in the dark. Both solutions were purified by NAP-5 and 10 columns, and mixed together immediately and incubated at 23 °C for 3 h. The products were purified by FPLC with buffer A (20 mM Tris) and gradient of buffer B (20 mM Tris + 1 M NaCl) over 40 min. After purification, the fractions were collected, and the buffer was exchanged to PBS (1×) using viva spin. The obtained products were analyzed by UV-Vis spectroscopy and native polyacrylamide gel electrophoresis (12%).

6.4.17 Preparation of Enzyme-AgNP Hybrids through DNA-Directed Immobilization

Mb-AgNP
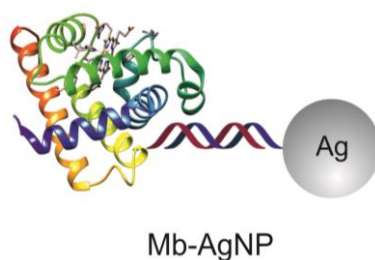
The immobilization of enzyme to the surface of Ag NPs was realized by DNA hybridization. 20 μL aqueous solution of DNA1-AgNP conjugates was mixed with 0.2 nmol Mb-*c*DNA (I) or (II) and incubated at 23 °C for 6 h. The product was collected by centrifugation, and analyzed by agarose gel electrophoresis (1%).

6.4.18 Enzymatic Activity of Mb-AgNP Hybrids

The enzymatic activity of the Mb-AgNP hybrids was tested using nonfluorescent N-acetyl-3,7-dihydroxyphenoxazine (Amplex Red), which could be oxidized into fluorescent resorufin by H_2O_2 in the presence of peroxidase enzymes. Different amounts of the Mb-AgNP hybrids (the Moles of Mb were 0, 7.25, 21.75 and 36.25 pmol) were mixed with 10 μL Amplex Red (1 mM) and 10 μL H_2O_2 (100 μM). The final volume of the mixtures was adjusted to 150 μL with phosphate buffer (0.1 M, pH = 6). The fluorescence of resorufin was recorded on a microplate reader (BioTek) (λ_{ex} = 540 nm and λ_{em} = 585 nm).

6.4.19 Preparation of Polymer-Coated Ag NPs through Diels-Alder Cycloaddition
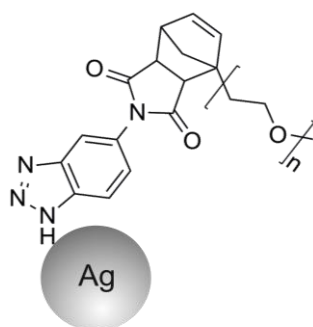
PEG-Ag

Diels-Alder cycloaddition could also be employed for the immobilization of other molecules to the surface of BTM-Ag NPs. Herewith, cyclopenta-1,3-diene-modified polyethylene glycol (CP-PEG, Mw ~2000 g/mol, provided by Prof. Christopher Barner-Kowollik's) (200 μM) was used to react with as-synthesized BTM-coated Ag NPs (200 μL) in

the mixture of H_2O and MeCN (v_{H_2O}: v_{MeCN} = 3: 2). After the addition of 0.3 M LiCl, the solution was incubated at 23 $^\circ$C for 2 h, and the product was analyzed by agarose gel electrophoresis (1%).

6.5 Syntheses and Properties of Copper NPs

6.5.1 Seed-Mediated growth of Cu NPs

Cu NPs were synthesized by a seed mediated growth method with slight modification.[387] 0.02 mmol $CuSO_4$ was dissolved 100 mL H_2O and the solution was purged with Ar for 10 min to remove the dissolved oxygen. 0.1 mmol $NaBH_4$ was dissolved in 1 mL H_2O and kept ice-cold before being added to the $CuSO_4$ solution under vigorous stirring. The Cu seeds were formed immediately, visualized by the appearance of a yellowish brown color.

0.02 mmol $CuSO_4$ was dissolved 100 mL H_2O and the solution was purged with Ar for 15 min, and then 1 mL aqueous solution of the Cu seeds was added. 0.04 mmol L-ascorbic acid was dissolved in 1 mL H_2O and added dropwise to the above mixture. The colour of the solution turned brown after 5 min indicating the formation of Cu NPs.

6.5.2 Polyvinylpyrrolidone (PVP)-Coated Cu NPs

PVP-coated Cu NPs were prepared using a previously reported method with slight modifications.[77] 2 mmol $CuSO_4$ and 6 mmol PVP (Mw ~40,000 g/mol) were dissolved in 20 mL ethylene glycol. The solution was purged with Ar. Then 0.016 mol L-ascorbic acid was added under vigorous stirring, and the colour of the solution turned from blue to brown immediately. The solution was heated to 80 $^\circ$C in an oil bath, and the reaction was stopped after 1 h, and the colour of the solution turned red. After cooling down to room temperature, the solution was diluted by absolute ethanol and centrifuged at 5000 rpm for 15 min to collect the NPs. The precipitation was washed with absolute ethanol three times to remove the excessive surfactant and finally redispersed in absolute ethanol for the following characterization.

6.5.3 Citrate-Coated Cu NPs

0.75 mmol $CuSO_4$ was dissolved in 10 mL H_2O and the solution was purged with Ar for 15 min. Then 10 mL aqueous solution containing 5 mmol trisodium citrate was added and the mixture was stirred at room temperature for 30 min. 1 mL H_2O containing 0.1 mmol $NaBH_4$,

which was kept ice-cold, was injected to the above mixture drop by drop. The colour of the solution turned from blue to dark brown. The obtained NPs were centrifuged and washed with ice-cold water three times to remove excessive citrate. The NPs were finally redispersed in absolute ethanol.

6.5.4 Cetyltrimethylammonium Bromide (CTAB)-Coated Cu NPs

0.75 mmol $CuSO_4$ was dissolved in 10 mL H_2O and the solution was purged with Ar for 15 min. Then 10 mL aqueous solution containing 5 mmol CTAB was added and the mixture was stirred at room temperature for 30 min. 1 mL ice-cold aqueous solution containing 0.1 mmol $NaBH_4$ was injected to the above mixture dropwise. The colour of the solution turned from blue to dark brown immediately, but then turned back to blue within 30 min.

6.5.5 Benzotriazole (BT) Derivatives-Coated Cu NPs

0.015 mmol $CuCl_2 \cdot 2H_2O$ were dissolved in 5 mL H_2O and stirred under Ar protection for 15 min. Then 0.115 mmol 5-amino-BT (or BTM) was dissolved in 1 mL MeCN and injected to the above solution, and the mixture was stirred under Ar protection for 30 min. 0.02 mmol $NaBH_4$ was dissolved in 1 mL H_2O and injected to the above mixture dropwise. The solution was stirred at room temperature overnight and the colour changed from greenish brown to black. The products were collected by centrifugation, washed with methanol and finally redispersed in MeCN for TEM characterization. However, no Cu NPs could be observed in the TEM images.

Therefore, the reaction was attempted again using different precursor and solvent. 0.046 mmol $CuBr_2$ was dissolved in methanol to give a yellow solution.[345] Then certain amount of BTM was added. Different ratios between BTM and $CuBr_2$ (1: 1 and 5: 1) were used. After the addition of BTM, the colour of the solution turned to green. The mixture was stirred under Ar protection at room temperature for 1 h. 0.46 mmol $NaBH_4$ was dissolved in 1 mL methanol and injected to the above solution drop by drop. The reaction was stirred under Ar protection at room temperature overnight, and the solution became blurry and the colour turned pale green. The products were collected by centrifugation, washed with methanol and finally redispersed in methanol for TEM characterization, which again did not show any NPs.

6.5.6 Iodide-Stablized Cu NPs

Iodide-stabilized Cu NPs were prepared using a reported method.[392] 0.01 mmol $CuSO_4$ and 0.01 mmol KI were mixed in 4 mL H_2O and stirred under Ar protection at room temperature for 1 h. Then 1 ml aqueous solution containing 0.06 mmol $NaBH_4$ was added dropwise and the color changed to wine-red. After stirring under Ar protection at room temperature for 2 h the color of the solution turned yellowish green.

6.5.7 DNA-Templated Synthesis of Cu NPs

Method 1: DNA-Templated Synthesis of Cu NPs by Using Sodium Ascorbate as Reductant

Cu NPs were prepared using DNA duplex as a template.[445] Aqueous solution (500 μL) containing the same amounts of DNA3 (500 nM) and *c*DNA3 (500 nM) in the buffer consisting of MOPS (20 mM, pH 7.5), NaCl (300 mM) and sodium ascorbate (2 mM) was purged with Ar, heated to 85 ℃ and slowly (5 ℃ / min) cooled down to 23 ℃. The formation of *ds*DNA was confirmed by agarose gel electrophoresis (1%) and the following staining with ethidium bromide (EtBr) (Figure 6.2). Desired amount of $CuSO_4$ or $CuCl_2$ (final concentration: 50-600 μM) was added. After incubation at room temperature for 30 min fluorescence spectroscopy was used to check if Cu NPs were obtained ($\lambda_{ex} = 340$ nm).
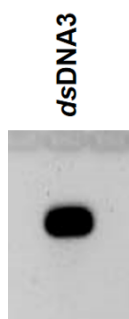
Figure 6. 2 Agarose gel image of *ds*DNA3 taken under the UV mode of the gel imaging system after staining the gel with EtBr

Method 2: DNA-Templated Synthesis of Cu NPs by Using Irgacure-2959 as Reductant

Aqueous solution (500 μL) containing equimolar amounts of DNA3 (500 nM) and *c*DNA3 (500 nM) in Tris buffer (20 mM) consisting of Irgacure-2959 (2 mM)[384] was purged with Ar, heated to 85 ℃ and slowly (5 ℃ / min) cooled down to 23 ℃. The formation of *ds*DNA was confirmed by agarose gel electrophoresis (1%) and the following staining with EtBr. $CuSO_4$ (final concentration: 100-1000 μM) was added and the mixture was irradiated

with UV lamp (λ = 365 nm) for 30 min. Fluorescence spectroscopy was used to check the formation of Cu NPs (λ_{ex} = 340 nm).

6.5.8 Oleylamine (OA)-Coated Cu NPs

The preparation of OA-Cu NPs followed a reported procedure with slight modification.[349] 0.1 mg of copper acetylacetonate was dissolved in 10 mL of OA in a 25 mL flask. The solution was degassed for 5 min and subsequently protected under a flow of Ar. The reaction mixture was heated to 230 °C by a heating mantle while being magnetically stirred and then kept at 230 °C for 5 h. The product was cooled to room temperature and washed with ethanol three times. The precipitation was redispersed in cyclohexane for TEM characterization.

Ligand exchange of OA-coated Cu NPs was performed by using 11-mercaptoundecanoic acid (MUA). 11 mg MUA was dissolved in 10 mL ethanol and added to 10 mg OA-Cu NPs. The mixtures were sonicated for 15 min and then magnetically stirred for 6 h under Ar protection. Finally, the Cu NPs were washed with ethanol for three times, and the resulting MUA-coated Cu NPs were redispersed in H_2O. However, the NPs precipitated after overnight.

6.5.9 Polyacrylic Acid (PAA)-Coated Cu NPs

Method 1: Synthesis of PAA-Cu NPs at 60 °C

PAA-coated Cu NPs were first prepared at 60 °C using a reported method with slight modification.[148] 0.017 mmol PAA and 0.05 mmol $CuCl_2$ $2H_2O$ were dissolved in 10 mL H_2O and heated in an oil bath at 60 °C for 20 min to give a light-blue solution. The pH of the solution was adjusted to 8 by adding 0.5 mL NaOH (0.5 M) dropwise. After stirring at 60 °C for 20 min, 1 mmol $N_2H_4 \cdot H_2O$ was added to the solution drop by drop. The color of the solution turned from blue to orange after several minutes. The reaction was stopped after 1 h and the color changed to reddish brown. After being kept undisturbed at room temperature overnight the color turned back to blue.

Method 2: Synthesis of PAA-Cu NPs at 23 °C

The reaction was carried out again at room temperature. 0.02 mmol PAA and 0.03 mmol $CuCl_2$ $2H_2O$ were dissolved in 5 mL H_2O and stirred at room temperature for 20 min to give a light-blue solution. The pH of the solution was adjusted to 8 by adding 100 μL NaOH (1 M) dropwise. Then $N_2H_4 \cdot H_2O$ (3 equv.) was added to the solution drop by drop and the mixture

was stirred at room temperature for 30 min and kept undisturbed for another 2 h. The color of the solution changed from blue to orange and finally to wine-red. The obtained Cu NPs were stable over months at 4 $^{\circ}$C.

6.5.10 L-ascorbic Acid (AA)-Coated Cu NPs

AA-coated Cu NPs were prepared by using a reported protocol with slight modification.[383] 1 mmol $CuCl_2$ $2H_2O$ was dissolved in 10 mL H_2O and heated to 80 $^{\circ}$C in an oil bath with magnetic stirring. 10 mL aqueous solution of L-ascorbic acid (0.5 M) was injected into the above solution drop by drop. The reaction was kept at 80 $^{\circ}$C overnight and the color of the solution became dark brown. The obtained Cu NPs were stable over months at 4 $^{\circ}$C.

6.5.11 Dopamine Linkers-Coated Cu NPs

Cu NPs were firstly prepared by using dopamine (DA) as a capping agent.[446] 0.5 mmol dopamine·HCl was dissolved in 5 mL H_2O and heated to 80 $^{\circ}$C in an oil bath with magnetic stirring. 0.5 mmol $CuCl_2$ $2H_2O$ was dissolved in 5 mL H_2O and injected to the above solution drop by drop. The reaction was kept at 80 $^{\circ}$C for 3 h and the color of the solution became dark brown.

The rest Cu NPs coated with dopamine derivatives (dopamine-maleimide (DoMal), norepinephrine-maleimide (NorMal), dopamine-triethylene glycol-maleimide (Do-TEG-Mal), DOPAC-triethylene glycol-amine (Do-TEG-Am) and DOPAC-triethylene glycol-alkyne (Do-TEG-Alkyne)) were prepared by using the similar synthetic procedures as DA-Cu NPs, except that the reaction time was different (3 ~ 15 h) when different capping agents were used. The reactions were normally stopped when the color of the solution became dark brown, and the NPs were stored at 4 $^{\circ}$C.

To prove that the Cu NPs were stabilized by dopamine linkers through the catechol groups, representative FTIR spectra of DA (**6**), DA-Cu, DoMal (**7**) and DoMal-Cu were recorded (Figure 6.3), which show that the stretching bands of catechol groups (-OH) around 3300 ~ 3500 cm^{-1} disappeared after the synthesis of Cu NPs indicating that the dopamine linkers indeed stabilized the Cu NPs through the coordination between catechol groups and Cu.

(a)

(b)

(c)
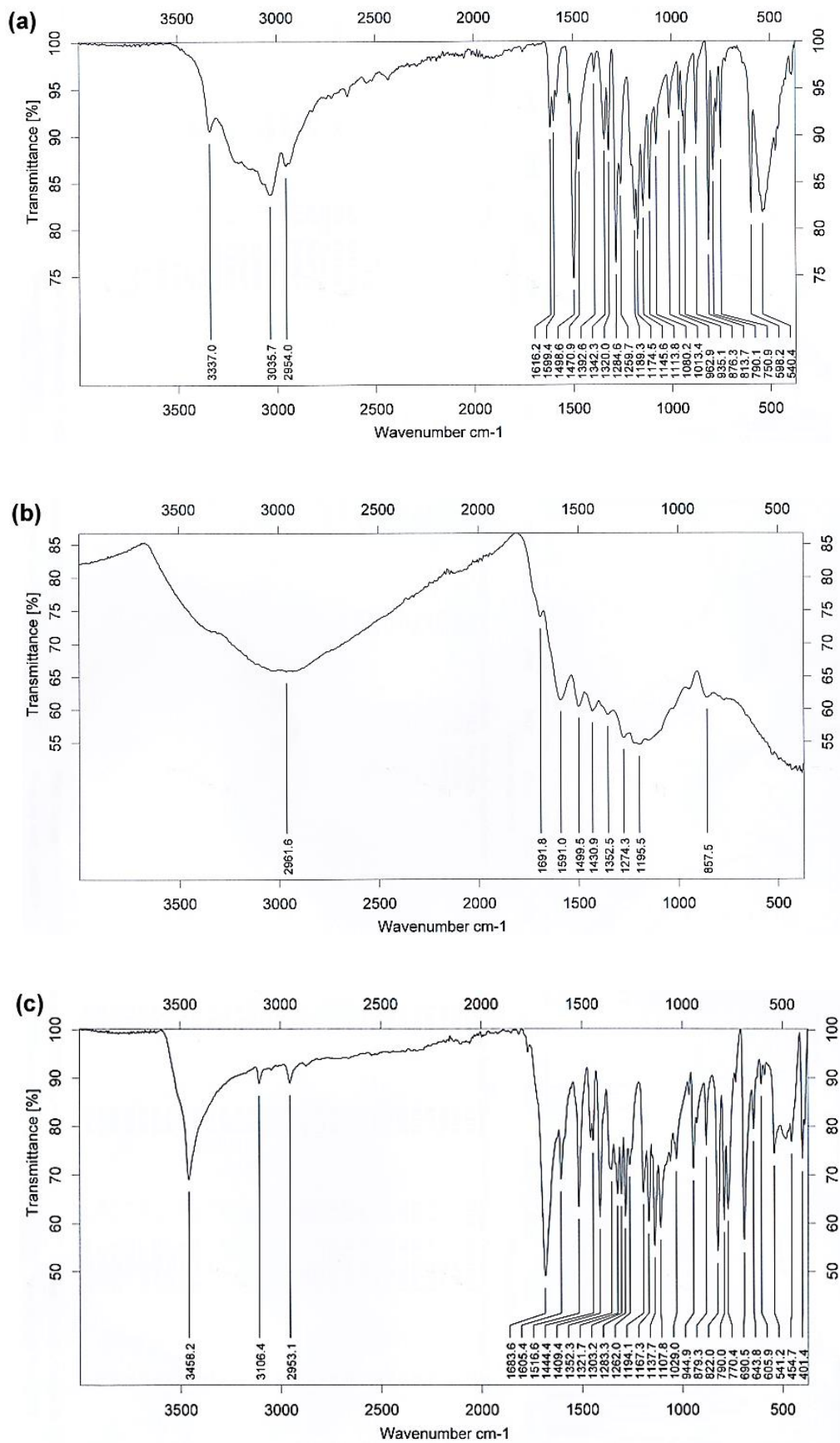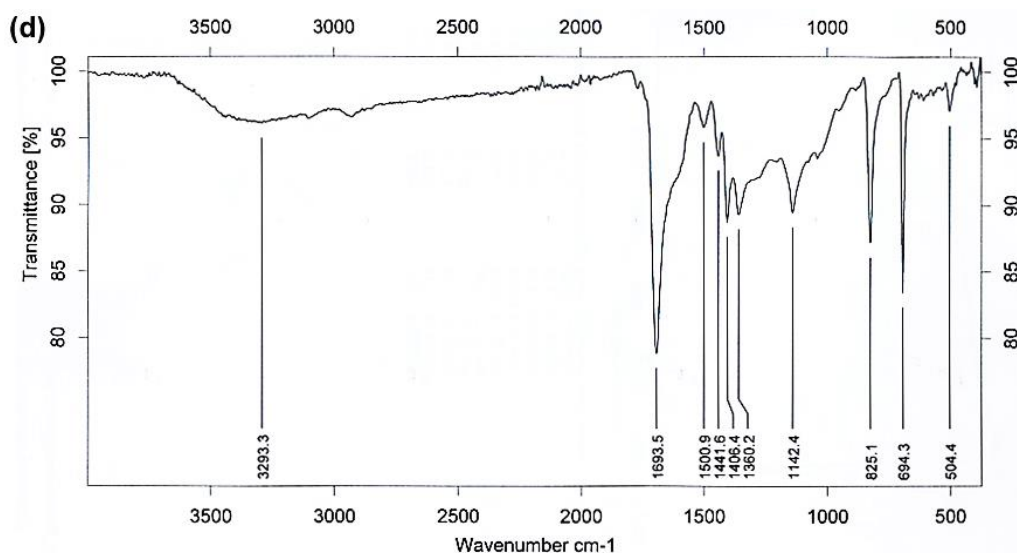
Figure 6. 3 FTIR spectra of (a) DA, (b) DA-Cu NPs, (c) DoMal and (d) DoMal-Cu NPs

6.5.12 Peroxidase Activity Tests for Cu NPs Using Amplex Red Assay

Peroxidase activity tests were performed by adding different volumes of AA- or dopamine linkers-coated Cu NPs (0 ~ 7 μL) to the mixture of 10 μL Amplex Red (AR, 1 mM) and 37.6 μL horseradish peroxidase (HRP, 50 U/mL). Phosphate buffer (0.1 M, pH = 6) was used to adjust the total volumes to 150 μL. A microplate reader was used to record the fluorescence signals of resorufin (λ_{ex} = 540 nm, λ_{em} = 585 nm, sensitivity: 95), which was formed by the oxidation of AR. Control experiments were done in the absence of Cu NPs (or HRP, or HRP and AR) or in the presence of corresponding ligands or CuCl$_2$ instead of Cu NPs.

6.5.13 Influence of Cu NPs on the Fluorescence of Resorufin

10 μL aqueous solutions of AA- or dopamine linkers-coated Cu NPs were mixed with 10 μL resorufin (100 μM). Phosphate buffer (pH = 6) was used to adjust the total volumes to 150 μL. Fluorescence signals of resorufin were recorded on a microplate reader (λ_{ex} = 540 nm, λ_{em} = 585 nm, sensitivity: 95). Control experiments were done by adding corresponding ligands instead of Cu NPs to resorufin.

6.5.14 Peroxidase Activity Tests for Cu NPs Using DCFH Assay

The ROS production ability of AA- and dopamine linkers-coated Cu NPs was confirmed again using 2,7-dichlorodihydrofluorescein (DCFH), which could be oxidized to fluorescent 2,7-dichlorofluorescein (DCF) by H$_2$O$_2$ in the presence of peroxidase. Firstly, 2,7-

205

dichlorodihydrofluorescein diacetate (DCFH-DA) was de-esterificated by NaOH (0.01 N), and then the reaction was stopped by adding sodium phosphate buffer (pH = 7.2).[76] 3 μL aqueous solutions of AA- or dopamine linkers-coated Cu NPs were added to the mixture of 100 μL DCFH (20.8 μM) and 25 μL HRP (50 U/mL). Fluorescence signals of DCF (λ_{ex} = 498 nm, λ_{em} = 535 nm, sensitivity: 80) were recorded on a microplate reader. Control experiments were done in the absence of Cu NPs, or in the presence of corresponding ligands or Cu (II) salt precursor instead of Cu NPs.

6.5.15 ROS Inhibition by Catalase

2 μL aqueous solutions of AA- or dopamine linkers-coated Cu NPs were mixed with 10 μL catalase (2,000 U/mL), then 37.6 μL HRP (50 U/mL) and 10 μL AR (1 mM) were added. Phosphate buffer (pH = 6) was used to adjust the total volumes to 150 μL. Fluorescence signals of the formed resorufin were recorded on a microplate reader (λ_{ex} = 540 nm, λ_{em} = 585 nm, sensitivity: 95).

6.5.16 H$_2$O$_2$ Calibration

The calibration curve was made by using H$_2$O$_2$ (50 μM) for the Amplex Red assay. Different volumes of H$_2$O$_2$ (50 μM, 0 ~ 5 μL) were added to the mixture of 10 μL AR (1 mM) and 37.6 μL HRP (50 U/mL). Phosphate buffer (pH = 6) was used to adjust the total volumes to 150 μL. A microplate reader was used to record the fluorescence signals of resorufin (λ_{ex} = 540 nm, λ_{em} = 585 nm, sensitivity: 95). By comparing the fluorescence intensity of resorufin obtained in the experiments using Cu NPs (3 μL) with that obtained in the experiments using H$_2$O$_2$, the ROS production ability of Cu NPs could be determined.

6.5.17 Superoxide Dismutase (SOD) Activity Assays of Cu NPs

The SOD-like activity of AA- and dopamine linkers-coated Cu NPs was tested employing a SOD activity assay, in which xanthine and xanthine oxidase (XO) were used as a source of superoxide.[447] 50 μL NaOH solution (0.02 M) of xanthine (2 mM) was mixed with 42.6 μL AA- or dopamine linkers-coated Cu NPs. 0.8 μL DMF solution of superoxide detection reagent (Orange) was added, followed by the addition of 100 μL PBS solution (1×) of XO (1 U/mL). PBS buffer (1×) was used to adjust the total volumes to 200 μL. The superoxide detection reagent (Orange®Enzo Life Science) could react with superoxide to afford a fluorescent product with an orange emission, and a microplate reader was used to record the

fluorescence signals of products (λ_{ex} = 484 nm, λ_{em} = 605 nm, sensitivity: 150). Controls were performed in the presence of corresponding ligands (or CuCl$_2$ or natural SOD from bovine erythrocytes) instead of Cu NPs.

6.5.18 SOD Activity Assays in the Presence of EDTA

To determine the influence of Cu^{2+} ions on the SOD activity assay of Cu NPs, the similar SOD activity assays of natural SOD, DoMal-Cu NPs, and CuCl$_2$ was performed in the presence of EDTA. The molar ratio between EDTA and natural SOD (or Cu precursor, or CuCl$_2$) was 1: 1, and the fluorescence was recorded on a microplate reader (λ_{ex} = 484 nm, λ_{em} = 605 nm, sensitivity: 150).

6.5.19 Enzyme Kinetics Studies of DoMal-Cu NPs and SOD

The enzyme kinetics studies of DoMal-Cu and SOD were performed as follows. 50 μL NaOH solution (0.02 M) of xanthine (2 mM) was mixed with 108 pmol DoMal-Cu or SOD. Different volumes (0.1, 0.2, 0.4, 0.6, or 0.8 μL) of superoxide detection reagent (Orange) were added, followed by the addition of 100 μL PBS solution (1×) of XO (1 U/mL). PBS buffer (1×) was used to adjust the total volumes to 200 μL. The fluorescence was recorded every minute over 1 h on a microplate reader (λ_{ex} = 484 nm, λ_{em} = 605 nm, sensitivity: 150).

6.5.20 Degradation of Rhodamine B (RB) and Methylene Blue (MB) by Cu NPs

The catalytic activity of AA- and dopamine linkers-coated Cu NPs for the degradation of RB and MB was tested by adding 10 μL AA- or dopamine linkers-coated Cu NPs to fluorescent dyes RB (20.8 μM) or MB (31.2 μM). Phosphate buffer (pH = 6) was used to adjust the total volumes to 150 μL. Fluorescence of RB (λ_{ex} = 540 nm, λ_{em} = 625 nm, sensitivity: 80) and MB (λex = 650 nm, λ_{em} = 685 nm, sensitivity: 150) was recorded on a microplate reader. Control experiments were carried out by adding CuCl$_2$ or corresponding ligands instead of Cu NPs to RB or MB.

6.5.21 Degradation of Chromomycin A3 (CMA) and Doxorubicin (DOX)

The catalytic activity of AA- and dopamine linkers-coated Cu NPs towards the degradation of CMA and DOX was tested by adding 10 μL AA- or dopamine linkers-coated Cu NPs to the solution of fluorescent CMA or DOX (20 μM). Fluorescence of CMA (λ_{ex} =

405 nm, λ_{em} = 555 nm, sensitivity: 100) and DOX (λ_{ex} = 499 nm, λ_{em} = 593 nm, sensitivity: 100) was recorded on a microplate reader. Control experiments were carried out by adding $CuCl_2$ or corresponding ligands instead of Cu NPs to RB or MB.

The recyclability of DA-coated Cu NPs for the degradation of CMA and DOX was performed in such a way that the Cu NPs were collected by centrifugation after the first round of degradation, and then used for the next round of reaction, and this procedure was repeated several times until the degradation efficiency decreased to around 50%.

6.6 Preparation and Properties of Hybrid TiO₂ Nanomaterials

6.6.1 Synthesis of Ethylene Glycol (EG)-Coated TiO₂ NPs

EG-coated TiO₂ NPs was synthesized by a polyol method with slight modification.[432] 0.2 mL TiCl₄ was added to 6 mL EG, which was previously heated to 60 °C under Ar protection. The colour of the solution became yellow, and then the temperature was increased to 75 °C and the solution was heat at 75 °C until it became clear. At this time, 0.1 mL H₂O was injected, and the reaction was refluxed at 160 °C for 3 h. After the solution was cooled down to room temperature, the NPs were precipitated from the solution by acetone and washed with acetone 3 times before TEM characterization.

6.6.2 Biofunctionalization of EG-TiO₂ NPs using Benzotriazole Linker

The biofunctionalization of EG-coated TiO₂ NPs with DNA strand was attempted using a bifunctional benzotriazole-maleimide (BTM, **4**) linker. The preparation of BTM-modified DNA1 has been described in 6.4.6. 20 μL EG-coated TiO₂ (20 μg/mL) was mixed with 2 nmol BTM-DNA1 in water, and incubated at room temperature for 1 d (or 4 d). The TiO₂ NPs were collected by centrifugation and washed with water 3 times to remove the free DNA. Then the NPs were characterized by agarose gel electrophoresis (1%).

6.6.3 Biofunctionalization of EG-TiO₂ NPs using Doapmine Linkers

1 mL aqueous solution of EG-coated TiO₂ NPs (1 mg/mL) was first incubated with 1 mL DoMal (**7**) and Do-TEG-Mal (**9**) (10 mM in the mixture of H₂O and MeCN (1: 1)) at room temperature for 2 h. The colour of the solutions turned orange and characterized by UV-Vis spectroscopy, which showed that the modification of EG-TiO₂ NPs with dopamine linkers was successful.

10 μL DoMal- or Do-TEG-Mal-modified TiO$_2$ NPs was mixed with 1 nmol furan-modified DNA1, which was synthesized in 6.4.13. After incubation at room temperature overnight, the products were analyzed by agarose gel electrophoresis (1%) and PAGE (21%). Then the bands in the gel pockets of PAGE were cut out and the NPs were extracted from the gel bands by ultrafiltration (Millipore) and characterized by TEM.

6.6.4 ROS Production by TiO$_2$ Nanomaterials

Different volumes (0 ~ 7 μL) of EG-TiO$_2$ NPs (or TiO$_2$ nanocubes or commercial TiO$_2$ NPs, 1 mg/mL in water) were added to a microplate and irradiated with UV light (365 nm) for 20 min. Then 10 μL Amplex Red (1 mM) and 37.6 μL HRP (50 U/mL) were added. Phosphate buffer (0.1 M, pH = 6) was used to adjust the total volumes to 150 μL. A microplate reader was used to record the fluorescence signals of resorufin (λ_{ex} = 540 nm, λ_{em} = 585 nm, sensitivity: 80), which was formed by the oxidation of AR. Controls were performed without UV light irradiation.

6.6.5 Copper-Free Click Reaction between Dopamine-Coumarin-Azide (DCA, 12) and Dopamine-Cyclooctyne (DCO, 13)

100 μL ethanol solution of DCA (**12**, 100 μM) and 100 μL ethanol solution (100 μM) of DCO (**13**) were mixed and incubated in dark at room temperature for 2 h or overnight, after which the fluorescence of the solution was recorded at λ_{ex} = 340 nm. However, the product was not fluorescent. Then the reaction was tried again using 100 μL DMSO solution of DCA (**12**) and 100 μL DMSO solution of DCO (**13**), but the product was still nonfluorescent.

To check if there was something wrong with both linkers, DCA (**12**) was used to undergo copper-catalyzed click reaction with triethylene glycol-alkyne (TEG-Alkyne, **15**). 100 μL DMSO solution of DCA (**12**, 100 μM) and 100 μL DMSO solution of TEG-Alkyne (**15**, 100 μM) were mixed, followed by the addition of 20 μL aqueous solution of sodium ascorbated (100 μM) and 40 μL aqueous solution of CuSO$_4$ (100 μM). The mixture was incubated at room temperature for 2 h or overnight. However, the obtained product was again not fluorescent, indicating that DCA (**12**) might not be pure or stable anymore. This was confirmed by the NMR spectrum of DCA, which showed the NMR signals of DCA, ^{1}H NMR (DMSO-d$_6$, 250 MHz) δ: 2.44-2.46 (2H, m, CH$_2$-C*H*$_2$), 3.26-3.30 (2H, m, C*H*$_2$-CH$_2$), 4.58 (2H, s, C*H*$_2$), 6.43-6.45 (1H, m, Ar-*H*), 6.58-6.63 (2H, m, Ar-*H*), 6.70-7.03 (2H, m, Ar-*H*), 7.62 (1H, s, Ar-*H*), 8.15-8.23 (1H, m, Ar-*H*), and also the signals of dopamine impurity,

^{1}H NMR (DMSO-d$_6$, 250 MHz) δ: 2.57-2.60 (2H, m, CH$_2$-CH_2), 6.38-6.41 (1H, m, Ar-*H*), 6.56-6.58 (2H, m, Ar-*H*).

Therefore, freshly prepared pure DCA (**12**) was used to react with DCO (**13**) in the following reaction. 100 μL DMSO solution of DCA (**12**, 100 μM) and 100 μL DMSO solution of DCO (**13**, 100 μM) were mixed and incubated at room temperature for 24 h, after which the fluorescence of the product was recorded. The product was also characterized by NMR and MS. ^{1}H NMR (DMSO-d$_6$, 250 MHz) δ: 1.23 (2H, m, CH_2), 1.39-1.54 (2H, m, CH_2), 1.35-1.57 (5H, m, CH_2), 2.18-2.29 (1H, m, CH_2), 2.99 (2H, s, CH$_2$-CH_2), 3.31-3.34 (4H, m, CH_2-CH_2), 4.49-4.66 (4H, m, CH_2), 6.42-6.47 (3H, m, Ar-H), 7.08-7.14 (3H, m, Ar-H), 7.76-7.78 (1H, m, Ar-H), 8.16-8.28 (2H, m, Ar-H), 8.54 (1H, s, Ar-H), 8.67 (2H, s, O*H*), 8.79 (2H, s, O*H*); m/z (FAB) for C$_{36}$H$_{36}$FN$_5$O$_9$ [M+H]$^+$: 702.3.

6.6.6 Preparation of TiO$_2$-Cu Nanocomposites

Preparation of DCA-Coated TiO$_2$ Nanomaterials

500 μL DMSO suspension of TiO$_2$ nanocubes or commercial TiO$_2$ NPs (2 mg/mL) was incubated with 500 μL DMSO solution of DCA (**12**, 5 mM) at room temperature for 2 h, after which the colour of the solution became yellow. The TiO$_2$ nanocubes or commercial TiO$_2$ NPs were collected by centrifugation, washed with DMSO, resuspended in 1 mL DMSO, and characterized by UV-Vis spectroscopy.

Synthesis of DCO-Coated Cu NPs

0.5 mmol DCO (**13**) was dissolved in 5 mL ethanol and heated to 80 $^{\circ}$C in an oil bath with magnetic stirring. 0.5 mmol CuCl$_2$ 2H$_2$O was dissolved in 5 mL ethanol and injected to the above solution drop by drop. The reaction was refluxed at 80 $^{\circ}$C for 8 h and the color of the solution became dark brown.

Click Reaction between DCA-Coated TiO$_2$ Nanomaterials and DCO-Coated Cu NPs

200 μL DMSO suspensions of DCA-coated TiO$_2$ nanocubes or commercial TiO$_2$ NPs was mixed with 200 μL ethanol solution of DCO-coated Cu NPs and incubated at room temperature for 24 h. Then the NPs were collected by centrifugation and redispersed in ethanol for TEM characterization. However, only TiO$_2$ nanocubes or commercial TiO$_2$ NPs could be observed, but no traces of smaller Cu NPs, indicating that the click reaction on the surface of NPs was not successful, which might be because the existence of ethanol in the

solvent system might influence the dispersity of DCA-modified TiO$_2$ nanomaterials as DCA (**12**) was not soluble in ethanol.

Then the reaction was performed again by evaporating the solvent (ethanol) of Cu NPs (200 μL) in speed vaccum. The dried Cu NPs were redispersed in 200 μL DMSO and mixed with 200 μL DMSO suspension of DCA-coated TiO$_2$ nanocubes or commercial TiO$_2$ NPs. The mixture was incubated at room temperature for 24 h, and then the NPs were collected by centrifugation and redispersed in ethanol for TEM characterization. However, there were again only TiO$_2$ nanocubes or NPs observed in the TEM images, and no Cu NPs could be observed.

The other possible reason for the failure of the click reaction on NPs might lie in the full or partial removal of the cyclooctyne functional group in the case of Cu NPs, as the preparation of DCO-Cu NPs was performed under refluxing at 80 $^{\circ}$C, which might affect the stability of DCO (**13**). Therefore, the NMR and MS of DCO were recorded both before and after heating its ethanol solution at 80 $^{\circ}$C for 8 h, which showed that the structure of DCO was intact after heating at 80 $^{\circ}$C for 8 h. ^{1}H NMR of DCO before heating (CDCl$_3$, 250 MHz) δ: 1.31-1.40 (2H, m, CH_2), 1.54-1.64 (1H, m, CH_2), 1.73-2.03 (4H, m, CH_2), 2.14-2.25 (3H, m, CH_2), 2.66 (2H, t, ^3J = 7.0, CH$_2$-CH_2), 3.45 (2H, q, ^3J = 6.7, CH_2-CH$_2$), 6.51 (1H, dd, ^4J = 1.8, ^3J = 8.0, Ar-H), 6.70 (1H, d, ^4J = 1.7, Ar-H), 6.77 (1H, d, ^3J = 8.0, Ar-H); m/z (FAB) for C$_{17}$H$_{20}$FNO$_3$ [M+H]$^+$: 306.2. ^{1}H NMR of DCO after heating (CDCl$_3$, 250 MHz) δ: 1.32-1.47 (1H, m, CH_2), 1.52-1.68 (2H, m, CH_2), 1.78-2.08 (4H, m, CH_2), 2.16-2.31 (3H, m, CH_2), 2.69 (2H, t, ^3J = 7.0, CH$_2$-CH_2), 3.47 (2H, q, ^3J = 6.6, CH_2-CH$_2$), 6.55 (1H, dd, ^4J = 2.0, ^3J = 8.0, Ar-H), 6.71 (1H, d, ^4J = 2.0, Ar-H), 6.78 (1H, d, ^3J = 8.0, Ar-H); m/z (FAB) for C$_{17}$H$_{20}$FNO$_3$ [M+H]$^+$: 306.2.

7 Abbreviations

AA	L-Ascorbic Acid
Abs	Absorbance
Ag	Silver
APS	Ammonium Persulfate
Ar	Argon
AR	Amplex Red (N-acetyl-3,7-dihydroxyphenoxazine)
a. u.	Arbitrary Unit
Au	Gold
BPE	1,2-Bis(4-pyridyl)ethylene
BT	Benzotriazole
BTM	Benzotriazole-Maleimide
c	Concentration
CDI	1,1'-Carbonyl Diimidazole
*c*DNA	Complementary Deoxyribonucleic Acid
CMA	Chromomycin A3
CPG	Controlled Pore Glass
CP-PEG	Cyclopenta-1,3-diene-Polyethylene Glycol
CTAB	Cetyltrimethylammonium Bromide
Cu	Copper
δ	Chemical Shift
d	day
DA	Dopamine
DCA	Dopamine-Coumarin-Azide
DCF	2,7-Dichlorofluorescein
DCFH	2,7-Dichlorodihydrofluorescein
DCM	Dichloromethane
DCO	Dopamine-Cyclooctyne
DIPEA	N,N-Diisopropylethylamine
DMF	Dimethylformamide
DMSO	Dimethyl Sulfoxide
DNA	Deoxyribonucleic Acid

DoMal	Dopamine-Maleimide
Do-TEG-Alkyne	Dopamine-Triethylene Glycol-Alkyne
Do-TEG-Am	Dopamine-Triethylene Glycol-Amine
Do-TEG-Mal	Dopamine-Triethylene Glycol-Maleimide
DOX	Doxorubicin
*ds*DNA	Double Stranded Deoxyribonucleic Acid
DTT	Dithiothreitol
e⁻	Electrons
EDC	1-Ethyl-3-(3-Dimethylaminopropyl)-Carbodiimide
EDTA	Ethylenediaminetetraacetic acid
EG	Ethylene Glycol
EtBr	Ethidium Bromide
em	Emission
EPR	Electron Paramagnetic Resonance
ESI-MS	Electrospray Ionization Mass Spectrometry
EtBr	Ethidium Bromide
eV	Electron Volt
ex	Excitation
FAB-MS	Fast Atom Bombardment Ionization Mass Spectrometry
FPLC	Fast Protein Liquid Chromatography
FTIR	Fourier Transform Infrared Spectroscopy
g	Gram
h	Hour
h⁺	Holes
HBTU	o-Benzotriazole-N,N,N',N'-Tetramethyl-Uronium-Hexafluoro-phosphate
HDA	Hexadecylamine
HOBt	Hydroxybenzotriazole
HOMO	Highest Occupied Molecule Orbital
HPLC	High Performance Liquid Chromatography
HRP	Horseradish Peroxidase
HRTEM	High Resolution Transmission Electron Microscopy
Hz	Hertz
Irgacure-2959	1-[4-(2-hydroxyethoxy)phenyl]-2-hydroxy-2-methyl-1-propane-1-one

J	Coupling Constant
L	Litre
λ	Wavelength
LUMO	Lowest Unoccupied Molecule Orbital
LSPR	Localized Surface Plasmon Resonance
μ	Micro
M	Moles per Litre
MAA	Mercaptoacetic Acid
MALDI	Matrix-Assisted Laser Desorption Ionization
Mb	Myoglobin
MB	Methylene Blue
MeCN	Acetonitrile
mg	Milligram
μg	Microgram
min	Minute
mL	Millilitre
μL	Microlitre
mM	Millimoles per Litre
μM	Micromoles per Litre
mmol	Millimole
μmol	Micromole
mol	Mole
MS	Mass Spectrometry
MUA	Mercaptoundecanoic Acid
mV	Millivolt
Mw	Molecular Weight
NHS	*N*-Hydroxysuccinimide
nm	Nanometer
nmol	Nanomole
nM	Nanomoles per Liter
NMR	Nuclear Magnetic Resonance
NorMal	Norepinephrine-Maleimide
NP	Nanoparticle
OA	Oleylamine

PAA	Polyacrylic Acid
PAGE	Polyacrylamide Gel Electrophoresis
PBS	Phosphate Buffered Saline
PEG	Polyethylene Glycol
pmol	Picomole
PVP	Polyvinylpyrrolidone
QDs	Quantum Dots
RB	Rhodamine B
RFU	Relative Fluorescence Unit
ROS	Reactive Oxygen Species
RT	Room Temperature
SAED	Selected Area Electron Diffraction
SERS	Surface Enhanced Raman Scattering
SOD	Superoxide Dismutase
*ss*DNA	Single Stranded Deoxyribonucleic Acid
SH	Thiol
Sulfo-SMCC	Sulfosuccinimidyl-4-(N-Maleimidomethyl) Cyclohexane-1-Carboxylate
TEG	Triethylene Glycol
TEM	Transmission Electron Microscopy
TEMED	Tetramethylethylenediamine
TFA	Trifluoroacetic Acid
TiO_2	Titanium Dioxide
TOF	Time of Flight
U/mL	Units per Milliliter
UV	Ultraviolet
V	Volume
Vis	Visible
XO	Xanthine Oxidase
ζ	Zeta Potential

8 Curriculum Vitae

Personal Details

Name	Cheng Chen
Nationality	Chinese

Education

04.2011~10.2014	**PhD**, Centre for Functional Nanostructures, Karlsruhe Institute of Technology, Germany Supervisor: Dr. Ljiljana Fruk *Thesis: Novel Strategies for the Preparation and Functionalization of Noble Metallic and Titanium Dioxide Nanoparticles*
09.2013	**Academic Visitor**, Rudjer Boskovic Institute, Croatia
07.2013~08.2013	**Academic Visitor**, Department of Pure and Applied Chemistry, University of Strathclyde, United Kingdom Supervisor: Dr. Ljiljana Fruk and Prof. Dr. Duncan Graham
09.2007~07.2010	**Master of Engineering**, Materials Physics & Chemistry, College of Chemistry and Chemical Engineering, Inner Mongolia University, China Supervisor: Prof. Dr. Jun Zhang *Thesis：Ionic Liquid-based Synthesis, Characterization, and Property Study of Rare Earth Fluorescent Nanomaterials*
11.2008~05.2010	**Exchange Student**, Inorganic Chemistry, College of Chemistry and Molecular Engineering, Peking University, China Supervisor: Prof. Dr. Chunhua Yan and Prof. Dr. Jun Zhang
09.2003~07.2007	**Bachelor of Science**, Materials Chemistry, College of Chemistry and Chemical Engineering, Inner Mongolia University, China Supervisor: Prof. Dr. Jun Zhang *Thesis: Preparation and Photocatalytic Property of Nanoscale TiO_2*
09.2004~07.2007	**Bachelor of Art**, English, College of Foreign Languages, Inner Mongolia University, China

9 Publications and Patents

Publications

1. **C. Chen**, A. Vigovskaya, J. B. Priebe, D. Hollmann, A. Brückner and L. Fruk, Catechol-Coated Copper Nanoparticles as Superoxide Dismutase Mimetics, *submitted*.

2. **C. Chen**, I. Ahmed and L. Fruk*, Reactive Oxygen Species Production by Catechol Stabilized Copper Nanoparticles, *Nanoscale*, **2013**, *5*, 11610-11614.

3. **C. Chen** and L. Fruk*, Functionalization of Maleimide-Coated Silver Nanoparticles through Diels-Alder Cycloaddition, *RSC Adv*., **2013**, *3*, 1709-1713.

4. F. Gao, C. F. Lv, J. X. Han, X. Y. Li, Q. Wang, J. Zhang*, **C. Chen**, Q. Li, X. F. Sun, J. C. Zheng, L. R. Bao, X. Li, CdTe-Montmorillonite Nanocomposites: Control Synthesis, UV Radiation- Dependent Photoluminescence and Enhanced Latent Fingerprint Detection, *J. Phys. Chem. C*, **2011**, *115*, 21574–21583.

5. **C. Chen**, L. D. Sun, Z. X. Li, L. L. Li, J. Zhang*, Y. W. Zhang, C. H. Yan*, Ionic Liquid-Based Route to Spherical $NaYF_4$ Nanoclusters with the Assistance of Microwave Radiation and Their Multicolor Upconversion Luminescence, *Langmuir*, **2010**, *26*, 8797-8803.

6. Z. X. Li, L. L. Li, H. P. Zhou, Q. Yuan, **C. Chen**, L. D. Sun, C, H. Yan*, Color Modification Action of An Upconversion Photonic Crystal, *Chem. Commun*., **2009**, 6616-6618.

Patents

1. Z. L. Liu, C. X. Yang, **C. Chen**, B. Liu, J. Zhang*, J. Y. Feng, X. W. Di, Method for Preparing Doped Nanometer Titanium Oxide Photocatalyst, **2010**, CN101301606B.

2. J. Zhang*, **C. Chen**, B. C. Liu, X. W. Di, J. Y. Feng, C. X. Yang, Z. L. Liu, Method for Preparing Doped Nanometer Titanium Oxide Photocatalyst, **2008**, CN101301606A.

The patents could be found using the publications' numbers on the website of Chinese Patent Search and Service System:

http://www.pss-system.gov.cn/sipopublicsearch/ensearch/searchEnHomeIndexAC.do

10 Acknowledgements

The collegues in the University of Strathclyde have also helped me a lot with my research and life in Glasgow. I want to thank Dr. David Thompson and Dr. Samuel Mabbott for their help with the Raman Spectroscopies and suggestions for SERS property study of Cu NPs, Dr. Narayana Sirimuthu for his help with SEM, and Jonathan Simpson for the synthesis of benzotriazole dyes.

I want to thank Dr. Philipp Müller, Pascal Bockstaller and Dr. Heike Störmer for their help with TEM, EDX and SAED characterizations, and there were always interesting and beautiful images.

For the EPR measurements, I want to say thank you to Prof. Angelika Brückner, Jacqueline B. Priebe and Dr. Dirk Hollmann. They have taught me the principle of EPR and showed me how to make the EPR measurements under different conditions.

During these 3.5 years, Dr. Christian Röthig, Ms. Renate Bender and Ms. Ursula Moesle have helped me with many administrative things, and I have bothered Mr. Andreas Elkeries many times with problems about computers, softwares, email addresses, etc. They were so nice and patient to help me to solve such kind of problems, and thank you so much.

I would also like to thank Prof. Dr, Chunhua Yan for recommending me to Dr. Ljiljana Fruk in 2010 so that I could have the chance to join such a great research team. Many thanks to Prof. Dr. Goran Baranović, Dr. Suzanna Segota, and Dr. Danijela Vojta for their companion during my visit to Rudjer Boskovic Institute.

I also want to thank my family and friends for all their love and encouragement. For my parents who have raised me up, support me for all my persuits, love and believe in me forever. For my husband who has always been on my side, loves me, supports me and encourages me. For all best friends who have spent lots of wonderful moments with me, and for all those unforgettable memories we have had together.

Last but not least, thanks to DAAD and CSC's financial support, so that I could come to Germany, do the interesting research work, and finish my PhD research smoothly. I really appreciated Mr. David Hildebrand, Ms. Marion Asten, Ms. Ye Yang, Ms. Yifei Zhang and Mr. Zheng Chen's help with my questions concerning the scholarship. Thank you!

Cheng Chen

Karlsruhe

24.10.2014

References

1. A. V. Whitney, J. W. Elam, S. L. Zou, A. V. Zinovev, P. C. Stair, G. C. Schatz and R. P. Van Duyne, *J. Phys. Chem. B*, 2005, **109**, 20522-20528.
2. D. Graham, D. G. Thompson, W. E. Smith and K. Faulds, *Nat. Nanotechnol.*, 2008, **3**, 548-551.
3. Z. Shen, H. W. Duan and H. Frey, *Adv. Mater.*, 2007, **19**, 349-352.
4. E. A. Karakhanov, A. L. Maximov, Y. S. Kardasheva, V. A. Skorkin, S. V. Kardashev, V. V. Predeina, M. Y. Talanova, E. Lurie-Luke, J. A. Seeley and S. L. Cron, *Appl. Catal. a-Gen.*, 2010, **385**, 62-72.
5. B. Dubertret, P. Skourides, D. J. Norris, V. Noireaux, A. H. Brivanlou and A. Libchaber, *Science*, 2002, **298**, 1759-1762.
6. S. W. Zeng, X. Yu, W. C. Law, Y. T. Zhang, R. Hu, X. Q. Dinh, H. P. Ho and K. T. Yong, *Sensor Actuat. B-Chem.*, 2013, **176**, 1128-1133.
7. A. Liebsch, *Phys. Rev. Lett.*, 1993, **71**, 145-148.
8. O. Wolf, M. Dasog, Z. Yang, I. Balberg, J. G. Veinot and O. Millo, *Nano Lett.*, 2013, **13**, 2516-2521.
9. S. K. Haram, A. Kshirsagar, Y. D. Gujarathi, P. P. Ingole, O. A. Nene, G. B. Markad and S. P. Nanavati, *J. Phys. Chem. C*, 2011, **115**, 6243-6249.
10. J. Y. Park, P. Daksha, G. H. Lee, S. Woo and Y. M. Chang, *Nanotechnology*, 2008, **19**, 365603–365609.
11. C. J. Xu and S. H. Sun, *Adv. Drug Deliv. Rev.*, 2013, **65**, 732-743.
12. L. L. Chng, N. Erathodiyil and J. Y. Ying, *Acc. Chem. Res.*, 2013, **46**, 1825-1837.
13. B. R. Cuenya, *Thin Solid Films*, 2010, **518**, 3127-3150.
14. X. H. Huang, P. K. Jain, I. H. El-Sayed and M. A. El-Sayed, *Nanomedicine*, 2007, **2**, 681-693.
15. G. Schmid and B. Corain, *Eur. J. Inorg. Chem.*, 2003, 3081-3098.
16. W. T. Yu, M. D. Porosoff and J. G. G. Chen, *Chem. Rev.*, 2012, **112**, 5780-5817.
17. D. G. Thompson, A. Enright, K. Faulds, W. E. Smith and D. Graham, *Anal. Chem.*, 2008, **80**, 2805-2810.
18. S. D. Brown, P. Nativo, J. A. Smith, D. Stirling, P. R. Edwards, B. Venugopal, D. J. Flint, J. A. Plumb, D. Graham and N. J. Wheate, *J. Am. Chem. Soc.*, 2010, **132**, 4678-4684.
19. M. F. Frasco and N. Chaniotakis, *Sensors-Basel*, 2009, **9**, 7266-7286.
20. M. K. Fan, G. F. S. Andrade and A. G. Brolo, *Anal. Chim. Acta.*, 2011, **693**, 7-25.
21. M. Samim, N. K. Kaushik and A. Maitra, *B Mater. Sci.*, 2007, **30**, 535-540.
22. M. G. Miljevic, B.; Bergfeldt, T.; Bockstaller, P.; Fruk, L, *Adv. Funct. Mater.*, 2014, **24**, 907-915.
23. W. J. Cho, Y. Kim and J. K. Kim, *ACS Nano*, 2012, **6**, 249-255.
24. W. Y. Li, P. H. C. Camargo, X. M. Lu and Y. N. Xia, *Nano. Lett.*, 2009, **9**, 485-490.
25. A. Tao, P. Sinsermsuksakul and P. Yang, *Nat. Nanotechnol.*, 2007, **2**, 435-440.
26. M. Fan, M. L. Andrade, M. Thompson and A. G. Brolo, *Anal. Chem.*, 2010, **82**, 6350-6352.
27. M. Rycenga, C. M. Cobley, J. Zeng, W. Y. Li, C. H. Moran, Q. Zhang, D. Qin and Y. N. Xia, *Chem. Rev.*, 2011, **111**, 3669-3712.
28. K. Loza, J. Diendorf, C. Sengstock, L. Ruiz-Gonzalez, J. M. Gonzalez-Calbet, M. Vallet-Regi, M. Koller and M. Epple, *J. Mater. Chem. B*, 2014, **2**, 1634-1643.
29. H. S. Li, H. B. Xia, D. Y. Wang and X. T. Tao, *Langmuir*, 2013, **29**, 5074-5079.

References

30. P. T. K. Chin, M. van der Linden, E. J. van Harten, A. Barendregt, M. T. M. Rood, A. J. Koster, F. W. B. van Leeuwen, C. D. Donega, A. J. R. Heck and A. Meijerink, *Nanotechnology*, 2013, **24**, 075703.

31. B. Wiley, Y. G. Sun, B. Mayers and Y. N. Xia, *Chem. Eur. J.*, 2005, **11**, 454-463.

32. B. Pietrobon, M. McEachran and V. Kitaev, *ACS Nano*, 2009, **3**, 21-26.

33. R. C. Jin, Y. C. Cao, E. C. Hao, G. S. Metraux, G. C. Schatz and C. A. Mirkin, *Nature*, 2003, **425**, 487-490.

34. S. Jang, Y. Seo, J. Choi, T. Kim, J. Cho, S. Kim and D. Kim, *Scripta Mater.*, 2010, **62**, 258-261.

35. N. G. Bastus, J. Comenge and V. Puntes, *Langmuir*, 2011, **27**, 11098-11105.

36. P. C. Lee and D. Meisel, *J. Phys. Chem.-Us*, 1982, **86**, 3391-3395.

37. M. Kamali, S. A. A. Ghorashi and M. A. Asadollahi, *Iran. J. Chem. Chem. Eng.*, 2012, **31**, 21-28.

38. X. Y. Dong, X. H. Ji, H. L. Wu, L. L. Zhao, J. Li and W. S. Yang, *J. Phys. Chem. C*, 2009, **113**, 6573-6576.

39. J. Lim, S. Lee and S. Yoon, *B. Kor. Chem. Soc.*, 2011, **32**, 4113-4116.

40. C. F. Li, D. X. Li, G. Q. Wan, J. Xu and W. G. Hou, *Nanoscale Res. Lett.*, 2011, **6**, 32.

41. M. Zhou, B. X. Wang, Z. Rozynek, Z. H. Xie, J. O. Fossum, X. F. Yu and S. Raaen, *Nanotechnology*, 2009, **20**, 505.

42. F. Fievet, J. P. Lagier, B. Blin, B. Beaudoin and M. Figlarz, *Solid State Ionics*, 1989, **32-3**, 198-205.

43. F. Kim, S. Connor, H. Song, T. Kuykendall and P. D. Yang, *Angew. Chem. Int. Ed.*, 2004, **43**, 3673-3677.

44. J. Y. Chen, T. Herricks, M. Geissler and Y. N. Xia, *J. Am. Chem. Soc.*, 2004, **126**, 10854-10855.

45. S. E. Skrabalak, B. J. Wiley, M. Kim, E. V. Formo and Y. N. Xia, *Nano Lett.*, 2008, **8**, 2077-2081.

46. C. Ducampsanguesa, R. Herreraurbina and M. Figlarz, *J. Solid State Chem.*, 1992, **100**, 272-280.

47. D. Kim, S. Jeong and J. Moon, *Nanotechnology*, 2006, **17**, 4019-4024.

48. H. J. Jiang, K. S. Moon, Z. Q. Zhang, S. Pothukuchi and C. P. Wong, *J. Nanopart. Res.*, 2006, **8**, 117-124.

49. W. Cai and J. Q. Wan, *J. Colloid Interface Sci.*, 2007, **305**, 366-370.

50. S. S. Horikoshi, N., *Microwaves in Nanoparticle Synthesis: Fundamentals and Applications*, 2013.

51. Y. Zhou, S. M. Jin, G. Z. Qiu and M. Yang, *Mat. Sci. Eng. B-Solid*, 2005, **122**, 222-225.

52. H. Gronbeck, A. Curioni and W. Andreoni, *J. Am. Chem. Soc.*, 2000, **122**, 3839-3842.

53. M. A. Neouze and U. Schubert, *Monatsh. Chem.*, 2008, **139**, 183-195.

54. X. L. Li, J. H. Zhang, W. Q. Xu, H. Y. Jia, X. Wang, B. Yang, B. Zhao, B. F. Li and Y. Ozaki, *Langmuir*, 2003, **19**, 4285-4290.

55. Y. A. Diaz-Fernandez, P. Pallavicini, L. Pasotti, C. Milanese, E. Pellicer, M. D. Baro, Y. Ren and L. Malavasi, *Nanoscale*, 2011, **3**, 4220-4225.

56. A. Andrieux-Ledier, B. Tremblay and A. Courty, *Langmuir*, 2013, **29**, 13140-13145.

57. A. Longo, G. Carotenuto, M. Palomba and S. De Nicola, *Polymers-Basel*, 2011, **3**, 1794-1804.

58. C. J. Murphy, L. B. Thompson, D. J. Chernak, J. A. Yang, S. T. Sivapalan, S. P. Boulos, J. Y. Huang, A. M. Alkilany and P. N. Sisco, *Curr. Opin. Colloid Interface Sci.*, 2011, **16**, 128-134.

59. Q. A. Zhang, W. Y. Li, C. Moran, J. Zeng, J. Y. Chen, L. P. Wen and Y. N. Xia, *J. Am. Chem. Soc.*, 2010, **132**, 11372-11378.

60.	R. L. Zong, X. L. Wang, S. K. Shi and Y. F. Zhu, *Phys. Chem. Chem. Phys.*, 2014, **16**, 4236-4241.

61.	W. X. Niu, L. Zhang and G. B. Xu, *Sci. China Chem.*, 2012, **55**, 2311-2317.

62.	J. C. Liu, F. He, T. M. Gunn, D. Y. Zhao and C. B. Roberts, *Langmuir*, 2009, **25**, 7116-7128.

63.	S. Giuffrida, G. Ventimiglia, S. Petralia, S. Conoci and S. Sortino, *Inorg. Chem.*, 2006, **45**, 508-510.

64.	K. L. McGilvray, M. R. Decan, D. S. Wang and J. C. Scaiano, *J. Am. Chem. Soc.*, 2006, **128**, 15980-15981.

65.	X. L. Zheng, W. Q. Xu, C. Corredor, S. P. Xu, J. An, B. Zhao and J. R. Lombardi, *J. Phys. Chem. C*, 2007, **111**, 14962-14967.

66.	M. A. El-Sheikh, *ScientificWorldJournal.*, 2014, **2014**, 514563.

67.	M. Grzelczak and L. M. Liz-Marzan, *Chem. Soc. Rev.*, 2014, **43**, 2089-2097.

68.	K. M. M. Abou El-Nour, A. Eftaiha, A. Al-Warthan and R. A. A. Ammar, *Arab. J. Chem.*, 2010, **3**, 135-140.

69.	D. Longano, N. Ditaranto, N. Cioffi, F. Di Niso, T. Sibillano, A. Ancona, A. Conte, M. A. Del Nobile, L. Sabbatini and L. Torsi, *Anal. Bioanal. Chem.*, 2012, **403**, 1179-1186.

70.	B. C. Ranu, R. Dey, T. Chatterjee and S. Ahammed, *ChemSusChem*, 2012, **5**, 22-44.

71.	Y. Lee, J. R. Choi, K. J. Lee, N. E. Stott and D. Kim, *Nanotechnology*, 2008, **19**, 415604.

72.	G. H. Chan, J. Zhao, E. M. Hicks, G. C. Schatz and R. P. Van Duyne, *Nano Lett.*, 2007, **7**, 1947-1952.

73.	M. Muniz-Miranda, C. Gellini and E. Giorgetti, *J. Phys. Chem. C*, 2011, **115**, 5021-5027.

74.	M. S. Usman, M. E. El Zowalaty, K. Shameli, N. Zainuddin, M. Salama and N. A. Ibrahim, *Int. J Nanomed.*, 2013, **8**, 4467-4478.

75.	S. Q. Qiu, J. X. Dong and G. X. Chen, *J. Colloid Interface Sci.*, 1999, **216**, 230-234.

76.	M. Shi, H. S. Kwon, Z. M. Peng, A. Elder and H. Yang, *ACS Nano*, 2012, **6**, 2157-2164.

77.	Y. H. Wang, P. L. Chen and M. H. Liu, *Nanotechnology*, 2006, **17**, 6000-6006.

78.	S. H. Wu and D. H. Chen, *J. Colloid Interface Sci.*, 2004, **273**, 165-169.

79.	M. F. Casula, Y. W. Jun, D. J. Zaziski, E. M. Chan, A. Corrias and A. P. Alivisatos, *J. Am. Chem. Soc.*, 2006, **128**, 1675-1682.

80.	H. X. Mai, Y. W. Zhang, R. Si, Z. G. Yan, L. D. Sun, L. P. You and C. H. Yan, *J. Am. Chem. Soc.*, 2006, **128**, 6426-6436.

81.	S. Chin, E. Park, M. Kim and J. Jurng, *Powder Technol.*, 2010, **201**, 171-176.

82.	Y. Z. Chen, D. L. Peng, D. P. Lin and X. H. Luo, *Nanotechnology*, 2007, **18**, 505703.

83.	S. Navaladian, B. Viswanathan, R. P. Viswanath and T. K. Varadarajan, *Nanoscale Res. Lett.*, 2007, **2**, 44-48.

84.	Y. H. Kim, Y. S. Kang, W. J. Lee, B. G. Jo and J. H. Jeong, *Mol. Cryst. Liq. Cryst.*, 2006, **445**, 231-238.

85.	B. K. Park, S. Jeong, D. Kim, J. Moon, S. Lim and J. S. Kim, *J. Colloid Interface Sci.*, 2007, **311**, 417-424.

86.	C. Kind, A. Weber and C. Feldmann, *J. Mater. Chem.*, 2012, **22**, 987-993.

87.	B. K. Park, S. Jeong, D. Kim, J. Moon, S. Lim and J. S. Kim, *J. Colloid Interface Sci.*, 2007, **311**, 417-424.

88.	Y. M. Long, Q. L. Zhao, Z. L. Zhang, Z. Q. Tian and D. W. Pang, *Analyst*, 2012, **137**, 805-815.

89.	Z. L. Xiao, C. Y. Han, W. K. Kwok, H. W. Wang, U. Welp, J. Wang and G. W. Crabtree, *J. Am. Chem. Soc.*, 2004, **126**, 2316-2317.

90.	C. M. Lopez and K. S. Choi, *Langmuir*, 2006, **22**, 10625-10629.

References

91.   K. S. Choi, *Dalton Trans.*, 2008, 5432-5438.
92.   T. Nychyporuk, V. Lysenko, B. Gautier and D. Barbier, *J. Appl. Phys.*, 2006, **100**.
93.   C. Pascal, J. L. Pascal, F. Favier, M. L. E. Moubtassim and C. Payen, *Chem. Mater.*, 1999, **11**, 141-147.
94.   O. Corduneanu, V. C. Diculescu, A. M. Chiorcea-Paquim and A. M. Oliveira-Brett, *J. Electroanal. Chem.*, 2008, **624**, 97-108.
95.   T. Gao, G. W. Meng, Y. W. Wang, S. H. Sun and L. Zhang, *J. Phys-Condens. Mat.*, 2002, **14**, 355-363.
96.   M. V. Mandke and H. M. Pathan, *J. Electroanal. Chem.*, 2012, **686**, 19-24.
97.   L. Rodriguez-Sanchez, M. C. Blanco and M. A. Lopez-Quintela, *J. Phys. Chem. B*, 2000, **104**, 9683-9688.
98.   R. Surudzic, Z. Jovanovic, N. A. Bibic, B. Nikolic and V. Miskovic-Stankovic, *J. Serb. Chem. Soc.*, 2013, **78**, 2087-2098.
99.   M. A. Lopez-Quintela, C. Tojo, M. C. Blanco, L. G. Rio and J. R. Leis, *Curr. Opin. Colloid Interface Sci.*, 2004, **9**, 264-278.
100.   R. A. S. Soomro, S. T. H.; Sirajuddin, Memon, N.; Shah, M. R.; Kalwar, H.; Hallam, K. R.; Shah, A., *Adv. Mater. Lett.*, 2013, **5**, 191-198.
101.   M. P. Pileni, *Nat Mater*, 2003, **2**, 145-150.
102.   B. J. Nehilla, M. Bergkvist, K. C. Popat and T. A. Desaid, *Int. J. Pharmaceut.*, 2008, **348**, 107-114.
103.   Y. Niidome, K. Honda, K. Higashimoto, H. Kawazumi, S. Yamada, N. Nakashima, Y. Sasaki, Y. Ishida and J. Kikuchi, *Chem. Commun.*, 2007, 3777-3779.
104.   Z. L. Wang, J. M. Yan, H. L. Wang, Y. Ping and Q. Jiang, *J. Mater. Chem. A*, 2013, **1**, 12721-12725.
105.   W. W. Guo, J. P. Yuan, Q. Z. Dong and E. K. Wang, *J. Am. Chem. Soc.*, 2010, **132**, 932-934.
106.   J. P. Xie, Y. G. Zheng and J. Y. Ying, *J. Am. Chem. Soc.*, 2009, **131**, 888-889.
107.   J. P. Xie, Y. G. Zheng and J. Y. Ying, *Chem. Commun.*, 2010, **46**, 961-963.
108.   A. Rotaru, S. Dutta, E. Jentzsch, K. Gothelf and A. Mokhir, *Angew. Chem. Int. Ed.*, 2010, **49**, 5665-5667.
109.   Z. X. Zhou, Y. Du and S. J. Dong, *Anal. Chem.*, 2011, **83**, 5122-5127.
110.   H. W. Shim, A. H. Lim, J. C. Kim, E. Jang, S. D. Seo, G. H. Lee, T. D. Kim and D. W. Kim, *Sci. Rep.*, 2013, **3**, 2325.
111.   R. Kaur, C. Giordano, M. Gradzielski and S. K. Mehta, *Chem. Asian J.*, 2014, **9**, 189-198.
112.   S. Magdassi, M. Grouchko and A. Kamyshny, *Materials*, 2010, **3**, 4626-4638.
113.   L. Chen, D. J. Zhang, J. M. Chen, H. D. Zhou and H. Q. Wan, *Mat. Sci. Eng. a-Struct.*, 2006, **415**, 156-161.
114.   J. Zhou, B. Song, G. L. Zhao, W. X. Dong and G. R. Han, *Appl. Phy.s a-Mater.*, 2012, **107**, 321-331.
115.   J. Zhang, L. P. Li and G. S. Li, *Int. J. Photoenergy*, 2012, 913630.
116.   T. Froschl, U. Hormann, P. Kubiak, G. Kucerova, M. Pfanzelt, C. K. Weiss, R. J. Behm, N. Husing, U. Kaiser, K. Landfester and M. Wohlfahrt-Mehrens, *Chem. Soc. Rev.*, 2012, **41**, 5313-5360.
117.   S. Gupta and M. Tripathi, *Chinese Sci. Bull.*, 2011, **56**, 1639-1657.
118.   K. Q. Huang, L. Chen, J. W. Xiong and M. X. Liao, *Int. J. Photoenergy*, 2012, 631435.
119.   S. M. Gupta and M. Tripathi, *Cent. Eur. J. Chem.*, 2012, **10**, 279-294.
120.   T. K. Tseng, Y. S. Lin, Y. J. Chen and H. Chu, *Int. J. Mol. Sci.*, 2010, **11**, 2336-2361.
121.   C. Burda, X. B. Chen, R. Narayanan and M. A. El-Sayed, *Chem. Rev.*, 2005, **105**, 1025-1102.

122.   T. Sugimoto, X. P. Zhou and A. Muramatsu, *J. Colloid Interface Sci.*, 2003, **259**, 53-61.

123.   S. Lee, I. S. Cho, J. H. Lee, D. H. Kim, D. W. Kim, J. Y. Kim, H. Shin, J. K. Lee, H. S. Jung, N. G. Park, K. Kim, M. J. Ko and K. S. Hong, *Chem. Mater.*, 2010, **22**, 1958-1965.

124.   B. Guo, Z. L. Liu, L. Hong, H. X. Jiang and J. Y. Lee, *Thin Solid Films*, 2005, **479**, 310-315.

125.   F. B. Li, X. Z. Li, C. H. Ao, S. C. Lee and M. F. Hou, *Chemosphere*, 2005, **59**, 787-800.

126.   D. P. Macwan, P. N. Dave and S. Chaturvedi, *J. Mater. Sci.*, 2011, **46**, 3669-3686.

127.   G. F. Zou, H. Li, Y. G. Zhang, K. Xiong and Y. T. Qian, *Nanotechnology*, 2006, **17**, S313-S320.

128.   Y. W. Jun, M. F. Casula, J. H. Sim, S. Y. Kim, J. Cheon and A. P. Alivisatos, *J. Am. Chem. Soc.*, 2003, **125**, 15981-15985.

129.   H. E. Wang, Z. H. Chen, Y. H. Leung, C. Y. Luan, C. P. Liu, Y. B. Tang, C. Yan, W. J. Zhang, J. A. Zapien, I. Bello and S. T. Lee, *Appl. Phys. Lett.*, 2010, **96**, 263104.

130.   W. Q. Wu, B. X. Lei, H. S. Rao, Y. F. Xu, Y. F. Wang, C. Y. Su and D. B. Kuang, *Sci. Rep.*, 2013, **3**, 1352

131.   H. S. Wu, L. D. Sun, H. P. Zhou and C. H. Yan, *Nanoscale*, 2012, **4**, 3242-3247.

132.   H. G. Yang, G. Liu, S. Z. Qiao, C. H. Sun, Y. G. Jin, S. C. Smith, J. Zou, H. M. Cheng and G. Q. Lu, *J. Am. Chem. Soc.*, 2009, **131**, 4078-4083.

133.   Z. F. Bian, J. A. Zhu, F. L. Cao, Y. N. Huo, Y. F. Lu and H. X. Li, *Chem. Commun.*, 2010, **46**, 8451-8453.

134.   X. L. Li, Q. Peng, J. X. Yi, X. Wang and Y. Li, Chem. Eur. J., 2006, **12**, 2383-2391.

135.   J. Zhang, L. P. Li, T. J. Yan and G. S. Li, *J. Phys. Chem. C*, 2011, **115**, 13820-13828.

136.   D. S. Kim and S. Y. Kwak, *Appl. Catal. a-Gen.*, 2007, **323**, 110-118.

137.   S. S. Mali, H. Kim, C. S. Shim, P. S. Patil, J. H. Kim and C. K. Hong, *Sci. Rep.*, 2013, **3**, 3004.

138.   K. Byrappa and T. Adschiri, *Prog. Cryst. Growth Charact. Mater.*, 2007, **53**, 117-166.

139.   C. Feldmann, *Adv Funct Mater*, 2003, **13**, 101-107.

140.   J. T. Jiu, M. Nogi, T. Sugahara, K. Suganuma, M. Tsujimoto and S. Isoda, *J. Nanopart. Res.*, 2012, **14**, 975.

141.   B. Geiseler and L. Fruk, *J. Mater. Chem.*, 2012, **22**, 735-741.

142.   S. K. Tripathy, T. Sahoo, M. Mohapatra, S. Anand and Y. T. Yu, *J. Phys. Chem. Solids*, 2009, **70**, 147-152.

143.   X. Chen and S. S. Mao, *Chem. Rev.*, 2007, **107**, 2891-2959.

144.   W. B. Hou and S. B. Cronin, *Adv. Funct. Mater.*, 2013, **23**, 1612-1619.

145.   K. L. Kelly, E. Coronado, L. L. Zhao and G. C. Schatz, *J. Phys. Chem. B*, 2003, **107**, 668-677.

146.   G. Singaravelu, J. S. Arockiamary, V. G. Kumar and K. Govindaraju, *Colloid Surface B*, 2007, **57**, 97-101.

147.   Y. X. Hu, J. P. Ge, D. Lim, T. R. Zhang and Y. D. Yin, *J. Solid. State. Chem.*, 2008, **181**, 1524-1529.

148.   Y. F. Wang, A. V. Biradar, G. Wang, K. K. Sharma, C. T. Duncan, S. Rangan and T. Asefa, *Chem. Eur. J.*, 2010, **16**, 10735-10743.

149.   H. Chen, X. Kou, Z. Yang, W. Ni and J. Wang, *Langmuir*, 2008, **24**, 5233-5237.

150.   J. Zeng, S. Roberts and Y. N. Xia, *Chem. Eur. J.*, 2010, **16**, 12559-12563.

151.   Y. Q. Zheng, Y. Y. Ma, J. Zeng, X. L. Zhong, M. S. Jin, Z. Y. Li and Y. N. Xia, *Chem. Asian J.*, 2013, **8**, 792-799.

152.   W. Hermoso, T. V. Alves, E. G. Moriya, F. R. Ornellas and P. H. C. Camargo, *Eur. Phys. J. D*, 2012, **66**, 135.

References

153.   E. Oh, K. Susumu, R. Goswami and H. Mattoussi, *Langmuir*, 2010, **26**, 7604-7613.
154.   S. Link and M. A. El-Sayed, *Int. Rev. Phys. Chem.*, 2000, **19**, 409-453.
155.   U. F. Kreibig, C. Fragstein., *Z. Phys.*, 1969, **224**, 307-323.
156.   B. N. J. Persson, *Surf. Sci.*, 1993, **281**, 153-162.
157.   T. Linnert, P. Mulvaney and A. Henglein, *J. Phys. Chem.-Us*, 1993, **97**, 679-682.
158.   M. Chen and L. Gao, *Inorg. Chem.*, 2006, **45**, 5145-5149.
159.   D. K. Lim, I. J. Kim and J. M. Nam, *Chem. Commun.*, 2008, 5312-5314.
160.   G. T. H., *Photoluminescence in Analysis of Surfaces and Interfaces in Encyclopedia of Anal. Chem.*, 2000, 9209–9231.
161.   B. Valeur and M. N. Berberan-Santos, *J. Chem. Educ.*, 2011, **88**, 731-738.
162.   J. P. Wilcoxon, J. E. Martin, F. Parsapour, B. Wiedenman and D. F. Kelley, *J. Chem. Phys.*, 1998, **108**, 9137-9143.
163.   T. P. Bigioni, R. L. Whetten and O. Dag, *J. Phys. Chem. B*, 2000, **104**, 6983-6986.
164.   S. Link, A. Beeby, S. FitzGerald, M. A. El-Sayed, T. G. Schaaff and R. L. Whetten, *J. Phys. Chem. B*, 2002, **106**, 3410-3415.
165.   J. Zheng, C. W. Zhang and R. M. Dickson, *Phys. Rev. Lett.*, 2004, **93**, 077402.
166.   T. J. Deerinck, *Toxicol. Pathol.*, 2008, **36**, 112-116.
167.   L. Li, Z. Li, H. Zhang, S. C. Zhang, I. Majeed and B. Tan, *Nanoscale*, 2013, **5**, 1986-1992.
168.   Z. Li, C. Q. Dong, L. C. Tang, X. Zhu, H. J. Chen and J. C. Ren, *Luminescence.*, 2011, **26**, 439-448.
169.   S. Mathew, S. A. Joseph, P. Radhakrishnan, V. P. N. Nampoori and C. P. G. Vallabhan, *J. Fluoresc.*, 2011, **21**, 1479-1484.
170.   C. C. Huang, H. Y. Liao, Y. C. Shiang, Z. H. Lin, Z. Yang and H. T. Chang, *J. Mater. Chem.*, 2009, **19**, 755-759.
171.   T. U. B. Rao and T. Pradeep, *Angew. Chem. Int. Ed.*, 2010, **49**, 3925-3929.
172.   J. Zheng, P. R. Nicovich and R. M. Dickson, *Annu. Rev. Phys. Chem.*, 2007, **58**, 409-431.
173.   X. Wu, T. Ming, X. Wang, P. N. Wang, J. F. Wang and J. Y. Chen, *ACS Nano*, 2010, **4**, 113-120.
174.   O. P. Siwach and P. Sen, *J. Lumin.*, 2009, **129**, 6-11.
175.   G. Lozano, D. J. Louwers, S. R. K. Rodriguez, S. Murai, O. T. A. Jansen, M. A. Verschuuren and J. G. Rivas, *Light Sci. Appl.*, 2013, **2**, e66.
176.   M. J. Ruedas-Rama, J. D. Walters, A. Orte and E. A. H. Hall, *Anal. Chim. Acta.*, 2012, **751**, 1-23.
177.   C. Zhou, S. Yang, J. Liu, M. Yu and J. Zheng, *Exp. Biol. Med. (Maywood)*, 2013, **238**, 1199-1209.
178.   J. Kneipp, H. Kneipp and K. Kneipp, *Chem. Soc. Rev.*, 2008, **37**, 1052-1060.
179.   Y. S. Huh, A. J. Chung and D. Erickson, *Microfluid. Nanofluid.*, 2009, **6**, 285-297.
180.   K. Kneipp, *Phys. Today*, 2007, **60**, 40-46.
181.   G. McNay, D. Eustace, W. E. Smith, K. Faulds and D. Graham, *Appl. Spectrosc.*, 2011, **65**, 825-837.
182.   B. Sharma, R. R. Frontiera, A. I. Henry, E. Ringe and R. P. Van Duyne, *Mater. Today*, 2012, **15**, 16-25.
183.   Y. P. Chen, X. W. Zheng, G. Chen, C. He, W. F. Zhu, S. Y. Feng, G. Q. Xi, R. Chen, F. H. Lan and H. S. Zeng, *Int. J. Nanomed.*, 2012, **7**, 73-82.
184.   D. A. Stuart, K. B. Biggs and R. P. Van Duyne, *Analyst*, 2006, **131**, 568-572.
185.   M. A. Mahmoud and M. A. El-Sayed, *J. Phys. Chem. Lett.*, 2013, **4**, 1541-1545.
186.   R. J. Stokes, A. Macaskill, P. J. Lundahl, W. E. Smith, K. Faulds and D. Graham, *Small*, 2007, **3**, 1593-1601.

187. A. G. Shen, L. F. Chen, W. Xie, J. C. Hu, A. Zeng, R. Richards and J. M. Hu, *Adv. Funct. Mater.*, 2010, **20**, 969-975.
188. S. M. Jang, J. S. Park, S. M. Shin, C. J. Yoon, B. K. Choi, M. S. Gong and S. W. Joo, *Langmuir*, 2004, **20**, 1922-1927.
189. E. Sr, W. E. Haskins and S. M. Nie, *J. Am. Chem. Soc.*, 1998, **120**, 8009-8010.
190. K. G. Stamplecoskie, J. C. Scaiano, V. S. Tiwari and H. Anis, *J. Phys. Chem. C*, 2011, **115**, 1403-1409.
191. G. V. P. Kumar, *J. Nanophotonics*, 2012, **6**, 064503.
192. L. Lu, A. Kobayashi, K. Tawa and Y. Ozaki, *Chem. Mater.*, 2006, **18**, 4894-4901.
193. J. M. McLellan, A. Siekkinen, J. Y. Chen and Y. N. Xia, *Chem. Phys. Lett.*, 2006, **427**, 122-126.
194. M. Rycenga, M. H. Kim, P. H. C. Camargo, C. Cobley, Z. Y. Li and Y. N. Xia, *J. Phys. Chem. A*, 2009, **113**, 3932-3939.
195. A. O. Pinchuk and G. C. Schatz, *Mater. Sci. Eng. B-Adv.*, 2008, **149**, 251-258.
196. K. Kneipp and H. Kneipp, *Isr J Chem*, 2006, **46**, 299-305.
197. C. Y. Wu, W. Y. Lo, C. R. Chiu and T. S. Yang, *J. Raman Spectrosc.*, 2006, **37**, 799-807.
198. T. Pal, N. R. Jana, A. Pal, J. A. Creighton and A. E. Beezer, *J. Indian Chem. Soc.*, 2000, **77**, 34-35.
199. Y. Wang, D. Li, P. Li, W. Wang, W. Ren, S. Dong and E. Wang, *J. Phys. Chem. C*, 2007, **111**, 16833-16839.
200. S. E. J. Bell and N. M. S. Sirimuthu, *J. Am. Chem. Soc.*, 2006, **128**, 15580-15581.
201. Y. Q. Wang, B. Yan and L. X. Chen, *Chem. Rev.*, 2013, **113**, 1391-1428.
202. A. Manke, L. Y. Wang and Y. Rojanasakul, *Biomed. Res. Int.*, 2013.
203. A. Sarkar, M. Ghosh and P. C. Sil, *J. Nanosci. Nanotechno.*, 2014, **14**, 730-743.
204. H. Kato, N. Sugino, S. Takiguchi, S. Kashida and Y. Nakamura, *Rev. Reprod.*, 1997, **2**, 81-83.
205. B. I. Ipe, M. Lehnig and C. M. Niemeyer, *Small*, 2005, **1**, 706-709.
206. Y. Li, W. Zhang, J. F. Niu and Y. S. Chen, *ACS Nano*, 2012, **6**, 5164-5173.
207. Y. W. Guo, C. P. Cheng, J. Wang, Z. Q. Wang, X. D. Jin, K. Li, P. L. Kang and J. Q. Gao, *J. Hazard Mater.*, 2011, **192**, 786-793.
208. B. I. Ipe and C. M. Niemeyer, *Angew. Chem. Int. Ed.*, 2006, **45**, 504-507.
209. A. Nel, T. Xia, L. Madler and N. Li, *Science*, 2006, **311**, 622-627.
210. W. W. He, Y. T. Zhou, W. G. Wamer, M. D. Boudreau and J. J. Yin, *Biomaterials*, 2012, **33**, 7547-7555.
211. W. He, Y. T. Zhou, W. G. Wamer, M. D. Boudreau and J. J. Yin, *Biomaterials*, 2012, **33**, 7547-7555.
212. O. Bondarenko, A. Ivask, A. Kakinen and A. Kahru, *Environ. Pollut.*, 2012, **169**, 81-89.
213. A. K. Chatterjee, R. Chakraborty and T. Basu, *Nanotechnology*, 2014, **25**, 135101.
214. H. L. Karlsson, P. Cronholm, Y. Hedberg, M. Thornberg, L. De Battice, S. Svedhem and I. O. Wallirider, *Toxicology*, 2013, **313**, 59-69.
215. W. S. Lin, Y. Xu, C. C. Huang, Y. F. Ma, K. B. Shannon, D. R. Chen and Y. W. Huang, *J. Nanopart. Res.*, 2009, **11**, 25-39.
216. S. J. Oh, H. Kim, Y. Liu, H. K. Han, K. Kwon, K. H. Chang, K. Park, Y. Kim, K. Shim, S. S. A. An and M. Y. Lee, *Toxicol. Lett.*, 2014, **225**, 422-432.
217. S. Sortino, *J. Mater. Chem.*, 2012, **22**, 301-318.
218. M. Pelaez, N. T. Nolan, S. C. Pillai, M. K. Seery, P. Falaras, A. G. Kontos, P. S. M. Dunlop, J. W. J. Hamilton, J. A. Byrne, K. O'Shea, M. H. Entezari and D. D. Dionysiou, *Appl. Catal. B-Environ.*, 2012, **125**, 331-349.
219. D. Astruc, F. Lu and J. R. Aranzaes, *Angew. Chem. Int. Ed.*, 2005, **44**, 7852-7872.

References

220.   P. V. Kamat and D. Meisel, *C. R. Chim.*, 2003, **6**, 999-1007.
221.   A. D., *Nanoparticles and Catalysis, Wiley*, 2008.
222.   D. Beydoun, R. Amal, G. Low and S. McEvoy, *J. Nanopart. Res.*, 1999, **1**, 439-458.
223.   H. Hirai, Y. Nakao and N. Toshima, *Chem. Lett.*, 1976, 905-910.
224.   M. Haruta, T. Kobayashi, H. Sano and N. Yamada, *Chem. Lett.*, 1987, 405-408.
225.   M. Haruta, *Catal. Today*, 1997, **36**, 153-166.
226.   A. Salehi-Khojin, H. R. M. Jhong, B. A. Rosen, W. Zhu, S. C. Ma, P. J. A. Kenis and R. I. Masel, *J. Phys. Chem. C*, 2013, **117**, 1627-1632.
227.   Y. L. S. J. L. W. C. G. Z., *ChemCatChem*, 2014.
228.   R. Xu, D. S. Wang, J. T. Zhang and Y. D. Li, *Chem. Asian J.*, 2006, **1**, 888-893.
229.   K. B. Zhou, R. P. Wang, B. Q. Xu and Y. D. Li, *Nanotechnology*, 2006, **17**, 3939-3943.
230.   J. F. Wang, J. X. Gong, Y. S. Xiong, J. D. Yang, Y. Gao, Y. L. Liu, X. Q. Lu and Z. Y. Tang, *Chem. Commun.*, 2011, **47**, 6894-6896.
231.   R. J. Tayade, P. K. Surolia, R. G. Kulkarni and R. V. Jasra, *Sci. Technol. Adv. Mat.*, 2007, **8**, 455-462.
232.   H. Yaghoubi, N. Taghavinia and E. K. Alamdari, *Surf. Coat. Tech.*, 2010, **204**, 1562-1568.
233.   J. B. Priebe, M. Karnahl, H. Junge, M. Beller, D. Hollmann and A. Bruckner, *Angew. Chem. Int. Ed.*, 2013, **52**, 11420-11424.
234.   F. Xu and L. T. Sun, *Energy Environ. Sci.*, 2011, **4**, 818-841.
235.   S. Y. Lee and S. J. Park, *J. Ind. Eng. Chem.*, 2013, **19**, 1761-1769.
236.   W. X. Li, *J. Aust. Ceram. Soc.*, 2013, **49**, 41-46.
237.   M. Ni, M. K. H. Leung, D. Y. C. Leung and K. Sumathy, *Renew. Sust. Energ. Rev.*, 2007, **11**, 401-425.
238.   A. L. Linsebigler, G. Q. Lu and J. T. Yates, *Chem. Rev.*, 1995, **95**, 735-758.
239.   M. N. Chong, B. Jin, C. W. K. Chow and C. Saint, *Water Res.*, 2010, **44**, 2997-3027.
240.   M. I. Baraton, *Recent Pat Nanotech*, 2012, **6**, 10-15.
241.   H. B. Shi, R. Magaye, V. Castranova and J. S. Zhao, *Part. Fibre Toxicol.*, 2013, **10**, 15.
242.   Z. F. Bian, T. Tachikawa, P. Zhang, M. Fujitsuka and T. Majima, *J. Am. Chem. Soc.*, 2014, **136**, 458-465.
243.   R. Mohammadi, B. Massoumi and M. Rabani, *Int. J. Photoenergy*, 2012.
244.   Q. P. Lu, Z. D. Lu, Y. Z. Lu, L. F. Lv, Y. Ning, H. X. Yu, Y. B. Hou and Y. D. Yin, *Nano Lett.*, 2013, **13**, 5698-5702.
245.   A. W. Maijenburg, J. Veerbeek, R. de Putter, S. A. Veldhuis, M. G. C. Zoontjes, G. Mul, J. M. Montero-Moreno, K. Nielsch, H. Schafer, M. Steinhart and J. E. ten Elshof, *J. Mater. Chem. A*, 2014, **2**, 2648-2656.
246.   E. Katz and I. Willner, *Angew. Chem. Int. Ed.*, 2004, **43**, 6042-6108.
247.   W. R. Algar, D. E. Prasuhn, M. H. Stewart, T. L. Jennings, J. B. Blanco-Canosa, P. E. Dawson and I. L. Medintz, *Bioconjugate Chem.*, 2011, **22**, 825-858.
248.   I. Willner, B. Basnar and B. Willner, *FEBS J.*, 2007, **274**, 302-309.
249.   B. N. Rospendowski, K. Kelly, C. R. Wolf and W. E. Smith, *J. Am. Chem. Soc.*, 1991, **113**, 1217-1225.
250.   H. Mattoussi, J. M. Mauro, E. R. Goldman, G. P. Anderson, V. C. Sundar, F. V. Mikulec and M. G. Bawendi, *J. Am. Chem. Soc.*, 2000, **122**, 12142-12150.
251.   J. S. Lee, A. K. R. Lytton-Jean, S. J. Hurst and C. A. Mirkin, *Nano Lett.*, 2007, **7**, 2112-2115.
252.   J. L. Brennan, N. S. Hatzakis, T. R. Tshikhudo, N. Dirvianskyte, V. Razumas, S. Patkar, J. Vind, A. Svendsen, R. J. M. Nolte, A. E. Rowan and M. Brust, *Bioconjugate Chem.*, 2006, **17**, 1373-1375.
253.   J. Pan and Q. W. Yang, *Anal. Bioanal. Chem.*, 2007, **388**, 279-286.

228

254. G. S. Lai, J. Wu, H. X. Ju and F. Yan, *Adv. Funct. Mater.*, 2011, **21**, 2938-2943.
255. K. E. Sapsford, W. R. Algar, L. Berti, K. B. Gemmill, B. J. Casey, E. Oh, M. H. Stewart and I. L. Medintz, *Chem. Rev.*, 2013, **113**, 1904-2074.
256. W. Shenton, S. A. Davis and S. Mann, *Adv. Mater.*, 1999, **11**, 449-452.
257. D. van Lierop, Z. Krpetic, L. Guerrini, I. A. Larmour, J. A. Dougan, K. Faulds and D. Graham, *Chem. Commun.*, 2012, **48**, 8192-8194.
258. M. H. Humphreys and S. Y. Lin, *Hypertension*, 1988, **11**, 397-410.
259. S. C. Wagner, M. Roskamp, H. Colfen, C. Bottcher, S. Schlecht and B. Koksch, *Org. Biomol. Chem.*, 2009, **7**, 46-51.
260. N. Shamim, L. Hong, K. Hidajat and M. S. Uddin, *J. Colloid Interface Sci.*, 2006, **304**, 1-8.
261. V. Hlady and J. Buijs, *Curr. Opin. Biotech.*, 1996, **7**, 72-77.
262. Z. Li, R. C. Jin, C. A. Mirkin and R. L. Letsinger, *Nucleic Acids Res.*, 2002, **30**, 1558-1562.
263. P. Thangadurai, S. Balaji and P. T. Manoharan, *Nanotechnology*, 2008, **19**, 435708.
264. M. H. Lin, Y. J. Liu, X. F. Chen, S. D. Fei, C. L. Ni, Y. P. Fang, C. B. Liu and Q. Y. Cai, *Biosens. Bioelectron.*, 2013, **45**, 82-88.
265. H. Basti, L. Ben Tahar, L. S. Smiri, F. Herbst, M. J. Vaulay, F. Chau, S. Ammar and S. Benderbous, *J. Colloid Interface Sci.*, 2010, **341**, 248-254.
266. A. P. Alivisatos, K. P. Johnsson, X. G. Peng, T. E. Wilson, C. J. Loweth, M. P. Bruchez and P. G. Schultz, *Nature*, 1996, **382**, 609-611.
267. C. A. Mirkin, R. L. Letsinger, R. C. Mucic and J. J. Storhoff, *Nature*, 1996, **382**, 607-609.
268. D. W. Shi, C. Song, Q. Jiang, Z. G. Wang and B. Q. Ding, *Chem. Commun.*, 2013, **49**, 2533-2535.
269. X. Zhang, T. Gouriye, K. Goeken, M. R. Servos, R. Gill and J. W. Liu, *J. Phys. Chem. C*, 2013, **117**, 15677-15684.
270. P. C. Patel, D. A. Giljohann, D. S. Seferos and C. A. Mirkin, *Proc. Natl. Acad. Sci. U.S.A.*, 2008, **105**, 17222-17226.
271. D. H. Tsai, F. W. DelRio, A. M. Keene, K. M. Tyner, R. I. MacCuspie, T. J. Cho, M. R. Zachariah and V. A. Hackley, *Langmuir*, 2011, **27**, 2464-2477.
272. J. L. Elechiguerra, J. L. Burt, J. R. Morones, A. Camacho-Bragado, X. Gao, H. H. Lara and M. J. Yacaman, *J. Nanobiotechnology*, 2005, **3**, 6.
273. U. Terranova and D. R. Bowler, *J. Phys. Chem. C*, 2010, **114**, 6491-6495.
274. T. Paunesku, T. Rajh, G. Wiederrecht, J. Maser, S. Vogt, N. Stojicevic, M. Protic, B. Lai, J. Oryhon, M. Thurnauer and G. Woloschak, *Nat. Mater.*, 2003, **2**, 343-346.
275. R. Bazak, J. Ressl, S. Raha, C. Doty, W. Liu, B. Wanzer, S. A. Salam, S. Elwany, T. Paunesku and G. E. Woloschak, *Nanoscale*, 2013, **5**, 11394-11399.
276. V. Singh, S. P. N. Nair and G. K. Aradhyam, *J. Nanobiotechnology*, 2013, **11**, 7.
277. Y. J. Zhang, R. Huang, X. F. Zhu, L. Z. Wang and C. X. Wu, *Chinese Sci. Bull.*, 2012, **57**, 238-246.
278. J. V. Staros, R. W. Wright and D. M. Swingle, *Anal. Biochem.*, 1986, **156**, 220-222.
279. B. Masereel, M. Dinguizli, C. Bouzin, N. Moniotte, O. Feron, B. Gallez, T. V. Borght, C. Michiels and S. Lucas, *J. Nanopart. Res.*, 2011, **13**, 1573-1580.
280. D. X. Li, Q. He, Y. Cui, L. Duan and J. B. Li, *Biochem. Biophys. Res. Commun.*, 2007, **355**, 488-493.
281. T. Lai, Q. N. Hou, H. A. Yang, X. G. Luo and M. R. Xi, *Acta Biochim. Biophys. Sinica*, 2010, **42**, 787-792.
282. L. J, *Click Chemistry for Biotechnology and Materials Science*, 2009.
283. M. T. Gokmen, J. Brassinne, R. A. Prasath and F. E. Du Prez, *Chem. Commun.*, 2011, **47**, 4652-4654.

References

284. C. Boyer, A. Granville, T. P. Davis and V. Bulmus, *J. Polym. Sci. Pol. Chem.*, 2009, **47**, 3773-3794.
285. C. Rissing and D. Y. Son, *Organometallics*, 2009, **28**, 3167-3172.
286. Y. Yuan, X. Wang, B. Mei, D. Zhang, A. Tang, L. An, X. He, J. Jiang and G. Liang, *Sci. Rep.*, 2013, **3**, 3523.
287. L. L. Li, Q. Yin, J. Cheng and Y. Lu, *Adv. Healthc. Mater.*, 2012, **1**, 567-572.
288. C. Y. Lee, P. C. T. Nguyen, D. W. Grainger, L. J. Gamble and D. G. Castner, *Anal. Chem.*, 2007, **79**, 4390-4400.
289. E. Oh, K. Susumu, J. B. Blanco-Canosa, I. L. Medintz, P. E. Dawson and H. Mattoussi, *Small*, 2010, **6**, 1273-1278.
290. H. J. Ba, J. Rodriguez-Fernandez, F. D. Stefani and J. Feldmann, *Nano Lett.*, 2010, **10**, 3006-3012.
291. J. E. Moses and A. D. Moorhouse, *Chem. So.c Rev.*, 2007, **36**, 1249-1262.
292. J. M. Baskin, J. A. Prescher, S. T. Laughlin, N. J. Agard, P. V. Chang, I. A. Miller, A. Lo, J. A. Codelli and C. R. Bertozzi, *Proc. Natl. Acad. Sci. U.S.A.*, 2007, **104**, 16793-16797.
293. M. Meldal and C. W. Tornoe, *Chem. Rev.*, 2008, **108**, 2952-3015.
294. J. L. Brennan, N. S. Hatzakis, T. R. Tshikhudo, N. Dirvianskyte, V. Razumas, S. Patkar, J. Vind, A. Svendsen, R. J. Nolte, A. E. Rowan and M. Brust, *Bioconjugate Chem.*, 2006, **17**, 1373-1375.
295. J. I. Cutler, D. Zheng, X. Xu, D. A. Giljohann and C. A. Mirkin, *Nano Lett.*, 2010, **10**, 1477-1480.
296. C. Schieber, A. Bestetti, J. P. Lim, A. D. Ryan, T. L. Nguyen, R. Eldridge, A. R. White, P. A. Gleeson, P. S. Donnelly, S. J. Williams and P. Mulvaney, *Angew. Chem. Int. Ed.*, 2012, **51**, 10523-10527.
297. A. Heuer-Jungemann, R. Kirkwood, A. H. El-Sagheer, T. Brown and A. G. Kanaras, *Nanoscale*, 2013, **5**, 7209-7212.
298. D. C. Rideout and R. Breslow, *J. Am. Chem. Soc.*, 1980, **102**, 7816-7817.
299. K. W. Hill, J. Taunton-Rigby, J. D. Carter, E. Kropp, K. Vagle, W. Pieken, D. P. McGee, G. M. Husar, M. Leuck, D. J. Anziano and D. P. Sebesta, *J. Org. Chem.*, 2001, **66**, 5352-5358.
300. A. D. de Araujo, J. M. Palomo, J. Cramer, M. Kohn, H. Schroder, R. Wacker, C. Niemeyer, K. Alexandrov and H. Waldmann, *Angew. Chem. Int. Ed.*, 2005, **45**, 296-301.
301. D. Graham, L. Fruk and W. E. Smith, *Analyst*, 2003, **128**, 692-699.
302. M. Proupin-Perez, R. Cosstick, L. M. Liz-Marzan, S.-M. V and M. Brust, *Nucleos. Nucleot. Nucl.*, 2005, **24**, 1075-1079.
303. M. Shi, J. H. Wosnick, K. Ho, A. Keating and M. S. Shoichet, *Angew. Chem. Int. Ed.*, 2007, **46**, 6126-6131.
304. Y. C. Lan, Y. L. Lu and Z. F. Ren, *Nano Energy*, 2013, **2**, 1031-1045.
305. G. Doria, J. Conde, B. Veigas, L. Giestas, C. Almeida, M. Assuncao, J. Rosa and P. V. Baptista, *Sensors-Basel*, 2012, **12**, 1657-1687.
306. S. W. Zeng, K. T. Yong, I. Roy, X. Q. Dinh, X. Yu and F. Luan, *Plasmonics*, 2011, **6**, 491-506.
307. E. Katz and I. Willner, *Angew. Chem. Int. Ed.*, 2004, **43**, 6042-6108.
308. J. Kirsch, C. Siltanen, Q. Zhou, A. Revzin and A. Simonian, *Chem. Soc. Rev.*, 2013, **42**, 8733-8768.
309. J. Zhou and Q. Yang, *Chem. Asian J.*, 2012, **7**, 2045-2050.
310. D. van Lierop, K. Faulds and D. Graham, *Anal. Chem.*, 2011, **83**, 5817-5821.
311. P. Hazarika, B. Ceyhan and C. M. Niemeyer, *Small*, 2005, **1**, 844-848.

312. J. Li, S. P. Song, X. F. Liu, L. H. Wang, D. Pan, Q. Huang, Y. Zhao and C. H. Fan, *Adv. Mater.*, 2008, **20**, 497-500.

313. H. Cai, N. N. Zhu, Y. Jiang, P. G. He and Y. Z. Fang, *Biosens. Bioelectro.n*, 2003, **18**, 1311-1319.

314. S. Lukman, K. M. M. Aung, J. Liu, B. Liu and X. D. Su, *ACS Appl. Mater. Inter.*, 2013, **5**, 12725-12734.

315. J. U. Menon, P. Jadeja, P. Tambe, K. Vu, B. H. Yuan and K. T. Nguyen, *Theranostics*, 2013, **3**, 152-166.

316. M. Segev-Bar and H. Haick, *ACS Nano*, 2013, **7**, 8366-8378.

317. W. H. Tan, H. Wang, Y. Chen, X. B. Zhang, H. Z. Zhu, C. Y. Yang, R. H. Yang and C. Liu, *Trends Biotechnol.*, 2011, **29**, 634-640.

318. W. Wu, S. Wieckowski, G. Pastorin, M. Benincasa, C. Klumpp, J. P. Briand, R. Gennaro, M. Prato and A. Bianco, *Angew. Chem. Int. Ed.*, 2005, **44**, 6358-6362.

319. A. K. Salem, P. C. Searson and K. W. Leong, *Nat Mater*, 2003, **2**, 668-671.

320. X. Q. Zhang, X. Y. Xu, R. Lam, D. Giljohann, D. Ho and C. A. Mirkin, *ACS Nano*, 2011, **5**, 6962-6970.

321. N. L. Rosi, D. A. Giljohann, C. S. Thaxton, A. K. R. Lytton-Jean, M. S. Han and C. A. Mirkin, *Science*, 2006, **312**, 1027-1030.

322. R. Arvizo, R. Bhattacharya and P. Mukherjee, *Expert Opin. Drug Deliv.*, 2010, **7**, 753-763.

323. D. S. Seferos, A. E. Prigodich, D. A. Giljohann, P. C. Patel and C. A. Mirkin, *Nano Lett.*, 2009, **9**, 308-311.

324. L. Song, V. H. B. Ho, C. Chen, Z. Q. Yang, D. S. Liu, R. J. Chen and D. J. Zhou, *Adv.Healthc. Mater.*, 2013, **2**, 275-280.

325. R. Khandelia, A. Jaiswal, S. S. Ghosh and A. Chattopadhyay, *Small*, 2013, **9**, 3494-3505.

326. H. L. Liu, M. Y. Hua, H. W. Yang, C. Y. Huang, P. C. Chu, J. S. Wu, I. C. Tseng, J. J. Wang, T. C. Yen, P. Y. Chen and K. C. Wei, *Proc. Natl. Acad. Sci. U.S.A*, 2010, **107**, 15205-15210.

327. S. Ghosh, U. Anand and S. Mukherjee, *Analyst*, 2013, **138**, 4270-4274.

328. Y. Qin, L. Sun, X. X. Li, Q. Q. Cao, H. Wang, X. F. Tang and L. Ye, *J. Mater. Chem.*, 2011, **21**, 18003-18010.

329. A. Z. Wilczewska, K. Niemirowicz, K. H. Markiewicz and H. Car, *Pharmacol. Rep.*, 2012, **64**, 1020-1037.

330. J. X. Xie, X. D. Zhang, H. Wang, H. Z. Zheng and Y. M. Huang, *TrAC Trend Anal. Chem.*, 2012, **39**, 114-129.

331. K. S. Park, M. I. Kim, D. Y. Cho and H. G. Park, *Small*, 2011, **7**, 1521-1525.

332. L. Z. Gao, J. Zhuang, L. Nie, J. B. Zhang, Y. Zhang, N. Gu, T. H. Wang, J. Feng, D. L. Yang, S. Perrett and X. Yan, *Nat. Nanotechnol.*, 2007, **2**, 577-583.

333. H. Deng, W. Shen, Y. Peng, X. Chen, G. Yi and Z. Gao, *Chem. Eur. J.*, 2012, **18**, 8906-8911.

334. A. Asati, S. Santra, C. Kaittanis, S. Nath and J. M. Perez, *Angew. Chem. Int. Ed.*, 2009, **48**, 2308-2312.

335. W. W. He, Y. T. Zhou, W. G. Warner, X. N. Hu, X. C. Wu, Z. Zheng, M. D. Boudreau and J. J. Yin, *Biomaterials*, 2013, **34**, 765-773.

336. L. Z. Hu, Y. L. Yuan, L. Zhang, J. M. Zhao, S. Majeed and G. B. Xu, *Anal. Chim. Acta*, 2013, **762**, 83-86.

337. J. M. Slocik, A. O. Govorov and R. R. Naik, *Angew. Chem. Int. Ed.*, 2008, **47**, 5335-5339.

338. L. Fruk, V. Rajendran, M. Spengler and C. M. Niemeyer, *ChemBioChem*, 2007, **8**, 2195-2198.

References

339.   B. Geiseler, M. Miljevic, P. Muller and L. Fruk, *J. Nanomater.*, 2012.

340.   L. L. Zhang, L. Han, P. Hu, L. Wang and S. J. Dong, *Chem. Commun.*, 2013, **49**, 10480-10482.

341.   X. N. Hu, J. B. Liu, S. Hou, T. Wen, W. Q. Liu, K. Zhang, W. W. He, Y. L. Ji, H. X. Ren, Q. Wang and X. C. Wu, *Sci. China Phys .Mech. Astron.*, 2011, **54**, 1749-1756.

342.   R. Subbiah, M. Veerapandian and K. S. Yun, *Curr. Med. Chem.*, 2010, **17**, 4559-4577.

343.   C. M. Shen, C. Hui, T. Z. Yang, C. W. Xiao, J. F. Tian, L. H. Bao, S. T. Chen, H. Ding and H. J. Gao, *Chem. Mater.*, 2008, **20**, 6939-6944.

344.   A. Grondin, D. C. Robson, W. E. Smith and D. Graham, *J. Chem. Soc. Perkin Trans. 2*, 2001, 2136-2141.

345.   K. Salorinne, X. Chen, R. W. Troff, M. Nissinen and H. Hakkinen, *Nanoscale*, 2012, **4**, 4095-4098.

346.   L. Fruk, A. Grondin, W. E. Smith and D. Graham, *Chem. Commun.*, 2002, 2100-2101.

347.   A. Enright, L. Fruk, A. Grondin, C. J. McHugh, W. E. Smith and D. Graham, *Analyst*, 2004, **129**, 975-978.

348.   S. A. McCarthy, G. L. Davies and Y. K. Gun'ko, *Nat. Protoc.*, 2012, **7**, 1677-1693.

349.   D. J. Lewis, T. M. Day, J. V. MacPherson and Z. Pikramenou, *Chem. Commun.*, 2006, 1433-1435.

350.   R. A. Sperling and W. J. Parak, *Phil. Trans. R Soc. A*, 2010, **368**, 1333-1383.

351.   L. Shang and G. U. Nienhaus, *Mater. Today*, 2013, **16**, 58-66.

352.   J. L. Wang, G. Zhang, Q. W. Li, H. Jiang, C. Y. Liu, C. Amatore and X. M. Wang, *Sci. Rep.*, 2013, **3**.

353.   J. Zheng, C. Zhou, M. X. Yu and J. B. Liu, *Nanoscale*, 2012, **4**, 4073-4083.

354.   S. Sadhu, P. S. Chowdhury and A. Patra, *J. Lumin.*, 2007, **126**, 387-392.

355.   S. Kim, D. H. Shin, D. Y. Shin, C. O. Kim, J. H. Park, S. B. Yang, S. H. Choi, S. J. Yoo and J. G. Kim, *J. Nanomater.*, 2012, 572746.

356.   J. R. Lakowicz, *Principles of Fluorescence Spectroscopy 3rd Edition, Springer*, 2006.

357.   A. C. Borin, L. Serrano-Andres, V. Ludwig and S. Canuto, *Phys. Chem. Chem. Phys.*, 2003, **5**, 5001-5009.

358.   W. Roth, D. Spangenberg, C. Janzen, A. Westphal and M. Schmitt, *Chem. Phys.*, 1999, **248**, 17-25.

359.   F. Li, H. Q. Zhang, B. Dever, X. F. Li and X. C. Le, *Bioconjugate Chem.*, 2013, **24**, 1790-1797.

360.   A. Steinbruck, A. Csaki, K. Ritter, M. Leich, J. M. Kohler and W. Fritzsche, *J. Biophotonics*, 2008, **1**, 104-113.

361.   S. K. Balani, T. Zhu, T. J. Yang, Z. Liu, B. He and F. W. Lee, *Drug Metab. and Dispos.*, 2002, **30**, 1059-1062.

362.   T. J. Strelevitz, R. S. Foti and M. B. Fisher, *J. Pharm. Sci.*, 2006, **95**, 1334-1341.

363.   R. Owczarzy, B. G. Moreira, Y. You, M. A. Behlke and J. A. Walder, *Biochemistry*, 2008, **47**, 5336-5353.

364.   C. Lin, Y. Liu, S. Rinker and H. Yan, *ChemPhysChem*, 2006, **7**, 1641-1647.

365.   D. Kendroira, *Biofunktionalisierung von Metallischen Nanopartikeln zur Entwicklung von Biosensoren*, 2013.

366.   S. A. A. Kates, F. , *Solid-Phase Synthesis: A Practical Guide*, 2000.

367.   A. Sudina, E. Volkov, T. Oretskaya, N. Naryshkin, M. Ivanovskaya and E. Kubareva, *IUBMB Life*, 2004, **56**, 139-143.

368.   H. Y. Wang and D. D. Weller, *Tetrahedron Lett.*, 1991, **32**, 7385-7388.

369.   L. Fruk and C. M. Niemeyer, *Angew. Chem. Int. Ed.*, 2005, **44**, 2603-2606.

370.   A. A. Mokhir, W. H. Connors and C. Richert, *Nucleic Acids Res.*, 2001, **29**, 3674-3684.

371.   S. Otto, F. Bertoncin and J. B. F. N. Engberts, *J. Am. Chem. Soc.* , 2006, **118**, 7702-7707.

372.   Z. Zhang, S. Zhang and M. S. Lin, *Analyst*, 2014, **139**, 2207-2213.

373.   Y. Chen, K. Munechika and D. S. Ginger, *Nano Lett.*, 2007, **7**, 690-696.

374.   C. M. Niemeyer and B. Ceyhan, *Angew. Chem. Int. Ed.*, 2001, **40**, 3685-+.

375.   A. C. Balazs, T. Emrick and T. P. Russell, *Science*, 2006, **314**, 1107-1110.

376.   N. Cioffi, L. Torsi, N. Ditaranto, G. Tantillo, L. Ghibelli, L. Sabbatini, T. Bleve-Zacheo, M. D'Alessio, P. G. Zambonin and E. Traversa, *Chem. Mater.*, 2005, **17**, 5255-5262.

377.   J. V. Jokerst, T. Lobovkina, R. N. Zare and S. S. Gambhir, *Nanomedicine.*, 2011, **6**, 715-728.

378.   D. F. Liu, W. Wu, J. J. Ling, S. Wen, N. Gu and X. Z. Zhang, *Adv. Funct .Mater.*, 2011, **21**, 1498-1504.

379.   V. Cauda, C. Argyo and T. Bein, *J. Mater. Chem.*, 2010, **20**, 8693-8699.

380.   D. P. K. Lankveld, R. G. Rayavarapu, P. Krystek, A. G. Oomen, H. W. Verharen, T. G. van Leeuwen, W. H. De Jong and S. Manohar, *Nanomedicine.*, 2011, **6**, 339-349.

381.   F. Alonso, Y. Moglie, G. Radivoy and M. Yus, *Tetrahedron Lett.*, 2009, **50**, 2358-2362.

382.   G. P. Jose, S. Santra, S. K. Mandal and T. K. Sengupta, *J. Nanobiotechnol.*, 2011, **9**, 9-18.

383.   J. Xiong, Y. Wang, Q. J. Xue and X. D. Wu, *Green Chem.*, 2011, **13**, 900-904.

384.   N. L. Pacioni, A. Pardoe, K. L. McGilvray, M. N. Chretien and J. C. Scaiano, *Photochem. Photobiol. Sci.*, 2010, **9**, 766-774.

385.   A. Marimuthu, J. Zhang and S. Linic, *Science*, 2013, **339**, 1590-1593.

386.   P. Kanninen, C. Johans, J. Merta and K. Kontturi, *J. Colloid Interface Sci.*, 2008, **318**, 88-95.

387.   N. R. Jana, Z. L. Wang, T. K. Sau and T. Pal, *Curr. Sci. India*, 2000, **79**, 1367-1370.

388.   N. Wiberg, *Inorganic Chemistry, Academic Press*, 2001.

389.   D. Malina, A. Sobczak-Kupiec, Z. Wzorek and Z. Kowalski, *Dig. J. Nanomater. Bios.*, 2012, **7**, 1527-1534.

390.   J. Ryu, H. S. Kim and H. T. Hahn, *J. Electron. Mater.*, 2011, **40**, 42-50.

391.   B. Thierry, J. Ng, T. Krieg and H. J. Griesser, *Chem. Commun.*, 2009, 1724-1726.

392.   S. Kapoor, R. Joshi and T. Mukherjee, *Chem. Phys. Lett.*, 2002, **354**, 443-448.

393.   A. L. Stepanov, X. Xiao, F. Ren, T. Kavetskyy and Y. N. Osin, *Rev. Adv. Mater. Sci.*, 2013, **34**, 107-122.

394.   G. Y. Liu, Y. Shao, K. Ma, Q. H. Cui, F. Wu and S. J. Xu, *Gold Bull.*, 2012, **45**, 69-74.

395.   G. Y. Lan, W. Y. Chen and H. T. Chang, *RSC Adv.*, 2011, **1**, 802-807.

396.   S. X. Dai, X. T. Zhang, T. F. Li, Z. L. Du and H. X. Dang, *Appl. Surf. Sci.*, 2005, **249**, 346-353.

397.   A. Bjorklund and S. B. Dunnett, *Trends Neurosci.*, 2007, **30**, 194-202.

398.   J. H. Waite, *Nat. Mater.*, 2008, **7**, 8-9.

399.   X. Fan, L. Lin, J. L. Dalsin and P. B. Messersmith, *J. Am. Chem. Soc.*, 2005, **127**, 15843-15847.

400.   R. Baron, M. Zayats and I. Willner, *Anal. Chem.*, 2005, **77**, 1566-1571.

401.   R. Bou, R. Codony, A. Tres, E. A. Decker and F. Guardiola, *Anal. Biochem.*, 2008, **377**, 1-15.

402.   A. Gomes, E. Fernandes and J. L. F. C. Lima, *J. Biochem. Biophys. Meth.*, 2005, **65**, 45-80.

403.   H. Weiner, E. Maser, D. W. Crabb and R. Lindahl, in *Advances in Experimental Medicine and Biology (Enzymology and Molecular Biology of Carbonyl Metabolism 7)*, 1999, p. 92.

References

404.   A. Gupta, B. Butts, K. A. Kwei, K. Dvorakova, S. P. Stratton, M. M. Briehl and G. T. Bowden, *Cancer Lett.*, 2001, **173**, 115-125.

405.   K. S. Rabe, M. Spengler, M. Erkelenz, J. Muller, V. J. Gandubert, H. Hayen and C. M. Niemeyer, *ChemBioChem*, 2009, **10**, 751-757.

406.   G. C. Yen and C. L. Hsieh, *Bioscience, Biotechnology, and Biochemistry*, 1997, **61**, 1646-1649.

407.   D. W. H. M. Rankin, N.; Morrison, C. , *Structural Methods in Molecular Inorganic Chemistry, 1st Ed.*, 2013.

408.   A. Haddy and G. Smith, *Comp. Biochem. Physiol. B*, 1999, **123**, 407-415.

409.   Y. Su, H. M. Brown, G. S. Li, X. D. Zhou, J. E. Amonette, J. L. Fulton, D. M. Camaioni and Z. C. Zhang, *Appl. Catal. a-Gen.*, 2011, **391**, 436-442.

410.   E. J. A. Ukpong, N. W.; and Prasad, J., *Afr. J. Pure Appl. Chem.*, 2010, **4**, 38-43.

411.   W. J. Barreto, S. R. G. Barreto, R. A. Ando, P. S. Santos, E. DiMauro and T. Jorge, *Spectrochim. Acta A*, 2008, **71**, 1419-1424.

412.   S. Lomnicki, H. Truong, E. Vejerano and B. Dellinger, *Environ. Sci. Technol.*, 2008, **42**, 4982-4988.

413.   V. Roginsky and T. Barsukova, *J. Chem. Soc. Perkin Trans. 2*, 2000, 1575-1582.

414.   J. A. Tainer, E. D. Getzoff, J. S. Richardson and D. C. Richardson, *Nature*, 1983, **306**, 284-287.

415.   A. Barik, B. Mishra, A. Kunwar, R. M. Kadam, L. Shen, S. Dutta, S. Padhye, A. K. Satpati, H. Y. Zhang and K. I. Priyadarsini, *Eur. J. Med. Chem.*, 2007, **42**, 431-439.

416.   R. Novotna, Z. Travnicek and R. Herchel, *Bioinorg. Chem. Appl.*, 2012, 704329.

417.   H. Ohtsu, Y. Shimazaki, A. Odani and O. Yamauchi, *Chem. Commun.*, 1999, 2393-2394.

418.   M. Hadizadeh, E. Keyhani, J. Keyhani and C. Khodadadi, *Acta Biochim. Biophys. Sin.*, 2009, **41**, 603-617.

419.   C. Oviedo and J. Rodriguez, *Quim. Nova*, 2003, **26**, 901-905.

420.   S. J. S. Flora and V. Pachauri, *Int. J. Environ. Res. Public Health*, 2010, **7**, 2745-2788.

421.   Y. Yamada, H. Saito, H. Tomioka and J. Jidoi, *J. Gen. Microbiol.*, 1987, **133**, 2007-2014.

422.   C. A. a. W. E. Smith, *Biological Molecules, 1st Ed. Chapman and Hall*, 1992, 92.

423.   G. M. Madhu, M. A. L. A. Raj and K. V. K. Pai, *J. Environ. Biol.*, 2009, **30**, 259-264.

424.   Y. J. Li and W. Chen, *Catal. Sci. Technol.*, 2011, **1**, 802-809.

425.   R. Libanori, T. R. Giraldi, E. Longo, E. R. Leite and C. Ribeiro, *J. Sol-Gel Sci. Technol.*, 2009, **49**, 95-100.

426.   K. Giribabu, R. Suresh, R. Manigandan, A. Vijayaraj, R. Prabu and V. Narayanan, *Bull. Korean Chem. Soc.*, 2012, **33**, 2910-2916.

427.   V. Homem and L. Santos, *J. Environ. Manage.*, 2011, **92**, 2304-2347.

428.   V. Yargeau and C. Leclair, *Water Sci. Technol.*, 2007, **55**, 321-326.

429.   J. H. O. S. Pereira, A. C. Reis, O. C. Nunes, M. T. Borges, V. J. P. Vilar and R. A. R. Boaventura, *Environ. Sci. Pollut. Res*, 2014, **21**, 1292-1303.

430.   A. Fernandez-Gonzalez, R. Badia and M. E. Diaz-Garcia, *Anal. Biochem.*, 2005, **341**, 113-121.

431.   H. R. Park, C. H. Oh, H. C. Lee, J. G. Choi, B. I. Jung and K. M. Bark, *Bull. Korean Chem. Soc.*, 2006, **27**, 2002-2010.

432.   P. Wang, D. J. Wang, H. Y. Li, T. F. Xie, H. Z. Wang and Z. L. Do, *J. Colloid Interface Sci.*, 2007, **314**, 337-340.

433.   B. Trouiller, R. Reliene, A. Westbrook, P. Solaimani and R. H. Schiestl, *Cancer Res.*, 2009, **69**, 8784-8789.

434.   A. M. Peterson, C. Pilz-Allen, T. Kolesnikova, H. Mohwald and D. Shchukin, *ACS Appl. Mater. Interfaces*, 2014, **6**, 1866-1871.

435. A. S. Levina, Z. R. Ismagilov, M. N. Repkova, N. V. Shikina, S. I. Baiborodin, N. V. Shatskaya, S. N. Zagrebelnyi and V. F. Zarytova, *Russ. J Bioorg. Chem.*, 2013, **39**, 77-86.

436. K. T. Thurn, T. Paunesku, A. G. Wu, E. M. B. Brown, B. Lai, S. Vogt, J. Maser, M. Aslam, V. Dravid, R. Bergan and G. E. Woloschak, *Small*, 2009, **5**, 1318-1325.

437. K. Ninomiya, A. Fukuda, C. Ogino and N. Shimizu, *Ultrason. Sonochem.*, 2014, **21**, 1624-1628.

438. A. S. Levina, M. N. Repkova, Z. R. Ismagilov, N. V. Shikina, E. G. Malygin, N. A. Mazurkova, V. V. Zinov'ev, A. A. Evdokimov, S. I. Baiborodin and V. F. Zarytova, *Sci. Rep.*, 2012, **2**.

439. K. O. Iwu, A. Galeckas, S. Diplas, F. Seland, A. Y. Kuznetsov and T. Norby, *Electrochim. Acta*, 2014, **115**, 66-74.

440. D. C. Bradley and M. J. Hillyer, *Trans. Faraday Soc.*, 1966, **62**, 2382-&.

441. C. J. Xu, K. M. Xu, H. W. Gu, R. K. Zheng, H. Liu, X. X. Zhang, Z. H. Guo and B. Xu, *J. Am. Chem. Soc.*, 2004, **126**, 9938-9939.

442. S. Yu, B. Liu, Q. Wang, Y. Gao, Y. Shi, X. Feng, X. An, L. Liu and J. Zhang, *ACS Appl. Mater. Interfaces*, 2014, **6**, 10283-10295.

443. J. Donovalova, M. Cigan, H. Stankovicova, J. Gaspar, M. Danko, A. Gaplovsky and P. Hrdlovic, *Molecules*, 2012, **17**, 3259-3276.

444. B. B. Raju and T. S. Varadarajan, *J. Phys. Chem.-Us*, 1994, **98**, 8903-8905.

445. A. Rotaru, S. Dutta, E. Jentzsch, K. Gothelf and A. Mokhir, *Angew. Chem. Int. Ed.*, 2010, **49**, 5665-5667.

446. J. Xiong, X. D. Wu and Q. J. Xue, *J. Colloid Interface Sci.*, 2013, **390**, 41-46.

447. A. Barik, B. Mishra, L. Shen, H. Mohan, R. M. Kadam, S. Dutta, H. Y. Zhang and K. I. Priyadarsini, *Free Radic. Bio. Med.*, 2005, **39**, 811-822.